PUMPING AND MODE-LOCKING TECHNIQUES FOR NEAR-INFRARED DYE AND COLOUR CENTRE LASERS.

Thesis submitted for the degree of Doctor of Philsophy of the University of London

by

Nigel John Langford, B.Sc., A.R.C.S.

Optics Group

Blackett Laboratory

Imperial College of Science and Technology

London SW7 2BZ   June 1988

Abstract.

Excitation schemes for dye and colour centre lasers have been studied and by a variety of mode-locking techniques ultrashort pulses have been generated in the red and near infra-red spectral regions. The laser active dye Rhodamine 700 was optically excited, using a krypton-ion pump laser, to provide a tunable source of coherent light in the 690 - 810 nm wavelength region. Synchronous excitation of this dye and exploitation of the technique of hybrid mode-locking resulted in the generation of pulses as short as 470 fs. Passive mode-locking of this active dye, using a variety of saturable absorbers, has also been demonstrated, and it was shown for the first time to be a reliable source of ultrashort pulses where durations of 430 fs have been recorded.

To extend the wavelength range over which ultrashort pulses may be produced the F_2^+ colour centre in a lithium flouride host crystal was studied. Laser operation was in the 0.8 - 1.0 μm wavelength range and short pulses, of 25 ps duration, were obtained by active mode-locking. The sub sequent development of a non-colinear excited LiF:F_2^+ colour centre laser enabled the characterisation of the synchronously mode-locked performance for both standing-wave and travelling-wave resonator configurations. Further pulse shortening was achieved by the hybrid technique whereby a saturable absorber folded section was added to the synchronously mode-locked linear cavity.The practicality of the passive mode-locking technique for the colour centre laser was also investigated for first time and subpicosecond (360 fs) pulses were obtained directly. By configuring a dispersion-optimised colliding pulse mode-locked ring cavity pulses as short as 180 fs were realised over the 850 - 875 nm tuning range.

The possibility of using electrical excitation as a convenient alternative to optical pmping has also been addressed. In the preliminary work the primary emphasis has been directed towards the electric field induced excitation of the self-trapped exciton in a caesium iodide crystal. Electroluminescence has been observed in the UV/blue (300-400 nm) spectral region.

Dedication

To Alison and Alexander

Contents

Chapter 1: Introduction.

The development of the laser has revolutionised both high resolution and time-domain spectroscopy. Prior to this, high resolution spectroscopy was restricted to the study of linear susceptibilities and their resonances and the optical probes used were normally filtered white light sources. These had very low spectral intensities and made the study of certain phenomena, such as non-linear optical transitions and forbidden transitions, impracticable. Similarly time-domain spectroscopy was hindered by the lack of suitable fast optical probes. However the realisation of both the highly tunable homogeneously broadened dye [1] and colour centre [2] lasers has opened many new avenues of research for both the time-domain and high-resolution spectroscopist, as well as many other aspects of science such as photobiology [3] and optical communications [4].

The homogeneously broadened nature of dye and colour centre gain media is a bonus to the laser physicist as it means that each excited dye molecule or colour centre is equally capable of contributing its energy at the desired frequency. Thus the insertion of frequency selective elements into the laser cavity means that the optical field will be at its strongest at the frequency governed by the tuning element and such elements can be inserted with little loss in efficiency. Hence by the introduction of highly selective frequency filters the lasing bandwidth can be limited to a single longitudinal mode. This strong spectral condensation together with the highly tunable nature of both dye and colour centre lasers means that a specific resonant transition in a material can be excited and the frequency of the probe light tuned through it to give an accurate mapping of the transition [5].

Conversely if the laser is made to oscillate with a large bandwidth and the longitudinal modes which constitute the bandwidth are forced to have the same phase relationship, then ultrashort pulses may be generated by the laser. Inducing a fixed phase relationship on the longitudinal modes is refered to as mode-locking and a comprehensive review of mode-locking has been given by New [6]. The duration of pulses generated by a mode-locked laser is related to the reciprocal of the lasing bandwidth and the pulses are temporally separated by the cavity round-trip period.

Various techniques can be applied to attain this mode-locked state, such as active mode-locking whereby an external modulation is used, or passive mode-locking, in which an intracavity flux related modulation is involved. In later chapters details of each technique will be described.

Tunable short pulse generation has been readily achieved using dye lasers as the active medium. Using the technique of passive mode-locking pulses as short as 19 fs have been generated directly from a dispersion-optimised Rhodamine 6G/ DODCI dye combination [7]. These pulses were generated at a wavelength of ~630 nm. Until recently pulses generated from actively mode-locked dye lasers could not match this duration with any degree of reliability. (Although it should be noted that Mourou et al have generated pulses as short as 70 fs from a hybrid mode-locked Rhodamine 6G/DQOCI combination [8].) Thus for experiments requiring ultrashort pulses, in the region of 100 fs, in wavelength regions beyond that covered by the Rhodamine 6G/DODCI combination indirect frequency shifting processes must be employed. An example of this is white light continuum generation [9] whereby the optical pulse is amplified in a dye amplifier [10] and then focussed into a transparent material such as glass, water or ethylene glycol. This produces a continuum which extends from the ultraviolet to the infrared which is then coupled into the sample of interest. The recent synthesis of new active dyes such as the Styryl family [11] combined with the development of new active/passive dye combinations for both purely passive [12] and dispersion-compensated hybridly mode-locked [13] dye lasers, has le d to the generation of ultrashort pulses with sub 100 fs durations from 490 nm [14] to ~ 1 μm [13].

For wavelengths beyond one micrometer, the thermal and photochemical stability of dyes are poor and for ultrashort pulse generation, complicated nonlinear frequency shifting techniques such as transient stimulated Raman scattering in various gaseous media [15], Raman scattering in optical fibres [16] or frequency mixing in non-linear media [17], must be employed. These methods result in the generation of near-infrared pulses, however the experimental complexity associated with their operation limits their usefulness. The family of laser active colour centres, which exhibit many of the features associated with organic dyes such as high emission and absorption cross-

sections, together with large homogeneously broadened luminescence bandwidths, has been demonstrated as a viable alternative for ultrashort pulse generation in the near infra-red spectral region. Laser action from colour centres has been reported to extend from ~0.8 μm (see chapter 5 and ref 2) to 4 μm [2] as well as in the ultraviolet/blue (345 - 420 nm) [18] and visible (500-600 nm) [19] spectral regions. However problems associated with the creation and stabilisation of the centres necessary for laser action have restricted the applications of colour centres as tunable light sources, even though the colour centre has been shown to operate with narrower linewidths than dye lasers [20], and is capable of generating femtosecond duration pulses (see chapters 6 and 7). For most colour centre lasers, stable laser operation is observed only at liquid nitrogen temperatures and this results in the need for specialist cryostats. Until recently the design of such cryostats has severely restricted the cavity configurations which can be constructed. In chapter 6 a novel inhouse-designed cryostat is described, which allows the configuration of both standing- and travelling-wave resonators to be configured. The ability of colour centre lasers to produce tunable short duration pulses in the near-infrared especially in the 1.3 μm [21] and 1.55 μm [22] regions has resulted in them becoming useful tools for the characterisation of optical fibres. By the addition of an external fibre-optic loop to the output from a synchronously mode-locked KCl:Tl colour centre laser resulting, in the so-called "soliton" laser [23] the broad homogeneously broadened nature of the colour centre gain medium has been fully exploited with the direct generation of pulses as short as 63 fs [24].

This thesis is primarily concerned with the generation of ultrashort pulses from both the near-infrared laser active dye Rhodamine 700 and near-infrared F_2^+ colour centre in a LiF host crystal. The pulses were generated using active, passive and hybrid techniques but in all three instances a krypton-ion pump laser was used as the excitation source. Noble ion lasers of this form are expensive and lack long term reliability and the final experimental chapter is concerned with the alternative of direct electrical excitation. In particular the self-trapped exciton in a CsI host lattice has been investigated in some preliminary work and the results obtained indicate that the self-trapped exciton electroluminesces in the 300 - 400 nm spectral region. This

could be developed to provide a tunable blue laser which is excited directly by an electrical source thus removing the need for an optical pump.

References:

1. See for example *Dye Lasers*; Ed F.P. Schafer Springer Verlag, Berlin 1973.

2. C.R. Pollock; J. Lumins., 35, 65, 1986.

3. L. Reekie, I. Ruddock and R. Illingworth, in *Picosecond Chemistry and Biology*. Eds. T. Doust and M. West. Science Reviews Limited. 1983.

4. See for example *Optical Fibre Telecommunication*, Ed. S.E. Miller and A.G. Chynoweth. Academic Press New York 1979.

5. B.D. Sinclair; PhD. Thesis University of St. Andrews 1987 and references therein.

6. G.H.C. New; Rep. Prog. Phys., 46, 887, 1983.

7. A. Finch, G. Chen, W. Sleat and W.Sibbett; J. Mod. Opts., (to be published).

8. G.A. Mourou and T. Sizer II ; Opt. Commun., 41,47, 1982.

9. R.L. Fork, C.V. Shank, R.Yen and C.V. Hirlimann; I.E.E.E. J. Quant. Electron., QE-19, 500, 1983.

10. T. Sizer II, J.D. Kafla, I.N. Duling III, C.W. Gabel and G.A. Mourou;I.E.E.E. J. Quant. Electron., QE-19, 506, 1983.

11. K. Kato; Opt. Lett., 9, 544, 1984

12. P.M.W. French; PhD. Thesis University of London 1987.

13. M.D. Dawson, T.F. Boggess and A.L. Smirl; Opt. Lett., 12, 254, 1987. and references therein.

14. P.M.W. French and J.R. Taylor; Appl. Phys. Lett., 50, 1708, 1987.

15. P.G. May and W. Sibbett; Appl. Phys. Lett., 43, 624, 1983.

16. A.S. Gouveia-Neto, A.S.L. Gomes and J.R. Taylor; I.E.E.E. J. Quant. Electron., QE-23, 1193, 1987.

17. D.Cotter and K.I. White; Opt. Commun., 49, 205, 1984.

18. B. Henderson; Opt. Lett., 6, 437, 1981.

19. S.C. Rand and L.G. Shazer; Opt. Lett., 10, 481, 1985.

20. N.D. Viera and L.F. Mollenauer; I.E.E.E. J. Quant. Electron., QE-21, 195, 1985.

21. L.F. Mollenauer and D.M. Bloom; Opt. Lett., 4, 247, 1979.

22. L.F. Mollenauer, N.D. Vieria and L. Szeto; Opt. Lett., 7, 414, 1982.

23. L.F. Mollenauer and R.H. Stolen; Opt. Lett., 9, 13, 1984.

24. F.M. Mitschke and L.F. Mollenauer; I.E.E.E. J. Quant. Electron., QE- 22, 2242, 1986.

Chapter 2: Organic Dyes, Colour Centres and Self-Trapped Excitons in Alkali Halide Crystals as Laser Active Gain Media.

2.1. Introduction

In the work presented here several different types of gain media were studied, including the near infra red dye laser, Rhodamine 700, the $LiF:F_2^+$ colour centre and the self-trapped exciton in CsI. The first two will be shown to be efficient sources of tunable radiation in the red and near infra-red spectral regions whilst the self-trapped exciton was studied only as a luminescence source which could be developed to give a tunable solid state laser in the blue spectral region. In this chapter a brief overview of all three as gain media will be given.

2.2. The Photophysics of an Organic Dye

A laser dye is a complex organic molecule containing many conjugated bonds which greatly influence the spectroscopic properties of the molecule. The basic mechanism for the absorption and emission of light is the same for each dye regardless of the spectral region in which laser action occurs. Laser action from organic dyes has been observed from 309 nm [1] to 1.8 μm [2].

The absorption of light can be explained in a semi-quantitative way using the free electron gas model. The dye is assumed to be a plane molecule with the atoms linked in a common plane by σ bonds whilst the π electrons form a charge cloud above and below the plane of the molecule. If the dye is of length l then the energy of a single π electron in the charge cloud is given by

$$E_n = \frac{h^2 n^2}{8ml^2}$$

(2.1)

where n is the quantum number of the electron Eigenstate, h is Planck's constant and m is the electron mass.

From this equation it can be seen that the transition wavelength is determined primarily by the length of the molecule and it predicts that transitions between energy Eigenstates will occur at specific wavelengths. In general, however, the absorption and emission lines are greatly broadened by the presence of rotational and vibrational sub-

levels. The vibronic sub-levels arise from the multi-atom nature of the molecule. When a transition between energy levels occurs there is a change in the density of the electron charge cloud associated with the molecule. A change of this nature alters the bond length between neighbouring atoms. The atoms experience a different coulombic force and start to vibrate about their equilibrium position with an amplitude governed by the new and old bond lengths. This results in the production of many vibronic sub-levels and associated with these are rotational levels which are broadened by collisions with, and electrostatic perturbations induced by, the surrounding solvent molecules.

The multi-electron nature of the charge cloud associated with a dye molecule gives rise to singlet and triplet electronic states which arise from the coupling of the electron
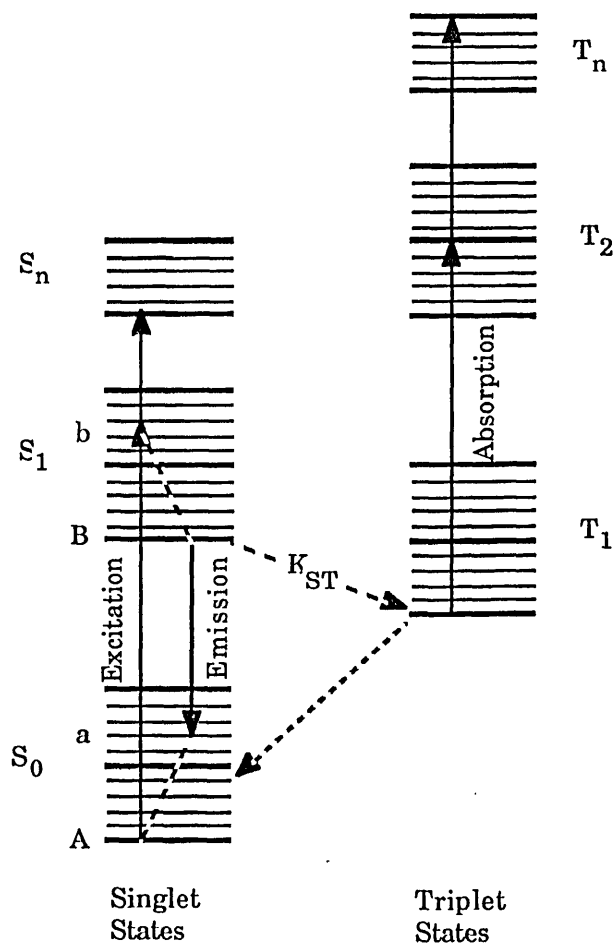

Fig 2.1:   The singlet and triplet states associated with optical transitions in an organic dye molecule (dotted lines are non-radiative decays).

spins. If the spins are anti-parallel then a singlet state is produced whilst the triplet state is formed when the electron spins are parallel. Both these states are broadened by the presence of the vibronic and rotational states, as illustrated in fig 2.1.The electronic states responsible for laser action are the ground and first excited singlet states, S_0 and S_1 respectively, and Fig 2.1. shows the electronic processes necessary for laser action. Absorption of a photon induces an electronic transition from the ground state of the S_0 singlet state to a sub-level in the first excited singlet S_{1b}. Transitions to higher order singlet or triplet states may occur, but these are regarded as sources of loss. The efficiency of the transition from S_0 to S_1 is governed by the absorption cross-section of the dye molecule $\sigma_a(\lambda)$ at the exciting wavelength, and the oscillator strength,f, of the interaction which for most dyes is assumed to be close to unity.

In the excited singlet state the molecule undergoes a series of non-radiative decays until the electron reaches the lowest lying state of S_{1B}. These transitions occur in times of the order of pico-seconds. The electron then undergoes a radiative decay from the ground state of the first excited singlet state to a sub-level in the S_0 singlet state, which has an efficiency determined by the emission cross-section $\sigma_e(\lambda)$.After the radiative decay the system then undergoes another series of non-radiative decays until the electron arrives at the S_0 ground state whence it can re-commence the electronic cycle again.

Ideally the transition from S_1 to S_0 would be a stimulated radiative decay induced by a photon, with the resulting photon mimicking the inducing photon. In practice however other pathways exist for this transition, such as spontaneous emission, internal conversion [3], and a transition from the excited singlet state S_1 to the ground triplet state T_1. Both the latter two decays are non-radiative and all three may be regarded as sources of loss. The transition S_1 to T_1 is referred to as inter-system crossing and can be induced by internal perturbations such as spin-spin/spin-orbit coupling due to the presence of heavy elements in the dye molecule. These elements produce a greater π electron charge cloud which increases the magnetic moment of the molecule resulting in an increase in the spin-orbit coupling. The inter-system transition can also be induced by external forces such as paramagnetic interactions

due to O_2 molecules present in the solvent. Both pathways result in losses. The S_1 - T_1 transition is more critical as it removes the electrons from the laser pathway for several micro-seconds because the transition from the T_1 to S_0 state is spin forbidden.

The presence of the triplet levels $T_1,T_2......$ indicate that absorption between the two states may occur with an efficiency given by $\sigma_t(\lambda)$. The absorption may occur at the excitation or emission wavelengths, but wherever it occurs it may be regarded as a source of loss. In order to reduce the effects of the triplet state absorptions the population in the lowest long triplet state must be minimised. This can be done by using triplet quenchers such as Cyclooctatetraene (C.O.T.) [4], the removal of gaseous oxygen from the dye solution [5] thus reducing the inter-system crossing, or by flowing the dye in a jet, thus removing the triplet levels from the pump source [6]. Once the effects of triplet state losses have been minimised organic dyes act as efficient gain media.

2.2.1.Optical Pumping of cw Organic Dye Lasers.

Following the rate equation analysis outlined for a simple two mirror c.w. dye laser cavity [7] the minimum pump power density necessary to reach laser threshold, $\dfrac{P_{th}}{A}$, is given by

$$\frac{P_{th}}{A}=\frac{N_c h\upsilon_p d}{\tau} \qquad (2.1)$$

where P_{th} is the threshold pump power, A is the pump spot area in the dye, d is the active length of the dye solution, $h\upsilon_p$ is the pump photon energy and τ is the radiative lifetime of the S_1 to S_0 transition.

The critical inversion N_c is related to dye and cavity parameters by

$$N_c =\frac{N}{Y(\lambda)} \{ \sigma_a(\lambda) +\frac{R(\lambda)}{N}\} \qquad (2.2)$$

Here $\qquad Y(\lambda) = \{\sigma_a(\lambda) +\sigma_e(\lambda) + K_{ST}\tau_T(\sigma_a(\lambda) - \sigma_T(\lambda))\}$ $\qquad (2.3)$

$$R(\lambda) = -\frac{\ln (R_1.R_2)}{2d} \qquad (2.4)$$

K_{ST} is the intersystem crossing rate constant, τ_T is the triplet lifetime, N the number density of dye molecules and $R_{1,2}$ the reflectivities of the mirrors which

form the cavity. For the case of minimum loss ($R_1 = R_2 = 1$) the calculated pump power density to take a 100 µm thick cell of Rhodamine 6G above threshold is ~ 5 kW/cm^2 at a pump wavelength of 530 nm (7). The first reported case of a c.w dye laser was made by Peterson et al [8] who focussed a c.w. argon ion laser to a spot size of ~ 20 µm to achieve the required power density.

Although organic dyes have been observed to lase at 1.8 µm, for wavelengths in excess of 800 nm the photo-chemical and thermal stability of the near-infrared dyes is poor. Also to increase the efficiency of the dyes dangerous solvents such as Dimethylsulpoxide [9] or Benzyl alcohol [10] are used. The spectral region 0.8 - 2.0 µm is also covered by the F_2^+ family of colour centres and these have been shown to be highly efficient sources of tunable radiation [11].

2.3. Definition of a Colour Centre.

The term colour centre refers to any defect which results in the coloration of an insulator. Colour centres can be regarded as simple point defects in a crystal lattice containing one or more electrons trapped at an ionic vacancy in the lattice. The presence of these electrons leads to the formation of energy levels which lie in the forbidden energy gap of the crystal. The energy levels give rise to optical absorptions
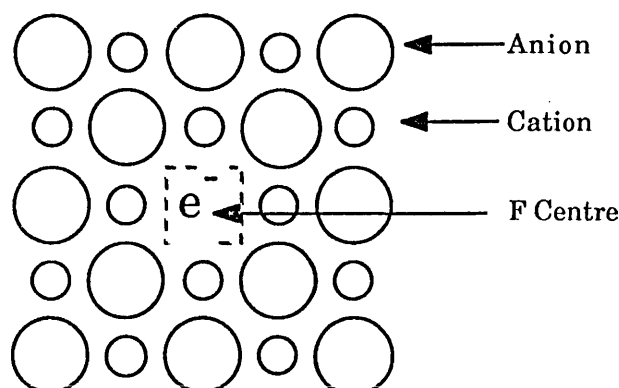

Fig 2.2:   A schematic of the F centre in a rock salt type lattice.

which colour the crystal. A simple rock salt lattice may act as the host to many different types of colour centre but the fundamental building block of each colour centre

is the F centre. This centre consists of an electron trapped at an anion vacancy, as illustrated in fig 2.2.

Although laser action has not been observed from the simple F centre many composite centres have been demonstrated as efficient laser active centres, which cover the spectral region from 0.8 - 4.0 μm, and a selection of these centres is described fully in ref 2.12.

2.3.1.The F_2^+ -Type Colour Centre.

The colour centre used in the work presented here was the F_2^+ centre.This centre consists of an F centre and anion vacancy lying in a lattice [110] direction [13], as depicted in fig 2.3.
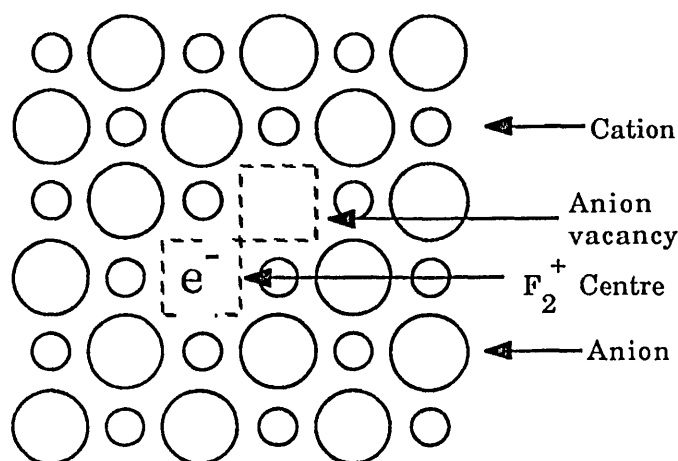
Fig 2.3: A schematic of the F_2^+ centre.

The coupling of the electron to the electric field associated with the two vacancies leads to the generation of new energy levels which are located in the band-gap of the crystal. The separation of these energy levels can be found approximately by treating the F_2^+ centre as a molecular hydrogen ion immersed in a dielectric medium. This approach was used by Herman, Wallis and Wallis [14], and Aegerter and Luty [15]. The model assumed the F_2^+ electron moved in the E field of the two point positive unit charges which were immersed in a dielectric medium, characterised by a dielectric constant ε(r). Solutions of the Schroedinger Equation describing this model yield electronic levels related to the free H_2^+ system by

$$E(F_2^+) = \frac{1}{\varepsilon(r)^2} E(H_2^+) \tag{2.5}$$

Discrepancies arise between the calculated and observed energy levels of the F_2^+ system using this model as it does not adequately consider the effects of the interaction between the phonon field of the lattice and the F_2^+ centre electron. The effects of the phonon field were considered by Wang [16,17], who assumed that the electron could move in a spherical region of the lattice enclosing one of the two vacancies. When the electron enters the sphere its motion is fast and so the point charge cannot follow the electron motion . Once the electron moves outside the sphere its motion is slow enough to allow the vacancy to follow the electron. In this way Wang was able to derive a Hamiltonian which describes the interaction of the phonon field with the field of the electron.

The wave-function Ψ and the potential V(r) used to solve the Shroedinger equation can be expanded by employing the adiabatic approximation and a configurational coordinate R . This is a normalized coordinate relating to the separation of the two anion vacancies. The potential V(R) can be expanded as a Taylor series.

$$V(R) = V(R_0) + A(R - R_0) + B(R - R_0)^2 \tag{2.6}$$

here R_0 is the equilibrium point, A is a constant relating to the coupling between the excited electronic state and the configurational coordinate R,which is normally non-zero, and B refers to the curvature of the excited state and ground state parabolas (see fig 2.4).

The wave function Ψ can be written as

$$\Psi = |\Phi(r)> |X(R)> \tag{2.7}$$

where $|\Phi(r)>$ is the electronic wave-function and $|X(R)>$ describes the lattice wavefunctions.

The electronic wave-functions $|\Phi(r)>$ are equivalent to those of the molecular hydrogen ion and hydrogen labelling such as 1s, 2p can be used to describe the electronic wave-functions and energy levels. It has been shown by Mollenauer [18] that the ground and first excited states of the F_2^+ centre are 1s and 2p states. The lattice wave-functions, $|X(R)>$, are those of a simple harmonic oscillator.

The energy levels of the system are determined by solving the overlap integral

$$E = \langle \Phi(r) \mid H_{eff} \mid \Phi(r) \rangle \qquad (2.8)$$

where $\quad H_{eff} = \langle X(R) \mid H \mid X(R) \rangle \qquad (2.9)$

with H being the actual Hamiltonian of the system.

Evaluation of equation (2.9) gives the energy Eigen values of the F_2^+ system as those of a simple harmonic oscillator. The ground state energy level is of the form

$$E_g = (n + \frac{1}{2}) h \omega_k \qquad (2.10)$$

and the first excited state has an energy given by

$$E_1 = (m + \frac{1}{2}) h \omega_k + E_0. \qquad (2.11)$$

E_0 is the zero phonon energy and defines the energy separation between the lowest lying ground and first excited states, ω_k is the angular frequency of a phonon with momentum k, and m,n refer to the vibration levels of the system. If the energy levels of the F_2^+ system are plotted against the configurational coordinate R as shown in fig 2.4 the optical transitions of the F_2^+ system can be understood. From this figure it can be seen that the ground state and first excited states do not lie directly above and below each other but in fact are slightly displaced from each other. This displacement arises from the nonzero A term in the Taylor expansion of the potential of the system (see eqn 2.6).

The probability of a transition from a state n in the ground state to a state m in the first excited state is given by considering the matrix element

$$Pmn = \langle \Psi \mid r \mid \Psi \rangle \qquad (2.12)$$

This can be expanded as

$$\mid \langle \Phi_m(r) \mid r \mid \Phi_n(r) \rangle \mid^2 \mid \langle X_m \mid X_n \rangle \mid^2 \qquad (2.13)$$

but $\mid \langle \Phi_m(r) \mid r \mid \Phi_n(r) \rangle \mid^2$ is the oscillator strength of the transition [19], which for the F_2^+ system is ~0.2 [20].

It is usually assumed that for an allowed transition the electronic dipole moment is independent of the nuclear coordinate (Frank-Condon approximation). Thus all the electronic transitions can be represented by straight vertical lines . The shape of the absorption band is determined by the overlap integral $\mid \langle X_m \mid X_n \rangle \mid^2$, which is normally non-zero because the vibrational wave-functions associated with different electronic

ENERGY

ABSORPTION

LUMINESCENCE

CONFIGURATIONAL   R
COORDINATE
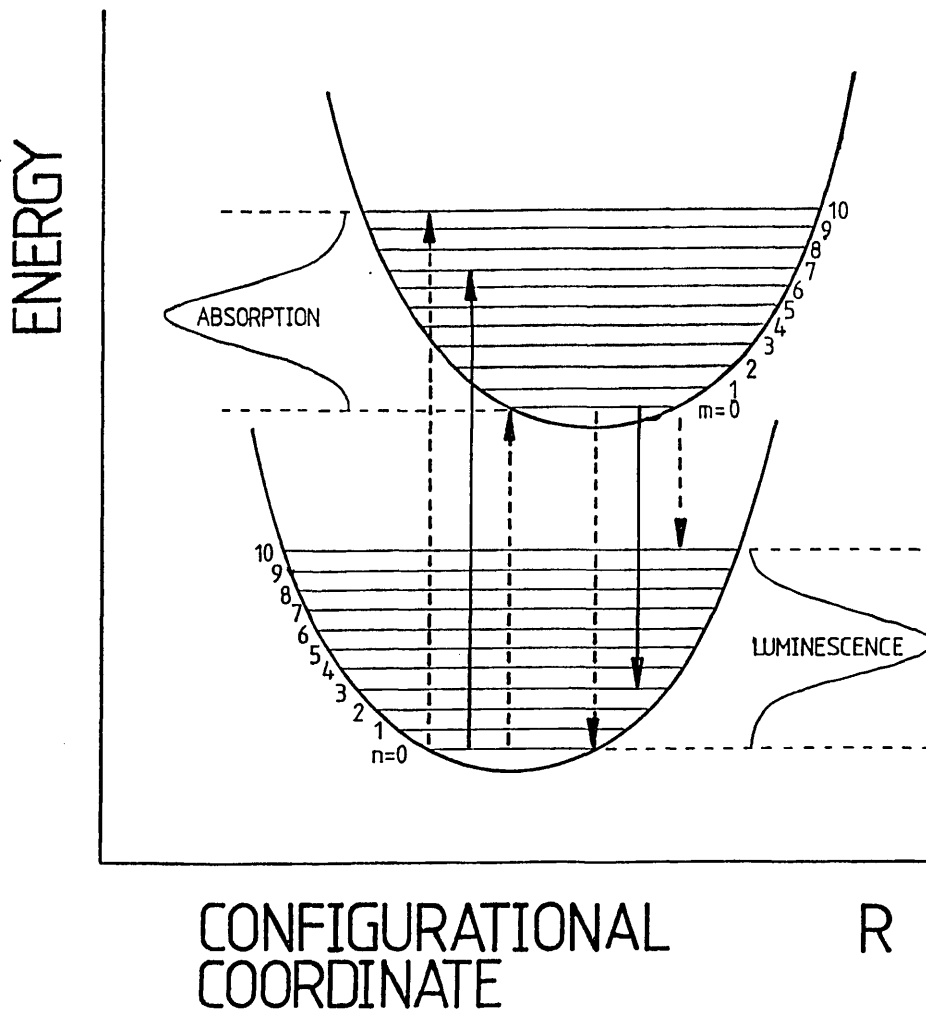
Fig 2.4:   A plot of the energy levels associated with the F_2^+ centre

against the configurational coordinate R (taken from ref

12).

states are not orthogonal. This integral can be evaluated to yield a transition

probability ,W_{0f}, to the fth level in the excited state in terms of the Huang Rhys factor

S_0, and can be regarded as the mean number of phonons generated in the transition.

Here W_{0f} is given by

$$W_{0f} = \frac{S_0 \exp -S_0}{f!}$$ (2.14)

with S_0 defined by

$$S_0 = \frac{\pi m \omega_k^2 (\delta R)^2}{\hbar \omega_k}$$ (2.15)

where ω_k is the phonon frequency, and δR is the change in the lattice co ordinate.

The laser-active cycle of the F_2^+ system is shown in fig 2.4., and fig 2.5. Absorption of a photon excites the centre electron from an s-type ground state (normal configuration) to a p-type first excited state. The lattice surrounding the defect relaxes by generating phonons until the electron reaches the lowest lying vibrational level of the first excited state (the relaxed excited state). From this state a radiative decay occurs, with a lifetime τ, enabling the centre electron to return to a vibrational level in the ground state. In order that the electron may return to its original ground state a further lattice relaxation occurs.

3dπ u

3dπ u

3d σ g

2s σ g

Excited
State
Absorptions

2pσ u

2p σ u

Absorption

Emission

1sσ g

1sσ g

1sσ g

2pσ u

Normal
Configuration

Relaxed
Configuration
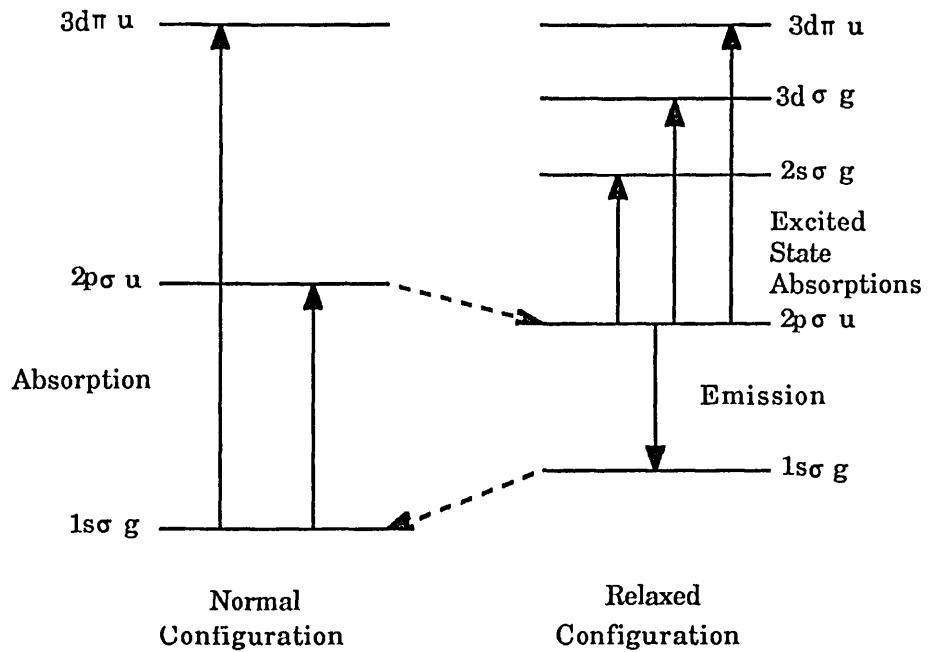
Fig 2.5:   The laser active transition associated with the F_2^+ centre depicted in terms of molecular hydrogen type labelling (Taken from ref 18).

The laser-active transition can be regarded as a $1s\sigma_g$ to a $2p\sigma_u$ transition, as shown in fig 2.5, and has several characteristics which make it suitable for laser action. these are: (i) the absorption and emission cross-sections are large, $\sim 10^{-16} cm^2$,[21], allowing for efficient absorption of the pump and high single pass gains with modest centre densities, (ii) the quantum efficiency is $\sim 100\%$ which results in low pump power thresholds [15], (iii) higher lying excited states are sufficiently removed from the

emitting $2p\sigma_u$ level so that no possibility of self-absorption in the laser tuning band exists, (iv) as the F_2^+ centre contains only one trapped electron,triplet states, are not present, and so the losses associated with the singlet-triplet transitions,which are common in dye lasers, are not observed, (v) an efficient four-level system is formed because the radiative lifetime of the relaxed excited state is long in comparison to the phonon lifetime [20]. This ensures that the relaxed excited state acts as a metastable state enabling a suitable population inversion, necessary for laser action, to be obtained.

The F_2^+ was first demonstrated as a laser active centre in 1977 [23] and the LiF:F_2^+centre used in this work was first demonstrated in 1978 by Mollenauer [25]. Although the F_2^+ has been shown to be a highly efficient centre with slope efficiencies as high as 50% being reported from a KF host lattice [24], it has not been exploited fully as a source of tunable radiation in the 0.8 -2.0 μm wavelength range as the long term stability of the F_2^+centre, in all its host lattices, is poor. This arises due to a number of problems associated with the centre. The first of these is the F_2^+ is positively charged with respect to the lattice and when the centres are formed, in order to maintain electrical neutrality in the lattice a density of electron traps equal to that of the F_2^+ concentration must be created. These negatively charged centres can take the form of F^- or higher order F^- centres which are easily ionised at room temperature and by the local heating associated with the pump beam. This results in reactions of the form

$$F^- + heat \longrightarrow F + e \qquad (2.12)$$

The following reaction may then occur

$$F_2^+ + e \longrightarrow F_2 \qquad (2.13)$$

which removes the F_2^+ centre from the laser active number density and these effects are depicted in fig 2.6 [27].

The second problem associated with the F_2^+ centre is related to its orientation in the lattice [22]. The F_2^+ centre as described previously lies in a lattice [110] direction and the laser emission is polarised in that direction. Thus the transition must be excited along the axis. In the crystal there are six possible [110] directions and the F_2^+ centre is not pinned to a specific [110] lattice direction . By exciting the F_2^+ centre to energy

levels other than the $2p\sigma_u$ level, via multi-photon absorption, the orientation of the centre

can be changed such that the centre rotates out of the pumped [110] direction [22]. If this

happens the gain of the system is reduced. However as the centre is reorientated there is

the possibility that the centre can migrate about the lattice and aggregate with other

centres thus losing their identities as F_2^+ centres and as a result the F_2^+ concentration
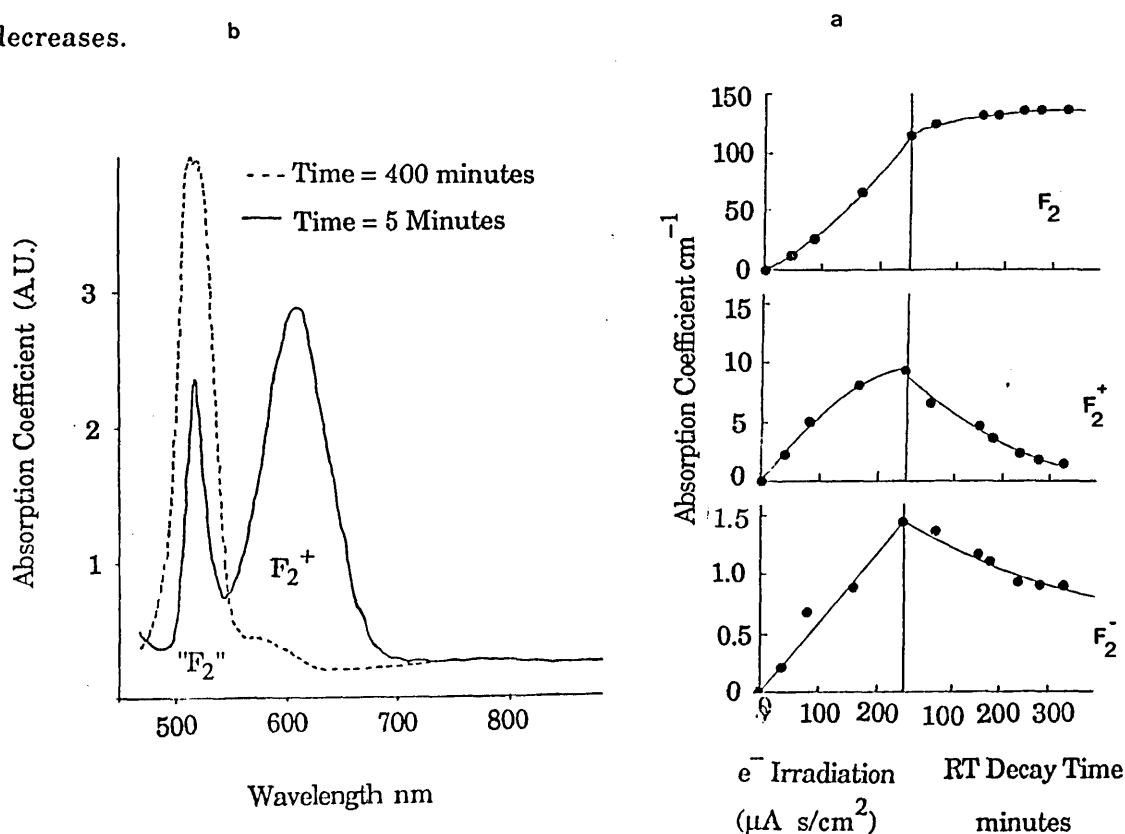
decreases.

Fig 2.6:   (a) The changes in the absorption coefficients of the F_2, F_2^+

and F_2^- centres after low temperature electron irradiation

then subsequent storage in the dark at room temperature

(taken from ref 26) and (b) a more detailed investigation of

the decay of the F_2^+ to F_2 centres at room temperature

(taken from ref 27).

These effects can be minimised, (i) by cooling the crystal to liquid nitrogen

temperatures, freezing the lattice, and so reducing the de-ionisation effects and

(ii) when an optical light chopper is used to reduce both the local heating in the crystal,

caused by the pump beam, and the exposure time to high photon fluxes. In order to cool

the crystal a variety of sophisticated laser cryostats have been developed and these will

be described in later chapters.

2.3.3. Optical Pumping of cw Colour Centre lasers.

The laser active cycle outlined consisted of four distinct processes: absorption, relaxation, emission and then relaxation to the ground state of the normal configuration. This can be regarded as a four level system. For this system, with a Gaussian luminescence band ($\delta\upsilon$ FWHM), the gain coefficient at band peak can be determined by following the treatment outlined in ref 2.20. and is given by

$$\alpha_0 = \frac{N^* \lambda_0^2 \eta}{8\pi\tau 1.07\delta\upsilon n^2} \qquad (2.14)$$

where N^* is the population in the relaxed excited state, λ_0 is the wave length at the band peak, η is the luminescence quantum efficiency, n the refractive index and τ the luminescence decay time.

The net optical gain is given by

$$\text{Net Gain} = \frac{I_{out}}{I_{in}} = R\exp(\alpha z) \qquad (2.15)$$

with z the gain path length, R the cavity losses and α the net gain coefficient which is given by

$$\alpha = \alpha_g - \alpha_e \qquad (2.16)$$

Here α_g is the gain coefficient evaluated for the inverted luminescence levels alone, and α_e is the coefficient of absorption losses in the crystal due to absorbing species at the laser wavelength.

The population in the relaxed excited state can be evaluated by considering the relationship

$$N^* = \frac{\beta I}{E\tau} \qquad (2.17)$$

which defines N^* as a function of the pump intensity I and the pump photon energy E. β is the absorption coefficient at the pump wavelength.

Substituting 2.17 into 2.14 gives

$$\alpha_0 = \frac{\lambda_0^2 \eta \beta I}{8\pi E 1.07\delta\upsilon n^2} \qquad (2.18)$$

For the case of a coaxially pumped gain medium the gain coefficient, α, can be expressed as

$$\alpha = \alpha_0 \exp{-\beta z} \qquad (2.19)$$

Thus the optical gain is given by

$$G = \exp\left(\alpha_0 \int_0^d \exp{-\beta z}\, dz\right) \qquad (2.20)$$

If the path length d is much greater than $\frac{1}{\beta}$ (which is the case in our experimental system as $d = 0.2$ cm and $b = 10 - 100$ cm^{-1}) then

$$G = \exp\left(\frac{\alpha_0}{\beta}\right) \qquad (2.21)$$

By combining this with the value for α_0 the gain is given by

$$\ln G = \alpha_0 = \frac{1}{8\pi} \frac{\lambda_0^2 \eta I}{E} \frac{1}{1.07\delta\upsilon} \frac{1}{n^2} \qquad (2.22)$$

For the LiF:F$_2^+$ centre studied in this work a value for the pump power density, at the threshold of laser action, of ~ 1 kW/cm^2 is evaluated. The various parameters used to evaluate this figure are listed in table 2.1.

Parameter	Value	Reference
n	1.39	29
λ	910 nm	28
$\delta\upsilon$	5×10^{13} Hz	20
τ	29 ns	30
η	~ 1	20

Table 1:   A listing of various parameters associated with the F$_2^+$ centre in LiF. (λ_0 is the peak luminescence wavelength, η the quantum efficiency, n the refractive index, $\delta\upsilon$ the FWHM of the luminescence, τ_1 the radiative lifetime).

2.4. Aberration Compensated Resonators

For both the organic dye and colour centre gain media to be efficiently operated, power densities well above those evaluated for threshold operation must be attained. Present day ion lasers, such as the krypton-ion laser which was used for all the optical

excitation described in this thesis, are capable of generating several Watts of pump power. Thus to generate the necessary power densities the pump beam must be focussed down to give a very tight beam waist. The requirement of such small beam waists together with the need for long cavities for tuning and mode-locking purposes leads to severe restrictions in cavity design which are only satisfied by the inclusion of internal focussing mirrors. The introduction of such elements to the cavity results in a new set of problems arising due to astigmatic aberrations [31].

An example of a long cavity with a region of tight focussing is shown in fig 2.7a., and this cavity was first analysed by Kogelnik et al [31]. The mirror M_2 acts as a lens of focal length f, imaging the mirror M_1 (radius of curvature R_1) close to the active medium, to give an image with radius of curvature R_2. The separation of the image of M_1 and the mirror M_3 (radius curvature R_3) is given by

$$d = d_1 - \frac{d_2 f}{(d_2 - f)} \qquad (2.23)$$

where $d_1 = R_3 + f + d$, $R_3 = 2f$ (in the case of the cavity shown in fig 2.7a.) and δ is an adjustment parameter.

For the cavity shown in fig 2.7a to be stable then the condition

$$0 \leq (1 - \frac{d}{R_1})(1 - \frac{d}{R_3}) \leq 1 \qquad (2.24)$$

must be satisfied.

By solving the inequality, limiting values of δ can be found and these are

$$\delta_{min} = \frac{f^2}{d_2 - R_1 - f} \qquad (2.25)$$

$$\delta_{max} = \frac{f^2}{d_2 - f} \qquad (2.26)$$

Thus a stability region, 2s, is obtained where

$$2s = \delta_{max} - \delta_{min} \qquad (2.27)$$

which can be expressed as

$$2s = \frac{-R_1 f^2}{(d_2 - f)(d_2 - f - R_1)} \qquad (2.28)$$

If R_1 tends to infinity and $d_2 \gg f$ then the stability region can be simplified to

$$2s \sim \frac{f^2}{d_2} \qquad (2.29)$$

The cavities illustrated in figs 2.7b,c have stability regions given by [32]

for 2.7b, $\quad 0 \le \delta \le \dfrac{f^2}{(d_1 - f)}, \quad \dfrac{f^2}{(d_1 - f)} \le \delta \le \dfrac{f^2}{(d_2 - f)} \qquad (2.30)$

for 2.7c $\quad 0 \le d \le \dfrac{4f^2}{(d_1 + d_2 + d_3 - 2f)} \qquad (2.31)$
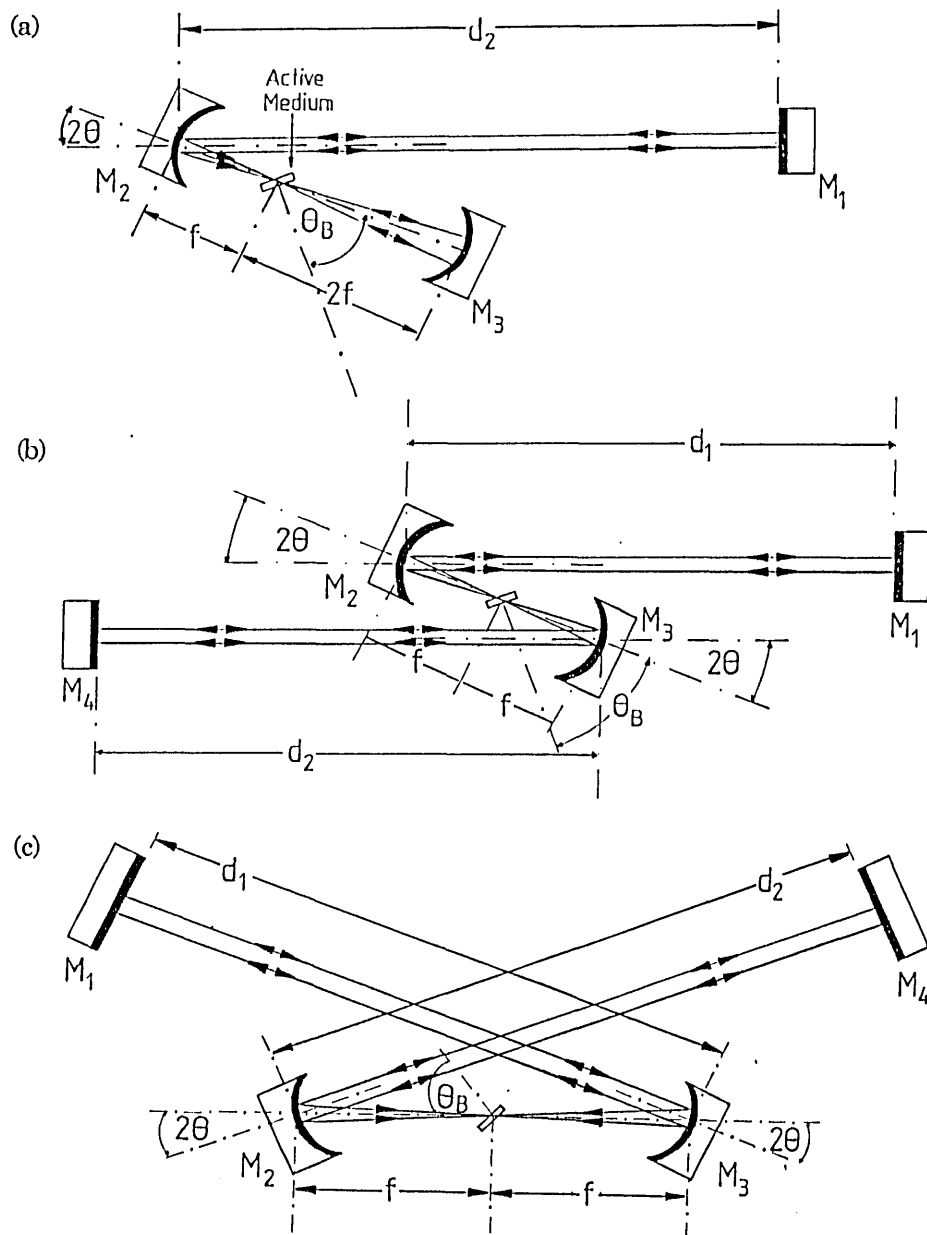

Fig 2.7: Examples of the cavity configurations used in the work presented in this thesis.

The beam diameter, ω_0, at the mode waist is described by the following equation

$$(\frac{\pi \omega_0^2}{\lambda})^2 = (\delta_{max} - \delta)(\delta - \delta_{min}) \qquad (2.32)$$

2.4.1. Astigmatic Compensation

The off-axis mirror M_2, of fig 2.7a, is used to focus the intracavity radiation into the gain medium, but the tangential and sagittal rays are focussed at different positions and this leads to the introduction of aberrations into the cavity, which are further compounded by the presence of the gain medium [33]. The aberrations produced by the off-axis mirror are astigmatic in nature and although they have little effect on the magnitude of the stability region they effect the location of both the tangential and sagittal regions.

The positions of the stability regions are given by

$$P(x) = d_x + R_1 + f_x + \delta_x \qquad (2.33)$$

$$P(y) = d_y + R_1 + f_y + \delta_y \qquad (2.34)$$

with

$$d_x = t\frac{(n^2+1)\frac{1}{2}}{n^2} \qquad (2.35)$$

$$d_y = t\frac{(n^2+1)\frac{1}{2}}{n^4} \qquad (2.36)$$

$$f_x = \frac{f}{\cos\theta} \qquad (2.37)$$

$$f_y = f\cos\theta \qquad (2.38)$$

With n the refractive index, t the thickness of the gain medium and f the focal length of the off-axis mirror. However by careful selection of the folding angle, 2θ, of the off-axis mirror M_2 the effects of these aberrations may be minimised and the three mirror cavity of fig 2.7a has been shown to be a suitable arrangement for compensating the astigmatism introduced by the Brewster angled faces of the gain medium, with that due to the off-axis mirror M_2. The condition for zero astigmatism is given by the making the folding angle, 2θ, satisfy the equation

$$Nt = f\sin\theta\tan\theta \qquad (2.39)$$

where
$$N = \frac{(n^2 - 1)(n^2 + 1)^{\frac{1}{2}}}{n^4} \qquad (2.40)$$

Astigmatic compensation is only achieved after one round trip of the cavity as the astigmatism introduced by the passage of the beam through both faces of the Brewster angled gain medium is compensated by a single reflection at the mirror M_2. Because of the asymmetrical arrangement of the mirrors M_2 and M_3, the astigmatism is not fully compensated within the gain medium and so the focal region of the beam is degraded . Therefore, the cavity can be totally astigmatically compensated with respect to stability but not with respect to focussing in the gain medium.

By using the cavities illustrated in fig 2.7b,c with two off-axis mirrors the above restriction can be removed [34]. In this case the astigmatism introduced by refraction at one Brewster angled face of the gain medium is compensated for by one reflection at one of the off-axis mirrors. Astigmatism can thus be compensated within the gain medium, so preserving a good focus, as well as ensuring the overall cavity stability. The condition for astigmatic compensation of the resonators in fig 2.7b,c is the same as that for cavity 2.7a but with the thickness of the gain medium replaced by a half of its value.Thus by careful selection of the folding angle of mirror M_2 the aberrations present in the cavity can be minimised and efficient performance of the laser can be achieved.

2.5. Electrical Excitation of Self-Trapped Excitons in Alkali Halide Crystals.

In order to achieve the necessary power densities to take both the organic dyes and colour centre lasers above threshold sophisticated resonators and high power pump lasers have to be used. For the work presented here a Spectra Physics 171 Kr^+ laser was used as the pump source. It is well known that high power ion lasers such as the Kr^+ are extremely inefficient, requiring ~45 kW of electrical power to generate ~5 W of optical power, and highly unreliable.

A more efficient and elegant way to obtain laser action from an alkali halide crystal, such as LIF or CsI,would be to electrically excite the defect responsible for the luminescence. Direct electrical excitation lasers already exist in the form of

semiconductor diode lasers [35]. In these lasers current is passed through a forward biased p-n junction, and lasing occurs by using the electron-hole recombination radiation as the photon flux. Although these lasers offer limited tunability in the near infra-red spectral region, a blue semiconductor laser has not been realised.

Electrical excitation of the self-trapped exciton has been studied and the results obtained will be presented in chapter 8. However, the electroluminescence observed from the self-trapped exciton in a variety of alkali halide hosts has been shown to cover the spectral region from 200 to 500 nm [36,37] and Vorob'ev et al have observed ultraviolet laser action from an extremely thin sample of NaCl [38].

2.5.1. The Self-trapped Exciton.

As in other materials, the exciton found in alkali halides consists of a bound electron hole pair [39]. A mobile exciton may be regarded as an excited negative ion, consisting of an electron in an orbital around a neutral halogen atom (X) and its surrounding nearest neighbour positive ions. The charge on these ions is unbalanced and consequently a long range coulomb force is generated which binds the electron. The hole can be regarded as the absence of an electron in a normally closed outer shell of the negative ion.

The process of self-trapping has been fully described by Seitz [40] and so only a brief outline will be given. A neutral atom located at a normal lattice point is unstable. The hole is used to form a covalent bond with a neighbouring negative ion and an excited $(X_2^2)^*$ molecule is formed in the lattice. The molecule is located in a lattice [110] direction as depicted in fig 2.8. The formation of this molecule occurs in a few picoseconds whilst the electron is still in its excited orbital. To lose energy the system undergoes a series of phonon decays and reduces the energy such that it is trapped at a single lattice point . This is the self-trapped exciton.The excited $(X_2^{2-})^*$ then returns to the ground state when the electron recombines with the hole to form a (X_2^{2-}) molecule. This recombination results in the production of energy and the dissipaton of this energy is determined by the temperature of the host lattice. If the temperature is low enough then the energy appears in the form of photons. The resulting (X_2^{2-}) molecule is

unstable in its ground state; when the electron and hole recombine strong Pauli and electrostatic repulsive forces return the X^- to their equilibrium position in the lattice. The temperature at which the decay of the self-trapped exciton is radiative is around 77 K [36,37] and to met this requirement a dewar was designed and this will be described in chapter 8.
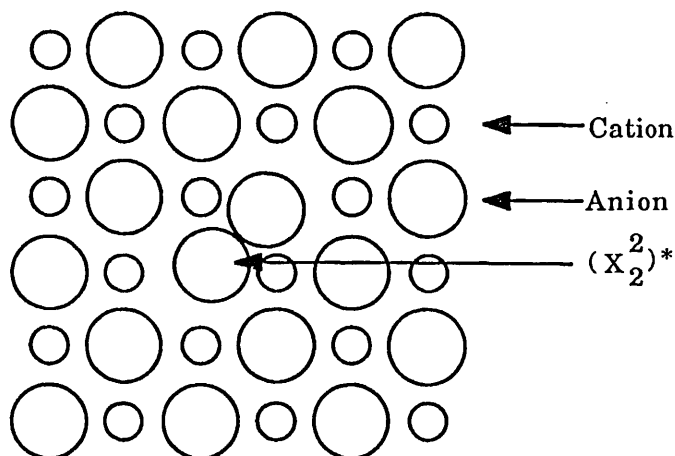

Fig 2.8:   A schematic of the self-trapped exciton.

The process outlined above for the production and decay of the exciton -excitation of the negative ion, relaxation to the self-trapped exciton, decay to give a (X_2^{2-}) molecule with emission of a photon followed by the relaxation of the (X_2^{2-}) to give the original X^- ions- can be seen to form a four level system consisting of excitation, nonradiative decay, radiative decay and finally non-radiatve decay which is characteristic of both organic dye and colour centre lasers. Thus the potential for an efficient laser exists.

2.5.2. Electrical Excitation and Conditions for Laser Operation

At present electroluminescence is thought to result from the impact ionisation of the emitting centre [38,41,42]. The idea that direct ionisation of the emitting centres by the applied potential has been discarded because the field strengths required by this mechanism ($\sim 10^7$ V/cm) greatly exceed those at which luminescence is observed ($\sim 10^5$ V/cm) [38]. Excitation by the injection of minority carriers at the electrodes which later recombine with majority carriers is also to be discounted, as electroluminescence is observed on both halves of a sinusodial applied potential.

A model for electroluminescence has been developed by Piper and Williams [40] and Alfrey and Taylor [41]. The model assumes that the electroluminescence is excited within a Mott-Schottky exhaustion region. The application of a strong electric field ($\sim10^5$ V/cm) field ionises electrons trapped at deep (~0.2 eV from the conduction bandedge) electron traps. These liberated electrons are accelerated by the applied field. They may then scatter off the negative ions in the lattice causing the excitation of the ion and hence the production of the self-trapped exciton and electroluminescence as outlined above.

To induce laser action via electrical excitation a population inversion must be attained and to achieve this a specific current density J must be applied to the crystal. The magnitude of this current density can be evaluated as follows. At threshold the input electrical power P_{in} is related to the optical output power P_{out} in the following way

$$P_{out} = \eta_{el}P_{in} = \eta_{exc}\eta P_{in} \qquad (2.41)$$

where the electrical efficiency η_{el} has been expressed in terms of the excitation efficiency η_{exc} and the luminescence quantum efficiency η. These two quantities, η_{exc} η , give the fraction of the input energy converted into the excitation of the luminescing levels and the fraction of those levels which actually decay radiatively.

The gain coefficient per pass (at the peak of the gain curve) for radiation passing through a medium of refractive index n, population inversion ΔN and length l is given by

$$\gamma = \frac{\Delta N\lambda^2 l}{4\pi^2 n^2\delta\upsilon\tau_{rad}} \qquad (2.42)$$

where λ is the wavelength (at band centre), $\delta\upsilon$ is the full width at half maximum height of the luminescence band which in this case is assumed to be a Lorentzian line shape and τ_{rad} is the radiative lifetime of the transition.

The luminescence output power at threshold is given by

$$P_{out} = \frac{\Delta Nh\upsilon\Omega}{\tau_{rad}} \qquad (2.43)$$

with $h\upsilon$ the energy of the radiated photon and Ω is the volume of the active medium.

Thus by combining equations 2.43,2.42 and 2.41 the input electrical power can be determined as

$$P_{in} = \frac{4\pi^2 n^2 \delta\upsilon h\upsilon\Omega\gamma}{\lambda^2 l\eta_{el}}$$

(2.44)

If the electrode applied to the surfaces of the crystal, of thickness d, is planar and of area A=wl and a voltage V is applied to the crystal inducing a current I to flow in the crystal then the input electrical power is given by IV. Thus the current density J is given by

$$J = \frac{4\pi^2 n^2 \delta\upsilon h\upsilon d\gamma}{\lambda^2 lV\eta_{el}}$$

(2.45)

By using the values listed in table 2.2 for the self-trapped exciton in KI a current density of 20 A/cm^2 is evaluated.

Parameter	Value	Reference
n	1.39	29
λ	297 nm	37
δυ	6×10^{13} Hz	37
d	100 μm	43
V	2000 V	43
l	10 mm	43
η	1	43

Table 2.2 : A listing of the parameters associated with the
electroluminescence of the self-trapped exciton in KI.

2.6. Conclusions.

In this chapter the pertinent photophysics of organic dyes, the F_2^+ colour centre and the self-trapped exciton have been described and the power densities and currents necessary to take the active centre above laser threshold have been evaluated. In order to achieve the high power densities needed for laser action to be observed from dye and colour centre lasers the pump beam must be focussed down to small spot areas. This results in the need for carefully designed optical resonators and a brief outline of the parameters which need to be considered has been presented. In later chapters examples

of both organic dye and colour centre lasers will be given and the results obtained indicate that both these gain media are highly tunable and efficient sources of laser radiation. Preliminary investigations into the electroluminescence from alkali halide crystals will also be be presented and the recorded data illustrates that the centre luminesces over a broad spectral range thus opening up the possibility for a tunable solid state blue laser.

References:

1. F.G. Zhang and F.P. Schafer; Appl. Phys. B., <u>26</u>, 211, 1981.

2. H.J. Polland, T. Elsaisser, A. Selmeier, W. Kaiser, M. Kussler, M.J. Marx, B. Sens and K.H. Drexhage; Appl. Phys. B., <u>32</u>, 53, 1983.

3. K.H. Drexhage in *Dye Lasers*. Ed F.P. Schafer Springer Verlag, Berlin 1973 Chp 4.

4. R. Pappulardo, H. Samelson and A. Lempicki; I.E.E.E. J. Quant. Elect .,QE <u>6</u>, 716, 1970.

5. J.B. Marling, D.W. Gregg and L. Wood; Appl. Phys. Lett., <u>17</u>, 527, 1970.

6. P.K. Runge; Opt. Commun., <u>5</u>, 311, 1972.

7. B.B. Snavely in *Dye Lasers*. Ed F.P. Schafer Springer Verlag, Berlin 1973 Chp 2.

8. O.G. Peterson, S.A. Tuccio and B.B. Snavely; Appl. Phys. Lett., <u>17</u>, 245, 1970.

9. M.Leduc and C.Weisbuch; Opt. Commun., <u>26</u>, 1, 1978.

10. W.Kranitzky, B.Kopanisky, W.Kaiser, K.H. Drexhage and G.A. Reynolds; Opt. Commun., <u>36</u>, 149, 1981.

11. L.F. Mollenauer in *Tunable Solid State Lasers* Eds J.C. White and L.F. Mollenauer Springer Verlag, Berlin 1986 Chp 6.

12. C.R. Pollock; J. Lumins., <u>35</u>, 65, 1986.

13. F Seitz; Rev. Mod. Phys.,<u>26</u>, 9, 1954.

14. R. Herman, M.C. Wallis and R.F. Wallis; Phys. Rev., <u>107</u>, 87, 1956.

15. M.A. Aegerter and F. Luty; Phys. Stat. Sol(b)., <u>43</u>, 227, 1971.

16. S.F. Wang; Prog Theor. Phys., <u>33</u>, 1001, 1965.

17. S.F. Wang; Prog Theor. Phys., <u>34</u>, 193, 1965.

18. L.F. Mollenauer; Phys. Rev. Lett., <u>43</u>, 1524, 1979.

19. F.P. Schafer, in *Dye Lasers*; Ed F.P. Schafer Springer Verlag Berlin 1973 Chapter 7.

20. L.F. Mollenauer; *Methods of Experimental Physics 15 Part B*. Academic Press, 1979. Chapter 6.

21. L.F. Mollenauer; XIth IQEC Boston 1980.

22. M.A. Aegerter and F. Luty; Phys. Stat. Sol(b)., <u>43</u>, 245, 1971.

23. L.F. Mollenauer; Opt. Lett., <u>1</u>, 164, 1977.

24. L.F. Mollenauer, B.M. Bloom and A.M. DelGaudio; Opt. Lett., <u>3</u>, 48, 1978.

25. L.F. Mollenauer and D.M. Bloom; Opt. Lett., <u>4</u>, 247, 1979.

26. W. Gellermann, A. Muller, D. Wandt, S. Wilk and F. Luty; J. Appl. Phys., <u>61</u>, 1297, 1987.

27. K. Smith; PhD. Thesis University of London 1985.

28. J. Nahum; Phys. Rev., <u>174</u>, 1000, 1968.

29. CRC Handbook.

30. L. Bosi, C. Bussolati and G. Spinolo; Phys. Lett., 32A, 159, 1970.

31. H.W. Kogelnik, E.P. Ippen, A. Diennes and C.V. Shank; I.E.E.E. J. Quant. Elect .., QE-12, 123, 1972.

32. F. Giberson, Chu. Chen, F.B. Dunning and F.K. Tittel; Appl. Opt., 21,172, 1982.

33. D.C. Hanna; I.E.E.E. J. Quant. Elect ., QE-5, 483, 1969.

34. A.I. Ferguson and M.H. Dunn; Opt. Commun., 20, 214, 1977.

35. J. Chen; PhD. Thesis University of London 1984.

36. S. Unger and K. Teegarden; Phys. Rev. Lett., 19, 1229, 1967.

37. C. Paracchini; Phys. Rev. B., 7, 1603, 1973.

38. G.A. Vorob'ev, S.G. Ekhanin, N.I. Lededva, S.N. Morev and N.S. Nesmelov; Sov. J. Phys., 18, 1774, 1976.

39. N.W. Aschroft and N.D. Mermin; *Solid State Physics*, Holt Saunders New York 1976.

40. F. Seitz in The Modern Theory of Solids. Mc Graw-Hill, New York 1940.

41. W.W. Piper and F.E. Williams; Brit. J. Appl. Phys., 6, 39, 1955.

42. G.F. Alfrey and J.B. Taylor; Proc. Phys. Soc. London., B68, 775, 1955.

43. R.W. Boyd, M.S. Malcuit and K.J. Teegarden; I.E.E.E. J. Quant. Elect .., QE-18, 1202, 1982.

Chapter 3 :Techniques for the Generation and Measurement of Ultrashort Pulses

3.1. Introduction

The previous chapter described the homogeneously broadened organic dye and colour centre gain media as well as the self-trapped exciton. To exploit the large gain bandwidths presented by the first two media, investigations were made into the possibilities of short pulse generation from these media. When optically excited the energy associated with the lasing photons is not distributed in the resonator in a random fashion but exists in well defined transverse modes. To each transverse mode there is a set of longitudinal modes since the laser resonator can support many standing waves. If the simple resonator shown in fig 3.1a has a mirror separation l then the frequency difference between each longitudinal modes is given by

$$\Delta \upsilon = \frac{c}{2l} \qquad\qquad (3.1)$$
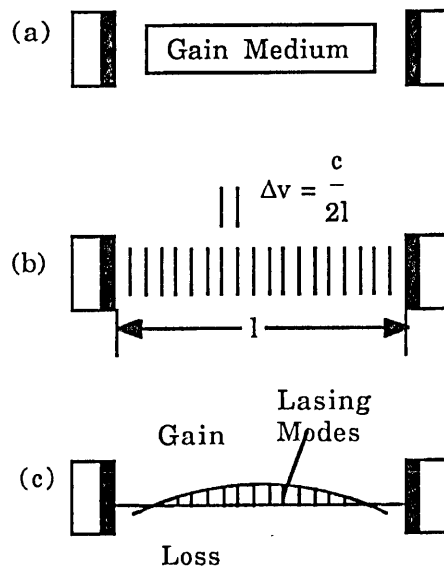
where c is the speed of light.

Fig 3.1: Simple representation of a laser resonator showing (a) the gain medium, (b) the longitudinal modes associated with the cavity and (c) those longitudinal modes which are above laser threshold.

Provided that the frequency of a specific longitudinal mode falls inside the gain bandwidth of the active medium and experiences enough gain to overcome the losses of the cavity then the mode will lase. As the gain bandwidth is usually quite broad then a large number of longitudinal modes may be supported. Each lasing mode is related only by their frequency spacing. The phase and amplitude of neighbouring modes varies in a random fashion due to competition between the modes and fluctuations in the gain medium. If a specific phase relationship can be maintained between the modes a well defined output is obtained from the laser. The fixing of the phase of the longitudinal modes gives rise to the technique of mode-locking and there are a variety of methods which can be applied to produce this state.

3.2. The Mode-Locking of a Laser.

The selection of a fundamental or TEM_{00} is achieved by the insertion of an aperture along the axis of the cavity, allowing only that mode to reach threshold. The control of the longitudinal modes associated with this transverse mode is a somewhat more complicated process but can be achieved in essentially two ways. The first is to produce a laser which operates on a single longitudinal mode. This can be achieved either by using a cavity length shorter than the mode spacing so that the laser operates at one modal frequency or by employing bandwidth-limiting intracavity filters to reduce the gain bandwidth of the laser until it can only support one longitudinal mode. Lasers of this type find extensive applications in high resolution spectroscopy [1].

An alternative scheme is to establish a fixed phase relationship between each mode and when this is accomplished the output from the laser consists of a series of short duration pulses, temporally separated by the cavity round trip time. The duration of these pulses is governed by the number of modes which have been locked in phase. Once the longitudinal modes are perfectly locked the duration of the emitted pulse $\Delta \tau$ is related to the bandwidth $\Delta \upsilon$ by

$$\Delta \tau \Delta \upsilon = \alpha \qquad (3.2)$$

where α is a constant determined by the pulse shape. A selection of pulses shapes and the corresponding value of α is listed in table 3.1.

3.3.Active Mode-locking.

This process as the name implies, uses an active element to impose a fixed phase relationship on the longitudinal modes. The active element may take the form of an external gain modulation or an internal loss modulation driven from an external source. Irrespective of the type of modulation, the modulation frequency must be matched to (or be a sub-multiple of) the resonator round-trip time [2]. This ensures that the intracavity flux will always be incident at the same point of the modulation cycle irrespective of the number of resonator transits.

3.3.1. Active Mode-locking by Acousto-Optic Modulation.

The production of ultrashort pulses by active mode-locking of the gain medium via an interaction with an acousto-optic modulator has proved to be a successful scheme and a wide variety of gain media have been mode-locked in such a fashion [3-6] . In the work presented here both the Kr^+ pump laser and the $LiF:F_2^+$ colour centre laser were actively mode-locked. The theory of acousto-optic mode-locking has been studied by many people [2,7-11]. The function of the modulator is to introduce a time varying loss into the laser resonator. The loss is based on the interaction of the intracavity flux with an acoustic wave (which in this case followed the Raman Nath model [12]). When an acoustic wave passes through a material, the changes in density associated with regions of compression and rarefraction produce a spatial variation of the refractive index. This appears as a phase grating to the incident light and as a result the light is diffracted. In order to produce a standing wave phase grating, the faces of the modulator are made parallel. The effects of the phase grating have been studied in both time [9] and frequency [10] domains. Although pulses as short as 10 ps have been generated from acousto-optically mode-locked dye lasers [3] and 35 ps from $Co:MgF_2$ lasers [4], a more effective form of active mode-locking is that of synchronous mode-locking.

3.3.2. Synchronous Mode-Locking.

Pulse generation via the technique of synchronous mode-locking was first demonstrated by Runge [13] and since then pulses have been produced by this method over the spectral region 420 nm [14] - 2.7μm [15]. Although relatively simple in principle, it is highly expensive in practice, requiring costly modulators and drive electronics for the pump laser and precision translation stages for the slave laser. The basic concept is to drive the slave laser with a train of pulses from the pump laser and arrange the timing of the slave laser pulse such that it returns to the gain medium to coincide with the pump pulse. In order to accomplish this the slave period must be a multiple or sub-multiple of the pump period. By meeting this requirement the gain medium can act as a pulse shortening element as it can induce losses on both the leading and trailing edges of the pulse. The leading edge of the pulse is controlled by timing the arrival of the pulse such that the peak of the pulse is amplified preferentially. If the pulse inside the cavity is of sufficient intensity it can induce a strong gain saturation effect which limits the amplification of the trailing edge of the pulse. Hence pulse compression can occur in the gain medium leading to short pulse production. As the modulation is applied to the gain medium, short pulses maybe generated over the entire lasing bandwidth of the gain medium and thus highly tunable short pulses can be generated via this method of mode-locking.

Theoretical investigations into the dependence of the slave laser pulse on such parameters as the pump pulse duration, pump pulse power and intracavity bandwidth have been performed and verified experimentally [16-23]. It has been found that the slave pulse is related to the square-root of the pump pulse duration [17] and varies as the inverse square-root of the intracavity bandwidth[18].

Cavity length dependences have been investigated by several researchers [16-18,22] and all have obtained similar results. They observed the behaviour of the pulse duration to be highly asymmetric for cavity length variations around the matching point. For negative detunings the slave pulses exhibit satellite pulses whilst for positive detunings the pulses are broadened. Studies were made on the effects of cavity length detuning on the pulse formation of synchronously mode-locked dye and colour centre

lasers. The results will be presented in later chapters. However in agreement with other authors [17,22] the shortest pulses were always observed for a slight negative detuning from the position of maximum second harmonic.

The need for such precise matching of the pump and slave cavity lengths results in the synchronously mode-locked laser being highly sensitive to cavity relaxations and pump pulse jitter. These affect the long term stability of the mode-locked pulse train produced by the slave laser. If these sources of jitter are eliminated, an intrinsic jitter still exists due to the stochastic nature of the low level of spontaneous emission present in the cavity. The effect of the spontaneous emission on the pulse formation process in a synchronously mode-locked laser has only recently been considered in a theoretical model [23] which shows that elimination of the intrinsic jitter and the production of short highly stable pulses are mutually exclusive.

3.4.Passive Mode-Locking.

The technique of passive mode-locking employs an intracavity saturable absorber as the mode-locking element. The saturable absorber acts as a switch with a specific saturation level. For intracavity intensities below the saturation level the absorber allows only low light transmission (typically 30 - 50% of the intracavity intensity is transmitted) , whilst for those above it appears transparent. This corresponds to a bleaching of the absorber and results in the confinement of the intracavity flux into a pulse which then propagates around the cavity. Mode-locking is only attained in the absorption band of the saturable absorber and so limits the tunability of the laser, but as there is no external driving force pulse formation is independent of the resonator period. This technique has been applied to a variety of organic dyes and has lead to short pulse production covering the entire visible spectrum from 490 -780 nm [24-26] and has le d to the direct generation of pulses as short as 19 fs from a dispersion optimised colliding pulse ring dye laser [27]. It has also been applied to semi-conductor lasers where a multiple quantum well served as the saturable absorber [28]. In later chapters the passive mode-locking of two new gain media, namely the Rhodamine 700 dye laser and the $LiF:F_2^+$ colour centre laser will be described.

Present day theories on passive mode-locking are based on the balancing of pulse

shaping mechanisms with pulse broadening processes. Initial theories [29-33] were

concerned with the effects of gain and absorber saturation on the pulse formation

process whilst later theories have taken into account the effects of self phase modulation

and group velocity dispersion [34,35]. The role of gain and absorber saturation were

first studied by New [29] who realised that for an optical pulse to be formed in the cavity

both the front and trailing portions of the pulse must experience a loss. The loss on the

leading edge of the pulse is induced by absorber saturation whilst on the trailing edge

by gain saturation. In order to satisfy this requirement New defined certain

experimental conditions relating to the cavity transit time and the recovery times of the

gain and absorber media. These are (i) the cavity transit time must be greater than the

gain recovery time,and (ii) the absorber recovery time must be less than that of the gain

recovery time.By carefully modelling the pulse formation process but ignoring the role

of bandwidth limitations New [30] was able to show that pulse compression occurred

while the system parameters remained inside a set of boundaries, referred to as

stability regions, (illustrated in fig 3.2). The magnitude of these stability regions is

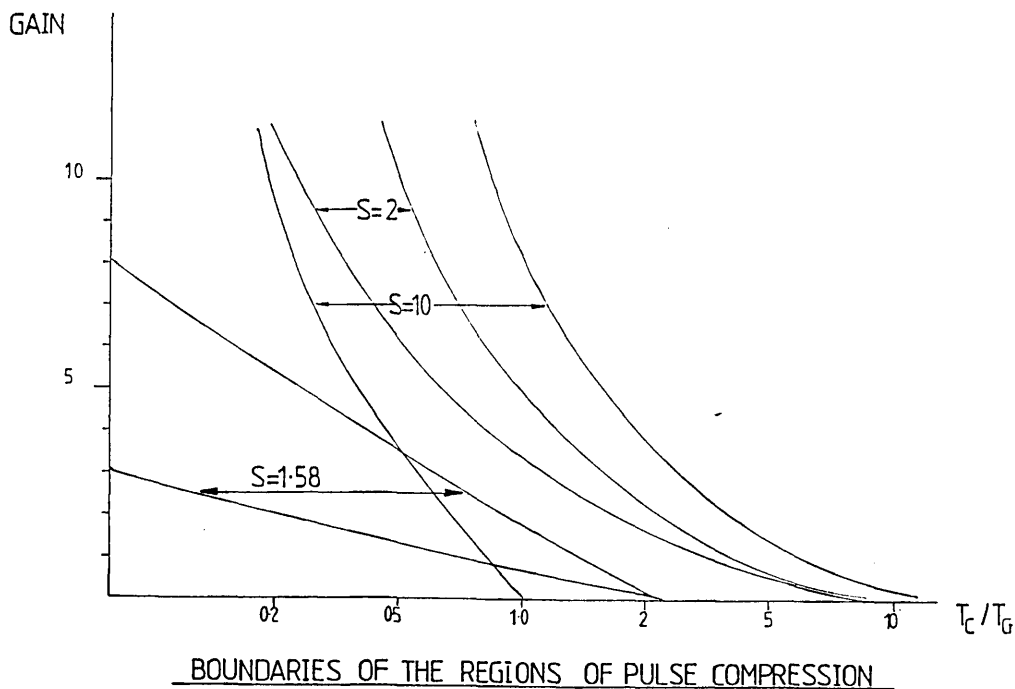BOUNDARIES OF THE REGIONS OF PULSE COMPRESSION

Fig 3.2:   A plot illustrating the stability regions for a passively
           mode-locked dye laser (taken from 30).

defined by the so-called S parameter. This parameter is related to the absorber cross-section and the gain cross-section as well as the intensities in the gain and passive media in the following way

$$S = k(\frac{\sigma_a I_g}{\sigma_g I_a}) \quad (= k(\frac{\sigma_a A_g}{A_a \sigma_g})) \tag{3.3}$$

where $\sigma_{a,g}$ are the absorber and gain cross-sections respectively, $I_{a,g}$ the intensities in the absorber and gain media and, $A_{a,g}$ are the focal areas in the absorber and gain media and k is a constant. Thus in order to increase the magnitude of the stability regions the S parameter must be as large as possible. This implies that the optical field which saturates the absorber must be greater than that which induces the gain saturation. This can be achieved by using mirrors in the passive folded section which have a shorter focal length compared to those around the gain medium. The process of colliding pulse mode-locking (CPM) [36] can also be exploited to enhance S. For a CPM laser the saturable absorber is placed in the centre of the resonator. As pulse formation is initiated by the absorber this timing arrangement ensures that the two counter-propagating pulses are synchronised to overlap precisely in the saturable absorber. This results in a coherent interaction occurring between the counter-propagating pulses in the saturable absorber. A standing wave is then established in the absorber, due to constructive interference between the two pulses, which leads to a modulation of the absorber saturation, and hence the formation of a transient grating. A direct result of the formation of this grating is a scattering of a portion of the pulse travelling in one direction into the opposite direction inducing more constructive interference. This results in the threshold for absorber saturation being reduced greatly, allowing the counter-propagating pulses to travel through the absorber with much reduced energy losses. Consequently, it appears as if there is a higher optical field in the absorber, due to this coherent interaction between the pulses, than in the gain medium and so the pulse shaping process is enhanced. In fact both Stix [33] and Kulkhe [37] predict that the pulse shaping process is so enhanced by the coherent interaction that the pulses produced from such a laser should be approximately three times shorter than those from passive systems where the pulses do not collide. As the saturation intensity in the absorber is

greater than that in the gain medium the S parameter is increased to give much broader stability regions and so the output pulses appear more stable under such operating conditions. (It should be noted that competition for the gain by the pulses is reduced by ensuring that the interval between pulse arrival times in the gain medium is long compared to the gain recovery time.)

Although colliding pulse mode-locking may assist in the pulse formation kinetics due to improved absorber and gain saturation, the pulses propagating in the cavity may still be broadened due to the effects of dispersion and frequency chirps. These effects are discussed in detail in chapter 7. However by carefully balancing the self phase modulation effects with those of group velocity dispersion, significant pulse shortening can occur in the laser [35] leading to the production of stable hyper-short pulses [27,38].

3.5. Hybrid Mode-Locking

This method of pulse generation combines both passive and synchronous techniques to yield highly stable ultrashort pulses which are in synchronism with an external frequency drive. The basic principle is to introduce a saturable absorber into the cavity of a synchronously mode-locked laser. The presence of the saturable absorber shortens the generated pulses, due to both absorber saturation and enhanced gain saturation. The absorber introduces a loss to the front portion of the pulse and so "sharpens" the leading edge of the pulse. The faster rising edge of the pulse then induces a greater gain saturation resulting in the trailing portion of the pulse experiencing more loss. The stability of the resulting pulse train is also greatly increased. Although hybrid mode-locking has been shown to be a reliable method for generating highly stable ultrashort pulses from synchronously mode-locked dye lasers [39-44] it greatly reduces the tunability of the synchronously mode-locked laser as hybrid pulse formation is only initiated in the wavelength range covered by the absorber. Outside the absorption band of the absorber, pulse formation is purely synchronous in nature. Hybrid mode-locking has been applied to both the Rhodamine 700 dye laser and the $LiF:F_2^+$ colour centre laser and the results obtained will be presented in chapters 4 and 6.

3.6. Methods of Ultrashort Pulse Measurement.

Initially, measurements of pulse durations were by made employing photodiode-oscilloscope combinations, but the advances made in ultrashort pulse generation have far outstripped improvements in the resolution of the photodiode-oscilloscope combination. As a direct consequence new techniques have been developed to measure the pulse durations and these fall into two distinct classes: linear processes such as electron-optical chronoscopy [45], and non-linear processes such as second harmonic autocorrelation [46].

3.6.1.The Electron Optical Streak Camera

The idea of measuring ultrafast optical events with a streak camera was pioneered by Zavoisky and Franchenko in 1956 [47], and has been developed by Bradley and Sibbett and co-workers to give predicted resolutions in the sub-picosecond regime [48,49]. The streak tube used in this work was the so-called Photochron II [50].The basic operation of a streak tube can be understood with reference to fig 3.3. A train of pulses from the mode-locked laser are incident upon the slit. The image of the slit is then focussed onto the photocathode by a lens. The pulse train when incident upon the photocathode causes the emission of electrons which are accelerated under the influence of a distributed potential gradient between the photocathode and the anode. After the anode the electrons are then deflected by a voltage ramp to give a spatial representation of the temporal profile of the pulse on the phosphor screen.
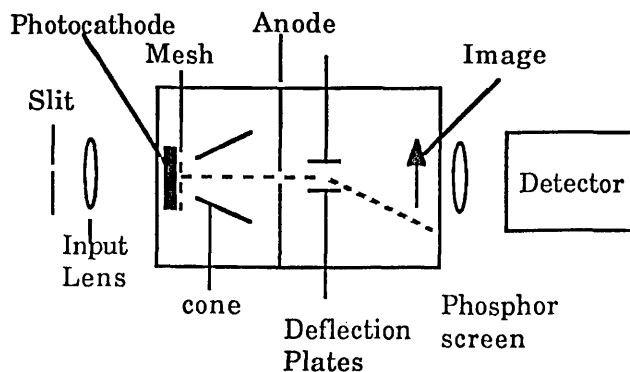
Fig 3.3:   A Photochron II streak camera.

Ideally, if all of the photoelectrons in the electron signal were emitted instantaneuosly from a single point on the photocathode and arrived simultaneously at the entrance of the deflectors via a perfect electron lens, and subsequently deflected by an ideal deflector then the streak image displayed on the phosphor screen would faithfully represent the temporal features of the input optical pulse. Unfortunately this is never the case and as a result of the initial energy and angular distributions of the electrons generated by the photocathode and inherent defects in the electrostatic focussing and deflection systems the temporal structure of the streak image is to some extent a deformation of that of the incident pulse and it is necessary to quantify this deformation in the most appropriate and accurate manner possible.

The temporal resolution of the streak camera was determined originally by assuming it arose from discrete quasi-independent contributions to which a Gaussian approximation could be applied [51]. This is usually applied in the form

$$\Delta\tau_{inst} = \{ (\Delta\tau_{phys})^2 + (\Delta\tau_{tech})^2 \}^{\frac{1}{2}} \qquad (3.4)$$

where $\Delta\tau_{inst}$ is the instrumental function of the streak tube and $\Delta\tau_{phys}$ and $\Delta\tau_{tech}$ represent the physical and technical time resolution components, respectively, that contribute to the overall resolution and can be quantified according to eqns. 3.5 and 3.6.

$$\Delta\tau_{phys}^2 = \Delta\tau_c^2 + \Delta\tau_k^2 + \Delta\tau_l^2 + \Delta\tau_d^2 + \Delta\tau_{pd}^2 \qquad (3.5)$$

where $\Delta\tau_c$ is the time dispersion of the photoelectrons in the photocathode and $\Delta\tau_k$, $\Delta\tau_l$, $\Delta\tau_d$, $\Delta\tau_{pd}$ are the transit time dispersions in the photocathode to mesh region, the focussing electron lens, the deflector plates, and the post-deflection sections, respectively.

$$\Delta\tau_{tech} = \frac{1}{v\delta} \qquad (3.6)$$

where v is the streak speed of the electrons at the phosphor screen and δ is the spatial resolution in the direction of the streak.

However recent theoretical studies [49] have shown this to be too simplistic an argument. Equation 3.4 assumes that the constituent factors are given the same weight and it follows that if they have equal values they would play the same role in the

deformation of the original signal. However this is not the case and it has been shown by Niu et al [49] that they do not have the same weight.

The dynamic spatial resolution, δ, of eqn. 3.6 was originally assumed to be a technical characteristic particular to each streak tube but it is in fact determined by both the electron-optical/electronic parameters and the physical time dispersion associated with the electron pulse that is deflected. Thus both the physical and technical time resolution limits cannot be treated as separate or distinct quantities.

A more exact method of evaluating the overall performance of the streak camera is to evaluate both the temporal and spatial modulation transfer functions of the streak tube. For a Photochron II streak camera with an applied potential of 20 kV/cm a temporal dispersion of 0.74 ps has been evaluated [49].

Although streak cameras may be used in single-shot mode giving sub-picosecond resolutions [52] the main advantage of the streak camera is that it may be operated in synchronism with the laser pulse train. This involves synchronising the deflecting voltage ramp with the pulse train, which results in a superpositioning and integration of the streaks associated with the repetitive light events without any reductions in the resolution capabilities of the streak tube.

As a synchronously operated streak camera was used throughout this work a brief description of this mode of operation is included here. The first reported case of a synchronously operated streak camera was made by Adams et al in 1978 [53] and the method of driving the deflection plates has changed little since then. The operation of a synchronously scanning streak camera may be described by referring to fig 3.4. A fraction (~10%) of the mode-locked pulse train is coupled onto a photodiode/tunnel diode combination. The tunnel diode is biased such that the laser pulse takes it above threshold so that a sine wave is produced at the frequency of the incident pulse train. This sine wave is frequency doubled and amplified to approximately 10 W before being coupled across the deflection plates of the streak tube. Coupling of the sine wave to the deflection plates is done through a moderate Q impedance network. Once amplified the peak-to-peak deflection voltage is about 3.5 kV, giving a linearity of the streak image over ~5 cm of the phosphor screen. The repetitive nature of the laser signal and

Optical Delay Line

Streak
Camera

Streak
Images

Tunnel-
diode   10 W   Time Delay

Beamsplitter   10 %

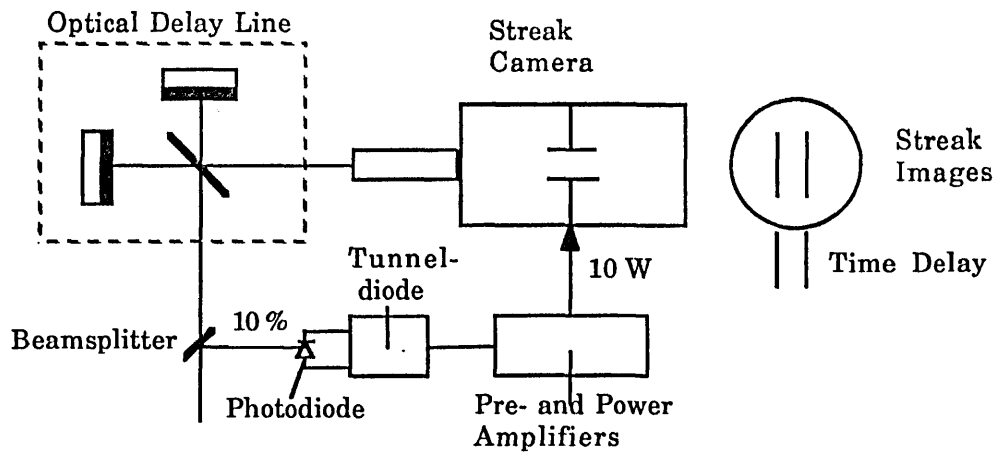Photodiode   Pre- and Power
Amplifiers

Fig 3.4:   The experimental arrangement used when measuring
pulse durations with a synchroscanning streak camera.

the low level of electronic jitter of the trigger signal, ensures the streak image

associated with each laser pulse is superimposed on the phosphor screen with picosecond

accuracy. This produces an integration effect which allows very low light levels to be

monitored. The streak images formed on the phosphor screen are then imaged onto the

vidicon image tube of an optical multi-channel analyser (OMA), which provides a real

time display of the streak images.The duration of the pulses incident upon the slit of the

streak camera are measured by splitting the beam into two portions and then

introducing a fixed delay between the two beams. The delayed and non-delayed pulses

are then scanned across the phosphor screen by the deflection voltage. Care has to be

taken to ensure that both pulses lie in the linear region of the deflecting sine wave to

avoid errors in time calibration and hence mis-measurements of the pulse duration.

The pulses are then stored by the OMA and as the temporal separation of the pulses is

known the pulse durations can then be evaluated.

Although a direct real-time display of the streak intensity profiles is obtained, the

recorded pulse duration differs from the actual duration due to jitter in the triggering

circuitry. This arises from accumulated variations in the interpulse separation and

phase drifts induced by amplitude fluctuations.

The best results obtained to date from a streak camera operated in synchronism

with a passively mode-locked dye laser are of the order of 1 picosecond [54]. The shortest

pulses recorded when the streak camera is operated in conjunction with a

synchronously mode-locked dye laser are 5 ps [55]. This difference arises from phase fluctuations in the trigger signal. The trigger signal is derived from the output pulse train of the dye laser and so any amplitude or pulse duration fluctations in the output pulse train introduce electronic jitter. The duration and amplitude of a synchronously mode-locked laser are highly sensitive to the degree of matching between the drive and slave frequencies. If the two frequencies drift apart due to cavity length fluctuations then a trigger jitter is induced.This jitter then manifests itself as a phase jitter when applied to the the streak tube.

The shortest pulse generated directly from a laser is 19fs [27]. Thus for linear pulse measurements employing electron-optical streak cameras to be valid requires the streak tubes to have femtosecond resolution and at present both theoretical and experimental studies into the design of such streak tubes are being undertaken.

3.6.2. Second Harmonic Generation Autocorrelation Measurements.

Pulse duration measurements made using this technique are based on the non-linear optical process of second harmonic generation. There are two types of autocorrelation technique and these are intensity [56], or interferometric [57], in nature. Intensity autocorrelations can be described as either first-order [58],or second-order [59], in nature. The second-order technique [59], is a background free method which requires that both beams are present in the crystal to generate the second harmonic signal. The resultant signal then propagates in a direction determined by the phase matching condition.In the first order process both fundamental-frequency beams propagate through the crystal co-linearily and the generated second harmonic signal follows the same path as the fundamental beams. This method was employed for the measurements reported in this thesis and so an outline of the experimental procedure is given.

The experimental configuration is illustrated in fig 3.5. The train of ultrashort light pulses is incident upon a Michelson interferometer type arrangement, where one arm provides a fixed time delay and the other a variable delay. The two beams are then recombined and focussed into a phase-matched second harmonic generating crystal.
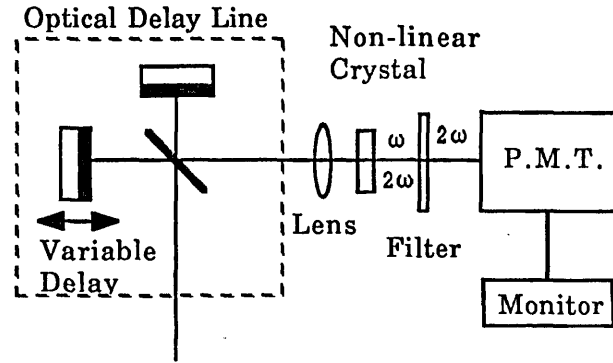
Fig 3.5:   Experimental configuration used for second harmonic
autocorrelation measurements.

By scanning the variable delay through the fixed delay using a stepping motor or a

vibrating mirror, the intensity of the generated second harmonic signal can be altered

due to the degree of overlap. This variation is then monitored by a photomultiplier tube-

oscilloscope combination to give a mapping of the correlation function of the pulses.

The resolution of this technique is determined by the phase matching bandwidth (and

hence thickness) of the second harmonic crystal [60].

It should be noted that monitoring the second harmonic signal does not provide a

direct indication of the pulse duration or shape but instead yields measurements of the

correlation function of the pulse. Therefore it is necessary to consider the relationship

between the signal E(t) and its correlation function G(t).The correlation function G(t)

describing a second harmonic experiment is given by

$$G^2(\tau) = \int_{-\infty}^{\infty} |E(t)|^2 |E(t+\tau)|^2 \, dt \tag{3.7}$$

where τ is the delay.

The half width of the correlation function gives a measure of the pulse duration if

the pulse shape is known.The correlation function is symmetric so it does not yield any

information about the pulse profile. To determine the pulse shape, higher order [61,62] or

interferometric [63] autocorrelation measurements must be made. The pulse duration

is related to the autocorrelation function through a simple relationship

$$\Delta\tau_p = \frac{\Delta\tau_a}{k} \tag{3.8}$$

where k is a constant determined by the pulse shape.

In first-order type autocorrelation the observed trace is related to the correlation function by the relationship

$$F(\tau) = c \left(1 + \frac{G^2(\tau)}{G^2(\tau - \infty)} + \Lambda(\tau) \right)$$ (3.9)

where c is a constant, 1 defines the background and $\Lambda(\tau)$ is a rapidly varying interference term, which averages to zero.

For the case of a perfectly mode-locked pulse train $G^2(\tau) = 2$ and hence $F(\tau)=3c$. This implies a signal to noise ratio of 3:1 between the peak of the pulse and the background. Any deviations from a 3:1 ratio imply imperfect mode-locking. For a perfectly mode-locked laser all the intracavity flux is contained in the pulse but for the incompletely mode-locked laser some interpulse intensity exists in the cavity and it has been shown by Von Der Linde [64] that if the signal to noise ratio is only 2.92:1 then only 10% of the cavity energy is maintained in the laser pulse.

There is a systematic error associated with pulse measurements made by second harmonic autocorrelation. The pulse widths measured are averages taken over many pulses ($\sim 10^9$) and as a result, the shape of the correlation function is sensitive to the distribution of pulse durations and not to the temporal features of an individual pulse [65]. For example, if an actively mode-locked laser is considered, any fluctuations in the cavity length lead to variations in the pulse shape and duration. As autocorrelation uses a continuous train of pulses the recorded function $G^2_{obs}(\tau)$ may be regarded as being a weighted average of the second-order autocorrelation functions of the individual pulses given by

$$G^2_{obs}(\tau) = \int_0^\infty G^2_{\tau_0}(\tau) p(\tau_0) d\tau_0$$ (3.10)

where $G^2_{\tau_0}$ is the autocorrelation function of a pulse of width τ_0 and $p(\tau_0)d\tau_0$ is the probability that the pulse has a width between τ_0 and $\tau_0 + d\tau_0$.

Since $G^2_{\tau_0}(\tau)$ depends on the square of the optical field (see eqn. 3.7), then the shortest pulses are most heavily weighted in such an average and as a result $G^2_{obs}(\tau)$ tends to peak nearer $\tau = 0$ when compared with $G^2_{\tau_0}(\tau)$ of an individual pulse. This leads to a mis-measurement of the pulse duration with the measured pulse tending to be

too short. This problem can be overcome by monitoring the pulse duration fluctuations. If the ratio of the square of the fundamental intensity to that of the second harmonic is considered , and providing the spatial distribution and the temporal pulse profiles do not change, this ratio is directly proportional to the pulse durations [65]. Although this will lead to a more valid representation of the pulse duration it was not implemented during the work performed in this thesis.

As already stated, the intensity autocorrelation reveals little information about the pulse shape and although streak cameras do provide a linear measuring device their temporal resolution at present is insufficient to be of much use for sub-picosecond pulses. An elegant way to obtain information about the pulse profile simultaneously with its duration is to exploit the technique of interferometric autocorrelation.

3.6.3. Interferometric Autocorrelation.

If the mirror which provides the variable delay is moved slowly enough then the autocorrelation signal is recorded with interferometric accuracy. The second harmonic signal $S(\tau)$ is proportional to

$$S(\tau) = \int_{-\infty}^{\infty} |\{ E(t) \, expi(wt + \phi) + E(t-\tau) expi(w(t - \tau)+ \phi(t-\tau))\}^2 |^2 \, dt \quad (3.11)$$

When the two arms of the delay line are matched $S(\tau)$ takes the form

$$S(\tau) = 2^4 \int_{-\infty}^{\infty} E^4(t)dt \quad (3.12)$$

This leads to autocorrelation signals of the form shown in fig 3.6 being recorded. For a correctly mode-locked laser contrast ratios of 8:1 are observed. As the profile is dependent upon the fourth power of the E fields combining in phase in the second harmonic generating crystal, the upper envelope is more sensitive to the pulse shape than the intensity autocorrelation previously described. Hence information about the pulse, such as whether the pulse is asymmetric or has experienced a chirp, may be obtained. The recorded interferometric signal is also self calibrating as the generated fringes are induced by the optical cycles in the fundamental frequency signal. Thus

interferometric autocorrelation can be seen to be a powerful technique for measuring hypershort pulses [63].
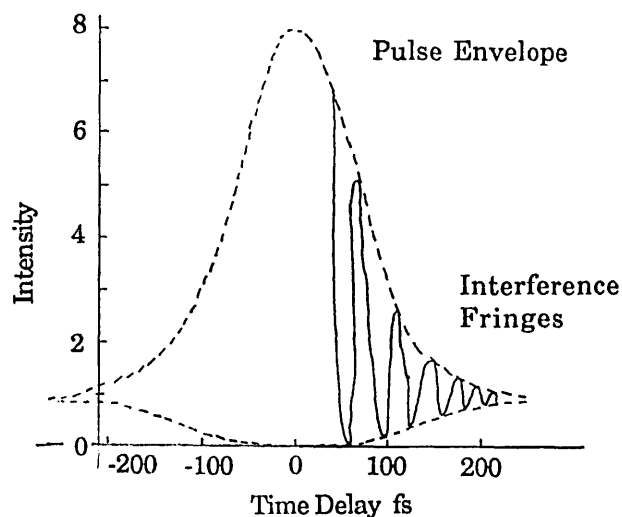

Fig 3.6:   A typical interferometric autocorrelation signal showing both the pulse envelope and the interference fringes associated with the signal.

However this technique was not implemented here as the pulses generated were not short enough to allow it to be used with any accuracy. In chapter 7 the dispersion-optimisation of a passively mode-locked colour centre laser is described.The shortest pulses generated from this laser were ~180 fs. These pulses were recorded at a wavelength of 850 nm. At this wavelength one optical cycle corresponds to 2.8 fs. (Also for a $Sech^2$ pulse shape which was assumed for these pulses there is a correction factor of 1.9 [27]). The number of fringes monitored on the oscilloscope screen, corresponding to a pulse of this duration, is ~120. To display the interferometric signal in a sensible fashion so that the number of interference fringes, calculated above, may be resolved whilst observing the pulse envelope is problematic.

3.7. Bandwidth Measurements

In order to estimate the degree of success of the mode-locking process employed the duration-bandwidth product has to be considered. These two quantities are related by eqn. 3.2. A list of possible pulse profiles and their corresponding value of a is given in table 3.1. The temporal duration of the pulse is determined by using one of the

Pulse Shape	Intensity Profile	α	k
Square	$1 \; (\frac{-\Delta t}{2} \leq t \leq \frac{\Delta t}{2})$	0.866	1
Gaussian	$\exp\left(\frac{-4\ln 2 t^2}{\Delta t}\right)$	0.441	$\sqrt{2}$
Sech^2	$\text{Sech}^2\left(\frac{1.76 t^2}{\Delta t^2}\right)$	0.315	1.55

Table 3.1:   A listing of the pulse shape together with the time-bandwidth product, α, and the autocorrelation constant, k.

measurement techniques described above and the bandwidth can be measured in the following way. Initial measurements of the laser bandwidth were made by placing photographic plates at the output of a monochromator. After the plates had been developed the recorded images were then analysed to give the bandwidth. An alternative scheme used was to place a photomultiplier tube at the output slit of the monochromator and record the spectrum directly. Both these methods of measuring the bandwidth were slow processes and did not yield real time information about the laser spectrum. As a result a real-time device was developed. This is illustrated in fig 3.7. It consists of a charged coupled device sensor (CCD) [66] placed at the exit slit of a monochromator. This gave a direct measurement of the spectral profile of the laser pulse which could be stored and displayed at a later time and so greatly simplified the process of recording the spectral information associated with the laser pulse train.
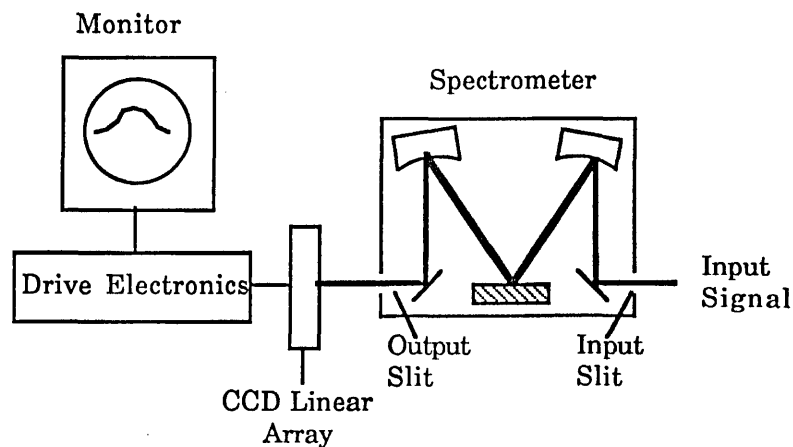
Fig 3.7:   The experimental set-up used to measure the laser bandwidth with a CCD linear array device.

3.8. Conclusions.

This chapter has given a brief outline of the mode-locking and measurement techniques used to generate and characterise the ultrashort pulses which will be described in later chapters. The main pulse measurement techniques used were those of intensity second harmonic autocorrelation and synchroscan streak camera measurements however the results obtained from both these types of measurements have to be treated with caution as they do not truly represent the pulses generated from the laser. In order to obtain a more accurate representation of the pulse train generated by the mode-locked laser interferometric autocorrelation techniques should be employed.

References:

1. B.D. Sinclair PhD Thesis University of St. Andrews 1987.
2. A Yariv; J. Appl. Phys., 36, 388, 1965.
3. A. Scavennec; Opt. Commun., 20, 335, 1977.
4. B.C. Johnson, P.F. Moulton and A. Mooradian; Opt. Lett., 10, 4, 1984.
5. M.D. Dawson PhD Thesis University of London 1985.
6. J.P. Willson PhD Thesis University of London 1982.
7. H. Haus; I.E.E.E. J. Quant. Elect ., 11, 323, 1975.
8. O. Mc. Duff and S.E. Harris; I.E.E.E. J. Quant. Elect ., QE 3, 101, 1967.
9. D.J. Kuizenga and A.E. Siegman; I.E.E.E. J. Quant. Elect ., QE 6, 694, 1970.
10. R. Alder; I.E.E.E. Spectrum, 4, 42, 1967.
11. G.H.C. New, L.A. Zenteno, and P.M. Radmore; Opt. Commun., 48, 149, 1976.
12. C.V. Raman and V.S. Nath; Proc. India. Ac. Sci., 2, 406, 1935.

13. P.K. Runge; Opt. Commun., 4, 195, 1971.
14. J.N. Eckstein, A.I. Ferguson, T.W. Hansch, C.A. Minard and C.K. Chan; Opt. Commun., 27, 466, 1978.
15. R. Illingworth and I.S. Ruddock; Opt. Commun., 61, 120, 1987.
16. N.J. Frigo, T. Daly and H. Mahr; I.E.E.E. J. Quant. Electon., QE-13, 101, 1977.
17. C.P. Ausschnitt, R.K. Jain and J.P. Heritage; I.E.E.E. J. Quant. Electon., QE-15, 912, 1979.
18. A. Scavannec; Opt. Commun., 17, 14, 1976.
19. D.A. Kim, J. Kuhl, R. Lambrich and D. Von Der Linde; Opt. Commun., 27, 123, 1978.
20. J. Herrmann and U. Motschmann; Appl. Phys. B., 27, 27, 1978.
21. J.M. Catherall, G.H.C. New, and P.M. Radmore; Opt. Lett., 7, 319, 1982.
22. P.G. May, W. Sibbett, K. Smith, J.R. Taylor and J.P. Wilson; Opt. Commun., 42, 285, 1982.
23. J.M. Catherall and G.H.C. New; I.E.E.E. J. Quant. Elect ., QE 22, 1593, 1986.
24. P.M.W. French and J.R. Taylor; Appl. Phys. Lett., 50, 1708, 1987.
25. E.P. Ippen C.V. Shank and A. Diennes; Appl. Phys. Lett., 21, 348,1972.
26. K. Smith, N. Langford, W. Sibbett and J.R. Taylor; Opt. Lett., 10, 559, 1985.
27. A. Finch private communication.
28. P.W. Smith, Y. Silverberg and D.A.W. Miller; J.O.S.A. B, 2, 1985.
29. G.H.C. New; Opt. Commun., 6, 188, 1972.
30. G.H.C. New; I.E.E.E. J. Quant. Elect ., QE- 10, 115, 1974.
31. H.A. Haus; I.E.E.E. J. Quant. Elect ., QE- 11, 736, 1975.

32. G.H.C. New, K.E. Orkney, and M.J.W. Nock; Opt. Quantum. Electron., 8, 425, 1976.

33. M.S. Stix and E.P. Ippen; I.E.E.E. J. Quant. Elech ., QE- 19, 520, 1983.

34. O.E. Martinez, R.L. Fork, and J.P. Gordon; J.O.S.A. B, 2, 753, 1985.

35. J.C. Diels, W. Dietel, J.J. Fontaine, W. Rudolph and B. Wilhelmi; J.O.S.A. B, 2, 682, 1985.

36. R.L. Fork, B.I. Greene and C.V. Shank; Appl. Phys. Lett., 38, 671, 1981.

37. D. Kulhke, W. Rudolph and B. Wilhelmi; I.E.E.E. J. Quant. Elect ., QE- 19, 570, 1983.

38. J.A. Valdmanis, R.L. Fork and J.P. Gordon; Opt. Lett., 10, 131, 1985.

39. G.W. Fehrenbach, K.J. Gruntz and R.G. Ulbrich; Appl. Phys. Lett., 33, 159, 1978.

40. Y. Aoyagi, Y. Segawa and S. Nariba; Japan J. Appl. Phys., 20, L1595, 1981.

41. Y. Ishida, K. Nagamima and T. Yajima; Japan J. Appl. Phys., 21, L312, 1982.

42. K. Smith, W. Sibbett and J.R. Taylor; Opt. Commun., 49, 359, 1984.

43. J. Dobler. H.H. Shulz and W. Zinth; Opt. Commun., 57, 487, 1986.

44. M.D. Dawson, T.F. Boggess and A.L. Smirl;Opt. Lett., 12, 123, 1976.

45. D.J. Bradley; in Ultrashort Light Pulses, Ed. S.L. Shapiro, Springer Verlag Berlin, 1977.

46. E.P. Ippen and C.V. Shank in *Ultrashort Light Pulses*, Ed. S.L. Shapiro, Springer Verlag, Berlin, 1977.

47. E.K. Zavoisky and S.D. Fanchenko; Sov. Phys. Doklady., 1, 285 1956

48. D.J. Bradley; Proc. 13th International Congress High Speed Photography and Photonics 1977.

49. W. Sibbett. H.Niu and M.R. Baggs; Rev. Sci. Instrum., 53, 563, 1982.

50. P.R. Bird, D.J. Bradley and W.Sibbett; Proc. 11th International Congress High Speed Photography and Photonics 1975.

51. D.J. Bradley, B. Liddy and W. Sibbett; Opt. Commun., 2, 391, 1971.

52. D.J. Bradley, W. Sibbett; Appl. Phys. Lett., 27, 382, 1975.

53. M.C. Adams, W. Sibbett and D.J. Bradley; Opt. Commun., 26, 273, 1978.

54. J.P. Wilson, W. Sibbett and W.E. Sleat; Opt. Commun., 42, 208, 1982.

55. K. Smith PhD Thesis University of London 1985.

56. H.P. Weber; J. Appl Phys. 38, 2331, 1967.

57. J.C. Diels, E.W. Van Stryland and D. Gold, in Proceedings of the first International Conference on Picosecond Phenomena. Springer Verlag 1978. p 117.

58. M. Maier, W. Kaiser and J.A. Giordmaine; Phys Rev. Lett., 17, 1275, 1966.

59. J.A. Armstrong; Appl. Phys. Lett., 10, 16, 1967.

60. I.S. Ruddock; Ph.D. Thesis University of London 1976.

61. E.I. Blount and F.R. Klander; J. Appl. Phys., 40, 2874, 1969.

62. H.P. Weber, R. Dandiker; Phys. Lett., <u>28A</u>, 77, 1968.

63. J.C. Diels, J.J. Fontaine, I.C. McMicheal and F.Simoni; Appl. Opt., <u>24</u>,1270, 1985.

64. D. Von Der Linde; I.E.E.E. J. Quant. Elect ., <u>8</u>, 328, 1972.

65. E.W. Van Stryland;Opt. Commun., <u>31</u>, 93, 1979.

66. Thanks to R. Zhang who built the drive electronics for the CCD and to IMEC (Belgium) for suppling the CCD.

Chapter 4: The Rhodamine 700 dye Laser.

4.1. Introduction.

The previous two chapters were concerned with colour centres and organic dyes as laser active media, the generation of ultrashort pulses and the measurements of these pulses. The original aim of this thesis was to develop the F_2^+ -type colour centre as a short pulse gain medium and exploit these pulses to study temporal propagation effects in optical fibres. It was mentioned in chapter 2 that this family of colour centres operates in the 0.8-2.0 μm spectral region [1]. As the field of short pulse generation and measurement was completely new to me it was decided to use a visible dye laser as a stepping stone so that I could familiarise myself with the aforementioned generation and measurement techniques without having the added complication of working in the infrared.

4.1.2. The cw Performance of the Rhodamine 700 Dye Laser.

This dye was first demonstrated as a highly efficient laser dye for the spectral region 695 - 810 nm by Marason [2] who used both an energy transfer scheme, using 4-dicyanomethylene-2-methyl-6-p-dimetylaminostyryl-4H-pyran, (DCM) as the donor and Rhodamine 700 (R700) as the acceptor, and also direct Kr^+ pumping to obtain efficient laser action from the dye. Jain [3] further extended the energy transfer system by synchronously pumping the DCM/R700 dye combination with an actively mode-locked Ar^+.Work by Johnston et al [4] showed that the tuning range could be extended to cover the region 695 -890 nm.

From the absorption curve for the laser active dye R700 shown in fig 4.1 it can be seen that the dye has a peak absorption centred on 650 nm and is well matched to the Kr^+ pump source used during this work. The absorption cross-section of the dye was calculated to be $\sim 7 \times 10^{-16}$ cm^2 and the radiative decay time was measured to be 2.8 ns [5].For most of the work presented in this chapter a Spectra Physics 375 dye laser served as the resonator, and its optical configuration is shown in fig 4.2. It is a simple three mirror cavity consisting of the retroreflecting end mirror M_1, the collimating mirror
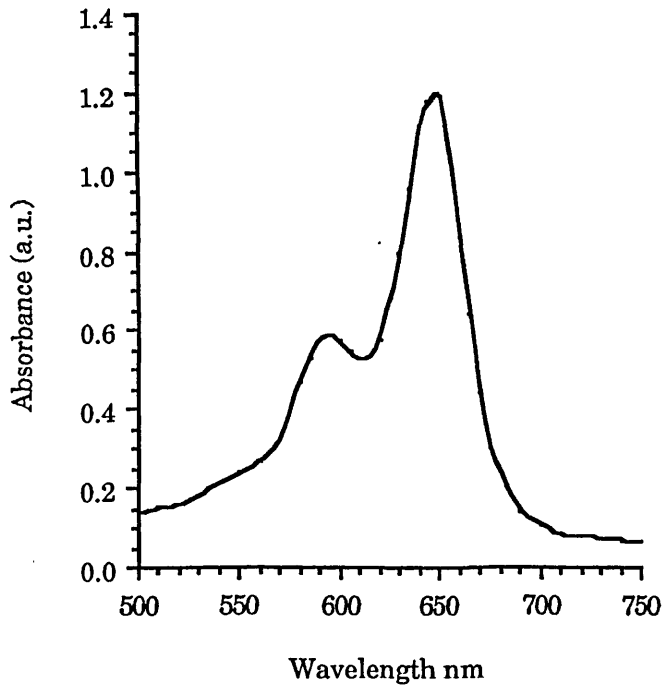
Fig 4.1   The absorption band of the laser active dye Rhodamine 700
in a methanolic solution (concentration 1×10^{-5}
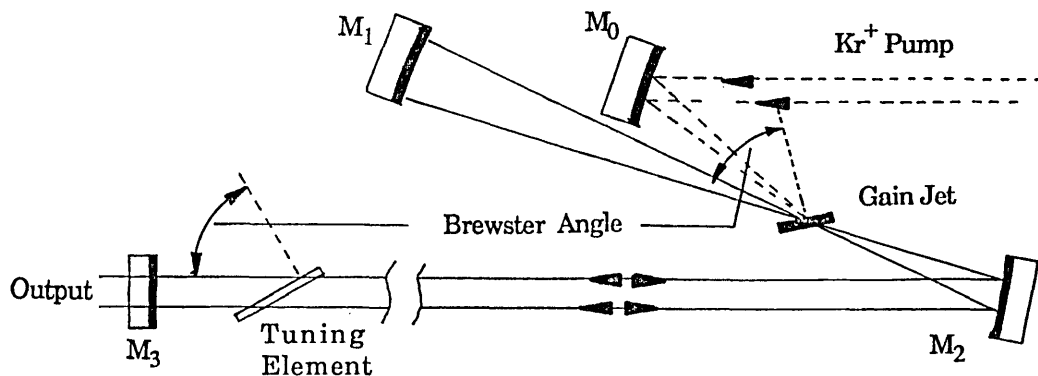mole/litre).

Fig 4.2:   The optical configuration of the Spectra Physics 375 dye
laser used in this chapter.

M_2 and the plane output coupler M_3 (T=3%). Both mirrors M_1 and M_2 had 5 cm radii of

curvature and were nominally 100% reflecting over the entire spectral region

700-800nm. The Kr^+ pump beam was coupled into the cavity via the 5 cm radius of

curvature mirror M_0. An ~200 μm thick Brewster angled dye jet was located at the

common focus M_0 and M_2 in which the active dye was dissolved. Frequency tuning of

the laser output was accomplished by using the Brewster angled dielectric wedge

inserted between mirrors M_2 and M_3. The laser active dye is driven through the nozzle of the dye jet by a Spectra Physics 376 Dye Circulator which provided dye stream velocities of up to 13 m/s. In order to remove any pressure fluctuations in the jet induced by pump motor variations an accumulator (Spectra Physics 372 B) was placed in series with the pump and the nozzle. The dye reservoir was placed in a constant temperature water bath, to minimise the temperature of the dye solution, thus avoiding possible thermal bleaching effects.

Typical dye concentrations ~1.2 x 10^{-3} mole/litre were used and at this concentration the performance characteristics of the dye laser, under continuous wave pumping, are shown in fig 4.3. Fig 4.3a shows the output power as a function of input power and it can be seen that the dye exhibits a slope efficiency of ~40%. The tuning range of the dye was found to be ~690 - 820 nm as illustrated in fig 4.3b. but no attempt was made to extend this range out to 890 nm [4] as the necessary mirrors were not available at the time.

4.2. The Synchronous Mode-Locking of the R700 Dye Laser.

4.2.1. Introduction.

As the dye laser proved to be highly efficient and user friendly it was decided to develop it into a pulse source so that I could become accustomed to the linear and non-linear measurement techniques described in chapter 3. The most direct way to generate short pulses is by the active process of synchronous mode-locking.

4.2.2. The Acousto-Optically Mode-Locked Kr^+ Pump Laser.

As described in chapter 3 synchronous mode-locking is a gain modulation technique and the gain modulation is provided by a mode-locked pump pulse. To satisfy this req uirement the Kr^+ pump laser was acousto-optically mode-locked. The end mirror of the Kr^+ was replaced by an acousto-optic modulator (Spectra Physics 342), which consisted of a Brewster angled quartz prism to which a piezo-electric transducer was bonded. The prism provided the necessary wavelength selection and the transducer induces the acoustic wave from the incident rf signal. The rf signal was amplified up
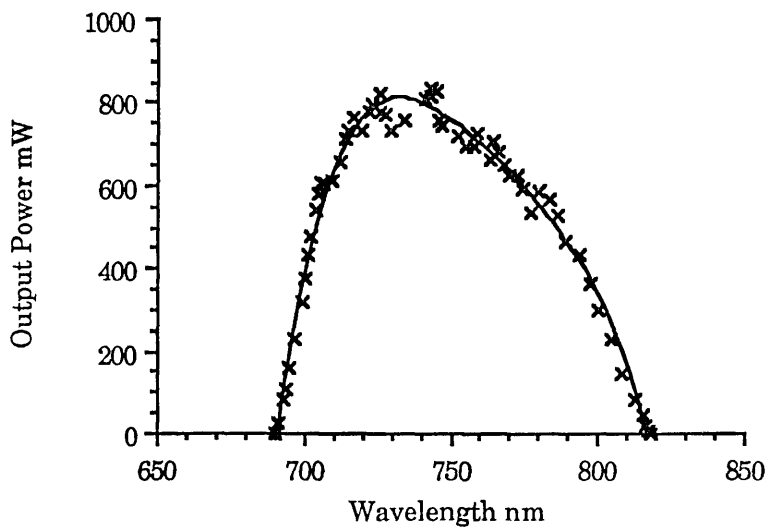
(a)
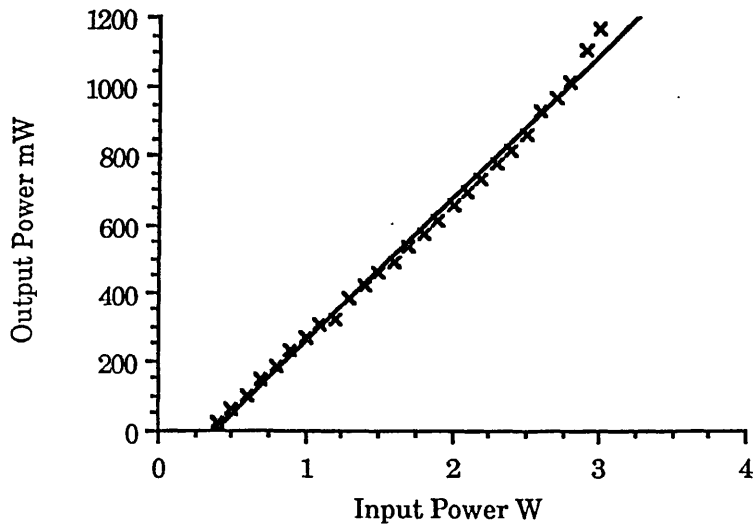
(b)

Fig 4.3:   The performance characteristics of the R700 dye laser (a)
            is a plot of output power against input power (T = 3%) and
            (b) exhibits the typical tuning range obtained from the
            laser active dye (T= 3%).

to a signal of 0.6 W   before being applied to the transducer. A drive frequency of

approximately 40.96MHz was selected, as this   matches   a resonant frequency of the

modulator. The degree of matching between the two was monitored using a standing

wave ratio meter (SWR). Under these operating conditions pulses as short as 80 ps,

depicted in fig 4.4, as measured on the synchronously scanning Photochron II streak

camera [6], were routinely observed.
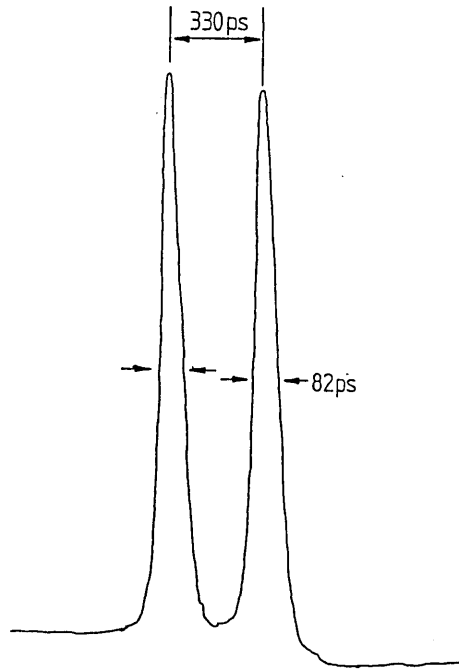
Fig 4.4:   Typical streak images of the pulse train emitted by the
           acousto-optically mode-locked Kr^+ pump laser.

4.2.3. The Synchronously Mode-Locked R700 Dye Laser.

The precise matching of the slave and pump resonator transit times is an essential

prerequisite for efficient mode-locking and to facilitate this the end mirror M_3 of the

dye laser was mounted on a precision translation stage. Coarse matching of the dye
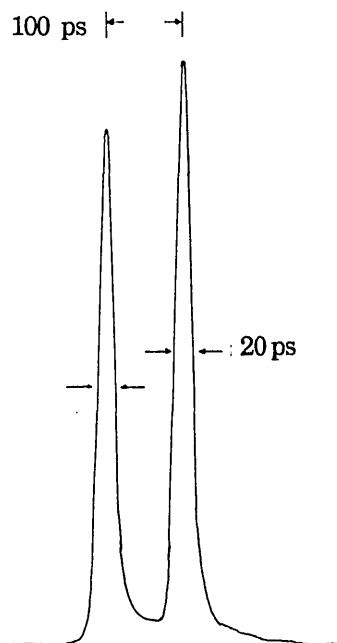
Fig 4.5:   Streak images of the synchronously mode-locked R700 dye
           laser pulse trains.

laser period to that of the Kr$^+$ was accomplished by monitoring the output pulse train produced by the dye laser on a fast photodiode/oscilloscope combination. For further optimisation the dye laser pulses were then coupled onto the slit of the synchroscanning Phtochron II streak camera and pulses as short as 20 ps were recorded, illustrated in fig 4.5.After optimisation on the streak camera the pulses were then fine tuned on a real time auto-correlator [7]. This consisted of the standard arrangement described in section 3.6.2. but the variable delay was provided by a rapidly scanning mirror. Once the pulses were fine tuned they were recorded by switching off the shaking mirror and then slowly scanning it using a stepping motor as the drive. The typical pulse duration observed from this laser was approximately 1 ps (assuming Gaussian pulse shapes) as illustrated in fig 4.6. The output power was ~50 mW giving peak pulse powers ~600 W.
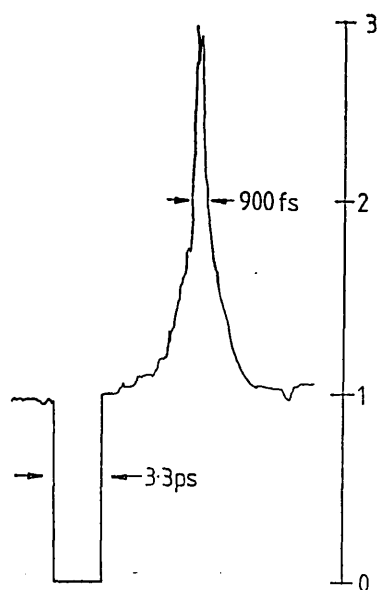
Fig 4.6:   Second harmonic autocorrelation traces of the pulses
            emitted by the synchronously mode-locked R700 dye laser.
            Recorded at a wavelength of 713 nm with 50 mW average
            power associated with the pulse train.

The dependence of the pulse duration on the cavity length was investigated, but instead of monitoring the pulses on the autocorrelator, the pulses were observed on a streak camera. This was chosen because at large cavity mismatches the non-linear technique of autocorrelation shows the pulses to consist of a coherence spike on a broad pedestal which is indicative of a noise-burst type structure circulating in the cavity.

This structure tends to conceal any information about the noise as it propagates and also masks any fluctuations of the noise. These fluctuations may be observed, however, using a streak camera. The camera was operated with a time resolution better than 10 ps and the behaviour of the pulses under both positive and negative cavity mismatch conditions as recorded by the streak camera, is shown in fig 4.7.
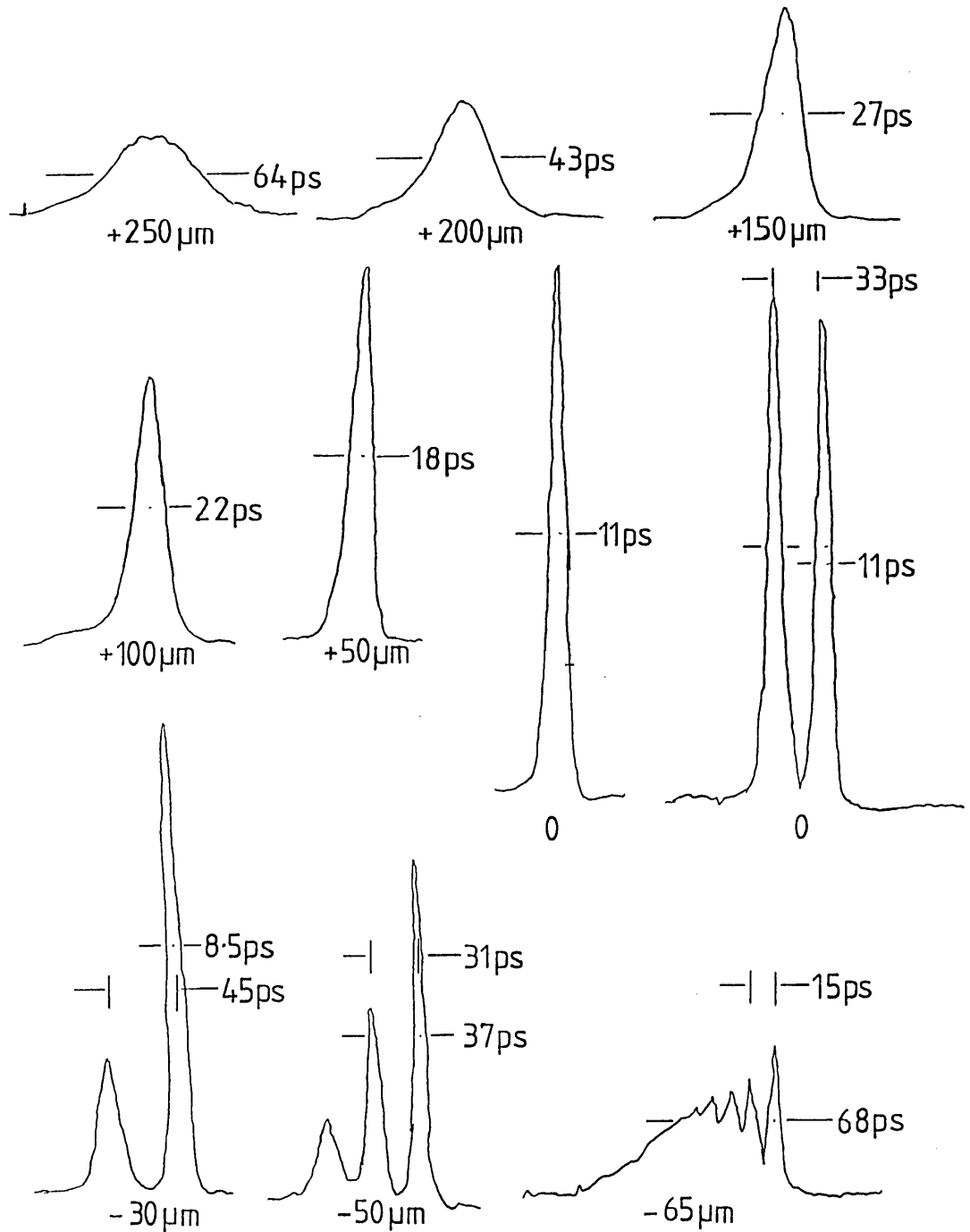

Fig 4.7:   The effects of cavity length variation on the pulses generated by the synchronously recorded R700 dye laser as recorded on the synchroscanning streak camera.

Under conditions of positive mismatch the pulses are broad and symmetric.For cavity detunings approaching the correct matching position the pulses narrow and beyond the optimum matching point, (defined as the position where the shortest pulses are observed on the streak camera with no satellites present), the pulses broaden and become asymmetric due to the development of satellite pulses. As the degree of negative detuning was increased the number of satellite pulses increased and the temporal separation between the main pulse and the first satellite pulse decreased, as illustrated in fig 4.7. The temporal variations of the pulse duration with respect to cavity length detuning is plotted in fig 4.8. From this plot it can be seen that the shortest pulses are recorded for a slight negative detuning which agrees with the behaviour observed for other synchronously mode-locked lasers [8-17].
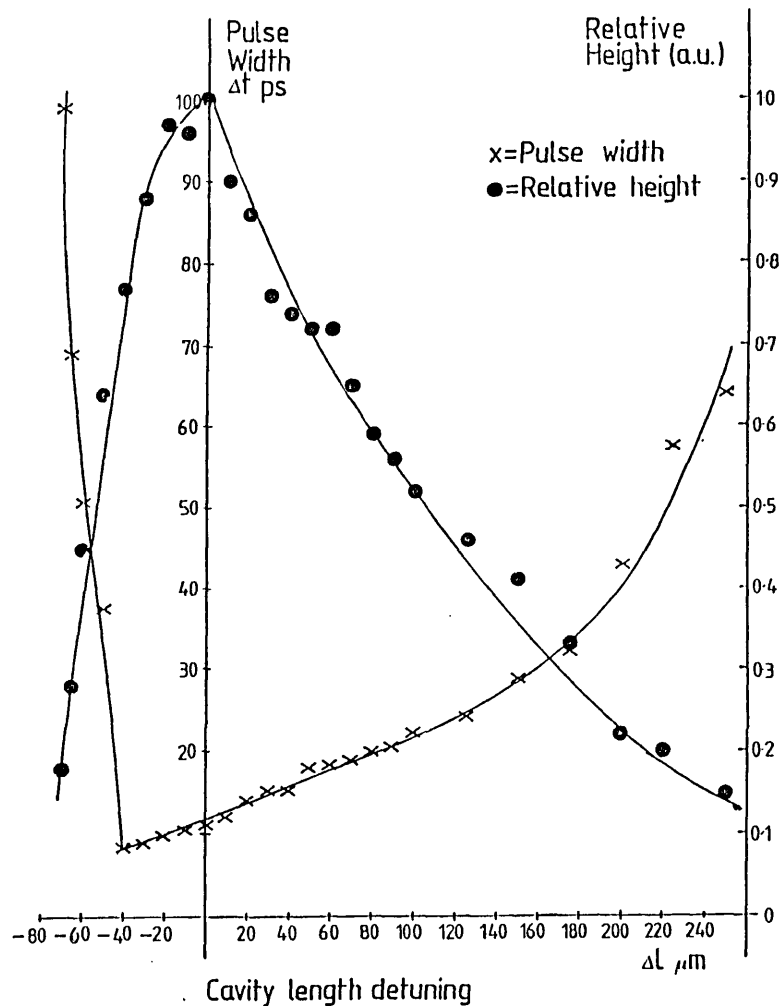
Fig 4.8:   The variation of pulse length and normalised pulse height against cavity length for the R700 dye laser.
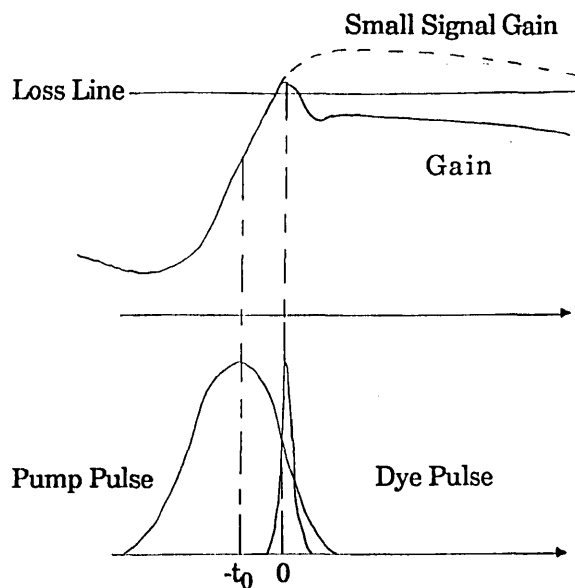
Fig 4.9:   A schematic of the time variation of the gain G due to the
          passage of the pump and the dye pulses through the active
          dye. The evolution of the gain Gs in the absence of the dye
          pulse is indicated by the dashed line (taken from ref 9).

This behaviour can be understood by referring to fig 4.9. To obtain a single well-defined pulse per cavity transit the dye laser pulse and its timing with respect to the pump pulse must be such that the gain remains below threshold after depletion by the circulating intracavity pulse. When the cavity length of the dye laser is set to match the period of the Kr^{+} pump pulse train, the peak of the dye laser pulse must pass through the gain medium slightly delayed from the point at which threshold was exceeded. Reducing the dye laser resonator period leads to an advancement of the dye laser pulse with respect to the pump pulse. This means that the dye laser pulse is moved further away from the peak of the gain signal. As a result the gain is not fully depleted by the front edge of the pulse. A direct consequence of this is that the trailing edge of the pulse is amplified, inducing a broadening of the pulse as well as production of satellite pulses. Futher detuning advances the pulse beyond the point where the intracavity losses are not exceeded and so laser action is inhibited. On the other hand, lengthening the cavity delays the pulse with respect to the pump pulse to a position where it experiences a higher net gain per pass but is broadened due a stronger amplification of the front edge of the pulse. Further lengthening of the cavity takes the dye laser pulse to a position where efficient mode-locking is precluded.

4.3. The Shortening of Laser Pulses by Exploiting both Gain and Absorber Saturation.

4.3.1. Introduction

For certain time domain spectroscopy experiments, such as the study of rotational relaxations in molecules [18], pulses with durations substantially shorter than a picosecond are often required. Pulses of this type may be generated from synchronously mode-locked dye lasers but to produce them routinely is quite difficult. To overcome this a variety of different schemes has been proposed. The first, demonstrated by French [19], is to select mirrors with the correct dispersion characteristics to form the resonator. A second and slightly more elegant scheme is to use a saturable absorber and exploit both absorber saturation and gain saturation as the pulse shaping processes. This can be applied to actively mode-locked lasers as well as passively mode-locked lasers.

4.3.2. The Hybrid Mode-locking of The R700 Dye Laser.

To familiarise myself with the role played by an intracavity saturable absorber the hybrid mode-locking of the R700 dye laser was investigated. Hybrid mode-locking has proved to be a reliable method for generating highly stable ultrashort pulses from synchronously mode-locked dye lasers [20-26]. In the work described here the R700 dye laser was hybridly mode-locked using the laser active dyes 1,1',3,3,3',3' Hexamethyl-indotria-carbocyanine-iodide, HITCI, and 3,3'Diethyl-oxatri-carbocyanine-iodide, DOTCI.

The resonator used in this work consisted of the Spectra Physics 375 dye laser described earlier (see 4.2.1) but an additional folded section was introduced into the cavity and the whole arrangement is shown in fig 4.10. The folded section consisted of two 10 cm radius of curvature mirrors. An ~200 μm Brewster angled dye was placed at the common focus of these two mirrors. The period of the R700 dye laser was matched directly to that of the Kr^+ and when the cavities were correctly matched, pulses as short as 1 ps, with average output powers as high as 50 mW were observed.
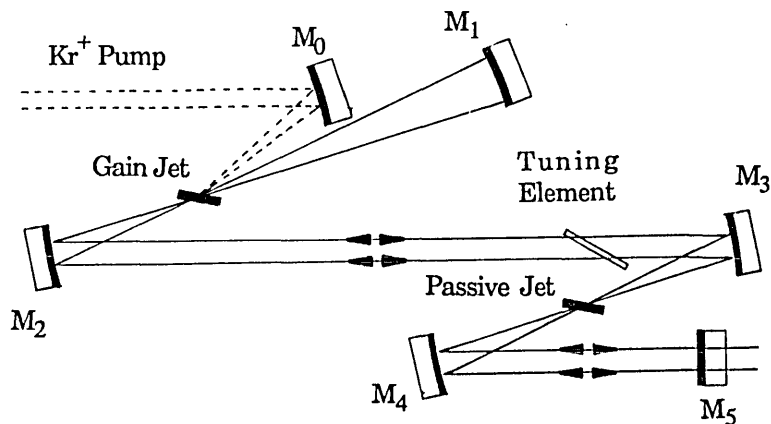
Fig 4.10: The arrangement of the optical elements used in the
investigations performed on the hybrid mode-locking of
the R700 dye laser.

To further shorten the duration of the pulses from the R700 dye laser a saturable

absorber was added to the passive dye jet. The saturable absorber used initially was the

laser active dye DOTCI. The absorption band of this dye (shown in fig 4.11) has a peak

absorption at ~680 nm, in an ethanolic solution, and an absorption cross-section

measured to be 9.8 x 10^{-16} cm^2. The dye also exhibits a strong photoisomer which has a
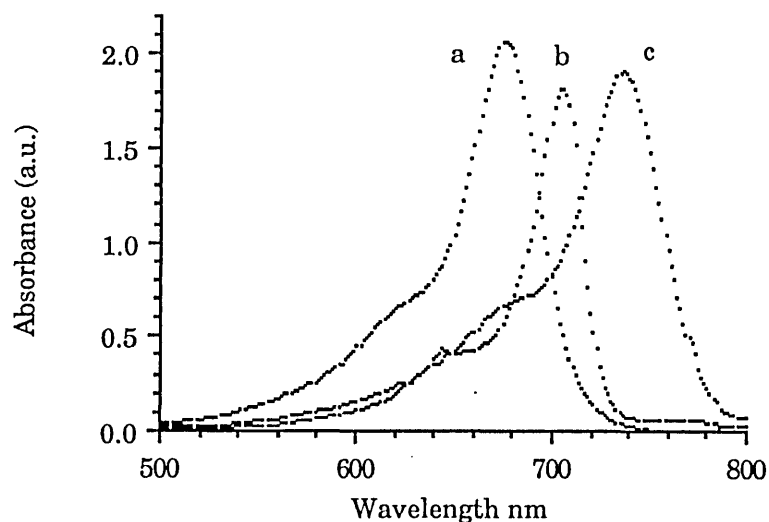
Fig 4.11: Absorption traces of 4 x 10^{-5} mole/litre ethanolic solutions
of (a) DOTCI, (b) DCI and (c) HITCI.

peak absorption at ~ 710 nm [27]. The wavelength of the laser was set to ~715 nm and the dependence of pulse duration upon absorber concentration was monitored on the autocorrelator, and is illustrated in fig 4.12a. At an absorber concentration of approximately 4×10^{-5} mole/litre pulses as short as 0.47 ps were observed,(see fig 4.12b). These pulses were tunable between 710 - 718 nm and had output powers of ~12 mW corresponding to peak powers of 320 W.
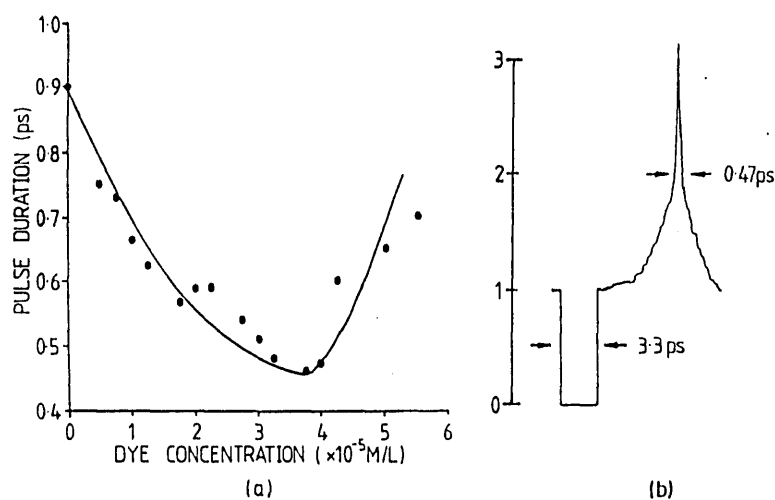
Fig 4.12:   (a) The dependence of the pulse duration on the DOTCI absorber concentration for hybrid mode-locked operation (λ = 713 nm) and (b) a typical autocorrelation trace taken with an absorber concentration of 4×10^{-5} mole/litre (λ = 713 nm).

Later work used the cavity shown in fig 4.13 where the actively mode-locked Kr^{+} pulse train (τ_p = 100 ps, P_{ave} = 1 W) was coupled into the cavity by the beam steering mirrors Ma,b via a small hole in mirror M_1. The pump beam was focussed into the active dye jet by mirror M_2 (10 cm radius of curvature) and rest of the cavity comprised the collimating mirror M_3 and the output coupler M_4 (T = 4%) which was mounted on a precision translation stage to give fine control over the cavity length. Mirrors $M_{1,2,3}$ were all nominally 100% reflecting over the spectral region 640 -860 nm and a Brewster angled dielectric wedge was used for frequency selection. The round trip time of the dye laser was matched to that of the Kr^{+} and pulses as short as 3 ps were rou tinely observed. From the autocorrelation trace shown in fig 4.14a., it can be deduced that the

TO AUTOCORRELATOR--←--

MODELOCKED KRYPTON ION
$t_p = 80ps$, AVE.POWER=1W

M_1

M_2

M_3

M_4

ACTIVE
JET

TUNING
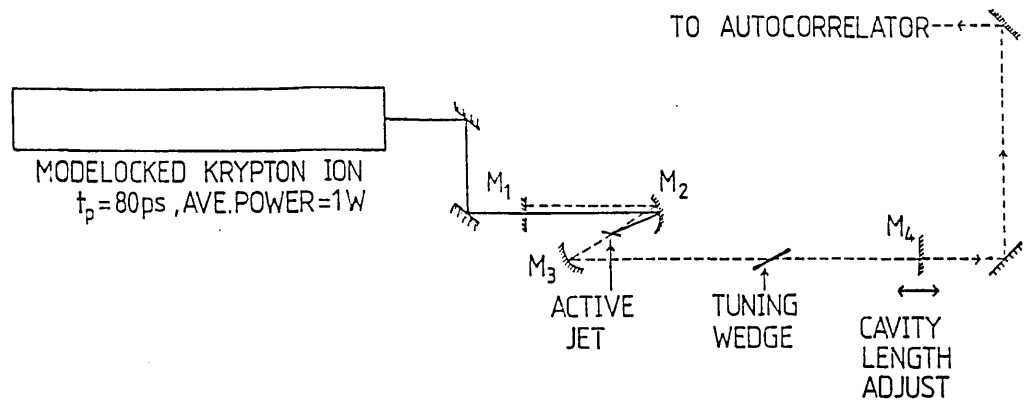WEDGE

CAVITY
LENGTH
ADJUST

Fig 4.13:   The modified cavity used for studies of the hybrid mode-
            locking of R700 with the laser active dye HITCI as the
            saturable absorber.

pulse train is extremely noisy. In order to "clean up" the train, and reduce the pulse

duration, a small amount of saturable absorber was added to the R700 circulator. In

this case the laser active dye HITCI was used. The absorption band of this dye (shown

in fig 4.11c.) has a peak absorption at ~740 nm, in an ethanolic solution, and an

absorption cross-section measured to be 9.1×10^{-16} cm^2. This dye also exhibits a strong

photoisomer which has a peak absorption at ~ 770 nm [27].

3
2
1
0

$t_p = 3.0ps$

$t_p = 0.64ps$

$t_p = 0.55ps$

3.3ps

3.3ps

3.3ps

(a)

(b)

(c)
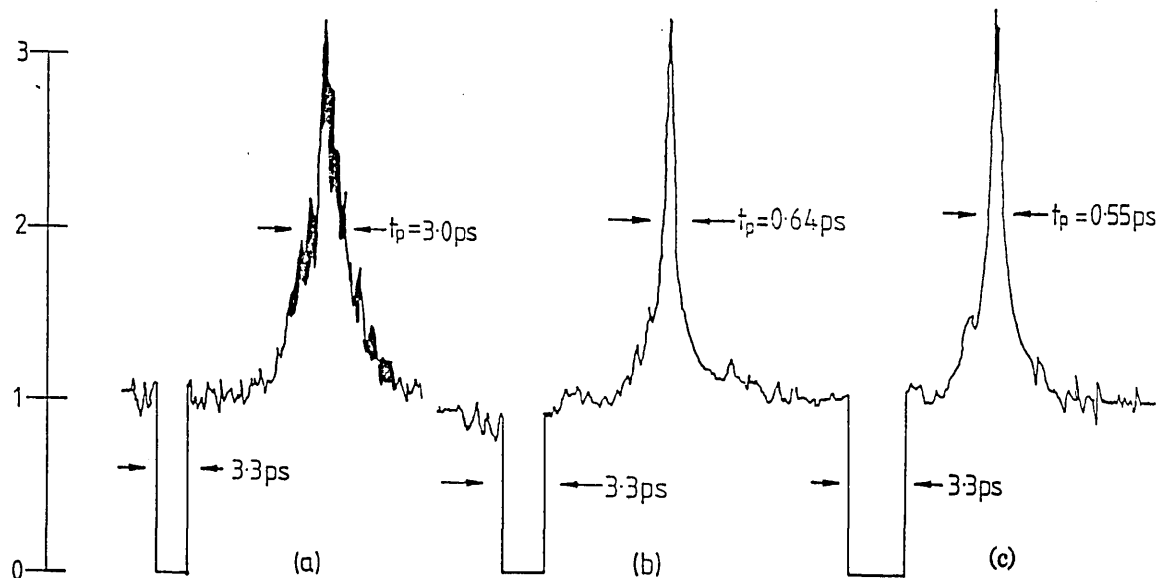
Fig 4.14:   The duration of the R700 dye laser pulses at 771 nm with (a)
            no   saturable   absorber   present,   (b)   an   absorber
            concentration of 3.4×10^{-5} mole/litre and (c) the shortest
            pulses generated at the absorber concentration of 3.4×10^{-5}
            mole/litre.

The wavelength of the dye laser tuned to 770 nm and the addition of a small concentration (0.5×10^{-5} mole/litre) of the saturable absorber to the R700 dye circulator resulted in a noticable reduction in the noise present on the pulse profile together with a slight pulse shortening. As the concentration of HITCI was increased the pulse shortening became more pronounced (see fig 4.14b) and at a concentration of 3.4×10^{-5} mole/litre pulses as short as 0.55 ps were produced, (see fig 4.14c) which were tunable from 770 - 785 nm. The effects of increasing absorber concentration on both pulse duration and pulse power are illustrated in fig 4.15.
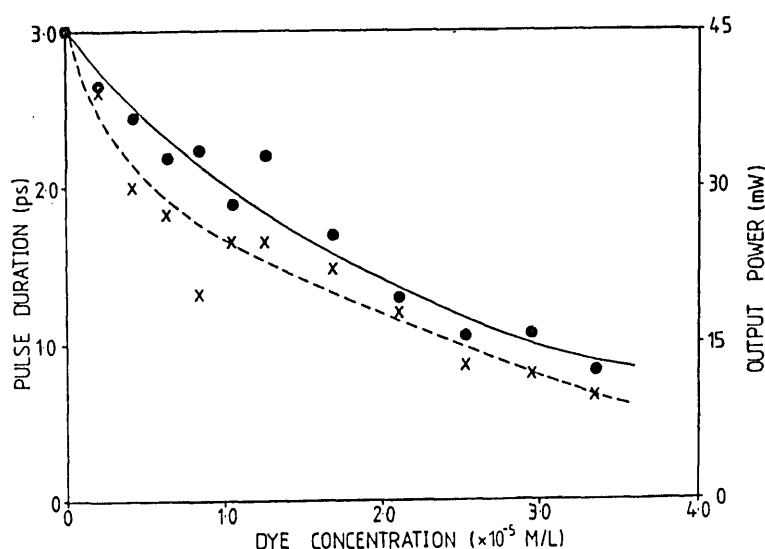
Fig 4.15:   The dependence of the pulse duration (dots) and the pulse average output power (crosses) on the absorber dye concentration for hybrid mode-locked operation at 771 nm.

4.4. The Passively Mode-Locked R700 Dye Laser.

The dependence of the pulse duration on the degree of matching between the pump and slave cavity lengths for both the purely sychronous and hybrid mode-locked R700 dye lasers is a limiting factor when used for the generation of ultrashort pulses. Any fluctuations in the drive or slave cavity lengths together with variations in the pump pulse duration lead to a degradation in the quality of the mode-locked pulses (see 4.2.3) and hence acts as a source of jitter. If the process of passive mode-locking could be implemented then the dependence of the pulse duration on the cavity length may be lifted and in this section the passive mode-locking of the R700 dye laser will be

described. This represented a major development in passively mode-locked cw dye lasers because since this work was reported [29] a wide range of active/passive combinations has been developed and passive mode-locking has been extended from 490 nm [28] to 780 nm [29] using dyes as the active media and 875 nm [30] using a colour centre as the active medium (see also chapter 7) . This range is to be compared to that which was previously restricted to the Rh6G/DODCI [31] combination or the quasi-cw flashlamp-pumped dye lasers which have been passively mode-locked [32-34].
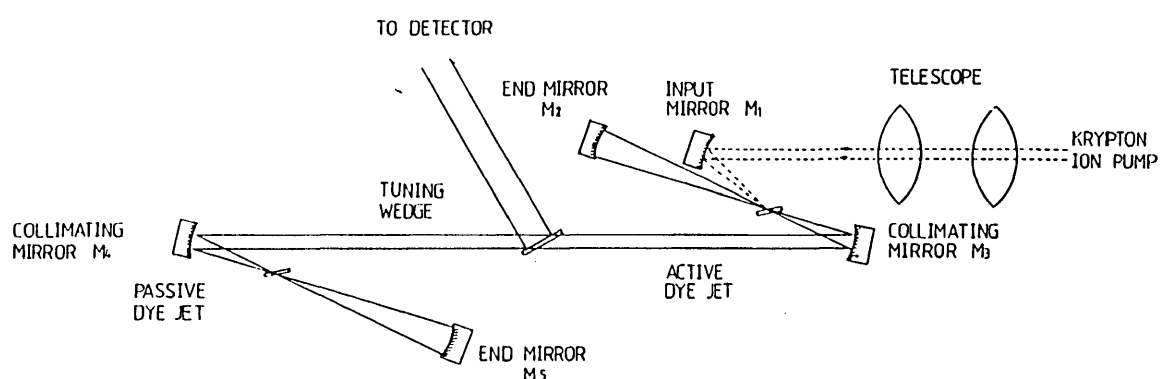
Fig 4.16: The passively mode-locked R700 dye laser cavity with external optics

The optical resonator used is illustrated in fig 4.16. It had a simple four mirror astigmatically compensated cavity [35] consisting of the gain folded section of the 375 dye laser and an independent passive folded section comprising the focussing mirror M_3 and the retro-reflecting mirror M_4. All the mirrors in the cavity were 5 cm radii of curvature mirrors and nominally 100% reflecting over the 700 - 800 nm spectral region. The two Brewster-angled dye jets, located at the foci of both the active and passive folded sections, were ~200 μm thick. The cavity was tuned using the standard dielectric tuning wedge,and the Brewster-angled reflection generated by the wedge served as the output signal. The Kr^+ pump beam, (P_{ave} 2.5 W), was coupled into the cavity using the beam steering mirrors and the telescope shown in fig 4.16. This telescope consisted of two anti-reflection coated 6 cm focal length lenses and although it

possessed unitary magnification it allowed for fine adjustments to be made to the size

and positioning of the focussed pump beam in the active jet.

As stated in chapter 3, for stable passive mode-locking to be achieved the S

parameter must be large. From the definition of the S parameter

$$S = K\frac{A_g \sigma_a}{A_a \sigma_g}.$$

(4.1)

where all symbols take the meanings described in 3.4. For the mirrors used in this

work the S parameter simply reduces to the ratio of the absorption cross-section to the

gain cross-section. The other requirements specified by New [36] for stable mode-

locking are satisfied as follows. The cavity period of 6.2 ns is much greater than the

gain recovery lifetime of 2.8 ns. The initial work was performed with the laser active

dye DOTCI with a lifetime measured to be 2.2 ns [5] and further work was performed

using the laser dye HITCI which had a lifetime of ~0.7 ns [37]. The concentration of the

DOTCI was 3×10^{-5} mole/litre and the pulse train produced by the combination of dyes

was monitored initially on a photodiode/sampling oscilloscope combination.

Subsequently the pulse train was monitored on a Photochron II streak camera which

revealed pulses as short as 12 ps from the dye laser, as shown in fig 4.17.

(a)   (b)   66 ps
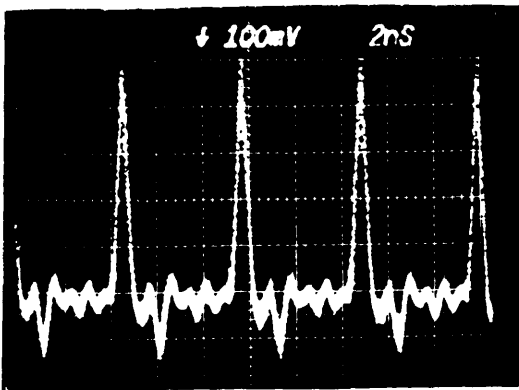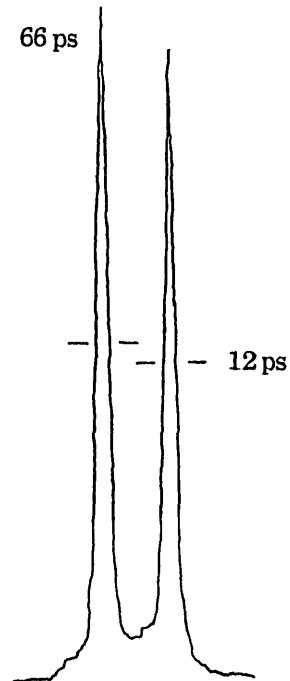

Fig 4.17:   (a) The passively mode-locked dye laser pulse train as
            recorded on a photodiode/oscilloscope combination and (b)
            the streak images associated the passively mode-locked
            pulse train.

The pulses were then coupled into an autocorrelator and pulses as short as 850 fs were measured over the 727 - 740 nm spectral region, illustrated in fig 4.18a. Average output powers as high as 20 mW, corresponding to peak powers of 1.5 kW were measured. These pulses were formed for pump powers ~200-400 mW above the mode-locking threshold (~ 2W). The addition of the fast recovery dye Diethyl-cryptocyanine, DCI (lifetime ~50 ps [37] and absorber cross-section 8.7×10^{-16} cm^2 at a wavelength of 705 nm (see fig 4.11)) lead to a reduction in the observed pulse duration. The shortest pulse durations were 350 fs, (see fig 4.18b), for this composite saturable absorber. Passive mode-locking of R700 was also demonstrated using HITCI as the saturable absorber. For an absorber concentration ~1 x 10^{-5} mole/litre, pulses of ~ 850 fs duration, (fig 4.18c), were generated over the 770-780 nm spectral region. These pulses had an average power of 10 mW giving rise to peak powers of 750 W per pulse.
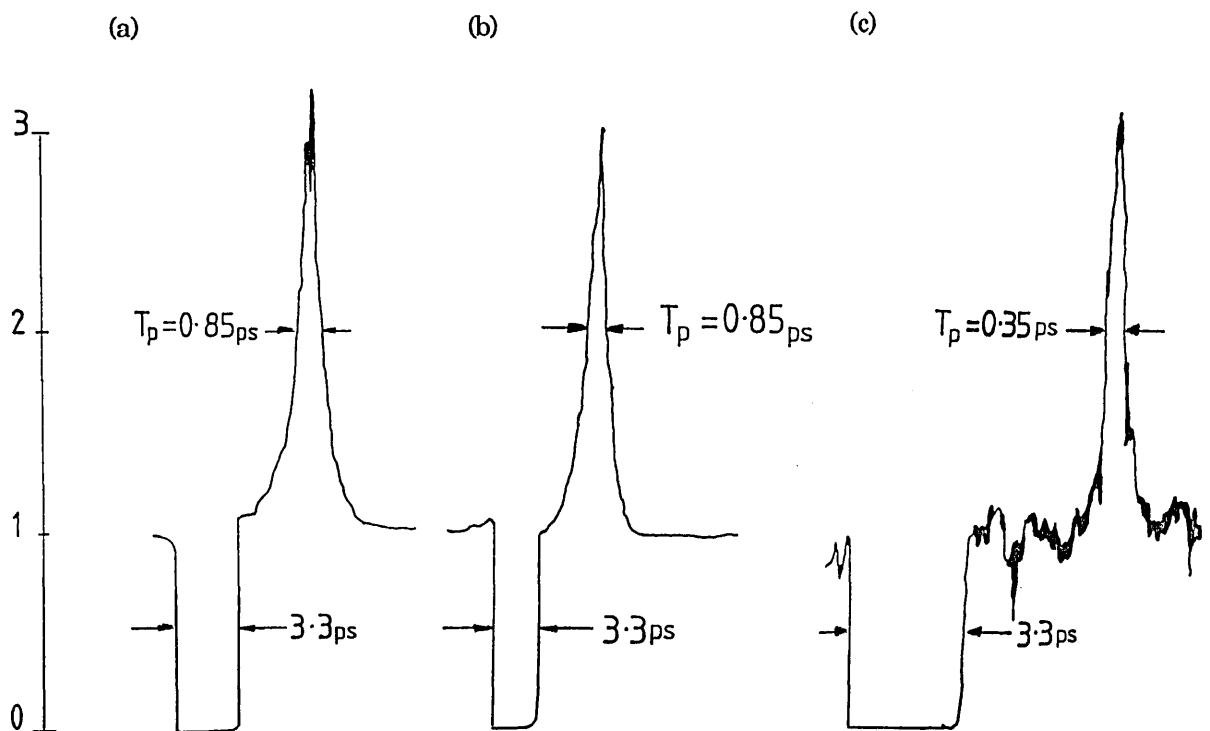
Fig 4.18: The autocorrelation traces recorded for the passively modelocked R700 dye laser with (a) DOTCI as the saturable absorber (λ= 730 nm), (b) the composite saturable absorber of DOTCI/DCI (λ = 740 nm) and (c) HITCI as the saturable absorber (λ = 770 nm).

For the main saturable absorbers, DOTCI and HITCI, described here no attempt was made to study the effects of varying the concentration on the pulse duration as the maximum power available from the Kr^+ at the time this experiment was performed was only 2.5 W and during the course of this investigation the power produced by the pump laser deteriorated quite rapidly.

4.5. Experimental Evaluation of Fibre Characteristics.

4.5.1. Introduction: Modal Dispersion in an Optical Fibre

Having studied the various experimental techniques available for ultrashort generation and the methods used to measure these pulses it was decided to apply the pulses generated by a synchronously mode-locked R700 dye laser as an experimental tool. It was mentioned in 4.1 that the original aim of this thesis was to study propagation effects in optical fibres at the zero dispersion wavelength. To become acquainted with optical fibres a study was made on a weakly multi-mode optical fibre.

When a laser pulse is coupled into an optical fibre, consisting of a core of refractive index n_1 and a cladding of index n_2 ($n_1 > n_2$) it is confined to the core by total internal reflections at the boundary between the cladding and the core. By solving the Maxwell equations associated with the propagation [38] it is found that several transverse electric and magnetic modes may be established in the fibre. These modes may be grouped together to form a set of linearly polarised modes, LP_{lm},(A mode of the form LP_{lm}, has m field maxima along a radius vector and 2l field maxima along the circumference.). The majority of the LP modes propagating in an optical fibre can be suppressed by making the refractive index difference between the cladding and the core as small as possible. When this is done only a few modes propagate down the fibre and the fibre is referred to as weakly guiding. Although several modes may propagate down a fibre at once they do not propagate with the same velocity and as a result a temporal separation will occur. The group delay of a particular mode group is dependent upon the material dispersion and the wave guide dispersion.

The modal dispersion can be found by following a treatment originally outlined by Gloge [39]. If an optical fibre consists of a core of radius a and refractive index n_c with a

cladding of refractive index n and extending to infinity, then a set of normalised parameters can be defined as

$$u = a(k^2 n_c^2 - \beta^2)^{\frac{1}{2}} \qquad (4.2)$$

$$w = a(\beta^2 - k^2 n^2)^{\frac{1}{2}} \qquad (4.3)$$

with β the propagation constant, and k the wave number in free space.

A normalised frequency v can be defined such that

$$v^2 = u^2 + w^2 \qquad (4.4)$$

which implies that

$$v = ak(n_c^2 - n^2)^{\frac{1}{2}} \qquad (4.5)$$

$$v = ak \, (n\Delta)^{\frac{1}{2}} \qquad (4.6)$$

with $\qquad \Delta = \dfrac{(n_c - n)(n_c + n)}{n} \qquad (4.7)$

Similarly the propagation constant can be interpreted in terms of a normalised constant given by

$$b(v) = 1 - \frac{[(\beta^2/n^2) - n^2]}{(n_c^2 - n^2)} \qquad (4.8)$$

which for small refractive index differences may be written as

$$b(v) = (\frac{\beta}{k} - 1)\frac{1}{(n_c - n)} \qquad (4.9)$$

giving $\qquad \beta = nk(\, b(v)\Delta + 1). \qquad (4.10)$

As a light pulse propagates down the optical fibre it experiences a group velocity dispersion given by

$$T_g = \frac{l}{c}\frac{d\beta}{dk} \qquad (4.11)$$

where l is the length of fibre, and c is the velocity of light in vacuum.

By inserting equation 4.9 into 4.10 and differentiating it is found that

$$T_g = \frac{l}{c}\left[\frac{dn(k)}{dk} + n\Delta\frac{dv(b)}{dv}\right] \qquad (4.12)$$

Here $\qquad \dfrac{dn(k)}{dk}$ characterises the material dispersion and is constant for all the modes, whilst

$n\Delta\dfrac{dv(b)}{dv}$ represents the wave guide dispersion

and can be expressed as

$$n\Delta\frac{dv(b)}{dv} = n\Delta(1-\frac{u^2}{v^2}(1-2K))$$ (4.13)

with K related to the field functions in the core and cladding. The curves associated with $\dfrac{dv(b)}{dv}$ are plotted in fig 4.19. The fields inside the core can be described by a set of

Bessel functions and those inside the cladding by a set of Hankel functions.Thus the

temporal difference between the LP_{lm} and LP_{01} modes is given by

$$\Delta T_{lm} = \frac{l\Delta n}{c}\{(\frac{dv(b)}{dv})_{lp} - (\frac{dv(b)}{dv})_{01}\}$$ (4.14)

By measuring the temporal separation of various modes, certain fibre parameters

may be evaluated. The typical separation between modes is ~100's ps and a streak

camera provides suitable resolutions for the measurement of such separations [40].
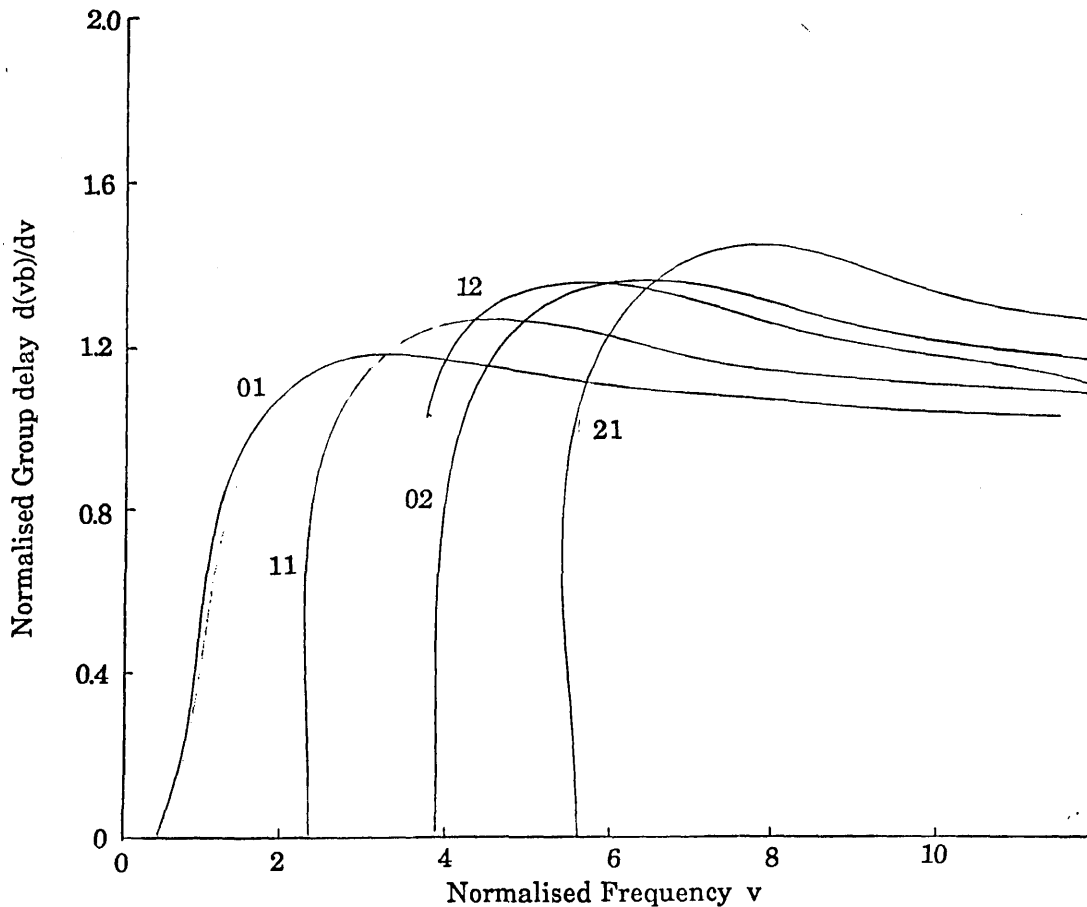
Fig 4.19: The normalised group delay $\dfrac{dv(b)}{dv}$ as a function of the

normalised frequency (taken from ref 40).

4.5.2. Experimental Determination of Fibre Characteristics Using a Synchroscanning Streak Camera in Conjunction with a R700 Dye laser.

The streak camera, when operated in a synchronous mode with a repetitive pulse source has been shown to be useful tool for the study of events in the pico-second time domain [41]. One possible application is the study of the propagation of ultrashort light pulses down an optical fibre.

A 51.5 m sample of optical fibre was used as the test fibre (this fibre was supplied by Optical Fibres Deeside Clwyd, Wales) and was nominally single mode at 1.3 μm with a core radius of a = 4.66 μm and refractive index difference $\Delta = 3.4 \times 10^{-3}$ [42]. However at the operational wavelength of the R700 dye laser the fibre was weakly multi-mode. The experimental arrangement employed is depicted in fig 4.20. The synchronously mode-locked R700 dye laser produced pulses of ~1 ps in duration. Although no attempt was made to continuously monitor these pulses on a real-time autocorrelator the stability of the pulse train produced by the dye laser was monitored on the photodiode/oscilloscope combination. Instead the pulses were measured on a Photochron II streak camera. A small portion of the output train from the dye laser (~ 10 mw) was coupled into the optical fibre by a 20 X microscope objective. The coupling into the fibre was arranged so as to avoid optical feedback into the dye laser as this adversely affects the mode-locked performance of the dye laser [43]. After passage through the fibre the light was then re-collimated using a 10 X microscope objective before being coupled onto the slit of the streak camera. The rest of the dye laser pulse train was used to trigger the streak camera drive electronics. With the wavelength of the dye laser tuned to 705 nm the following modes were observed: the fundamental LP_{01} together with the LP_{11} and LP_{21} which were orthogonally polarised.The LP modes generated by the pulse propagating down the fibre were characterised by observing their field patterns on a screen and the polarisation of each set of modes was determined by using a linear polariser. The streaked images associated with modes showing their temporal separations together with their mode groups are shown in fig 4.21.It was found that the temporal separation of the LP21 and LP_{01} mode groups was 93 ps and that of the
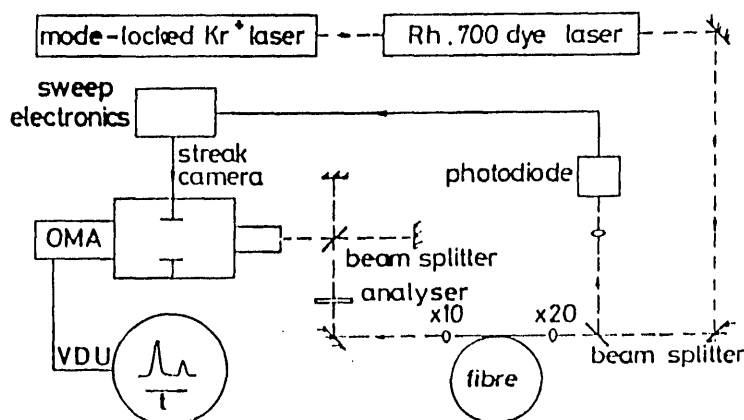
Fig 4.20: The experimental arrangement used to study the effects of
modal dispersion in optical fibres.

LP$_{11}$ and LP$_{01}$ was 105 ps.Using these two values, the core radius and refractive index

difference of the optical fibre could be evaluated. The derivatives $\frac{dv(b)}{dv}_{21,11,01}$ were

taken from the plot shown in fig 4.19. (This plot is taken from Fig 4 of ref 39).

Assuming a normalised frequency, v, ~4.12 and the values for $\frac{dv(b)}{dv}$ obtained from the

plot in fig 4.22, a value of Δ, $3.4 \pm 0.2 \times 10^{-3}$ was deduced using equation (4.14). The size

of the core radius, a, was also evaluated, using the expression for the normalised

frequency, (eqn. 4.6), and was found to be 4.64 ± 0.1 μm. The two values estimated from

the results obtained agree with those supplied by the manufacturer.
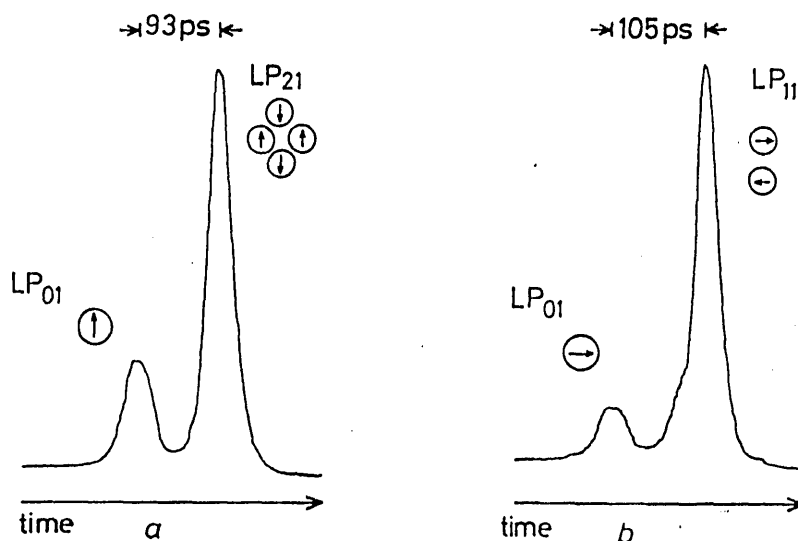
Fig 4.21: The temporal displacement of (a) the LP$_{01}$ and LP$_{21}$ mode
groups (vertically polarised) and (b) the LP$_{01}$ and LP$_{11}$
mode groups (horizontally polarised) for λ= 705 nm.

The cut-off wavelengths for the LP_{21} and LP_{11} modes were determined to be 755 ± 40 nm and 1.203 ± 0.06 μm respectively. As the cut-off wavelength for the LP_{21} mode lay well within the tuning range of the R700 dye laser the laser was tuned until the LP_{21} mode was no longer observed. This wavelength was found to be 745 nm. At this wavelength only the LP_{11} and LP_{01} modes were observed to propagate. The temporal separation of these two modes was found to be ~ 94 ps, as shown in fig 4.22, which agrees with the predicted value of, 96 ps obtained from equation 4.14, when a corrected normalised frequency which takes into account the change in wavelength has been used.
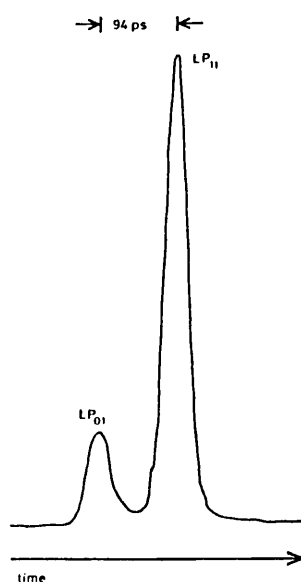
Fig 4.22:   The temporal displacement of the LP_{01} and the LP_{11} mode groups at a wavelength of 745 nm.
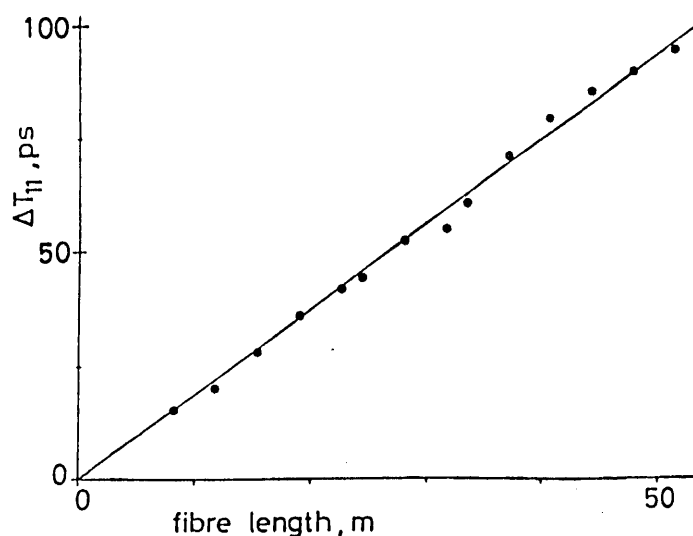
Fig 4.23:   A plot of the relative group delay of the LP_{01} and LP_{11} mode groups ($\Delta T11$) as a function of the fibre length (λ= 745 nm).

Equation 4.14 indicates that there is a linear relationship between the modal delay and the length of optical fibre. To verify this the length of optical fibre was continually reduced and the temporal separation measured. The variation between modal separation and the length of optical fibre are plotted in fig 4.23 and a gradient of 1.84 ps/m was estimated which agrees closely with the predicted value of 1.86 ps/m.

4.6.Conclusions

In this chapter the generation of ultrashort pulses from a R700 dye laser has been described. Pulses have been generated by exploiting both active and passive techniques with the passive arrangement being the first to cover a wavelength region different from that of the R6G/DODCI combination.The pulses generated by the active mode-locked R700 dye laser were used to characterise an optical fibre and values have been deduced for the core radius and refractive index difference between the core and the cladding using a streak camera based time domain studies. The use of a tunable pulse source has enabled the experimental determination of the cut-off wavelength of the LP_{21} mode group.

References:

1. L.F. Mollenauer in *Tunable Solid State Lasers* Eds J.C. White and L.F. Mollenauer Springer Verlag, Berlin 1986 Chp 6.

2. E.G. Marason; Opt. Commun., 40, 212, 1982.

3. R.K. Jain; Appl. Phys. Lett., 40, 295, 1982.

4. T.F. Johnston Jr., R.H. Brady, and W. Proffitt; Appl. Opts., 21, 2307, 1982.

5. T. Doust; Private Communication.

6. M.C. Adams, W. Sibbett and D.J. Bradley; Opt. Commun., 26, 273, 1978.

7. H. Harde and H. Burggrat; Opt. Commun., 38, 211, 1981.

8. N.J. Frigo, T. Daly and H. Mahr; I.E.E.E. J. Quant. Elect ., QE-13, 101, 1977.

9. C.P. Ausschnitt, R.K. Jain and J.P. Heritage; I.E.E.E. J. Quant. Elect ., QE-15, 912, 1979.

10. A. Scavannec; Opt. Commun., 17, 14, 1976.

11. P.G. May, W. Sibbett, K. Smith, J.R. Taylor and J.P. Wilson; Opt. Commun., 42, 285, 1982.

12. T.T. Basiev, N.S. Vorobiev, S.N. Mirov, V.V. Osiko, P.P. Pashinin, V. Postolov, and A.M. Prokhorov; J.E.T.P. Lett., 31, 291, 1980.

13. L.F. Mollenauer, N.D. Vieria and L. Szeto; Opt. Lett., 7, 414, 1982.

14. L. Isganitus, M.G. Sceats and K.R. German; Opt. Lett., 5, 123, 1980.

15. L.F. Mollenauer and D.M. Bloom; Opt. Lett., 4, 247, 1979.

16. R. Illingworth and I. Ruddock; Opt. Commun., 61, 120, 1987.

17. L. Reekie, I. Ruddock and R. Illingworth, in *Picosecond Chemistry and Biology*. Eds. T. Doust and M. West. Science Reviews Limited. 1983.

18. G.R. Fleming in *Applications of Ultrafast Chemistry*, Oxford University Press. 1986.

19. P.M.W. French; PhD. Thesis University of London 1987.

20. G.W. Fehrenbach, K.J. Gruntz and R.G. Ulbrich; Appl. Phys. Lett., 33, 159, 1978.

21. Y. Aoyagi, Y. Segawa and S. Nariba; Japan J. Appl. Phys., 20, L1595, 1981.

22. Y. Ishida, K. Nagamima and T. Yajima; Japan J. Appl. Phys., 21, L312, 1982.

23. G.A. Mourou and T. Sizer II; Opt. Commun., 41, 47, 1982.

24. K. Smith, W. Sibbett and J.R. Taylor; Opt. Commun., 49, 359, 1984.

25. J. Dobler. H.H. Shulz and W. Zinth; Opt. Commun., 57, 487, 1986.

26. M.D. Dawson, T.F. Boggess and A.L. Smirl;Opt. Lett., 12, 123, 1976.

27. J.P. Fouassier, D.J. Lougnot and J. Faure; Opt. Commun., 23, 263, 1977.

28. P.M.W. French and J.R. Taylor; Appl. Phys. Lett., 50, 1708, 1987.

29. K. Smith, N. Langford, W. Sibbett and J.R. Taylor; Opt. Lett., 10, 559, 1985.

30. N. Langford, K. Smith and W. Sibbett; Opt. Lett., 12, 903, 1987.

31. E.P. Ippen C.V. Shank and A. Diennes; Appl. Phys. Lett., 21, 348, 1972.

32. R. Wyatt; Opt. Commun., 38, 64, 1981.

33. W. Sibbett and J.R. Taylor;I.E.E.E. J. Quant. Elect ., QE-19, 558, 1983.

34. W. Sibbett and J.R. Taylor;I.E.E.E. J. Quant. Elect ., QE-20, 108, 1984.

35. H. Kogelnik. E.P. Ippen, C.V. Shank and A. Diennes; I.E.E.E. J. Quant. Elect ., 8, 372, 1972.

36. G.H.C. New; Opt. Commun., 6, 123, 1974.

37. J.R. Taylor. Private communication.

38. W. Sibbett and J.R. Taylor; in *Picosecond Chemistry and Biology*. Eds. T. Doust and M. West. Science Reviews Limited. 1983.

39. E. Snitzer; J.O.S.A., 51, 491, 1961.

40. D. Gloge; Appl. Opts., 10, 2252, 1971.

41. J.P. Wilson, W. Sibbett and P.G. May; Proc. 3rd Int. Conf. Picosecond Phenomena. Garmisch-Partenkirchen 149, 1982.

42. S. Hauge Optical Fibres Deeside Clwyd Wales. Private communication.

43. M. Hassinger and F.E. Lythe; Opt. Commun., 48,125, 1983.

Chapter 5: The LiF:F$_2^+$ Colour Centre Laser.

5.1. Introduction.

The previous chapter gave an outline of the generation and measurement studies made on the near-infrared laser active dye R700. This dye exhibited many of the characteristics of an F$_2^+$-type colour centre in that it had a large homogeneously broadened flourescence bandwidth and high gain and absorber cross-sections (typically 10^{-16} cm^2). However the aim of this thesis was to develop short pulse lasers in the near-infrared using colour centres as the gain medium. This chapter gives an outline of my initial studies in the field of colour centre lasers.

5.2. The Production of F$_2^+$ Centres in a LiF Host Crystal.

As described in 2.3, colour centres are simple point defects in an alkali halide lattice. The centre studied in this chapter was the F$_2^+$centre in LiF which was first observed as a laser active centre by Mollenauer in 1978 [1] and was further studied by Smith [2]. The centres are formed in the LiF host lattice by the established technique of electron damage and the method used is outlined in ref 5.2 and so a brief description of the production process is now given.

Boules of nominally pure LiF are annealed just below their melting point (~1000 K) in a vacuum oven for ~ 24 hours before they are allowed to cool back to room temperature. This removes any internal stresses and strains which may cause the boule to fracture when cut. Once annealed a [100] crystal lattice direction is located and the crystals are then cut and polished to give 2 x 10 x 10 mm crystal samples. Once prepared the crystals are encased in an aluminium-foil jacket and then subjected to a low temperature, (approximately 77 K in this case), irradiation with 1.5 MeV electrons, generated by a Van de Graaff generator [3]. The typical current densities incident upon the crystal are 0.5 μA/cm^2 and exposure times are typically of the order of 3 minutes. The aluminium-foil protects the surfaces of the crystals from any damage induced by the liquid nitrogen during the irradiation and subsequent storage. It also allows for the identification of the crystals after irradiation.Exposure of the crystal to the electron

beam results in the production of anion vacancies and F centres in the crystal lattice which are frozen into the lattice by cooling and storing the crystal at 77 K.

When needed, a crystal is selected from the storage dewar and allowed to warm up to room temperature. During the warming up period the crystal is kept in its aluminium jacket to protect the optical surfaces from condensation. Once the crystal has come up to room temperature, it is then removed from its foil jacket and the optical surfaces are inspected for any signs of damage. The crystal is then mounted on the cold finger (see 5.3.1) and re-cooled to 77 K. The annealing process out-lined above occurs in reduced light conditions to avoid photo-ionisaton of the F centres. The time taken from extraction of the crystal from the liquid nitrogen storage dewar to its subsequent re-cooling to 77 K, (~10 mins), is sufficient to allow the production of a high density of F_2^+ centres which are created in the following way. When the crystal is at room temperature the anion vacancies become mobile and migrate around the lattice. They may collide with the F centres forming F_2^+ centres but the F_2^+ centre is not the only species produced. During the irradiation process electrons are liberated into the lattice and they too become highly mobile when the crystal is warmed to room temperature. These electrons may also collide with the F centres to form F^- centres. In fact a whole variety of centres are produced ranging from F^- to F_3^+ centres [4]. Of these centres the F_2^- centre is important as it exhibits a peak absorption at 960 nm which is part of the region covered by the F_2^+ luminescence [4] and so acts as a source of loss in the crystal. These centres are easily ionised at room temperature and the liberated electron is passed into the conduction band of the lattice [5]. The F_2^+ is a strong electron trap which can capture these electrons and hence they lose their identity. This effect can be visualised by reference to fig 2.5.

5.3. The Colour Centre Laser.

5.3.1. The Resonator/Cryostat Assembly.

With reference to fig 5.1. and table 2.1 it can be seen that the absorption peak of the LiF:F_2^+ centre is situated around 645 nm and is well matched to the 647 nm and 676 nm lines of the Kr^+ laser used as the pump source. Optical excitation of the centre results in

the production of a broad luminsecence band extending from 0.8-1.0 μm   peaking around 910 nm (see fig 5.1). The high gain cross-section (~4.1 x 10^{-16} cm^2 [5]) allows for efficient laser operation to be attained with only modest centre densities (10^{17}-10^{18} /cm^3) and relatively thin crystals (~2 mm thick).

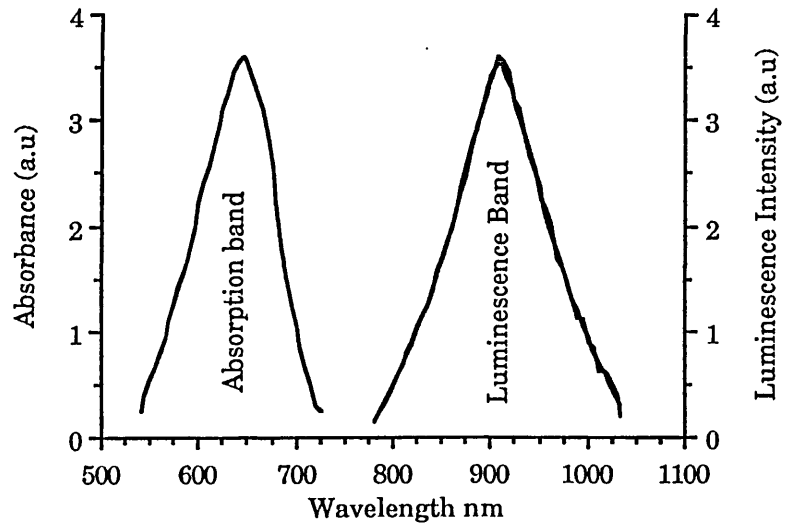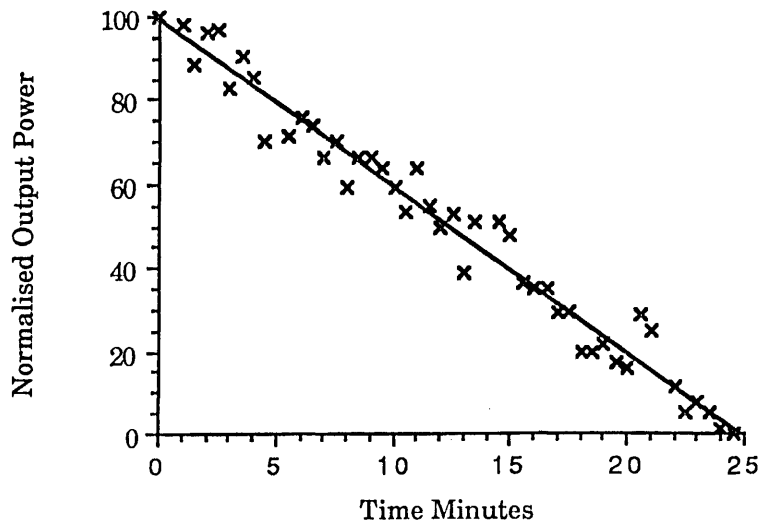Fig 5.1:   The absorption and luminescence bands of the LiF:F$_2$$^+$ centre (taken from ref 4).

Fig 5.2:   The decay of the normalised output power from the LiF:F$_2$$^+$ colour centre laser operating at room temperature as a function of time.

(a)

(b)
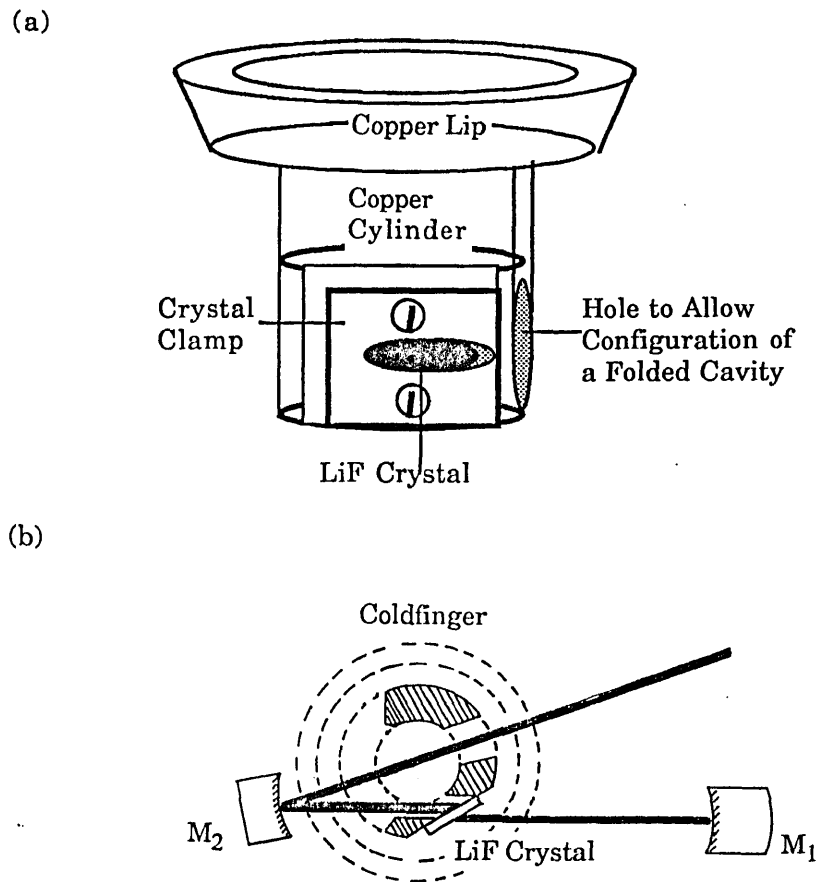
Fig 5.3:   (a) The vertical cold finger and (b) a schematic of the
holes present in the cold finger to allow the
development of a folded cavity and the processing of the
crystal.

Although the F_2^+ centre will lase at room temperature it is   stable for about

30 minutes only (see fig 5.2). Efficient long-term stable operation is obtained from the

$LiF:F_2^+$ centre if it is cooled to 77k. This was accomplished by using liquid nitrogen as

the coolant. To minimise the liquid nitrogen   boil-off rate and eliminate problems

associated with water condensation the crystal must be maintained in a suitable

vacuum enclosure. The resonator/cryostat combination which was used for the initial

studies of the $LiF:F_2^+$ centre has been fully described in ref 5.2. However a brief

description will be given as this will help me to illustrate inherent problems in its

design, which were overcome in later work by a radical redesign of the

cryostsat/resonator combination. The components of this initial laser can be

categorised as follows;(i) the cold finger, used for making thermal contact between the crystal and the liquid nitrogen reservoir,(ii) the vacuum assembly, and (iii) the optical resonator. These are described in greater detail in ref 5.2. The crystal is attached by a spring loaded clamping plate to the vertical cold finger shown in fig 5.3. Care has to be exercised to avoid damaging the crystal when attaching it. To improve the thermal contact between the crystal and the cold finger a sheet of indium is placed between the two. To maximise the thermal gradient between the cold finger and the base of the optical resonator a P.T.F.E. pad, with a locating pin (these are not illustrated in fig.5.3a), is attached to the bottom of the coldfinger. The locating pin ensures that the cold finger is inserted into the laser cavity with the crystal presented at Brewster-angle to the intracavity flux. To allow the development of a folded cavity, a set of holes has been drilled through the walls of the coldfinger (see fig 5.3b).Once the crystal is located in the resonator chamber thermal contact can be made between the coldfinger and liquid nitrogen coolant . The liquid nitrogen cryostat is shown in fig 5.4. The vacuum space, present to reduce the boil-off rate of the liquid nitrogen, is formed by the outer wall of the cryostat and the base plate. In the base plate is a gate valve which separates the cryostat vacuum space from the resonator vacuum space. To make thermal contact between the liquid nitrogen reservoir and the cold finger a set of extendible stainless steel bellows are attached to the bottom of the liquid nitrogen can. These bellows are detachable and a piece of indium wire is used to make the vacuum seal between the bellows and the liquid nitrogen can. The fabrication of a good vacuum seal was difficult and as a result high boil-off rates were experienced (typical hold-times of about 18 hours for the 5 litre liquid nitrogen can were observed).

To make thermal contact between the coldfinger and the coolant the liquid nitrogen dewar was placed on top of the resonator chamber. Vacuum integrity between the two was maintained by the O ring seal shown in fig 5.4. The resonator chamber was then evacuated using a rotary pump . Once the pressures in the two chambers were equal the gate valve was opened and the bellows extended, as described in ref 5.2, until thermal contact was made with the cold finger. This was indicated by an increase in the boil-off rate. Once thermal contact had been established the system was allowed to stand for
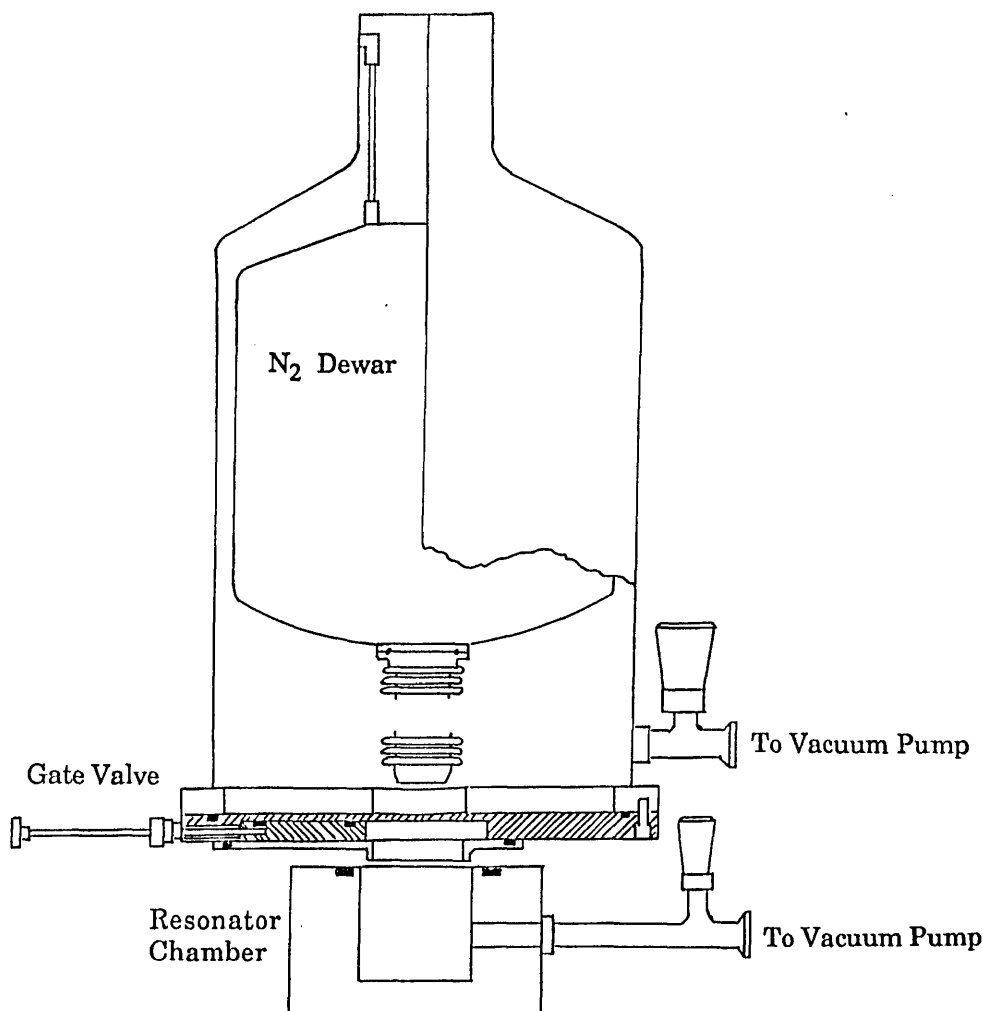
Fig 5.4:   The resonator/cryostat combination showing both the
           resonator chamber and the liquid nitrogen dewar.

approximately half an hour to ensure that the crystal was fully cooled before optical

excitation. The typical insertion time, from extraction of the crystal from the liquid

nitrogen store to making thermal contact between the cold finger and the stainless steel

bellows, was ~10 minutes.

The resonator chamber shown in fig 5.5. includes the two curved mirrors M_1 and

M_2 (radii of curvature 37.5 and 50 mm respectively). It also incorporates three

windows namely: the Brewster-angled Infrasil window, which allows the radiation

from the $LiF:F_2^+$ centre to be coupled out of the chamber whilst maintaining vacuum

integrity, the processing window, which allows for external processing of the crystal,

and the observation port. In order that the crystal be optically excited, the Kr^+ pump

beam is coupled into the cavity via the mirror M_1. The back surface of the mirror is

curved with a radius of curvature of 16 mm which means that the complete input coupler

acts as a lens of focal length 27 mm . The dielectric coating on M_1 is dichroic with low

reflectivity at 647 nm and 676 nm pump wavelengths but high reflectivity in the

luminescence band from 950- 1350 nm. In later work a slightly different input mirror

was used with a suitable dielectric coating to allow the full tuning range of the

F_2^+ centre to be exploited (800 - 1000 nm), however an additional 10 mm focal length

lens was necessary to allow optimum focussing of the pump beam into the crystal.
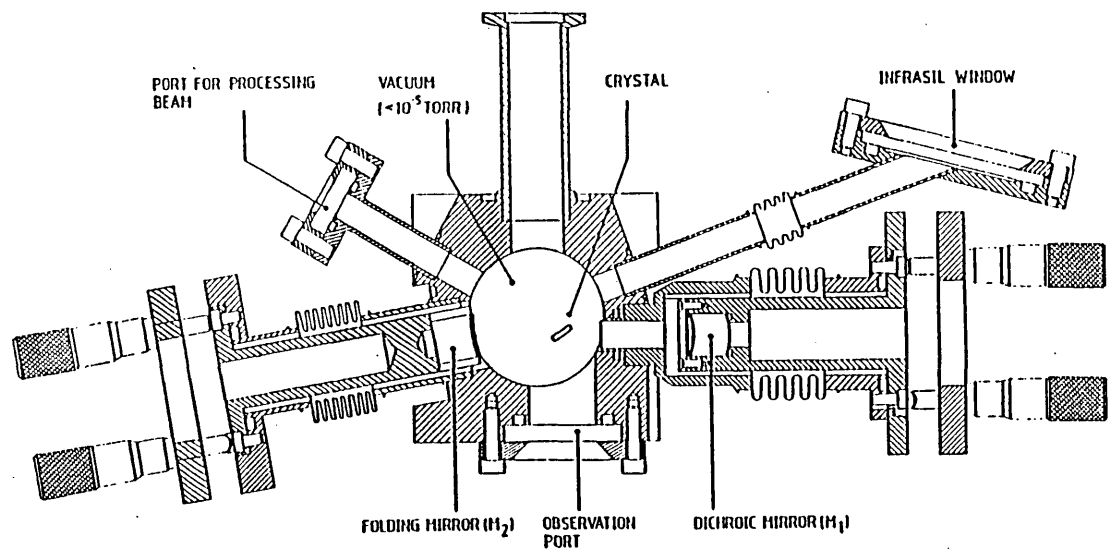
Fig 5.5: The resonator chamber showing the internal optics
and windows.

The cavity was completed by the output coupler M_3. With the three mirrors arranged

to form an astigmatically compensated cavity as described in 2.4.1. and for a crystal

thickness of 2 mm , the folding angle, 2θ, was calculated, using eqn. 2.39, to be 20°. A

stability region of 1.25 mm was calculated from eqn. 2.29 assuming a cavity length, d_2,

of 50 cm and a focal length,f, of 25 mm.

As both mirrors M_1 and M_2 were inside the vacuum chamber, all movements were

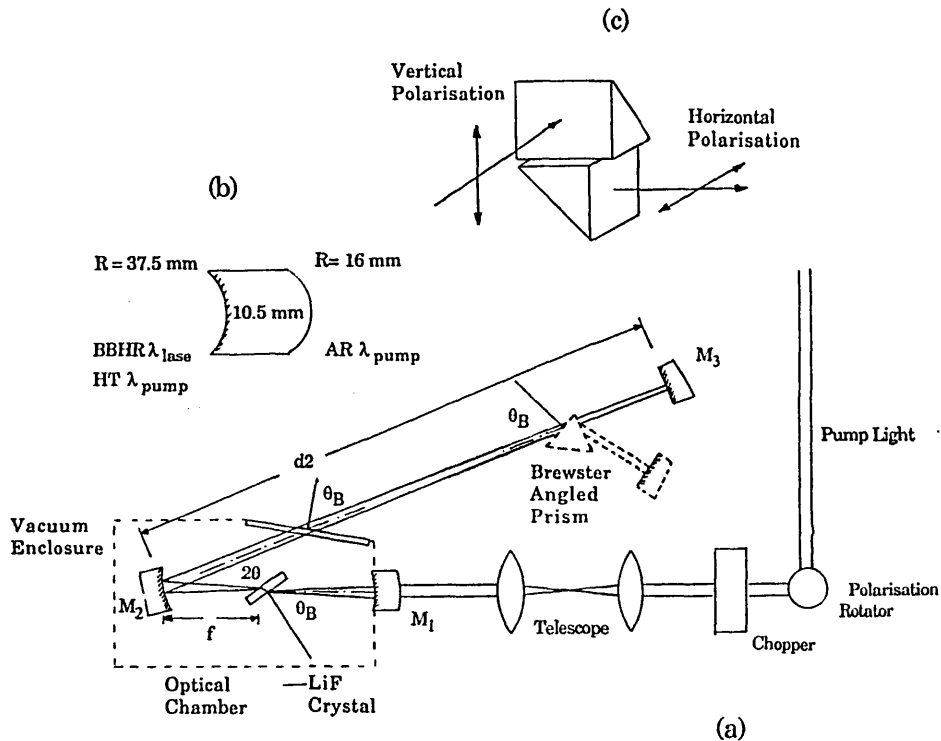made using translation stages and micrometers attached to flexible bellows. However

(c)

Vertical Polarisation

Horizontal Polarisation

(b)

R = 37.5 mm   R= 16 mm

10.5 mm

BBHR λ_{lase} AR λ_{pump} M_3

HT λ_{pump}

θ_B

Pump Light

d2

θ_B **Brewster Angled Prism**

Vacuum Enclosure

2θ

M_2 θ_B M_1 **Telescope**

f   **Chopper**

Polarisation Rotator

Optical Chamber   **—LiF Crystal**

(a)

Fig 5.6:   (a) The original LiF:F$_2^+$ resonator showing both the
            resonator optics and the external beam stearing optics,
            (b) the input coupler and (c) the prism assembly used
            for polarisation rotation.

the presence of the bellows meant that fine control of both the pump spot and the cavity

alignment could not be achieved readily and so most of the alignment had to be

performed prior to the evacuation of the crystal chamber. By the addition of an

extracavity telescope of unitary magnification, comprising two 60 mm focal length

lenses with anti-reflection coatings centred around 650 nm, it was possible to fine tune

the focussing of the pump beam enabling better optimisation of the colour centre laser.

To excite the crystal efficiently, the polarisation of the Kr$^+$ had to be rotated from

vertical to horizontal polarisation and this was accomplished using the anti-reflection

coated prism assembly illustrated in fig 5.6. The complete cavity including external

beam steering components is shown in fig 5.6.

5.3.2. The cw Performance Characteristics of The LiF:F$_2^+$ Laser.

In this section the cw performance of the LiF:F$_2^+$ Laser is described. As the

luminescence band of the F$_2^+$ centre covers the spectral region from 750 -1100 nm, an
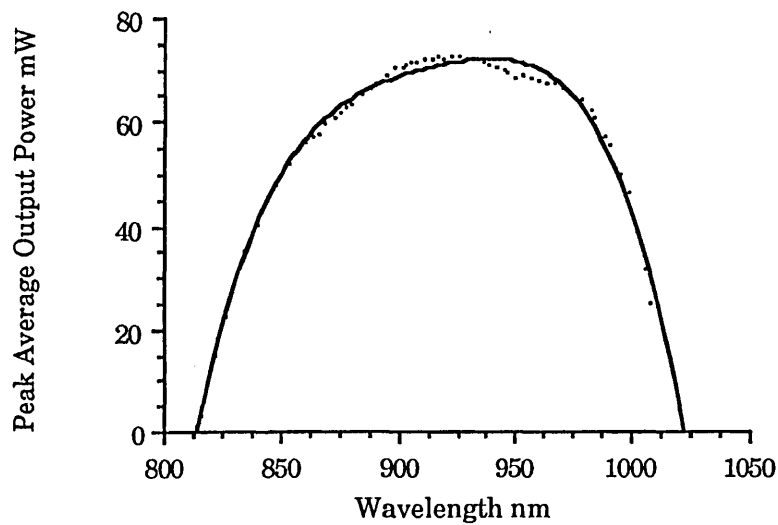
(a)
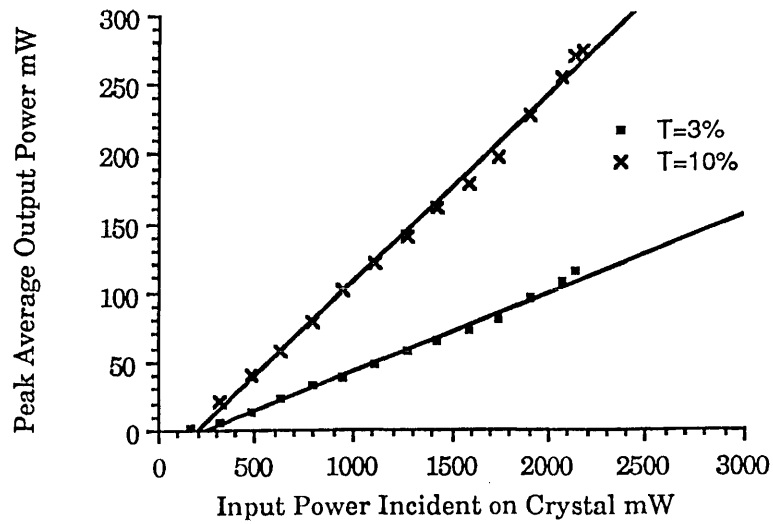
(b)

Fig 5.7:   The performance characteristics of the $LiF:F_2^+$ colour

centre laser (a) illustrates the peak average output

power observed from the centre as a function of input

power for two different transmission output couplers

(T= 3% and 10%), whilst (b) shows the tuning range of

the colour centre laser for a constant 1.9 W pump power

and a 3% output coupling.

infra-red viewer was used to observe the luminescence spots and laser beams. For the

F_2^+ centres under investigation here typical thresholds for laser action of ~150 mW

were routinely observed for a 3% output coupling. Fig.5.7a shows plots of the performance of the laser with regards to peak average output power against input power for two different transmission output couplers (T= 3% and 10%). The slope efficiencies observed were ~7% (T=3%) and ~18% (T=10%). The peak average power was evaluated by measuring the output power and multiplying by the chopping factor. For the work carried out here a chopping factor of ~13 was used and under these conditions the laser operated for ~150 hours before the laser emission stopped (This loss of laser action may be a result of the centre decays outlined in 2.3 or the result of ice forming on the crystal due to leaks in the vacuum chamber allowing water vapour into the resonator chamber). By measuring the output power for a selection of different transmission output couplers (T = 3%,10% and 37%) the small signal gain g_0, internal losses, l_i and optimum output coupler, T_{opt} could be evaulated.

The formulae used to estimate these quantities were (taken from [6])

$$P_{out} = \frac{kT}{\lambda^3}(\frac{T}{l_i + g_o}+1)$$ (5.1)

and $$T_{opt} = -l_i + \sqrt{l_i g_o}$$ (5.2)

were k is aconstant, and λ is the lasing wavelength

The values obtained were T_{opt} ~20%, go ~0.86 nepers and li ~13%.

Although reasonable efficiencies were observed for the $LiF:F_2^+$ system it should be noted that the cavity was strongly under-coupled and a T=20% transmission output coupler should be employed to obtain the optimum performance from the F_2^+ colour centre laser, however during the course of this work such a mirror was not available. These values agree with those predicted by Mollenauer for his $LiF:F_2^+$ laser [1].

The tuning range of the $LiF:F_2^+$ laser is shown in fig 5.7b. This was taken using a Brewster-angled prism as the tuning element . One of the Brewster-angled reflections from the prism served as a monitor signal which was coupled onto a monochromator. The pump power incident upon the crystal was 1.9 W (for higher pump powers it was found that the laser tended to oscillate on two or more wavelength bands). The output from the $LiF:F_2^+$ centre was observed to be tunable from 820 - 1000 nm (using the second input coupling mirror described in 5.3.1.). It should be noted that the longer wavelength

side of the tuning curve was not limited by the luminescent properties of the active centre but by the cavity optics employed (broad-band high reflectors 800-1000 nm). The output spectrum of the laser was also monitored on a .S1 PMT/chart recorder arrangement and it was seen that the spectrum was highly structured as illustrated in fig 5.8. This effect was attributed to Fabry-Perot type etalon effects in the cavity. The thickness of these etalons was deduced to be equal to a combination of the Brewster-angled window and the crystal [2].

1.45 nm —

885   886   887   888   889

Wavelength nm
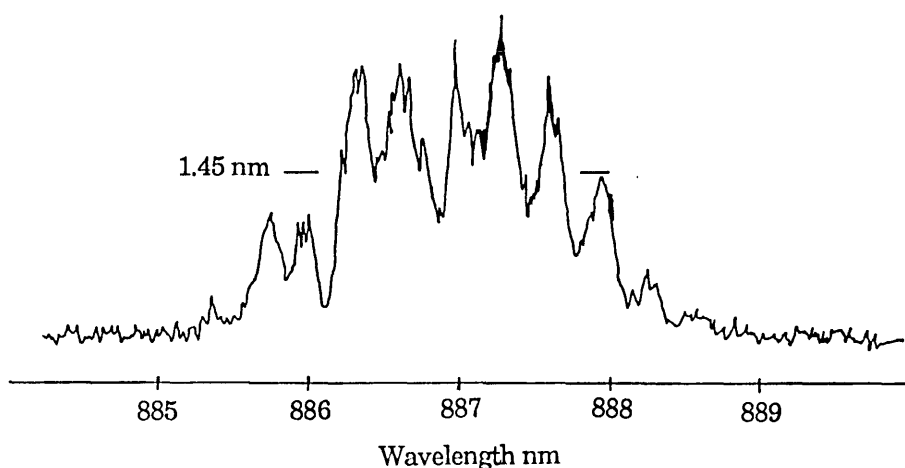
Fig 5.8:   The laser active bandwidth recorded from the LiF:F_2^+ colour centre laser operating at ~887 nm.

5.4. The Active Mode-Locking of the LiF:F_2^+ Laser.

5.4.1. Introduction.

The large homogeneously broadened luminescence bandwidth associated with the LiF:F_2^+ centre as well as its high gain cross-section and relatively short luminescence lifetime (29 ns [7]) should make a laser based on this centre a viable source of ultrashort pulses. To exploit these features I studied the active mode-locking of the colour centre laser.

5.4.2. The Acousto-Optically Mode-locked Colour Centre Laser.

The resonator described in 5.3.2 was modified by the insertion of an acousto-optic modulator (Spectra Physics 342 Modulator) between the folded mirror M_2 and the end mirror M_3. Under normal operating conditions the modulator is maintained in a

constant temperature oven to minimise the effects of temperature variations on the resonant frequency. (Any change in the heat load induces a variation in the modulator thickness which in turn affects the resonant frequency. The resonant frequency is also affected by the temperature dependent nature of the speed of sound and it should be noted that a 1° change in temperature leads to a 4.6 MHz drift in the resonant frequency). In the experiment performed here, to ensure that the intracavity flux passed through the same portion of the modulator cycle [8], the constant temperature oven was removed and replaced by a paper cowling. Although this cowling offered protection against external draughts it did not protect the modulator from internal temperature fluctuations arising from the interaction between the acoustic wave and the intracavity flux. This resulted in the resonant frequency drifting over a period of hours. A drive frequency of 79.5 MHz, amplified up to 1.4 W before being coupled to the modulator, was selected. This allowed the colour centre laser to be operated with a short, ~75 cm, cavity length (which corresponds to a cavity period of 5 ns).
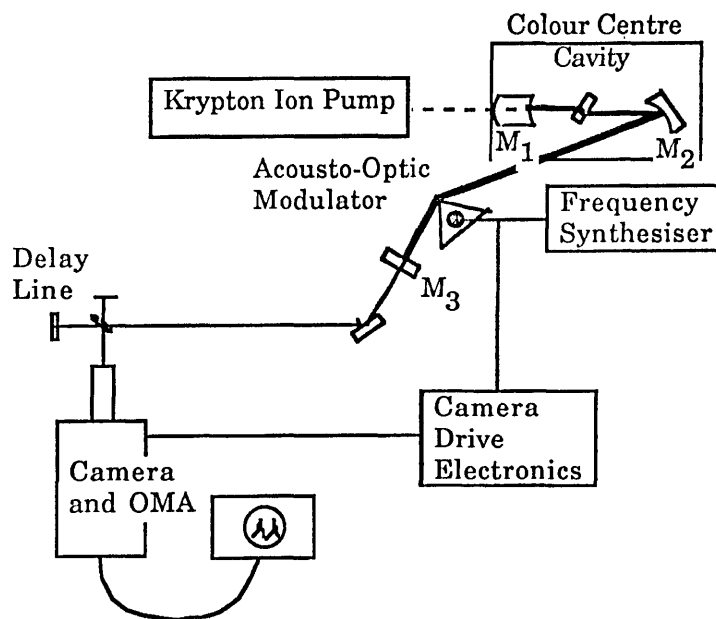
Fig 5.9:   The experimental arrangement used for the acousto-optic mode-locking of the $LiF:F_2^+$ colour centre laser.

To ensure a good match between the modulator and the resonator frequencies, the output coupler M_3 was mounted on a precision translation stage. The generated pulses

were measured using a synchroscan Photochron II streak camera and to ensure that the deflection voltage applied across the streak plates was in phase with the generated pulses the drive signal for the camera was taken from the frequency synthesiser. Using this method to drive the streak camera results in a greater system jitter and hence slightly broader pulses [9]. The experimental arrangement is shown in fig 5.9. A typical pulse generated by the acousto-optically mode-locked LiF:F_2^+ system is depicted in fig 5.10. The duration of these pulses was found to be ~25 ps with output powers of 5 mW, corresponding to peak powers of 13 W. They were recorded at a wavelength of 865 nm but pulses were observed across the entire tuning range of the laser.
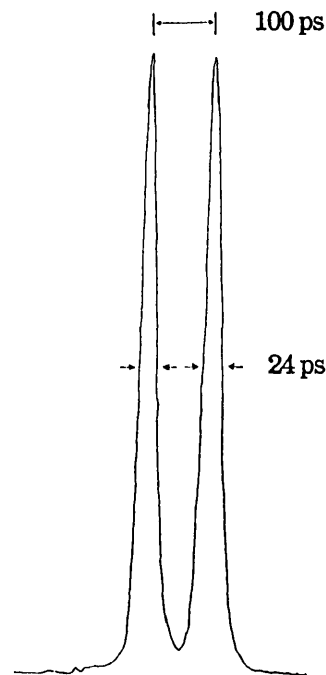
Fig 5.10:   The streak images associated with the shortest pulses generated from the acousto-optically mode-locked colour centre laser.

By considering the theoretical equation for t_p, the pulse width for an amplitude modulated homogeneously broadened laser, derived by Kuizenga [8]

$$t_p = \frac{\sqrt{2\ln 2}}{\pi} \left(\frac{g_0}{\delta l}\right)^{\frac{1}{4}} \left(\frac{1}{\Delta f f_m}\right)^{\frac{1}{2}} \tag{5.3}$$

nepers

where g_0 is the saturated gain taken to be 0.86, δl the modulation efficiency assumed to be 0.1, Δf the gain bandwidth which for LiF:F_2^+ is ~5 x 10^{13} Hz [5], and f_m is

the modulation frequency, in this case 79.5×10^6 Hz, pulses as short as 10ps are predicted.

The discrepancy between the calculated and observed pulse widths may arise from a number of sources: (i) When measuring the pulses the deflection voltage was derived from the frequency synthesiser and in this mode of operation a large interpulse jitter is introduced into the system which results in a reduction in resolution of the system[9].(ii) The predicted value of 10 ps assumes that the pulses are bandwidth limited and that the bandwidth is a smooth function. However, as illustrated in fig 5.8, the bandwidth is very strongly modulated due to Fabry-Perot etalon effects arising from internal reflections in the crystal and Infrasil window. This "channelling" will lead to some form of bandwidth restriction and hence broader pulses than those predicted.This has been observed by Johnston for his acousto-optically mode-locked MgF:Co laser [10].

It should also be noted that the calculation was performed using an equation derived for the active mode-locking of a Nd:YAG laser [8]. For this laser the lifetime of the excited gain medium ,230 μs, is greater than that of the cavity round trip time, typically 12 ns. This ensures that the laser gain is essentially time-independent and the saturation of the gain medium merely determines the value of the gain in relation to the average power in the cavity. However for the $LiF:F_2^+$ laser the gain recovery time, 29 ns, is comparable to the cavity round trip time, 5 ns, and so gain saturation should play an important part in the pulse formation process and the role of gain saturation is indicated by the reduction in the output power observed from the actively mode-locked colour centre laser when compared to the unmode-locked situation

It is well known that for an actively mode-locked laser the cavity length must be matched to the modulation frequency [8], thus cavity length detuning effects are important and these were investigated. Fig 5.11 shows the variation of the pulse duration with cavity length detuning. The results indicate that the cavity length detuning is asymmetric about the zero point (defined as the point of shortest pulses with no evidence of satellite pulses), with rapidly broadening pulses exhibiting a multi-pulse structure for negative detunings, whilst for cavity lengths greater than the
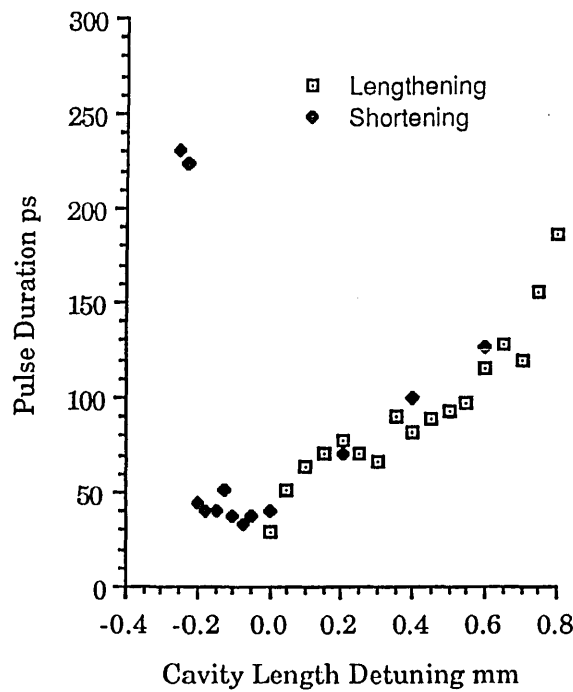
Fig 5.11:   The variation of pulse shape as a function of cavity
            length detuning.

optimum, the pulses broaden but remain symmetrical as illustrated in fig 5.12.These

results can be interpreted as follows. When the cavity length is correctly matched to the

modulation frequency an equilibrium condition is established whereby the pulse is

shortened by passage through the modulator but broadened by the gain medium. In fact

the modulator can be regarded as a filter influencing both the leading and trailing

edges of the pulse.For negative detuning the front edge of the pulse arrives at the

modulation cycle too early and so experiences a greater loss but any noise associated

with the tail of the pulse passes through the modulator. The pulse then propagates

through the gain medium where it is amplified. As the front portion of pulse has been

depleted by passage through the modulator, it does not fully deplete the gain and there is

still gain available to amplify the trailing edge of the pulse, and this may include

noise on the trailing edge. This results in the development of the observed multi-

pulsing. As the cavity length is further detuned, the front edge of the pulse is further

attenuated and more intracavity noise is allowed through the modulator which allows

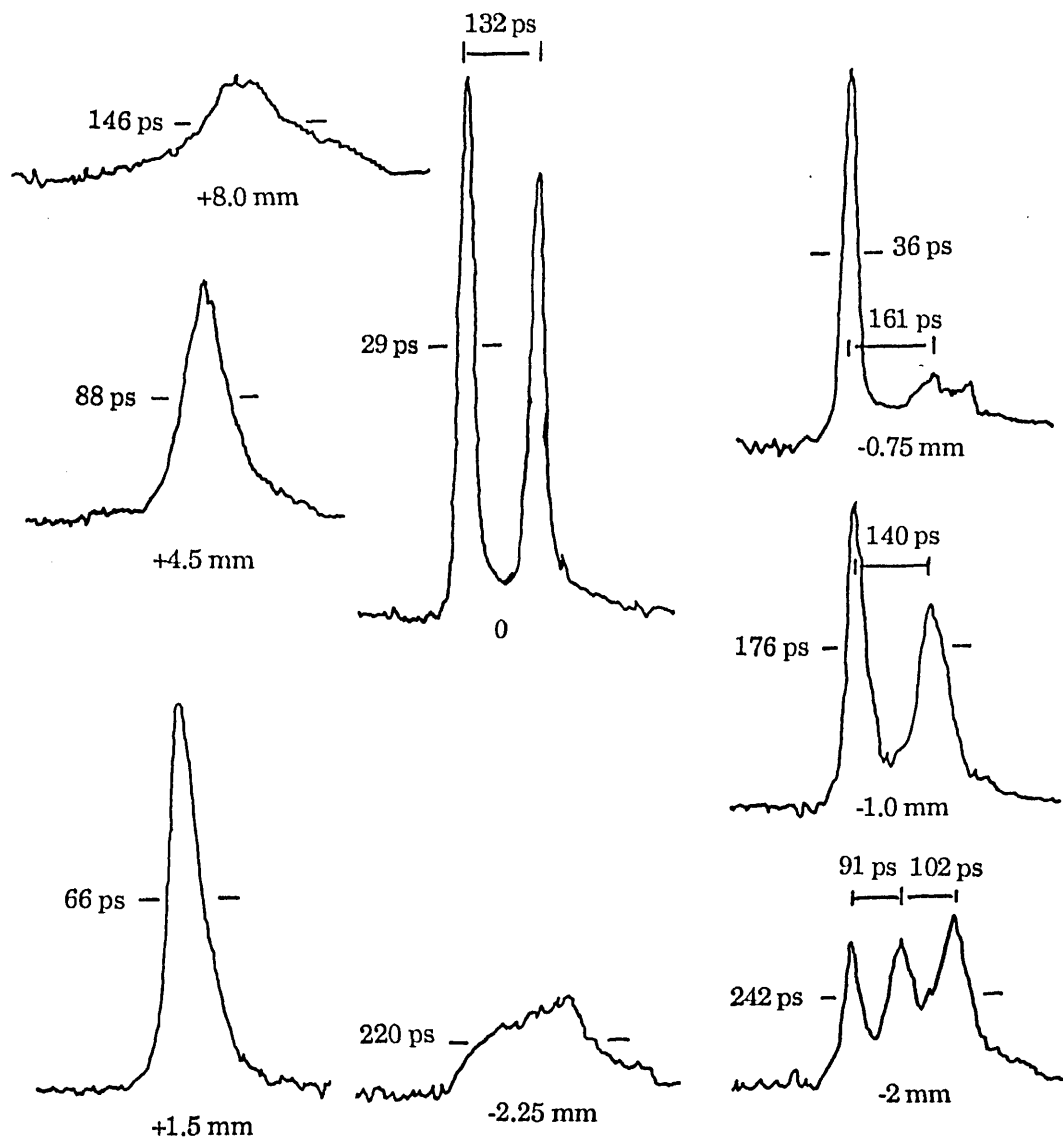the development of more satellite pulses, with none of the pulses being energetic enough

Fig 5.12:   The effects of cavity length detuning on the pulse shape
of the pulses generated from the acousto-optically
mode-locked colour centre laser.

to fully saturate the gain medium. This continues with further detuning until a single

broad pulse is observed. When the cavity is lengthened, (positively detuned), the pulse

arrives slightly later at the modulator and so the front edge of the pulse does not

experience the requisite loss to balance the broadening effects induced by the gain

medium.

From the plot illustrated in fig 5.11. it can be seen that the position of the shortest

pulse has altered to ~ -0.05 mm and the pulse width has broadened slightly to 33 ps.

These changes were attributed to a drift in the resonant frequency of the modulator. As mentioned previously, the experiments were performed with the modulator exposed to the atmosphere and no attempt was made to house the modulator in a constant temperature environment. As the experiment proceeded the modulator heated up leading to a shift in the resonant frequency. This in turn leads to a mismatch between the drive frequency and the resonance and hence a decrease in the modulation efficiency, thus resulting in an increase in the pulse duration (see eqn 5.3). Owing to this drift in resonant frequency no attempt was made to measure the effect of detuning the modulation frequency on the pulse duration.

5.4.3. The Synchronous Mode-Locking of the $LiF:F_2^+$ Colour Centre Laser.

A more efficient way to exploit the large homogeneous bandwidth of the F_2^+ laser and generate short pulses is to exploit synchronous mode-locking. Using an actively mode-locked Kr^+ laser as the pump source, Mollenauer has generated pulses as short as 4 ps from a $LiF:F_2^+$ system [11].

In the investigations carried out here the cavity period of the colour centre laser was taken to be half of the pump period. Although pulses as short as 20 ps see fig 5.13 were recorded, using a streak camera operated in synchronism with the laser pulse train, a second harmonic signal could not be observed. The reason for this was attributed to the effects of optical feedback degrading the pump laser pulse train. When monitoring the pump pulse train on the photodiode/oscilloscope combination it was observed that the train was seriously degraded by a diffuse reflection arising from the input coupler of the colour centre laser re-entering the pump resonator. Attempts were made to minimise the effects of this reflection by firstly positioning the input coupler at a given distance from the cavity where the feedback had minimum effect [12], (this was determined by reflecting a small portion of the light of a microscope slide into the cavity and watching the pump pulses on both the photodoide/oscilloscope combination and on the Photochron II streak camera), and secondly by mis-aligning the cavity sufficiently to reduce the amount of light re-entering the pump cavity. Although the first step taken reduced the effect of the feedback light it did not fully compensate for it and

the second resulted in much higher thresholds being observed. Thus attempts to synchronously mode-lock the laser active colour centre in this resonator were abandoned.
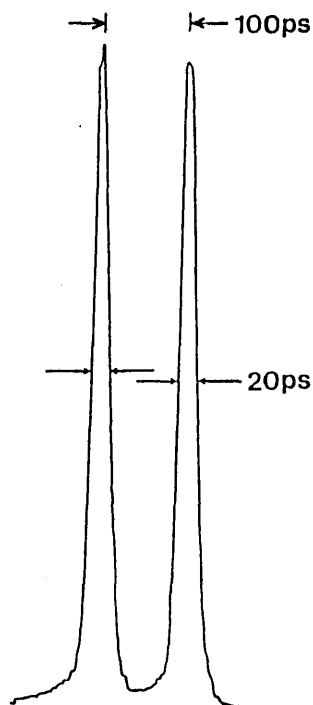

Fig 5.13:   Streak images associated with the synchronously mode-locked colour centre laser.

5.5. Conclusions.

In this chapter the performance characteristics of the home-built resonator $LiF:F_2^+$ laser were described. As with the R700 dye laser described in chapter 4, efficient operation was observed. However, unlike the R700 dye laser, short pulses could not be generated from the laser. This was a direct result of the colinear pumping of the centre, in that a small reflection of the back surface of the input coupler was reflected into the Kr^+ pump laser acvity, which resulted in a degradation of the Kr^+ pump train. A possible way of overcoming this problem is to use a non-colinear pumping scheme, as described in chapter 4 for the R700 dye laser, but due to the fact that the input and folding mirrors were located in the vacuum space of the resonator chamber, this could not be implimented. Thus a new resonator/cryostat combination was designed and this will be described in the next chapter.

References:

1. L.F. Mollenauer, B.M. Bloom and A.M. DelGaudio; Opt. Lett., 3, 48, 1978.

2. K. Smith; PhD. Thesis University of London 1985.

3. Thanks to A. Holman of The University of Reading for operating the Van De Graaff Generator.

4. J. Nahum; Phys. Rev., 174, 1000, 1968.

5. W. Gellermann, A. Muller, D. Wandt, S. Wilk and F. Luty; J. Appl. Phys., 61, 1297, 1987.

6. A. Yariv; *Optical Electronics* 3rd Edition Holt Sanders New York 1986 Chapter 4.

7. L. Bosi, C. Bussolati and G. Spinolo; Phys. Lett., 32A, 159, 1970.

8. D.J. Kuizenga and A.E. Siegman; I.E.E.E. J. Quant. Elect ., QE6, 694, 1970.

9. W. Sibbett; Proc. 13th International Conference on High Speed Photography and Photonics 1979.

10. B.C. Johnson, P.F. Moulton and A. Mooradian; Opt. Lett., 10, 4, 1984.

11. L.F. Mollenauer and D.M. Bloom; Opt. Lett., 4, 247, 1979.

12. M. Hassinger and F. Lytle; Opt. Commun., 48, 125, 1983.

Chapter 6:The Redesigned LiF:F$_2^+$ Colour Centre Laser.

6.1. Introduction.

The previous chapter described the performance characteristics of F$_2^+$ centres in a LiF host crystal. Although efficient performance was observed from the centre, certain operational problems were encountered, arising from the design of the resonator/cryostat combination and the manner in which the centres were optically excited.The first shortcoming related to the location of the mirrors M$_1$ and M$_2$ inside the vacuum space (see fig 5.5). Adjustment of these mirrors was made through the intermediacy of flexible bellows, which, on evacuation, tended to be rather insensitive to fine control, inhibiting the optimisation of the cavity . Also, as described in the previous chapter, it was difficult to maintain a reasonable vacuum in the cryostat and so the vacuum chambers had to be continuously pumped using either a diffusion pump or roughing pump. This resulted in the "backstreaming" of the vacuum pump oil into the resonator chamber which contaminated the mirrors, and over a period of several months the quality of the mirrors deteriorated, thus affecting the overall performance of the laser. The pump which was used to evacuate the chamber also suffered from mechanical vibrations which were coupled to the resonator chamber by the vacuum hosing connecting the chamber to the pump. These vibrations lead to resonator instability and could, if it was possible to synchronously mode-lock this cavity, degrade the mode-locked stability. The final and most restrictive problem encountered with the system arose from the colinear excitation of the crystal, whereby both the pump and laser beams follow the same path through the crystal. Although this arrangement allows for efficient operation it presents its own problems. The input coupler used in this work had a high quality anti-reflection coating applied to its back surface , but this did not prevent the production of a low intensity reflection which returned to the pump laser. Under continuous wave operation the presence of this feedback spot is of little significance but under mode-locked operation this reflected spot can seriously affect both the duration and stability of the output pulse train from the pump laser [1]. One possible solution to this problem is to use a Faraday rotator but this is an expensive

device and a more effective solution is to use a non-colinear pumping arrangement as applied to dye lasers.

6.2 The cw Performance Characteristics of the Redesigned LiF:F_2^+ Colour Centre Laser.

6.2.1 Introduction.

In order to resolve these problems, a resonator/cryostat combination was developed in which only the laser active crystal was maintained in the vacuum space, unlike any commercially available or home constructed colour centre resonator [2]. This arrangement allows for total control over the positioning of the resonator mirrors and enables both standing and travelling-wave resonators to be configured with both colinear or non-colinear pumping geometries. The resonator/cryostat is shown in figs 6.1 and 6.2 can be divided into three distinct parts; the cold finger (see fig 6.3), the cold face and the main vacuum chamber.
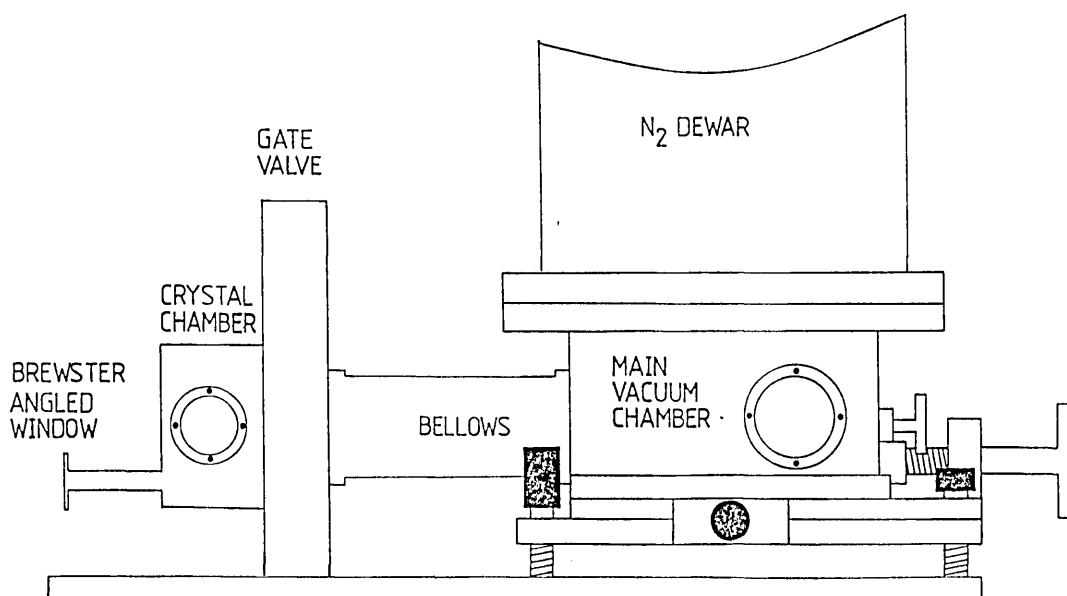
Fig 6.1:   A schematic of the redesigned colour centre cryostat showing the cold face , the cold arm and the liquid nitrogen dewar.

100
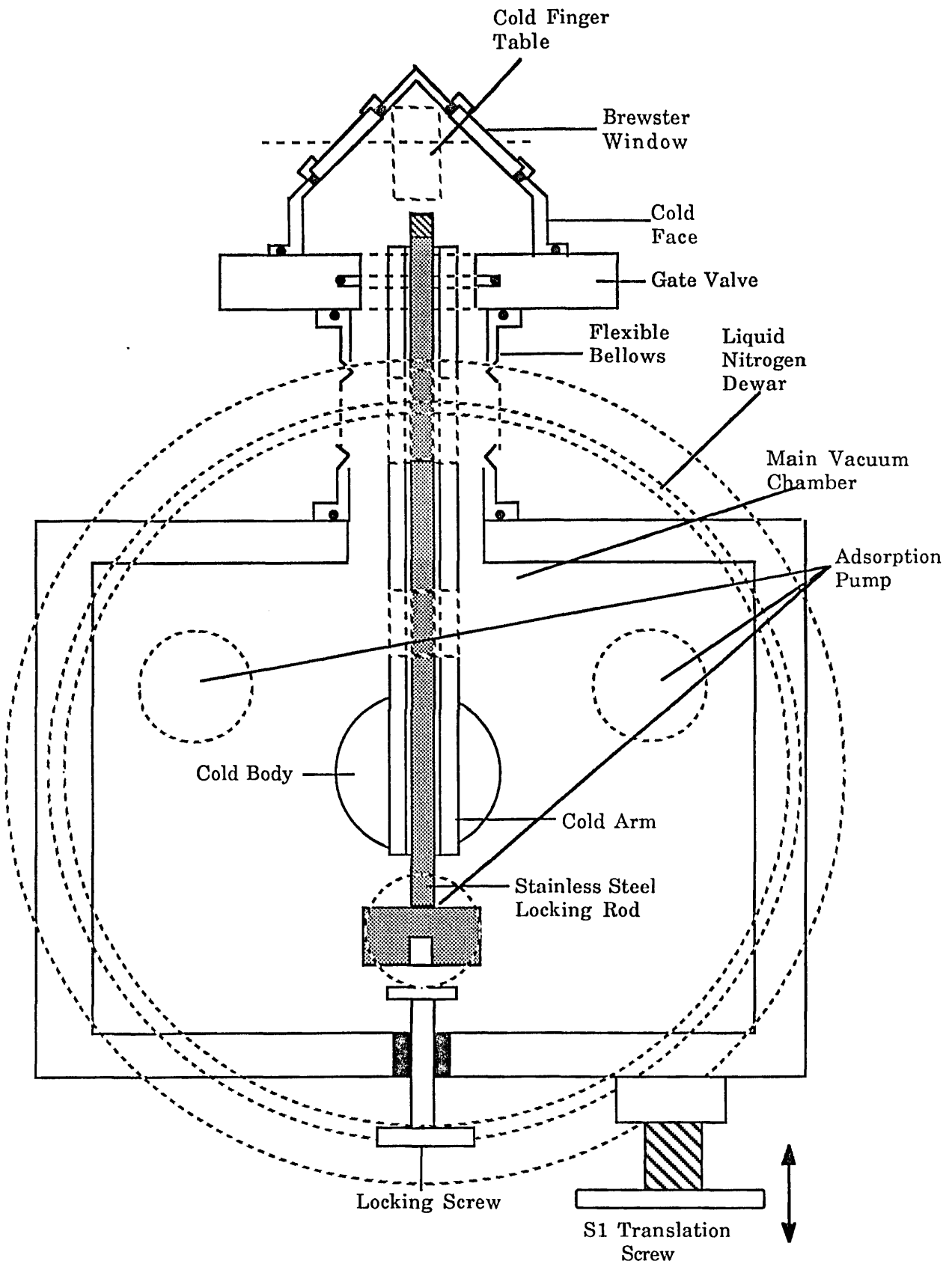
Fig 6.2: A schematic of the redesigned dewar showing the cold face, cold arm and cold body.

a

Coldfinger
locating   b
groove

A - A'

Locking
-screw holes
for crystal
clamp

Brewster
Angled
Facet
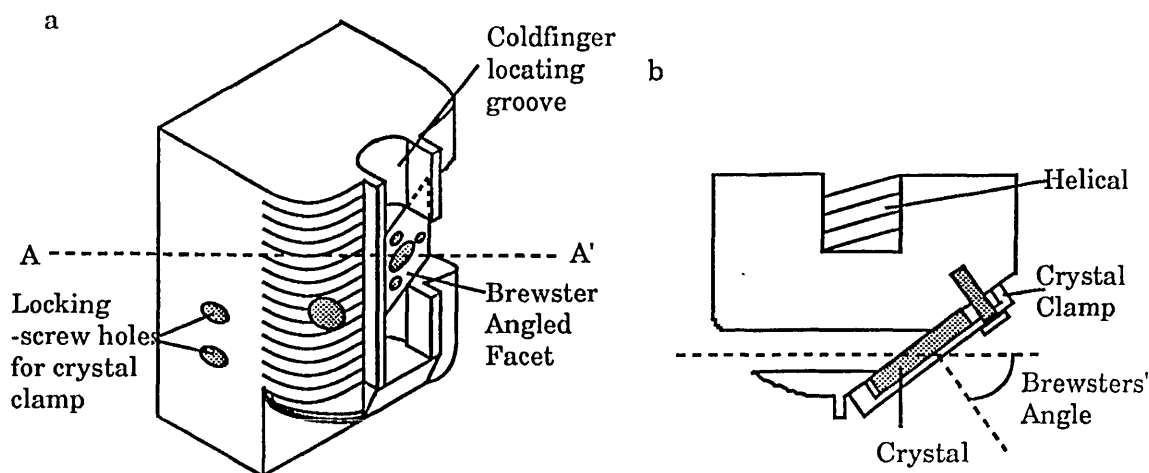
Helical

Crystal
Clamp

Brewsters'
Angle

Crystal

Fig 6.3:   (a) The horizontal cold finger and (b) a plan view of the
coldfinger taken on the line AA'.

The laser active crystal is mounted on the horizontal cold finger which is kept in

thermal contact with the liquid nitrogen temperature bath by a horizontal cold arm.

The cold face allows optical access to the crystal via the two Brewster-angled windows

and it also enables the crystal to be correctly positioned during the loading process. The

main vacuum chamber holds the liquid nitrogen dewar. To remove the need for

continuous vacuum pumping of this chamber three adsorption pumps are attached to the

liquid nitrogen dewar. These internal pumps result in liquid nitrogen hold times well

in excess of 36 hours for the 5 litre volume used as the temperature bath, which is a

marked inprovement on the original assembly.

6.2.2. Loading the Laser Active Crystal.

An irradiated crystal is removed from the liquid nitrogen store and processed as

described in 5.3.1. Once a region of strong coloration has been observed, the crystal is

placed in the clamp (illustrated in fig 6.2) with the coloured region closest to the two

threaded studs. The clamp is attached to the Brewster-angled facet on the cold finger

thus positioning the crystal in the correct orientation. The whole assembly is then

inserted into the cold face and maintained in the correct position by a locating groove

and table in the cold face. This small chamber is then sealed and evacuated. When the

pressures in the two chambers are equal the gate value of fig 6.2 is opened. The main

dewar is then translated until the cold arm makes contact with the cold finger which is

then attached to the cold arm by screwing a threaded stainless steel rod into the helical in the back of the cold finger. To ensure that good thermal contact is made between the two components a sheet of indium foil is placed between them and a thermal grease is applied behind the indium sheeting. This procedure can be performed in approximately five minutes. As for the original assembly, the crystal is left to stand for about half an hour before it is optically excited.

6.2.3. The cw Performance of the $LiF:F_2^+$ Centre Under Non-Colinear Pumping Conditions.

With only the active crystal located inside the vacuum space maximum flexibility over cavity design is afforded allowing both standing and travelling-wave resonators to be constructed and characterised.The basic linear cavity configuration is shown in fig 6.4. The polarisation of the chopped Kr^+ pump beam was rotated using two optical periscopes and this pump beam was coupled into the Brewster-angled LiF crystal by the plane mirror M_0 and the curved mirror M_1 (broad-band high reflector 640 - 960 nm, radius of curvature is 10 cm). The mirror M_2 (5 cm radius of curvature) acted as a retroreflector and the cavity was completed by the the plane end mirror M_3 which served as an output coupler. Frequency selection was effected by employing either a dielectric wedge or a Brewster-angled prism.
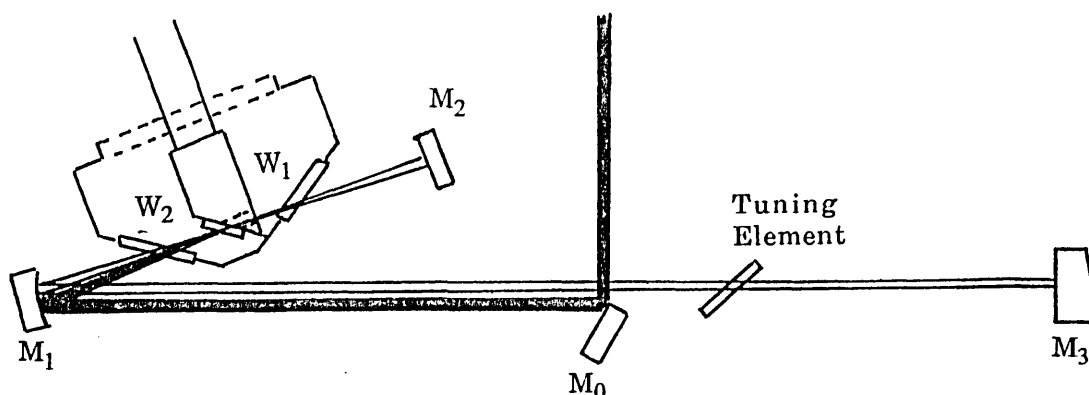

Fig 6.4:   The basic non-colinear excited colour centre laser cavity.

Astigmatic compensation of the cavity was ensured by selecting the folding angle such that it satisfied eqn. 2.39. However the presence of the Brewster-angled window between the folding mirror M_1 and the active crystal resulted in a further aberration term being included in 2.39 and so the folding angle, 2θ, was determined by the following equation.

$$fsin\theta tan\theta = (tgNg + tcNc) \tag{6.1}$$

where $t_{g,c}$ is the thicknesses of the window and crystal, $N_{g,c}$ are the normalised values for the crystal and window as defined by eqn. 2.40, and f is the focal length of the mirror M_1. Taking both the thickness of the Brewster-angled window and the thickness of the crystal to be 2 mm and n_g as 1.45 [3] and n_c as 1.39 [4], a folding angle of 22° was evaluated. By considering eqn. 2.29 a stability region of 5 mm was estimated (assuming a 50 cm cavity length).

The performance characteristics of this cavity were comparable to those obtained for the original cavity. Typical laser thresholds of 150 mW were routinely observed and thresholds as low as 70 mW have been recorded. The laser output power was measured as a function of input power, and slope efficiencies of 13% (3% transmission output coupler) and 25% (10% output coupling) were recorded, as shown in fig 6.5a. Again a 20% transmission output coupler was not available. This performance is somewhat better than that described for the original design (see 5.3.2), which may be a result of different crystals being used. A more valid comparison can be made by considering the values obtained for the small signal gain, g_0, and internal losses, l_i, associated with the two cavities. By using the equations outlined in 5.3.2 it was found that g_0 was 1.3 nepers, l_i, was 14% and t_{opt}, the optimum output coupling, was 22%. These values indicate that the non-colinear excitation of the $LiF:F_2^+$ colour centre is a viable process and as this excitation scheme eliminates the problems associated with optical feedback it should be possible to exploit the large homogeneously broadened bandwidth presented by this laser and generate short pulses from the laser via the technique of synchronous mode-locking.

The tuning range of the F_2^+ centre in this cavity is shown in fig 6.5b. It can be seen that the laser tunes from ~815 - 965 nm. The long wavelength side of the laser emission

is restricted to 965 nm, by reflectivity characteristics of the folding mirror M_1 used to

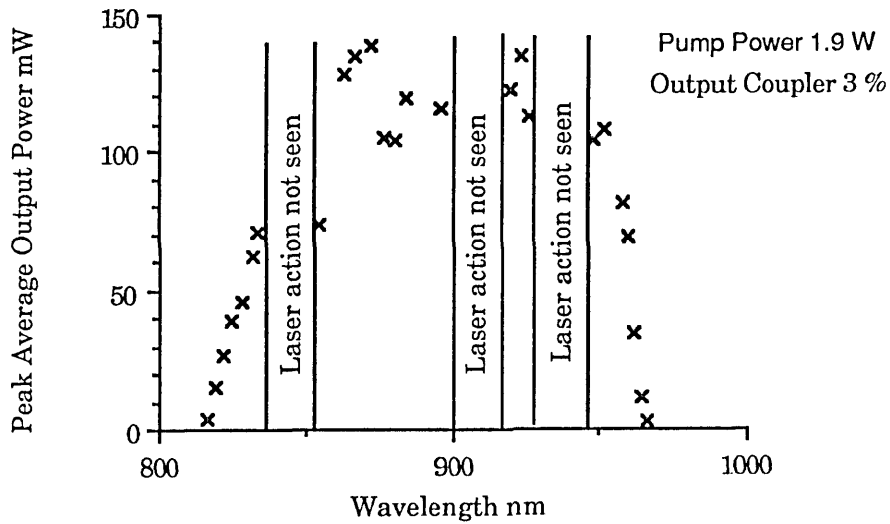focus the Kr^+ pump beam into the gain medium.

(a)
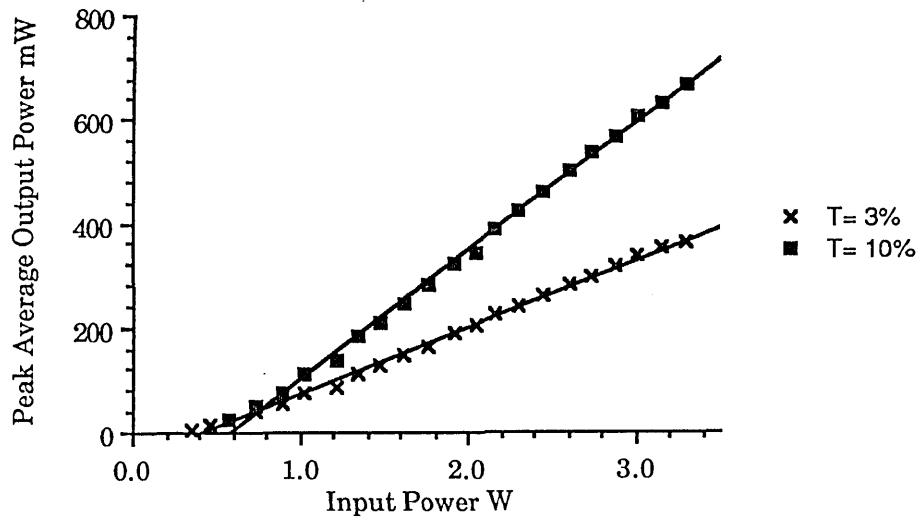
(b)

Fig 6.5:   The performance charateristics of the non-colinear
excited $LiF:F_2^+$ colour centre laser (a) represents the peak
average output power as a function of the input power for
two different output couplings and (b) the tunability of the
colour centre laser.

As all the reflecting optical components were located outside the vacuum chamber the configuration of a travelling-wave resonator was straightforward and this is illustrated in fig 6.6. The retroreflecting end mirror M_2 was replaced by another 10 cm radius of curvature mirror which served as a collimating mirror. The resonator was then completed by the plane 100% reflecting mirror M_4 which was oriented, together with M_3, to satisfy the travelling-wave conditions. With the ring employed in this work, thresholds of ~300 mW were observed and the output powers observed in both arms were comparable to those generated by the simple linear cavity. No attempt was made to operate the cavity in a unidirectional single longitudinal mode [5] but this has been demonstrated by other researchers using ring colour centre lasers [6,7]. For some applications relating to semiconductor studies, single longitudinal mode operation of this resonator will be evaluated.
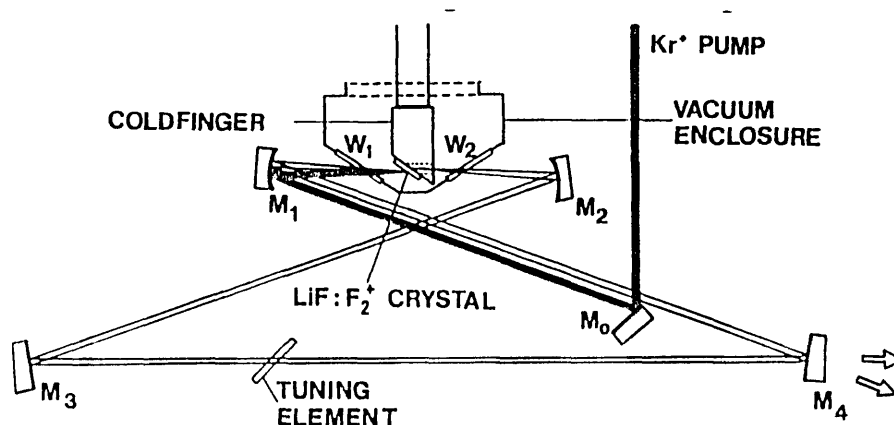
Fig 6.6:   A schematic of the ring colour centre cavity

The laser exhibited tunability over the 820-960 nm spectral region but certain wavelengths were excluded due to losses associated with the dielectric coatings of the mirrors used in the active folded section (see fig 6.5). One region of loss covered the 845-860 nm wavelength range. This would limit the role of the colour centre as a source for studies of exitonic resonances in GaAlAs multiple quantum well structures for example [8] but this could be overcome by replacing the mirrors used in the folded section with others which were totally reflecting over the full range of the F_2^+ luminescence band as well as being 100% reflecting at the Kr^+ pump laser wavelengths.

When the pump beam was chopped with a duty cycle reduction of 10X stable operation from the same active spot in the crystal was observed for approximately 200 hours before the threshold of the crystal doubled. The increase in threshold was attributed to the gradual de-ionisation of the F_2^+ centres through electron capture and the creation of other centres induced by the orientational rotation effect described in section 2.3. By relocating the crystal and finding another laser active spot the useful laser active lifetime of the crystal could be extended by another 50 hours. The improvement in the usable laser active lifetime was attributed to better thermal contact between the laser active crystal and the liquid nitrogen temperature bath. In the original laser (see chapter 5) thermal contact between the coldfinger and the temperature bath was accomplished through a set of stainless steel bellows. These bellows only came into contact with the lip of the copper cold finger and the nature of contact between the two was poor which resulted in bad thermal contact. Due to the presence of the holes in the original cold finger, to allow the formation of a folded cavity, the mass of copper near to the crystal was small and so the thermal mass was low. This meant that the heat dissipated into the crystal by the pump beam and the non-radiative decays associated with the laser active transitions could not be removed efficiently from the crystal. The modified cold finger of the new dewar was a solid block of copper (see fig 6.3) in good thermal contact with the copper cold arm. This results in the more efficient extraction of heat from the crystal thus reducing the thermal de-ionisation of the laser active centres. Although chopped laser operation at liquid nitrogen temperature was observed for longer periods than in the old system, due to the improved thermal contact between the coldfinger and the temperature bath, under true continuous wave operation efficient laser operation was observed for ~2 hours. This time interval is defined as the period over which the output power dropped below 50% of its initial value. This degradation was attributed to the poor thermal conductivity of the crystal. Under chopped operation the instantaneous heating of the crystal when the chopper blade is open by both the pump beam and the laser transition itself can be removed by the liquid nitrogen coolant when the window is closed. For continuous wave excitation,however, the heat dissipated into the crystal is

not removed quickly enough. Thus the crystal heats up which results in the de-ioisation of the centres. Also the crystal may be exposed to a greater density of pump photons which may induce a greater re-orientational bleaching effect, as described in chapter 2. Thus, even though the new design of resonator allows for longer stable operation from the F_2^+ laser it is still necessary to operate the F_2^+ laser with a chopped pump beam to reduce the thermal and rotational bleaching effects.

6.3. The Synchronous Mode-Locking of the LiF:F_2^+ Colour Centre Laser.

Initial investigations into the mode-locked behaviour of the redesigned resonator were performed using the simple three mirror cavity depicted in fig 6.4 and all the optical elements were the same as described in 6.2.3.. The end mirror, M_3, was mounted on a precision translation stage to allow matching between the pump and slave laser periods. The acousto-optically mode-locked Kr^+ generated pulses ~100 ps in duration, (as measured on a Photochron II Synchroscan streak camera [9]), with ~1 W of time averaged power and at a repetition frequency of 82 MHz. Preliminary investigations were carried out with a colour centre laser repetition rate of 164 Mhz.

(a)   (b)   100 ps
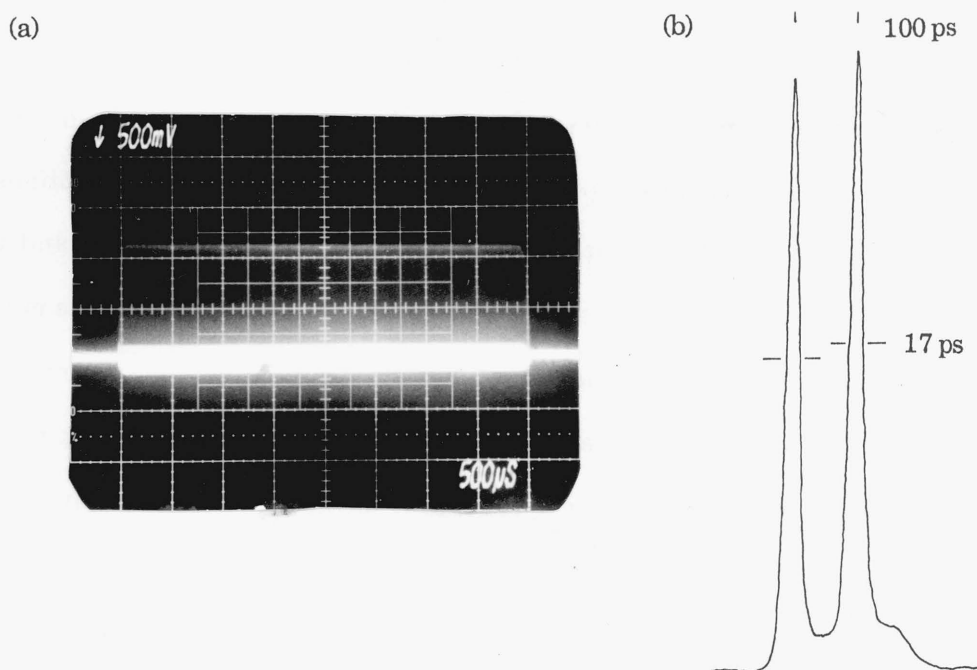

Fig 6.7:   (a) An oscillogram of the chopped pulse trains emitted by the synchronously mode-locked colour centre laser and (b) the streak images associated with these pulse trains.

As short pulses were observed from the simple linear cavity it was decided to configure a bi-directional travelling-wave resonator similar to that depicted in fig 6.6. Under synchronously mode-locked conditions, with a ring resonator frequency of ~82 Mhz, pulses as short as 700 fs, see fig 6.10, (again assuming Gaussian pulseshapes) centred around 870 nm were routinely generated with output powers of 20 mW in both arms. This corresponds to pulse peak powers of 150 W. These pulses were observed over the entire tuning range of the F_2^+ centre. The bandwidth of these pulses was found to be ~1.8 nm giving a time bandwidth product of 0.49 which should be compared to that value for bandwidth limited Gaussian pulse profiles (0.44).

Fig 6.10: The shortest pulses generated from the synchronously mode-locked ring colour centre laser.

The pulses generated from the travelling-wave resonator were a factor of two shorter than those produced from the linear cavity. Similar reductions in the pulse duration of ring dye lasers have been observed [10].This reduction may be attributed to a coherent interaction occurring in the gain medium [10,11] which enhances the gain saturation. Under the influence of the Kr^+ pump pulse train, two colour centre pulses are generated, which counter-propagate. After one round trip of the resonator the pulses collide in the gain medium and this collision leads to the formation of a standing-wave in the gain medium. This, in turn, induces the production of a transient grating, due to

not removed quickly enough. Thus the crystal heats up which results in the de-ioisation of the centres. Also the crystal may be exposed to a greater density of pump photons which may induce a greater re-orientational bleaching effect, as described in chapter 2. Thus, even though the new design of resonator allows for longer stable operation from the F_2^+ laser it is still necessary to operate the F_2^+ laser with a chopped pump beam to reduce the thermal and rotational bleaching effects.

6.3. The Synchronous Mode-Locking of the LiF:F_2^+ Colour Centre Laser.

Initial investigations into the mode-locked behaviour of the redesigned resonator were performed using the simple three mirror cavity depicted in fig 6.4 and all the optical elements were the same as described in 6.2.3. The end mirror, M_3, was mounted on a precision translation stage to allow matching between the pump and slave laser periods. The acousto-optically mode-locked Kr^+ generated pulses ~100 ps in duration, (as measured on a Photochron II Synchroscan streak camera [9]), with ~1 W of time averaged power and at a repetition frequency of 82 MHz. Preliminary investigations were carried out with a colour centre laser repetition rate of 164 Mhz.
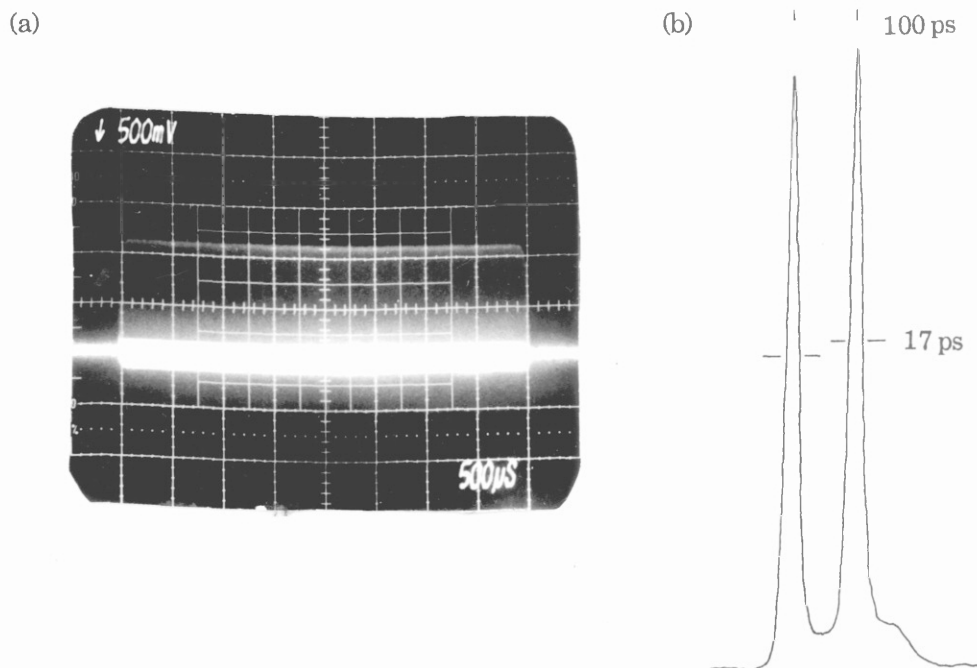
(a)

(b) 100 ps

17 ps

Fig 6.7: (a) An oscillogram of the chopped pulse trains emitted by the synchronously mode-locked colour centre laser and (b) the streak images associated with these pulse trains.

Optimisation of the colour centre laser pulses was performed in a fashion analogous to that described for the R700 dye laser. The streak camera results obtained indicated that pulses as short as 17 ps could be observed. These are illustrated in fig 6.7 together with typical pulse trains recorded from the photodiode/oscilloscope combination.The trigger signal used to drive the streak camera could have been taken from either the Kr^+ pulse train, the frequency synthesiser or the chopped colour centre pulse train. However the first choice would have resulted in a reduction in the pump power incident on the laser active gain medium and the second selection has been shown to increase the phase jitter and so degrade the overall temporal resolution [9]. Thus the trigger signal was derived from the colour centre beam. Since this was a chopped beam the trigger signal had to be established during each pulse train. This resulted in a loss of phase between successive pulse trains with the direct consequence that the streak images corresponding to successive trains of pulses were not precisely superimposed on the phosphor screen thereby introducing a slight broadening of the recorded images. As the streak camera was used solely for initial matching of the pump and colour centre cavity lengths, no attempt was made to determine the best method of driving the streak camera. The pulses incident upon the slit of the streak camera were therefore expected to be somewhat shorter than the recorded streak images.After optimisation on the streak camera the pulses were then further optimised on the real-time autocorrelator. Since the laser was chopped at ~25 Hz and the scanning mirror operated at ~25 Hz , a beating effect was observed between the mirror and the output signal which caused the scanned image to drift across the screen of the monitoring oscilloscope. This was rectified by synchronising the vibrating mirror with the chopper. After optimisation on the real-time autocorrelator the output pulses were measured by slowly scanning one of the mirrors of the autocorrelator through the introduced time delay. The typical pulse duration observed from this laser was between 2-3 ps (assuming Gaussian pulse shapes) as illustrated in fig 6.8a. Simultaneous measurement of the bandwidth,(shown in fig 6.8b), gave a value of 0.62 nm which corresponded to a time bandwidth product of 0.5. The average output power associated with these pulses was ~30 mW (T=3%) which corresponds to pulse peak powers of 75 W .
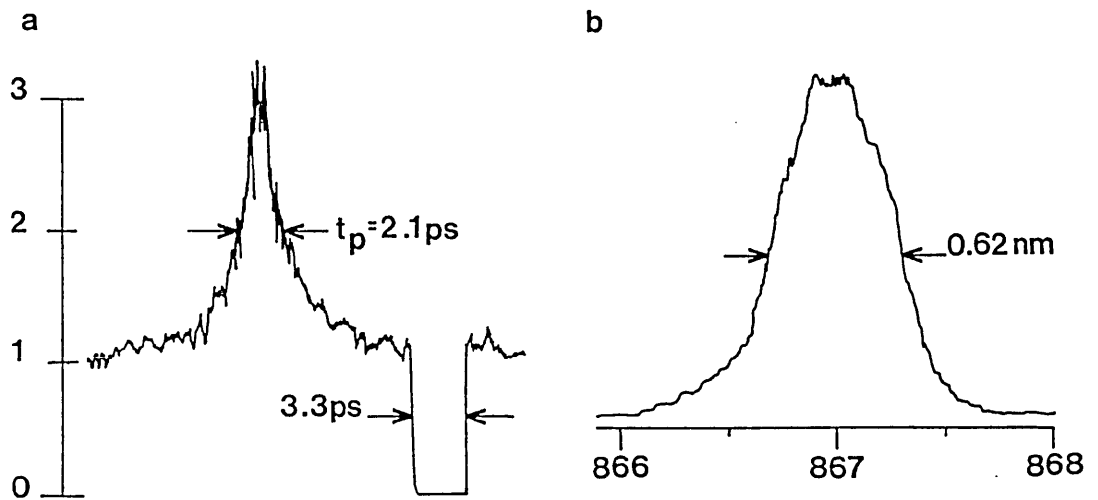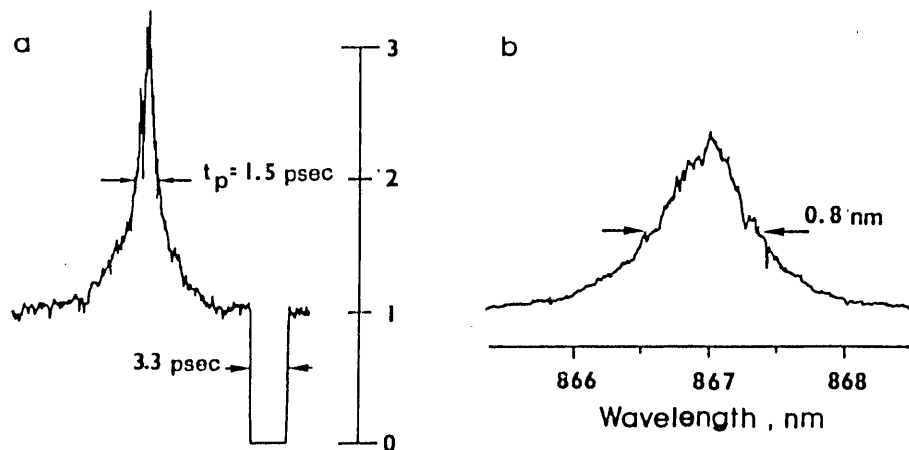
Fig 6.8: (a) The autocorrelation trace of the typical pulses emitted
from the synchronously mode-locked colour centre laser
together with (b) their mode-locked bandwidth .

The shortest pulses (shown together with their bandwidth in fig 6.9a,b.) observed

from the system were ~1.5 ps in duration (assuming a Gaussian pulse shape) and the

bandwidth was 0.8 nm. This gave a time bandwidth product of 0.48 which is close to that

value associated with bandwidth limited Gaussian pulses (0.44). The average output

power associated with these pulses was 20 mW giving peak powers of 50 W. These

pulses were generated over the entire tuning range of the laser.

Fig 6.9: (a) The autocorrelation trace of the shortest pulse emitted
from the synchronously mode-locked colour centre laser
together with (b) its mode-locked bandwidth .

As short pulses were observed from the simple linear cavity it was decided to configure a bi-directional travelling-wave resonator similar to that depicted in fig 6.6. Under synchronously mode-locked conditions, with a ring resonator frequency of ~82 Mhz, pulses as short as 700 fs, see fig 6.10, (again assuming Gaussian pulseshapes) centred around 870 nm were routinely generated with output powers of 20 mW in both arms. This corresponds to pulse peak powers of 150 W. These pulses were observed over the entire tuning range of the F_2^+ centre. The bandwidth of these pulses was found to be ~1.8 nm giving a time bandwidth product of 0.49 which should be compared to that value for bandwidth limited Gaussian pulse profiles (0.44).

Fig 6.10: The shortest pulses generated from the synchronously mode-locked ring colour centre laser.

The pulses generated from the travelling-wave resonator were a factor of two shorter than those produced from the linear cavity. Similar reductions in the pulse duration of ring dye lasers have been observed [10].This reduction may be attributed to a coherent interaction occurring in the gain medium [10,11] which enhances the gain saturation. Under the influence of the Kr^+ pump pulse train, two colour centre pulses are generated, which counter-propagate. After one round trip of the resonator the pulses collide in the gain medium and this collision leads to the formation of a standing-wave in the gain medium. This, in turn, induces the production of a transient grating, due to

a modulation of the gain saturation, and scatters a portion of the pulse travelling in one direction into the counter-propagating direction and induces more constructive interference. The effect of this transient grating on the pulse formation kinetics of the synchronously mode-locked laser can be understood as follows. For a synchronously mode-locked laser pulse formation is initiated by gain saturation which results in the trailing edge of the pulse experiencing a depleted gain, and as a result loss. Hence a compression of the pulse occurs. The rate of gain saturation is determined primarily by the rate of change of the optical field of the leading edge of the pulse [12]. For the case where a transient grating is present the apparent field in the gain medium is increased. As a result the rate of gain saturation is increased and so the trailing portion of the pulse experiences a more depleted gain. This can be interpreted as an advancement of the position where the cavity losses exceed the small signal gain and so the pulse is compressed.

Under the pumping conditions described above the active lifetime of the laser crystals was less than that for the continuous wave pumping used earlier. Typical lifetimes ~100 hours were routinely observed and altering the position of the laser active spot only increased the crystal lifetime by ~20 hours. The lifetime in this case was defined by the stability of the pulses under mode-locked operation. For a fresh crystal the generated pulses were highly stable and exhibited little interpulse noise. As the crystal aged the pulses became unstable and the noise level increased. As stated in 3.3.3. pulse formation in a synchronously mode-locked laser is initiated by gain saturation and this depends upon the number of pump photons absorbed [13]. This, in turn, is governed by the number of absorbing centres present. If the centre density decays, reducing the number of absorbing centres, then effective gain saturation may be precluded, affecting the pulse formation processes in the laser. The fading of the F_2^+ centre density was attributed to the orientational bleaching effects associated with the high photon density of the pump pulse [14].

6.3.1. The Effects of Cavity Length Detuning and Pump Power Variation on Pulse Formation.

The pulses produced by this laser are the shortest yet reported for a synchronously mode-locked LiF:F_2^+ laser. As for the case of the R700 dye laser (see 4.2.3) the duration of these pulses is critically dependent on the match between cavity periods of the colour centre and Kr^+ pump lasers and also on the pump power incident upon the gain medium. The effects of pump power variation and cavity length detuning on the production of ultrashort pulses from colour centre lasers have been investigated by several authors [13,15-19] and preliminary investigations carried out on F_2^+ centres [17] indicate some similarity between these centres and dye lasers [12]. However the development of colour centre lasers with gain cross sections and radiative decay times far removed from those of dye lasers has revealed substantial behavioural deviations between the two [13].In this section the mode-locked behaviour of the standing travelling-wave resonators will be described. The linear cavity employed is illustrated in fig 6.11. With this type of configuration care had to be taken to ensure the cavity was asymmetric in that the separation between mirrors $M_1 M_2$ was greater than that of $M_3 M_4$ ensuring that the laser operated in a uni-directional fashion and avoided any possible coherent interactions in the gain medium (Although these effects have
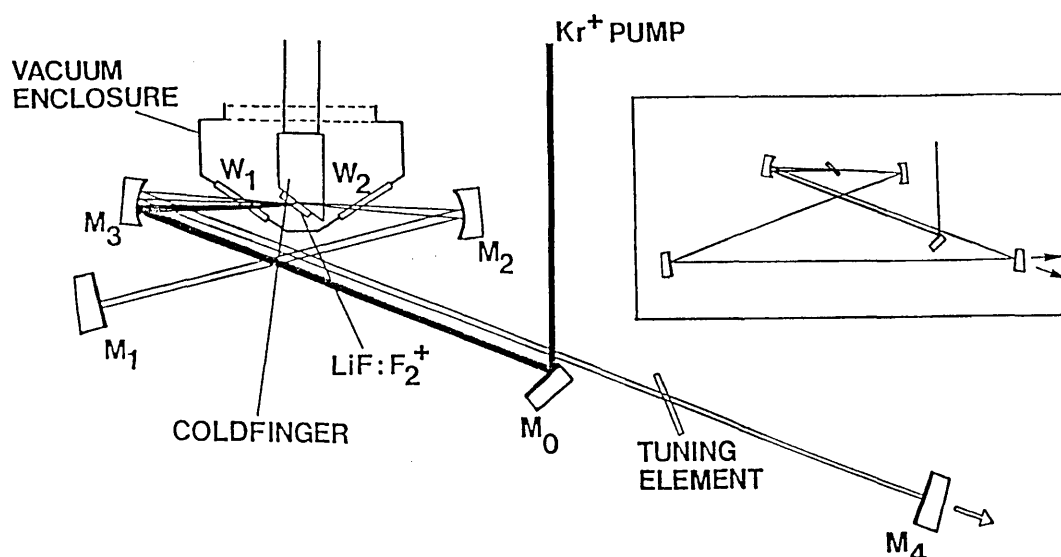

Fig 6.11:   The simple linear cavity used to study the effects of cavity
            length and pump power detuning on the pulse duration of
            the synchronously mode-locked colour centre laser.

been shown to be beneficial in a travelling-wave resonator, exploitation of a coherent interaction in a standing-wave system is extremely difficult as it requires positioning of the gain medium in the centre of the resonator to submicron accuracy). The period of the colour centre laser was matched to that of the Kr^+ pump laser (~12.4 ns) and the pulses produced by the laser were monitored using the real time autocorrelator and digital storage oscilloscope.

The variation of the second harmonic signal with respect to cavity length detuning was studied by blocking one arm of the autocorrelator delay line. The results obtained are illustrated in fig 6.12a, which shows the behaviour of both the time averaged fundamental and second harmonic powers as a function of cavity-length detuning for .
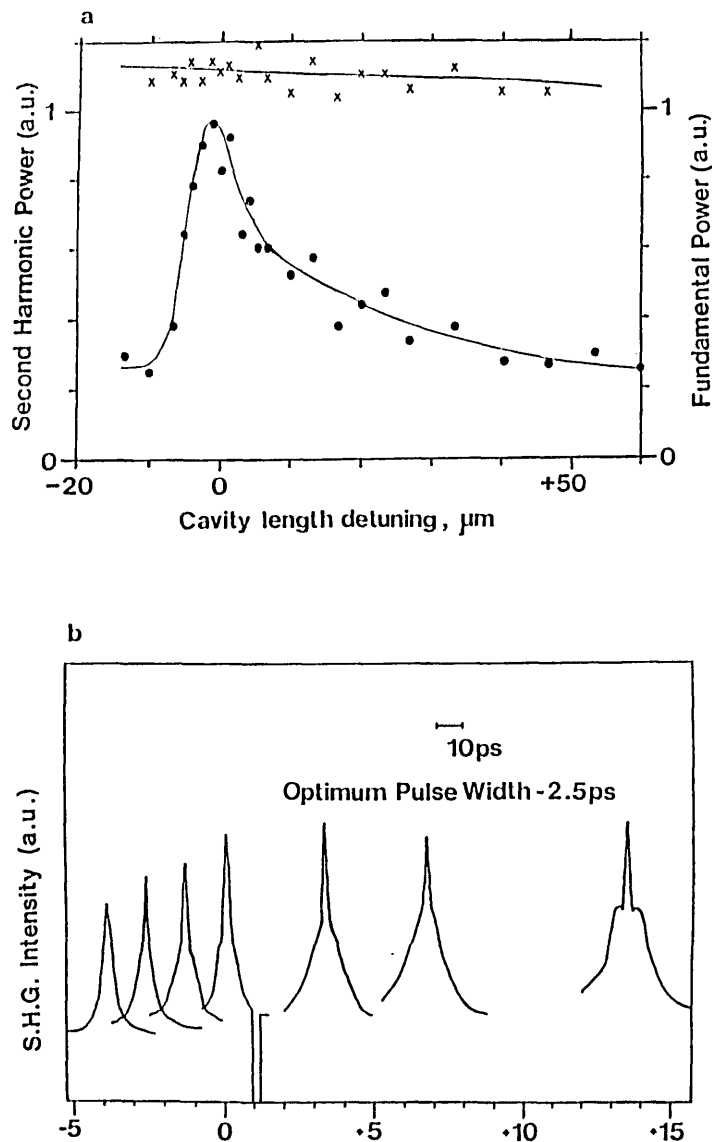
Fig 6.12: The variation with respect to cavity length detuning of (a) the second harmonic intensity (dots) and the fundamental power (crosses) and (b) pulse shape.

fixed pump power and pulse duration. It can be seen that despite almost constant fundamental output power over the ~80 μm round trip detuning, the second harmonic signal showed a distinct asymmetry about the zero detuning point. (This point was defined as the cavity length at which maximum second harmonic was observed.) The full width at half maximum of this asymmetry was ~15 μm.

The enhancement observed in the second harmonic signal as the cavity length was adjusted towards the zero point is indicative of a pulse shortening. This can be seen more clearly in fig 6.12b, which shows the effect of cavity detuning on the pulse shape. These results were taken with both arms of the autocorrelator open. For cavity lengths in excess of the zero point broad pulses with a definite coherence spike were observed. As the cavity length was tuned to the zero point the shoulders associated with the coherence spike decreased and the pulses narrowed. At the zero point the pulses exhibited slight shoulders and further reductions in the cavity length (~2.7 μm) resulted in these disappearing. At this point the shortest pulses were observed. For further detunings there was a marked reduction in the contrast ratio and then a total loss of mode-locking (~5 μm detuning). This behaviour agrees with that observed for other F_2^+ systems [17] and also for dye lasers [12] and can be understood in an analogous fashion to dye lasers (see 4.3.2). Similar effects were observed for the ring cavity .

The effect of pump power variations on the pulse duration, for both the standing- and travelling-wave resonators, is depicted in fig 6.13. From this figure it can be seen that short pulses can be generated from the colour centre laser for pump powers only twice above threshold. This agrees with the behaviour observed for synchronously mode-locked dye lasers [12] but differs significantly with that seen in other classes of colour centre lasers, most notably the KCl:Tl laser [13]. For the KCl:Tl system two distinct thresholds exist for mode-locking. The first power threshold defines laser action and corresponds to the production of pulses ~25 ps duration whilst the second, where the centres are pumped many times above threshold, marks the onset of short pulse formation. In this regime pulses as short as 5 ps have been observed [13].
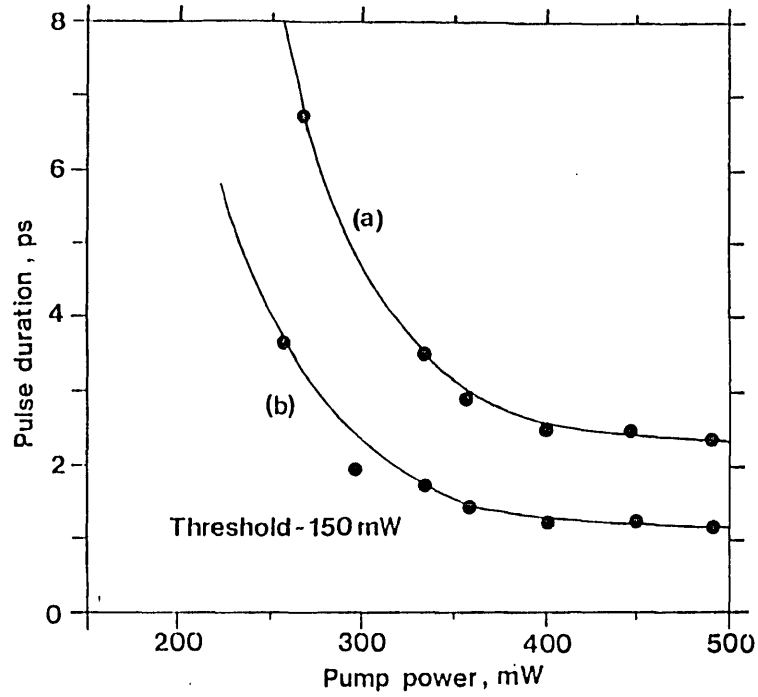
8

6

Pulse duration , ps

(a)

4

(b)

2

Threshold - 150 mW

0

200   300   400   500

Pump power, mW

Fig 6.13: The variation of pulse duration as a function of pump power for the synchronously mode-locked $LiF:F_2^+$ colour centre laser.

The difference in performance between the two centres is associated with their spontaneous decay times,τ_l, and gain cross sections, σ_g.The ability of a laser to produce a short pulse is determined primarily by a balance between two factors;(i) the ability of gain saturation to shape the pulse by introducing losses to the trailing edge of the pulse and(ii) the pulse broadening effects produced by various dispersive elements in the cavity. From fig 6.14, the effects of increasing the pump power on the gain and pulse shaping processes can be seen. The rate of gain saturation ΔG initiated by a single pump pulse is given by

$$\Delta G = \exp\frac{n\sigma_g}{a}$$ (6.1)

where n is the number of pump photons absorbed , related to the input intensity,a is the area of the focussed pump spot and σ_g is the gain cross-section.Thus the rate of gain saturation is proportional to the gain-cross section.For the LiF: F_2^+ centre the gain cross section is ~4 x 10^{-16} cm^2 [20], whilst in the KCl:Tl system it is 3 x 10^{-17} cm^2 [13]. Thus the rate of gain saturation induced by a single pulse is ~10^4 times greater in the LiF: F_2^+ system when compared to the KCl:Tl system. Thus for the same pump power, pulse formation in the LiF: F_2^+ system should be more effective.
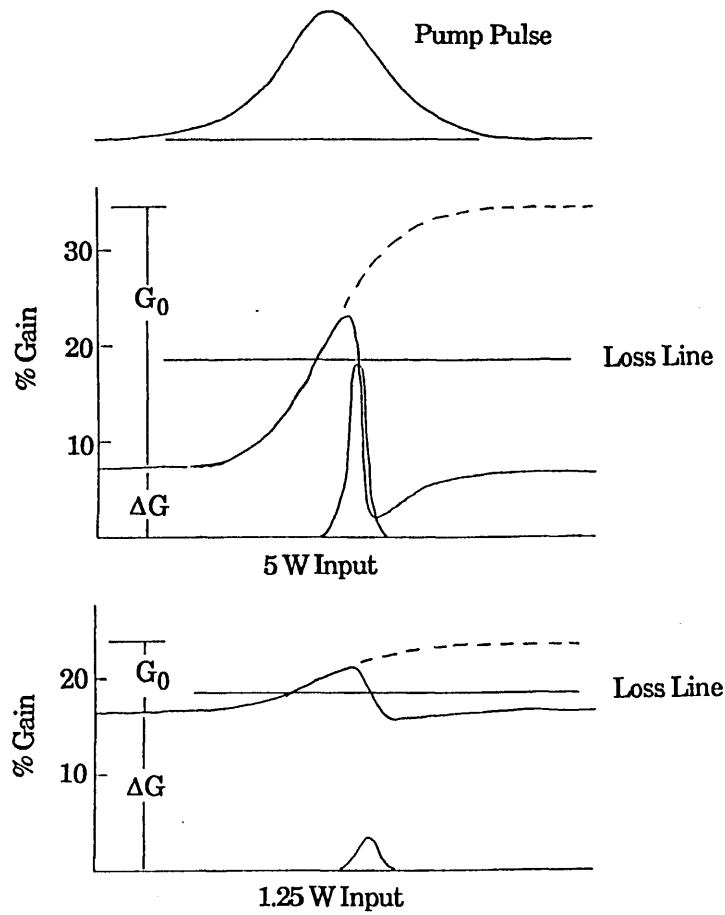
Fig 6.14: The evolution of the gain in a mode-locked KCl:Tl laser.
(a) Pump pulse ~ 80 ps duration. (b) and (c) The dashed
curve shows the effect of the pump pulse alone and the solid
curve represents the change in gain due to the presence of
the colour centre pulse (taken from 13).

Also the long lifetime associated with the KCl:Tl centre (~1.3 µs) [13], means that

the gain does not decay significantly, through spontaneous emission, between pump

pulses. This results in the small signal gain rising above threshold after several pump

pulses have been incident upon the crystal. Hence at low pump powers where effective

gain saturation is difficult to achieve the stored gain tends to amplify the trailing edge

of the pulse. At high pump powers gain saturation is more readily achieved and so the

trailing edge of the pulse can experience a greater loss due to the stronger depletion of

the gain This is illustrated in fig 6.14. In the $LiF:F_2^+$ system the gain recovery time is

~29 ns [20] and so the stored gain can decay quite rapidly below threshold by

spontaneous emission. Thus it is very difficult for the small signal gain to be taken

above threshold by the absorption of many pump pulses. Hence the ratio of the rate of

gain saturation to the small signal gain remains large thus allowing the production of ultrashort pulses at relatively low pump powers.

Although the effects of cavity length detuning and pump power variations on pulse formation and duration have been investigated, the pulses produced will still depend upon other parameters such as available lasing bandwidth [21] and pump pulse duration [12].

6.4. The Hybrid Mode-Locking of the F_2^+ Colour Centre Laser.

The key to successful pulse formation in a synchronously mode-locked laser is a strong gain saturation inducing a compression of the trailing edge of the pulse. Further pulse shortening can be effected through hybrid mode-locking whereby a small amount of saturable absorber is added to the cavity enhancing the pulse shaping kinetics which are now a combination of both gain and absorber saturation. This technique has already been used to great effect in 4.3.2.

The resonator employed was the same as that of 6.3.2 except that an additional folded section was inserted in the cavity. This folded section consisted of two 5 cm radius of curvature mirrors (Spectra Physics G3845-010, BBHR 800-950 nm). Located at the common focus of these two mirrors was a Brewster angled dye jet (thickness ~200 μm) which was mounted on a precision xyz translation stage allowing precise adjustment of the jet position. The saturable absorber employed in this work was the laser active dye 5,5'-dichloro-11-diphenylamino-3,3'-diethyl-10,12,-ethylene-thia-tri-carbo-cyanine-perchlorate IR 140. This dye exhibits a strong absorption, (as shown in fig 6.15), peaking at 810 nm, for an ethanolic solution, with an absorption cross section ~6 x 10^{-16} cm^2. The dye also has an equally strong photoisomer, peaking at the slightly longer wavelength of 865 nm [22]. The lifetime of the dye is approximately 1 ns, which is comparable to other polymethine-cyanine dyes [23]. It was first used as the saturable absorber in the hybrid mode-locking of a Styryl 9 dye laser [24] and has since been used for dye lasers having dispersion-compensated cavities to produce sub 100 fs duration pulses [25,26].

For an initially low concentration (~5 x 10^{-6} mole/litre) no significant pulse
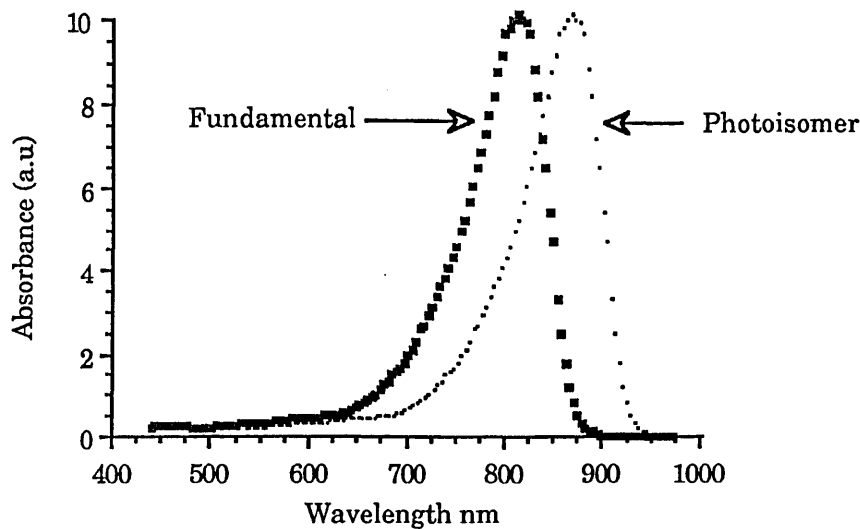
Fig 6.15:   The absorption band of the laser dye IR140 and its
photoisomer recorded in a propylene carbonate solution.

shortening was observed for the initial 1.7 ps pulses.However it was noticed that the

interpulse noise associated with the pulse train was substantially reduced. Further

additions of saturable absorber led to a distinct pulse compression resulting in the

generation of pulses as short as 550 fs at a concentration of 2.5 x 10^{-5} mole/litre. These

pulses are illustrated in fig 6.16. They were recorded at a wavelength of 871 nm and

tunability covered the region 865 - 880 nm.

As the mirrors forming the gain folded section frustrated laser operation in the

850-865 nm wavelength range, the hybrid laser could not be tuned into this region. This

is disadvantageous, as the S parameter (see 3.4, eqn. 3.2) depends upon the ratio of

absorber cross-section to gain cross-section. For this laser as the operational

wavelength is increased both the gain cross-section and photoisomer absorption cross-

section increase which may lead to a reduction in the S parameter. Hence shorter

pulses may be generated from this laser if it is operated around 850 nm. The stability of

the output pulse train from the laser was also observed to improve after the addition of

the saturable absorber.The average output power of the pulse trains was measured to be

~13 mW giving peak powers of 300 W. No attempt was made to construct a hybridly

mode-locked travelling-wave colour centre laser as the constraint of positioning the

passive dye jet at exactly half the cavity period (or some sub-multiple) proves to be too restrictive to justify it as a valid source for ultrashort pulse generation.
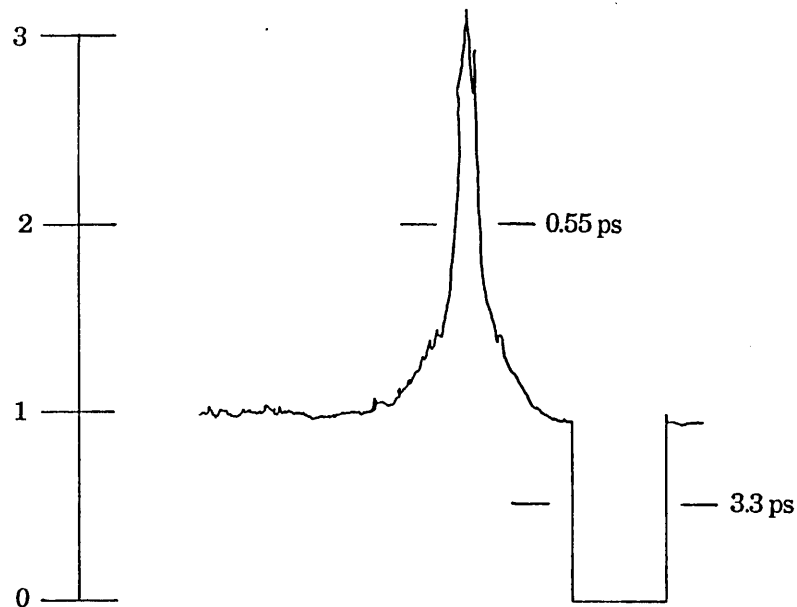

Fig 6.16:   The   shortest   pulse   generated   from   the   hybrid LiF:F_2^+/IR140 laser. The absorber concentration was 2.5 x 10 $^{-5}$ mole/litre and the operational wavelength was 871 nm.

6.5. Conclusions.

In this chapter the performance characteristics of a novel non-colinear pumped LiF:F_2^+ colour centre laser have been described. The laser has been shown to be tunable over 820 - 965 nm in both standing and travelling-wave cavities. By using the technique of synchronous mode-locking, pulses as short as 700 fs have been generated directly from the ring laser and these are the shortest pulses produced, to date, from this type of laser active centre. The influence of cavity length detuning and pump power variations on the pulse duration has been studied and shows some similarity to the performance exhibited by dye lasers when operated under the same conditions. Through the addition of a saturable absorber, pulses as short as 550 fs have been obtained from this laser over the spectral region of 865 - 880 nm. As the gain cross-section and gain recovery time are comparable to those of dye lasers and the performance under sychronous conditions was similar to that observed for the R700 dye

laser it was decided to attempt to use passive mode-locking as a pulse production

technique for this centre. The results of this investigation will be described in the next

chapter.

References:

1. M. Hassinger and F.E. Lythe; Opt. Commun., 48, 125, 1983.

2. L.F. Mollenauer in *Tunable Solid State Lasers*. Eds J.C. White and L.F. Mollenauer Springer Verlag Berlin 1987.

3. CRC Handbook.

4. American Institute of Physics Handbook p6.91.

5. G. Trenec, P. Nacher and M. Leduc; Opt. Commun., 43, 37, 1982.

6. K.W. Giberson, Chu Cheng, F.B. Dunning and F.K. Tittel; Appl. Opts., 21, 172, 1982.

7. G. Trenec, P. Nacher and M. Leduc; Opt. Commun., 43, 37, 1982.

8. D.A.B. Miller; Eigth National Conference on Lasers and Quantum Electronics QE8 1987 St Andrews.

9. W. Sibbett; Proc. 13th International Conference on High Speed Photography and Photonics 1979.

10. P.G. May, W. Sibbett and J.R. Taylor;Appl. Phys. B., 26, 179, 1981.

11. J.P. Heritage and E.D. Issacs; in Digest of Conference on Lasers and Electro-Optics (Washington DC.) Paper WL3 1981.

12. C.P. Ausschnitt, R.K. Jain and J.P. Heritage; I.E.E.E. J. Quant. Elect ., QE-15, 912, 1979.

13. L.F. Mollenauer, N.D. Vieria and L. Szeto; Opt. Lett., 7, 414, 1982.

14. M. Aegerter and F. Luty; Phys. Sol. Stat. B., 43, 227, 1971.

15. T.T. Basiev, N.S. Vorobiev, S.N. Mirov, V.V. Osiko, P.P. Pashinin, V. Postolov, and A.M. Prokhorov; J.E.T.P. Lett., 31, 291, 1980.

16. L. Isganitus, M.G. Sceats and K.R. German; Opt. Lett., 5, 123, 1980.

17. L.F. Mollenauer and D.M. Bloom; Opt. Lett., 4, 247, 1979.

18. R. Illingworth and I. Ruddock; Opt. Commun., 61, 120, 1987.

19. L. Reekie, I. Ruddock and R. Illingworth, in *Picosecond Chemistry and Biology*. Eds. T. Doust and M. West. Science Reviews Limited. 1983.

20. L. Bosi, C. Bussolati and G. Spinolo; Phys. Lett., 32A, 159, 1970.

21. D.A. Kim, J. Kuhl, R. Lambrich and D. Von Der Linde; Opt. Commun., 27, 123, 1978.

22. J.P. Fouassier, D.J. Lougnot and J. Faure; Opt. Commun., 23, 393, 1977.

23. J.P. Fouassier, D.J. Lougnot and J. Faure; Opt. Commun., 18, 293, 1978.

24. K. Smith, W. Sibbett and J.R. Taylor; Opt. Commun., 49, 359, 1984.

25. J. Dobler, H.H. Shuclz and W. Zinth; Opt. Commun., 57, 407, 1986.

26. M.D. Dawson, T.F. Boggess and A.L. Smirl; Opt. Lett., 12, 254, 1987.

Chapter 7:The Passive Mode-Locking of the LiF:F_2^+ Laser.

7.1. Introduction.

In the previous chapter a synchronously mode-locked colour centre laser was described and the direct generation of pulses as short as 700 fs was reported.Although the technique of synchronous pumping can lead to the production of short pulses it is not a practical process for lasers with the F_2^+ centre as the gain medium because the high peak powers associated with the mode-locked pump pulse lead to an orientational bleaching effect [1] which greatly reduces the useful lifetime of the centre.Passive mode-locking, where pulses are formed through the intermediacy of a saturable absorber, offers a possible solution since short pulses may be generated from the colour centre laser at reduced peak power levels, thus reducing the orientational bleaching effect. This technique has been applied to a variety of organic dyes and has led to short pulse production in the 490 -780 nm spectral range [2-4] and to the direct generation of pulses ~20-30 fs from a dispersion-compensated colliding pulse ring dye laser [5,6]. It has also been applied to semi-conductor lasers where a multiple quantum well served as the saturable absorber [7].In this chapter the passive mode-locking of a continuous wave chopped colour centre laser is reported for the first time in both standing-wave and travelling-wave resonator configurations.

7.2. The Passive Mode-Locking of the Standing-wave Resonator.

The cavity employed in the initial investigation of the passive mode-locking of the LiF:F_2^+ colour centre laser is illustrated in fig 7.1. Mirror M_1 was a plane 100% retro-reflecting mirror and the gain folded section was formed by the two 10 cm radius of curvature mirrors M_2 and M_3 described in chapter 6. The laser active LiF:F_2^+ crystal was located at the common focus of these two mirrors and the Kr^+ pump beam was coupled into the active crystal via mirror M_3. The passive folded section was formed by the mirrors M_4 and M_5 which were the same as those used for the hybrid mode-locking of the colour centre (see section 6.4). The ~200 μm thick Brewster-angled dye jet was located at the common focus of these two mirrors and the cavity was completed by the
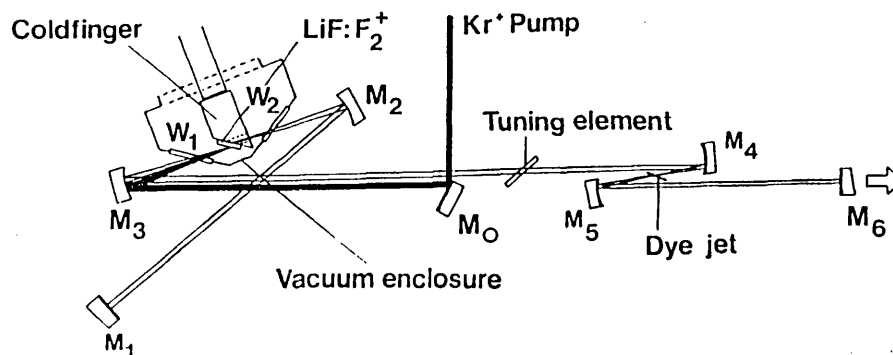
Fig 7.1:   The cavity configuration used in the initial studies of
the passive mode-locking of the $LiF:F_2^+$ centre.

3% output coupler M_6. The lasing wavelength was controlled by either the dielectric tuning wedge, (illustrated), or a Brewster-angled prism. The round trip time of the cavity was set initially to 13 ns. The absorbing dye selected was the laser dye IR 140 which was described in the previous chapter.

As mentioned in 3.4, for the evolution of steady state stable pulses certain system constraints have to be satisfied [8,9].The first condition, namely the relaxation time of the saturable absorber being less than that of the amplifying medium, is easily satisfied in this system as the gain recovery time for the F_2^+ centre in LiF is ~29 ns [10] whilst the absorber lifetime is ~1 ns [11].The condition relating to the S parameter [9] is satisfied by ensuring that the mirrors around the gain medium have a longer focal length than those in the passive folded section. In this system the gain mirrors had 5 cm focal lengths whilst those in the passive section had 2.5 cm focal lengths. This meant that the intracavity flux when focussed into the absorber was 4 times more intense than that in the gain medium. This value has not taken into account the contribution to the S parameter due to the ratio of the absorption to emission cross-sections. Although values for these two quantities have been quoted previously, the effect and magnitude of the absorber photoiosomer is not accurately known and so any calculations made tend to be rough estimates only. For the round trip time of 13 ns used in these preliminary studies the condition requiring that the cavity period exceeds the gain recovery time, 29 ns, was

not satisfied. This simply implies that the laser has to be operated further above threshold before mode-locking can be initiated [12].

The pulses produced by the laser were monitored in the following way. Pulse train stability was measured using a photodiode/oscilloscope combination. Bandwidths were measured using a CCD sensor coupled to a 25 cm monochromator. The signal for this was derived from the Brewster-angled reflection off the tuning element. The actual pulses generated were measured using a real time auto-correlator and digital storage oscilloscope.

Initial investigations were carried out with the concentration set at 9×10^{-5} mole/litre and the laser produced trains of stable output pulses as shown in fig 7.2. The duration of these pulses was measured to be 1.3 ps (assuming $Sech^2$ intenstity profiles) as shown in fig 7.3a. The bandwidth measured was 1.75 nm (Fig 7.3b) giving a time-bandwidth product of 0.9, which is far removed from the predicted value assumed for bandwidth limited $Sech^2$ pulse shapes (0.315). If a Gaussian pulse shape is assumed then the pulse duration is 1.4 ps and the time bandwidth product is 0.98 which again is not very close to the value associated for bandwidth limited pulses (0.44). The discrepancy between the observed time-bandwidth product and the theoretical value was attributed to the presence of intracavity dispersion (see 7.4).The average output power associated with the pulses was measured to be 10 mW
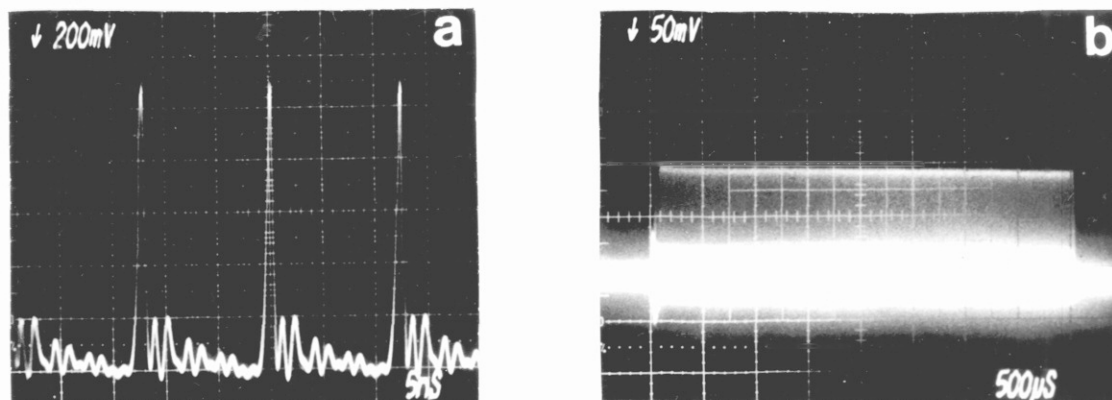

Fig 7.2:   Oscillograms of the chopped output pulse train from the
linear passively mode-locked colour centre laser.

a

3

2   →| |← t_p=1.3psec

b

→| |← 1.75nm

1

3.3psec →| |←
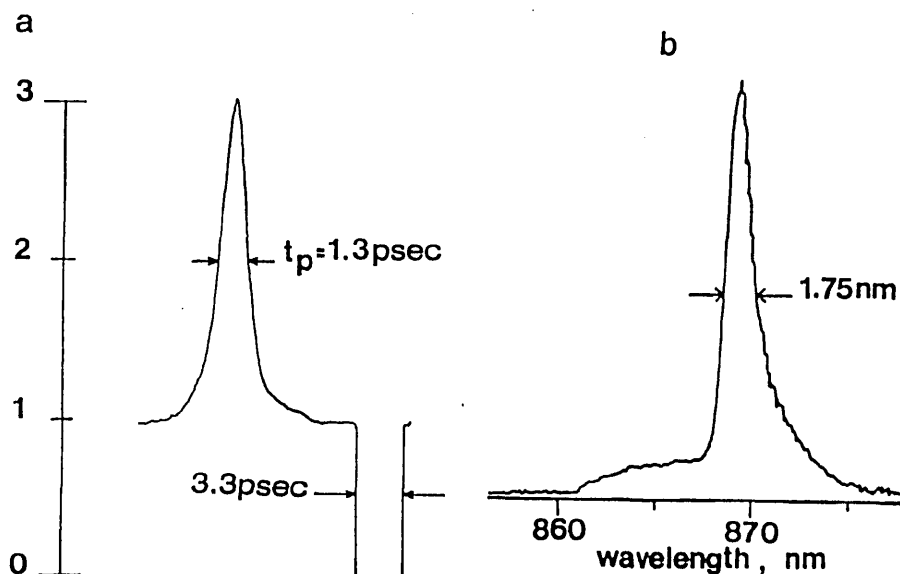
860   870
wavelength , nm

0

Fig 7.3:   (a) The autocorrelation signal from the passively
mode-locked colour centre together with (b) the
associated spectrum.

resulting in peak pulse powers of 100 W.These pulses were tunable over the 870-880 nm

spectral range. Pulse formation was observed for powers ~200-400 mW above the mode-

locked threshold, which in turn was ~500 mW above the laser threshold. As this

standing-wave resonator was used as a test configuration to investigate the possibility

of passive mode-locking of the LiF:F_2^+ laser, no attempts were made to investigate the

effects of concentration tuning on the pulse duration.

7.3. The Colliding Pulse Mode-Locked Colour Centre Laser.

Although the standing-wave resonator enabled pulses as short as 1.3 ps to be

generated from the passively mode-locked LiF:F_2^+ laser and the oscillogram shown in

fig 7.2 gives the impression of good pulse stability the actual stability of the

autocorrelation signal associated with the mode-locked pulse trains was poor.

Theoretical predictions have indicated that shorter duration pulses with much

improved long timescale stability should be observed [12] when the technique of

colliding pulse mode-locking [13] is implemented. To verify this a colliding pulse

mode-locked ring colour centre laser was configured. The optical components used to

form the travelling-wave resonator were the same as those described in 7.2 with
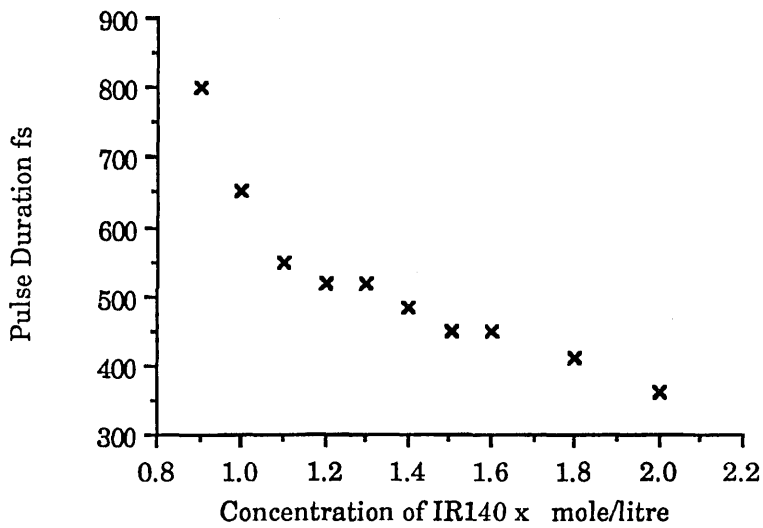
Fig 7.4: A plot of the pulse duration as a function of the dye concentration for the passively mode-locked colliding pulse ring colour centre laser.

the exception that mirrors M_1 and M_2 were aligned to form a travelling-wave resonator. Care was taken to ensure that the temporal separation between the gain and passive folded sections was one quarter of the total cavity period, which in this case was 13 ns. The concentration of the saturable absorber added to the passive circulator was increased until optimum pulses were observed. The variation of pulse duration as a function of the saturable absorber concentration is shown in fig 7.4. This concentration was found to be 2×10^{-4} mole/litre and the typical pulse duration observed was ~390 fs. The bandwidth associated with these pulses was 2.3 nm leading to a time bandwidth product of 0.6 for the $Sech^2$ pulse shapes assumed here. These pulses together with their associated bandwidth are depicted in fig 7.5. The peak power associated with these pulses was 200 W, corresponding to average output powers of 5 mW, per arm. The shortest pulses generated in this configuration had durations of 360 fs and bandwidths of 2.9 nm (see fig 7.6) which gave a time-bandwidth product of 0.42 for the assumed $Sech^2$ pulse shape.

The behaviour of the laser with respect to pump power variations is shown in fig 7.7. For pump powers just above mode-locking threshold, (2.1 W), very broad and unstable
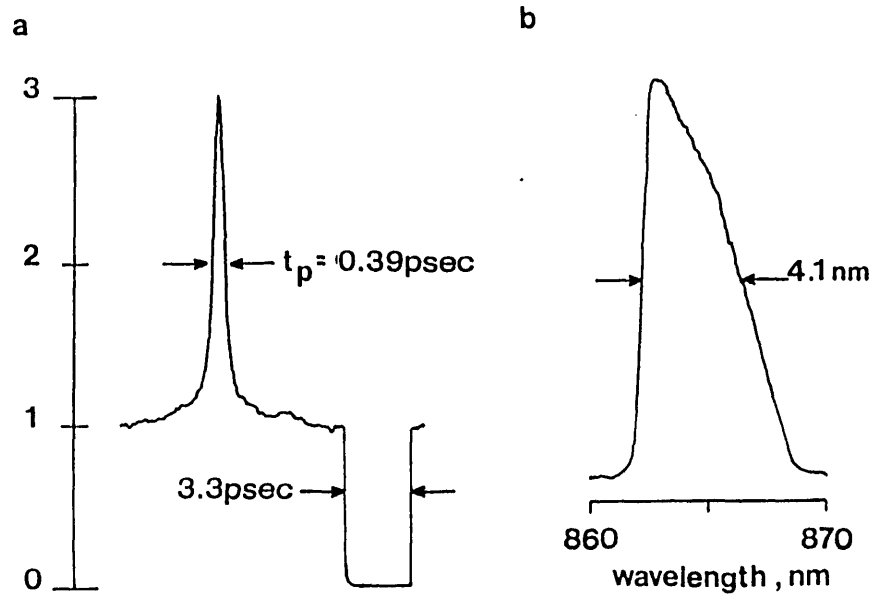
Fig 7.5: (a) The autocorrelation signal of the typical pulse trains generated from the colliding pulse laser together with their associated spectrum (b)
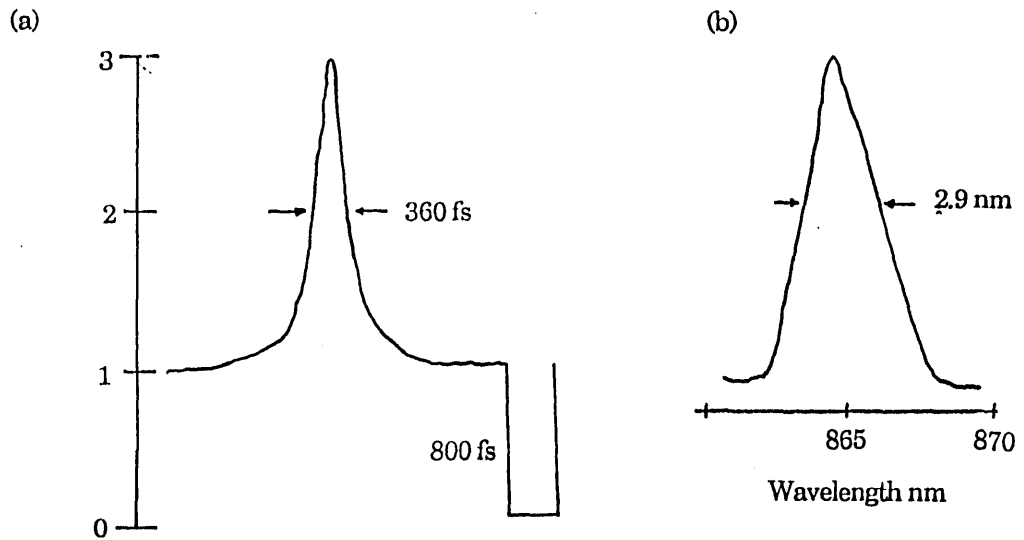

Fig 7.6: (a) The autocorrelation signal of the shortest pulse trains generated from the colliding pulse laser together with their associated spectrum (b)

pulses were observed. As the pump power was increased the pulses showed a significant narrowing until mode-locking was lost at a pump power of 2.5 W. Throughout the variation of pump power against pulse duration the contrast ratios of the recorded

autocorrelation signals remained three to one, indicating that the mode-locking was successful at all times.
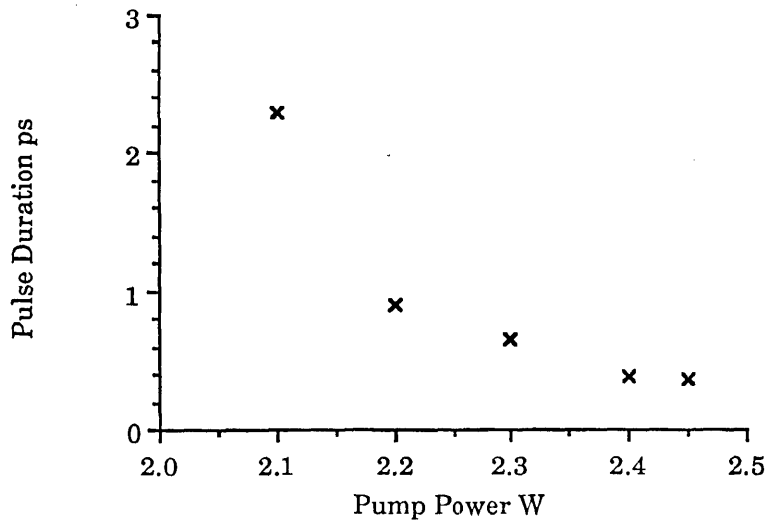
Fig 7.7:   A plot of pulse duration as a function of input power for the colliding pulse mode-locked ring colour centre laser.

The loss of mode-locking at high and low pump powers can be interpreted as follows. Pulse formation, as mentioned previously, depends strongly on the saturation of both the absorber and gain media. At the low pump powers associated with the mode-locking threshold the pulse intracavity intensity is sufficient to induce only a weak saturation of the absorber and gain media. This results in the S parameter, see eqn. 3. ., being quite small. Thus the magnitude of the stability region is also small and hence both the stability is poor and as the gain and absorber saturation are weak the generated pulses are broad. However, as the pump power is increased the intracavity intensity associated with the pulse increases, inducing a much stronger saturation of the absorber and gain media. This leads to an increase in the S parameter and hence the generation of more stable and shorter duration pulses. If the pump power is further increased then the intracavity intensity becomes too high resulting in earlier parts of the leading edge of the pulse saturating the absorber. This gives the absorber little chance to play a role in shaping the leading edge of the pulse and in fact bleaching of the absorber in this way leads to a total loss of mode-locking.

7.4. Dispersion-Compensation of the Passively Mode-Locked LiF:F$_2^+$ Laser

7.4.1. Sources of Intracavity Dispersion.

The time-bandwidth products of the mode-locked pulses generated in both the standing and travelling-wave resonator configurations were substantially greater than those predicted for Sech^2 pulse shapes. These discrepancies were attributed to the effects of intracavity group velocity dispersion and frequency chirps arising from various non-linear processes, such as self phase modulation occurring in both the passive and active media, which induce a loss of phase between the cavity modes forming the optical pulse. By balancing the self phase modulation effects with those introduced by the group velocity dispersion, significant pulse shaping and shortening [14] can occur in the laser leading to the production of hypershort optical pulses [5,6].

A frequency chirped pulse is one in which the carrier frequency changes smoothly over the duration of the pulse. This means that the time variation of the carrier wave can be expressed by an expansion of the form

$$\phi(\tau) = \omega\tau + \frac{1}{2}\beta\tau^2 + \psi\tau^3 + ... \tag{7.1}$$

For a linear chirp, ψ and higher order coefficients are zero. Such linear pulse chirps can be induced by: (i) passage through dispersive elements in the cavity, (ii) self phase modulation associated with the gain and absorber solvents and the off resonance absorption and emission in the absorber and gain media and finally, (iii) the dielectric mirrors which form the optical resonator.

The frequency chirp arising from an intracavity optical element is assumed to be linear and this includes passage of the optical pulse through transparent objects in the cavity, the unsaturated gain of the amplifier and the unsaturated loss of the absorber.

If a Gaussian pulse of the form

$$E(t) = E_0 \exp{-\left(\frac{2\ln 2 t^2}{\tau^2}\right)} \exp{i\omega_1 t} \tag{7.2}$$

is assumed to pass through a material whose phase varies slowly with frequency the phase can be expanded as a Taylor series of the form

$$\phi(\omega) = \phi(\omega_l) + (\frac{d\phi}{d\omega_l})(\omega - \omega_l) + \frac{1}{2}\frac{d^2\phi}{d\omega^2_l}(\omega - \omega_l)^2 + .. \tag{7.3}$$

The output pulse is then determined by transforming into frequency space, adding the phase contribution and then re-transforming back to the time domain. The resultant pulse is of the form

$$E_{out} = \frac{E_0}{(1+a)4}\frac{1}{} \exp -\frac{t^2}{4\beta(1+a)} \exp i(\omega_l t + \phi_{out} t) \tag{7.4}$$

with $$\beta = \frac{\tau^2}{8\ln 2} \tag{7.5}$$

$$a = \frac{\phi''^2}{4\beta^2} \tag{7.6}$$

$$\phi_{out} = \frac{-\phi'' t^2}{(2\phi''^2 + 8\beta^2)} - \frac{1}{2}\arctan(\frac{\phi''}{2\beta}) \tag{7.7}$$

$$\phi'' = (\frac{d^2\phi}{d\omega^2})_l \tag{7.8}$$

$$\frac{\tau_{out}}{\tau_{in}} = (1+a)\frac{1}{2} \tag{7.9}$$

Thus the effects of dispersion are to firstly broaden the output pulse τ_{out} by a factor $(1+a)^{\frac{1}{2}}$ and secondly to introduce a frequency chirp, with a sign opposite to that of ϕ''. For a transparent material of length l_e the phase shift $\phi(\omega)$ is given by

$$\phi(\omega) = \frac{-\omega n(\omega)l_e}{c} \tag{7.10}$$

By double differentiation with respect to ω and then transforming into wavelength, the frequency chirp is found to take the form

$$\phi'' = \frac{-l_e \lambda^3}{2\pi c^2}(\frac{d^2 n}{d\lambda^2}) \tag{7.11}$$

Thus it can be seen that the chirp introduced by the passage through the material is positive and so always causes a pulse broadening and up-chirp.

The resonator which allowed the studies of the passively mode-locked LiF:F$_2^+$ laser is shown in fig 7.1. Optical access to the crystal is allowed by the two Brewster-angled Infrasil windows W_1 and W_2. Under continuous wave operation these windows

introduce little loss to the system but for mode-locked operation they are a major source of intracavity dispersion. The passage of an optical pulse through a transparent medium leads to the development of an up-chirp on the pulse together with a broadening of the pulse. The magnitude of the dispersion is given by 7.11, using the values for $(\frac{d^2n}{d\lambda^2})_{SiO_2}$ obtained from the Sellmeier equations in [14]. The dispersion on a pulse as it passes through the Infrasil windows is -75 fs^2 per window. Similarily the passage of the pulse through the Brewster-angled laser active crystal also results in the development of a chirp and pulse broadening. For the pulses travelling in through the gain medium the dispersion experienced is -43 fs^2 and $(\frac{d^2n}{d\lambda^2})_{LiF}$ was evaluated using the values given in ref 15.

The role of mirror dispersion as a limit to the generation of ultrashort pulses from passively mode-locked dye lasers has been the subject of several recent theoretical and experimental investigations [16-23]. Fork et al [19] generated 65 fs pulses by limiting the dispersion produced by the mirrors in their cavity whilst French [20] has been able to control the pulse duration from both synchronous and passive systems simply by altering the angles of his mirrors.

A standard narrow band laser mirror consists of a series of high and low refractive index layers each $\frac{\lambda}{4}$ thick which are deposited on a glass substrate. The material which normally forms the high refractive index layers is TiO_2 (n= 2.28) whilst the low refractive index layers are made from SiO_2 (n=1.45). The reflected wave is produced by the interference of the multiple reflections which take place within the structure. This induces a phase shift on the reflected wave which in turn brings about a chirp. The magnitude of this chirp is governed by how close the operational wavelength is to the construction wavelength. If the mismatch between the two is small then the net dispersion introduced is small, and conversely if the mismatch is severe then large amounts of chirp can be introduced into the cavity [21].

Broad band laser mirrors, however, are constructed in a slightly different fashion. The same high and low layers are present but they are of varying thickness so that

reflections from these mirrors will always be off resonance. The amount of dispersion introduced by these mirrors depends upon their construction which may take one of the following forms: (i) several $\frac{\lambda}{4}$ stacks with different central wavelengths superimposed on each other, or (ii) a single stack made of a series of alternating high and low refractive index layers with their construction wavelength varying in a geometrical progression, and finally (iii) a single stack with thickness increasing in an arithmetic series.

The method of construction of mirrors plays an important role in determining the amount of dispersion introduced into the cavity, since on one side of the construction wavelength the phase shift introduced varies rapidly with respect to wavelength whilst on the other side it is a slowly varying function.The position of the two regions depends
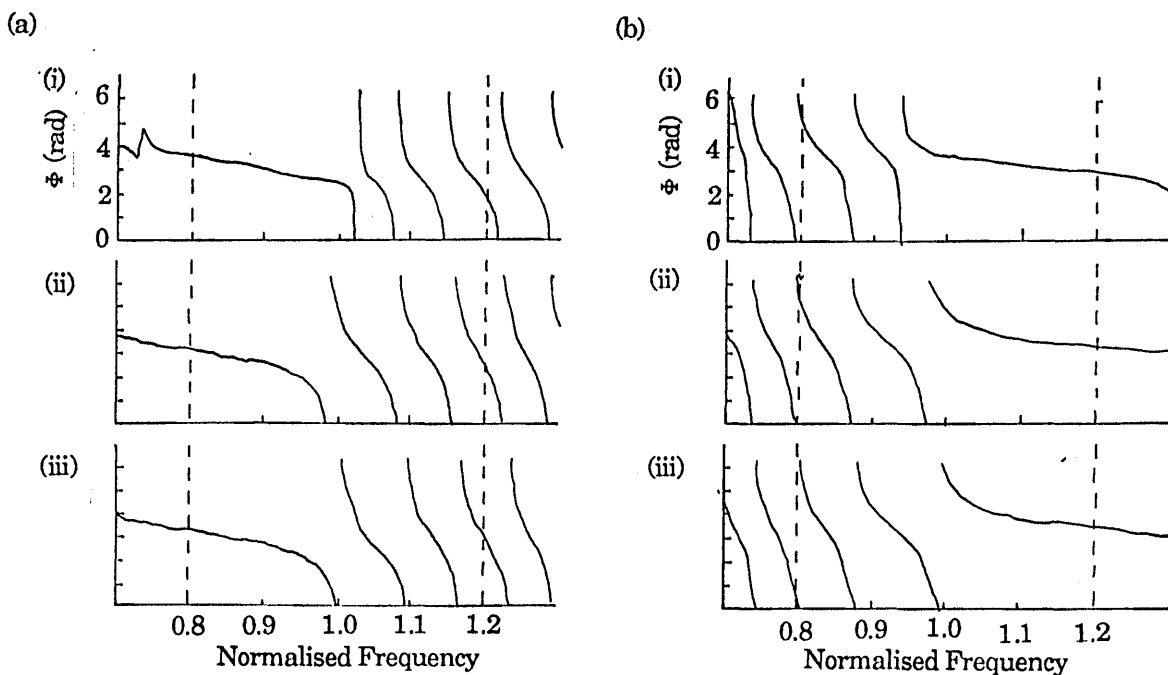
Fig 7.8:   Mirror phase shift Φ as a function of the normalised frequency for (a): (i) two quarter wave stacks with slightly overlapping high frequency zones (the high frequency stack is on top), (ii) a structure with layer thickness decreasing as a geometric progression and (iii) a structure with layer thickness decreasing as an arithmetic progression. The curves of (b) are when the layers are reversed (taken from ref 23).

on how the mirror was made (see fig 7.8). This can have serious effects on the pulse duration and shape. On the slowly varying dispersive side, the pulse is reflected primarily by the outer layers of the mirror structure, whilst on the rapidly varying side the reflection occurs from the inner surfaces. Hence the pulse has to pass through the outer layers twice and so is strongly affected by the material dispersions of the coating. This explains why certain double stack dielectric mirrors have the low frequency coating on the outside and the higher frequency one on the inside [22]. The operation of broad band dielectric mirrors on the high dispersion side can lead to distinct pulse shaping properties [18,21,23], due to the fact that the pulse is affected by quadratic and third order phase terms in the complex reflectivity term. The mirrors which formed the gain folded section were broad band high reflectors covering the 640 - 960 nm spectral region. The method of construction of these mirrors was unknown and so the dispersive effects of these mirrors could not be determined. The mirrors in the passive folded were single stack mirrors which covered the spectral region 820 - 960 nm. The deposition details for the final two mirrors which completed the optical cavity were also unknown. Thus the effects of the mirrors on the sign of the intracavity dispersion could not be evaluated.

Another source of intracavity frequency chirp in lasers arises from self phase modulation [5]. At present it is believed that there are two possible sources of self phase modulation in a passively mode-locked laser which are referred to as positive and negative self phase modulation and they lead to up-and down -chirps respectively. Negative self phase modulation is derived from an off-resonance excitation of the saturable absorber [24]. Saturation of the absorber results in its refractive index decreasing with time inducing a down-chirp on the optical pulse [25]. This type of self phase modulation has been considered by Khulke [26] to be the source of the down-chirp observed by Diels [22]. A small contribution to the negative phase modulation is also induced by the off resonance transitions in the gain medium [24], however as the intensity of the pulse in the gain medium is much less than that in the absorbing medium this effect is negligible and only comes into prominence for extremely short optical pulses [24].

The main source of positive self phase modulation is the non-linear optical Kerr effect [28] with a small component entering from the time dependent saturation of the gain medium [5]. The optical Kerr effect is a direct consequence of the intensity dependence of the refractive index of the solvent in which the saturable absorber is dissolved.The phase change, $\delta\phi$, introduced by the passage through a material of length l at a wavelength λ is given by

$$\delta\phi = \frac{2\pi\Delta n l}{\lambda} \qquad (7.12)$$

where $\Delta n = \frac{1}{2} n_2 E^2_{peak}$, n_2 is the non-linear refractive index of the material.

Here $n_2 E^2_{peak}$ can be replaced by a time averaged intensity, so that $\Delta n = N_2 I$, thus the change in phase is a function of intensity. So for a time varying intensity $I(t)$

$$\delta\phi(t) = \frac{2\pi l N_2 I(t)}{\lambda} \qquad (7.13)$$

and the induced pulse chirp is given by

$$\delta\omega = -\frac{d\phi(t)}{dt} \qquad (7.14)$$

$$\delta\omega = -\frac{2\pi l N_2}{\lambda} \frac{dI(t)}{dt} \qquad (7.15)$$

Hence for an optical pulse propagating through the non-linear medium the frequencies of the leading edge are lowered whilst those at the trailing edge are raised causing a broadening of the pulse spectrum and hence an up-chirp.

The two types of self phase modulation tend to compete against each other reducing the total amount of self phase modulation and thus limiting the pulse shaping processes which are used to compress the pulses. However the degree of competition between the two is governed by the intracavity pulse intensity and the thickness of the absorber jet. It has been shown that the predominant chirp produced on a pulse is from the optical Kerr effect when the pulse intensity in the saturable absorber exceeds the saturation intensity of the saturable absorber and its photoisomer by ~10 X [29]. It is believed that once the photoisomer has been saturated deeply it plays no further part in the pulse shaping mechanism and only the ground state of the absorber is effective for this [29]. Deep saturation of the photoisomer limits the pulse shaping to the leading edge of the

pulse and so the negative self phase modulation is present only on the leading edge of the pulse. Further pulse shaping and chirping take place due to the optical Kerr effect in the dye jet and the time dependent gain saturation associated with the central portion of the optical pulse [29].It has also been postulated that an up-chirp arises from low intensity pulses in the cavity due to the phase memory of the saturable absorber, which also compensates for the chirp induced by the off resonance absorption [24]. The value of this small signal chirp depends on the frequency bandwidth of the laser, the linear optical dispersion parameters of the absorption transition and the frequency detuning away from the absorber transition [24]. Calculations made by Miranda et al [30] have shown that for pulse energies ~5 nJ the optical Kerr effect dominates the off resonance saturation as the major source of chirp. To overcome this the passive dye jet is made extremely thin (typical jet thickness ~50 µm [24]).

7.4.2. Chirp Control by the Introduction of Group Velocity Dispersion.

The compression of optical pulses which exhibit a residual chirp by controlling the group velocity dispersion was first proposed by Treacy [31].A residual down-chirp on a pulse can be compensated for by the addition of an equal amount of positive group velocity dispersion and has been demonstrated by Diels to be a suitable way of controlling the pulse duration [27]. The controllable positive dispersion is introduced by altering the amount of glass in the cavity that the beam travels through, which in Diels' case is provided by translating the tuning prism across the beam. The compression occurs because the down-chirped trailing edge of the pulse sees a lower refractive index than the leading edge thus the leading edge of the pulse propagates more slowly than the trailing edge of the pulse and so the pulse is compresssed as it passes through the glass.

Control of a residual up-chirp is brought about by the introduction of a suitable negative GVD. This is usually introduced to the optical resonator by using either a prism delay line [32] or by a set of Gires-Turnois interferometers [33-37]. It should be noted that for fibre optic compressors the up-chirp induced by passage through the optical fibre is compensated for by a pair of gratings which produce the necessary negative group velocity dispersion [38,39].

The prism sequence shown in fig 7.9 can be used as a source of negative dispersion. The prisms are manufactured such that at Brewster-angle incidence minimum deviation of the beam is attained. This minimises the losses associated with insertion of the prisms. The four prism sequence is required for the following reason. The first prism disperses the beam whilst the second, separated by l, recollimates the dispersed beam parallel to the direction of propagation. The third and fourth prisms are arranged in the opposite sense to the first two so that they reform the beam and re-direct it along the original path.

"Red" Spectral
Components

"Blue" Spectral
Components
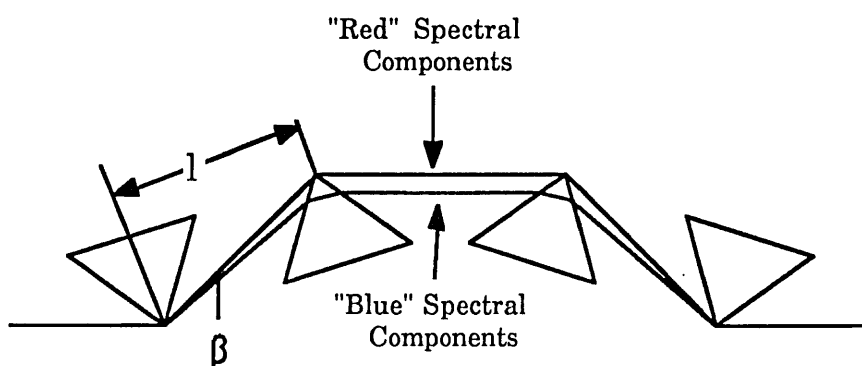
Fig 7.9:   A schematic of the prism sequence used to introduced a variable amount of negative group velocity into the colour centre cavity.

Two contributions to the dispersion arise. The first is the positive dispersion introduced by the passage of the light through the prism itself and the second is a negative group velocity dispersion introduced by the separation of the prisms. The existence of this negative dispersion enables pulse compression to occur. The prism sequence illustrated in fig 7.9 was first analysed by Gordon [34]. By considering the optical path length P, $(P = \int n(x)dx$, of the mode axis in the resonator), it was found that the group velocity dispersion (GVD) constant D was related to P by

$$D = (\frac{\lambda}{cL}) \frac{d^2P}{d\lambda^2}$$ (7.18)

Thus if $\frac{d^2P}{d\lambda^2}$ is negative then the GVD is negative. For the prism sequence illustrated the value of $\frac{d^2P}{d\lambda^2}$ is given by

$$\frac{d^2P}{d\lambda^2} = 4l\ \{(\frac{d^2n}{d\lambda^2} + (2n - \frac{1}{n^3})(\frac{dn}{d\lambda})^2)\ \sin\beta) - 2(\frac{dn}{d\lambda})^2\ \cos\beta\} \qquad (7.19)$$

where β is the angle of deviation between the 'red' and the 'blue' beams, and l is the separation of the prisms. The values of $n, \frac{dn}{d\lambda}$ and, $\frac{d^2n}{d\lambda^2}$ can be evaluated from Sellmier equations [14].and were found, for a wavelength of 875 nm to be

$$n = 1.45,\ \frac{dn}{d\lambda} = -0.015\ m^{-1}, and\ \frac{d^2n}{d\lambda^2} = 0.026\ m^{-2}$$

By setting $\frac{d^2P}{d\lambda^2}$ to zero a minimum value of l was evaluated as 112.8 mm. For separations greater than this minimum value the prism arrangement starts to introduce a negative group velocity dispersion. This negative component arises from the angular dispersion caused by the refraction at the optical surfaces of the prism. From fig 7.9 it can be seen that the shorter wavelength spectral components have less distance to travel to the next prism than the longer wavelength components and so they experience a smaller phase delay [29]. The magnitude of the negative group velocity dispersion can then be controlled by translating one of the prisms across the beam in the manner described by Diels [24].

Thus the main pulse shaping processes in a passively mode-locked laser, where the saturable absorber lifetime is slow in comparison to the duration of the pulse, are gain and absorber saturation combined with the pulse shaping kinetics due to the balancing of the intracavity self phase modulation with the group velocity dispersion of the cavity.

7.4.4 Dispersion-Compensated $LiF:F_2^+$ Resonators.

It is thought that the main source of intracavity dispersion in both the linear and ring resonators is due to the passage of the pulse through the Brewster-angled windows and crystal and the reflections from the mirrors which comprise the gain folded section. To overcome this problem and generate bandwidth limited pulses from the colour centre laser a prism sequence similar to that described above was inserted into both the linear and ring resonators. The apex angle of the prisms was evaluated to be $\sim$69° 5′ to give minimum deviation for Brewster incidence. The prisms were mounted

on optical tables which allowed for tilt control. In order to adjust the amount of glass in the cavity the prisms were mounted on translation stages. The separation between the prisms was estimated to be 50 cm to give a total cavity negative group velocity dispersion to compensate solely for the positive group velocity dispersion introduced by the windows, the material of the prisms and the Brewster-angled $LiF:F_2^+$ gain medium.

7.4.5. The Linear Dispersion-Optimised Resonator.

The prelimary studies of the mode-locked behaviour of the dispersion compensated resonators were performed with the cavity illustrated in fig 7.10. Although a prism separation of 50 cm was evaluated an initial separation of 25 cm was used. This length was selected in order to allow dispersion compensation studies to be carried out for prism separations greater than and less than the optimum value. The cavity period was ~13 ns and the concentration of the saturable absorber was set at 9×10^{-5} mole/litre to allow a direct comparison between the non-compensated resonator described in 7.2 and compensated resonators to be undertaken.
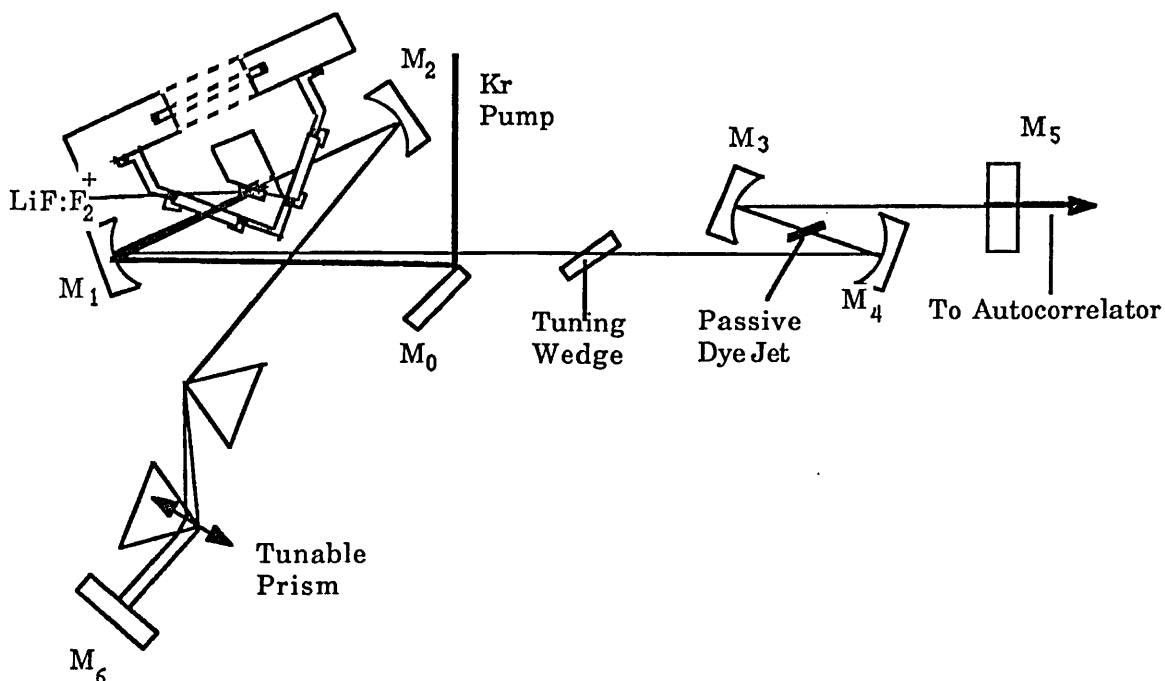
Fig 7.10: The simple linear dispersion-compensated resonator

Under these operating conditions no significant pulse shortening was observed but
a novel relationship between the pulse evolution and the pump power incident upon the
crystal was recorded. The variation is seen, together with the pulse spectrum, in
fig 7.11. It can be characterised as follows; for pump powers just above mode-locking
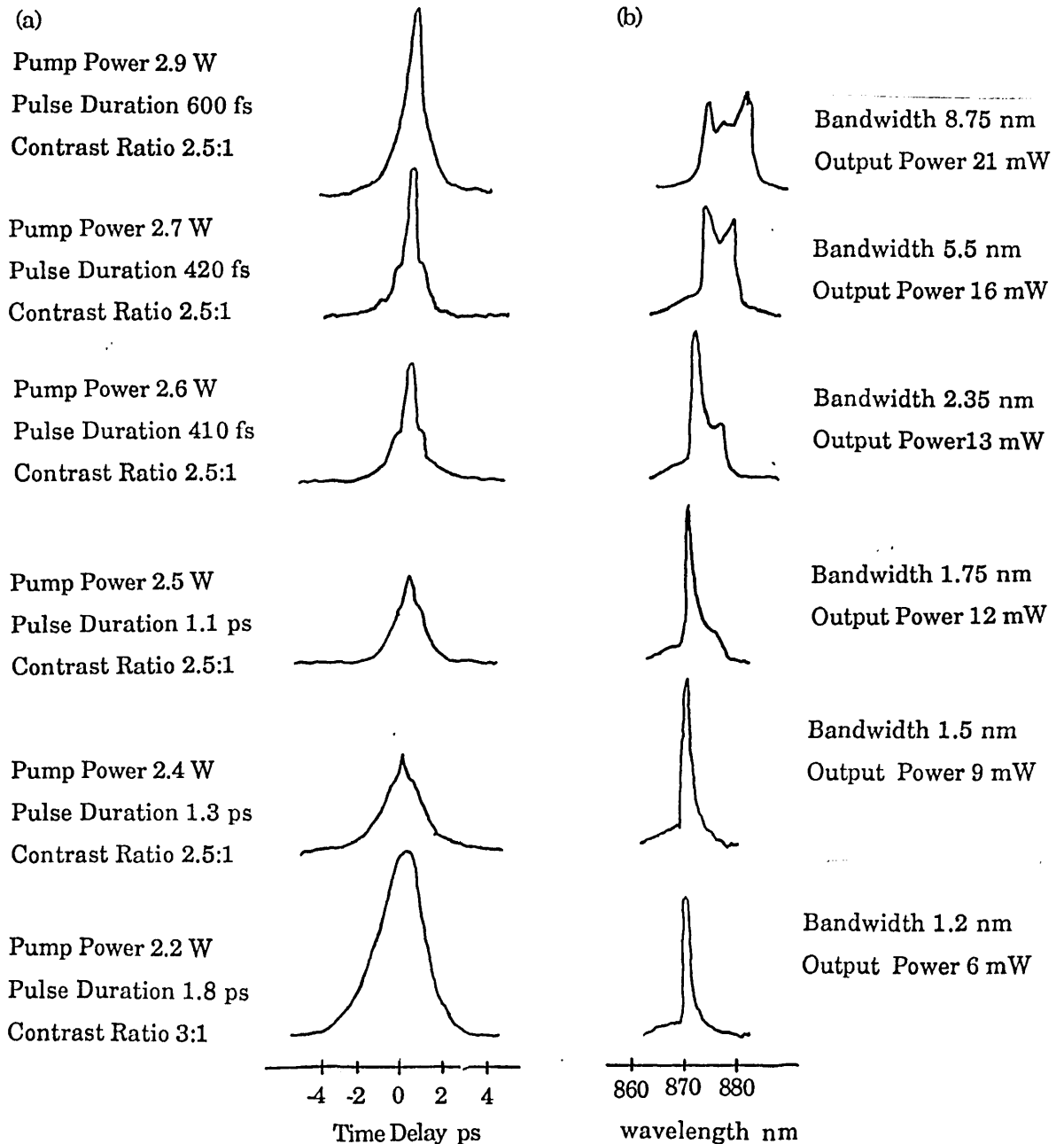threshold   (2 W), the pulses were broad,(~1 ps). As the pump power was increased the

(a)

Pump Power 2.9 W
Pulse Duration 600 fs
Contrast Ratio 2.5:1

Pump Power 2.7 W
Pulse Duration 420 fs
Contrast Ratio 2.5:1

Pump Power 2.6 W
Pulse Duration 410 fs
Contrast Ratio 2.5:1

Pump Power 2.5 W
Pulse Duration 1.1 ps
Contrast Ratio 2.5:1

Pump Power 2.4 W
Pulse Duration 1.3 ps
Contrast Ratio 2.5:1

Pump Power 2.2 W
Pulse Duration 1.8 ps
Contrast Ratio 3:1

(b)

Bandwidth 8.75 nm
Output Power 21 mW

Bandwidth 5.5 nm
Output Power 16 mW

Bandwidth 2.35 nm
Output Power 13 mW

Bandwidth 1.75 nm
Output Power 12 mW

Bandwidth 1.5 nm
Output Power 9 mW

Bandwidth 1.2 nm
Output Power 6 mW

-4 -2 0 2 4
Time Delay ps

860 870 880
wavelength nm

Fig 7.11:   The evolution of (a) the colour centre laser pulse and
(b) the pulse spectrum as a function of the pump power
incident upon the gain medium.

second harmonic signal in the autocorrelator increased and a "spike" evolved from the centre of the pulse as indicated in fig 7. 10. The duration of this spike was evaluated to be ~400 fs and the separation between the peak of the spike and the "shoulders" of the autocorrelation trace was also ~400 fs (see fig 7. 11).Associated with the development of this "spike" a shift in the operating wavelength to longer wavelengths was observed together with a broadening of the recorded spectra.

Initially this behaviour was thought to be associated with the development of optical solitons leading to the formation of double pulses in the cavity [42,43]. Although the second harmonic signal was observed to increase as the "spike" evolved from the centre of the pulse, the contrast ratio of the recorded signal decreased from the normal 3:1 ratio associated with correctly phase-locked pulses to a value of 2.5:1. Adjustments made to the alignment of the autocorrelator did not induce a 3:1 contrast ratio and observation of the chopped pulse trains on a photodiode/osciloscope combination indicated that they were very unstable and consisted mainly of relaxation oscillations (see fig 7.12).These observations indicated that the pulse trains originating from the passively mode-locked $LiF:F_2^+$ laser were incompletely mode-locked. The pulse generated by the laser can be regarded as containing two distinct sets of longitudinal modes. One set corresponds to the modes which are correctly phase-locked and the other set to a group of modes which do not have any distinct phase relationship between themselves or the other set of locked modes.
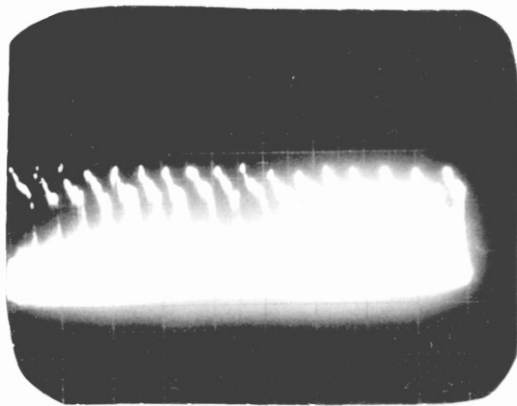
Fig 7.12:   Oscillogram of the chopped pulse train emitted by the
colour centre laser for an autocorrelation signal with a
2.5:1 contrast ratio.

The group of unlocked modes may be associated with the additional spectral component that develops as the pump power is increased (see fig 7.11). The effect of these modes can be interpreted by following an argument proposed originally by Von Der Linde [42].As stated in chapter 3, the intensity autocorrelation function $G^2(\tau)$ is given by

$$G^2(\tau) = <E(t)E(t+\tau)E^*(t)E^*(t+\tau)> \qquad (7.19)$$

where $E(t)$ is the electric field of the optical pulse. For the colinear autocorrelation techniques used to measure the pulses generated here the intensity is given by

$$I(\tau) = c \left(1 + 2\frac{G^2(\tau)}{G^2(0)} \right) \qquad (7.20)$$

This leads to contrast ratios of the form

$$k = \frac{I(0)}{I(t \sim \infty)} \qquad (7.21)$$

If the optical wave consists of a set of locked and unlocked modes , the electric field $E(t)$ can be written as

$$E(t) = E_p(t) + E_b(t). \qquad (7.22)$$

where $E_p(t)$ is the field of the locked modes and $E_b(t)$ is the field of the unlocked modes.

Substitution of 7.22 into 7.21,7.20,7.19 leads to a contrast ratio of the form

$$K(b) = \frac{3 + 6(\frac{1}{\beta^2} - 1)(\frac{t_p}{t})\alpha}{1 + 4(\frac{1}{\beta^2} - 1)(\frac{t_p}{t})\alpha} \qquad (7.23)$$

with β the ratio of pulse energy to total energy , t_p the pulse duration, t the cavity round trip time, and α the form factor, given by

$$\alpha = \frac{\frac{1}{t_p} \{ \int_{\frac{\tau p}{2}}^{\frac{-\tau p}{2}} |E_p|^2 \, dt \}^2}{\int_{\frac{\tau p}{2}}^{\frac{-\tau p}{2}} |E_p|^4 \, dt}, \qquad (7.24)$$

For a $Sech^2$ pulse this is calculated to be 0.31. Thus for a contrast ratio of 2.5, with $t_p \sim 1$ ps and $t \sim 10$ ns it can be seen that only 3% of the cavity energy is associated with the pulse .

The recorded autocorrelation traces are similar to those observed by Valdmanis and Fork when their dispersion compensated ring laser was operated with the passive dye jet too close to the focus of the mirrors forming the passive folded section, resulting in the generation of a greater positive self phase modulation component [43]. The effect of controlling the amount of positive group velocity dispersion on both the pulse duration and shape was investigated by translating one of the prisms across the beam and also varying the position of the passive dye jet. No noticable variation was observed in the behaviour outlined previously . This is to be expected, for at low pump powers the pulses are too broad for solitonic type pulse shaping processes to dominate whilst at the high pump powers the pulses were improperly mode-locked and so prism tuning should have little, or no, effect.

These effects can be explained as follows; at low pump powers the output power associated with the pulse train is low (~3 mW) and so the corresponding intracavity power is also low. This low intracavity power does not induce a large positive self phase modulation in the passive dye jet due to the optical Kerr effect. As the pump power is increased the output power and hence intracavity intensity increase and the pulse is compressed by enhanced gain and absorber saturation. For 2.9 W pump power the average output power from the colour centre laser was 20 mW corresponding to a peak power of ~520 W. The compression of the pulse results in additional spectral components being excited and hence the bandwidth broadens. As the pulse shortens and the intracavity power increases, the power density in the passive dye jet increases resulting in a greater self phase modulation. This results in the pulses generated in the laser experiencing a greater up-chirp. This means that "blue" spectral components are up-shifted in frequency and so move further away from the central frequency components whilst the "red" components are down-shifted. This results in a further broadening of the pulse spectrum and for the case of the high pump powers incident upon the active medium the observed spectra show the classical shape associated with positive self phase modulation [44]. As the pulse propagates around the cavity the spectral components experience a greater up-chirp due to the passsage through the Brewster-angled windows and gain medium. This leads to the spectral components in the wings

of the pulse spectrum losing their phase relationship with the central components. Thus although there is an increase in the second harmonic signal, indicating strong pulse shortening, the generated pulses are not completely phase-locked which results in the generation of the recorded autocorrelation traces. This behaviour was not observed in the non-compensated cavity as the presence of the negative dispersion introduced by the prism sequence was sufficient to compensate for part of the positive dispersion introduced by the effects described above but not for it all.

To try to eliminate this effect the separation of the prisms was increased to 70 cm but due to lack of space on the optical table an additional mirror had to be employed to allow the construction of the necessary cavity configuration. The need for 70 cm between the prisms meant that the resonator length was increased and hence the cavity period was also increased from 13 ns to 18 ns. To ascertain whether efficient mode-locked operation was possible from a cavity of such a length, or whether comatic aberrations [44] were too dominant to allow efficient laser operation (no attempt was made to compensate for comatic aberrations in any of the cavities described in this thesis and
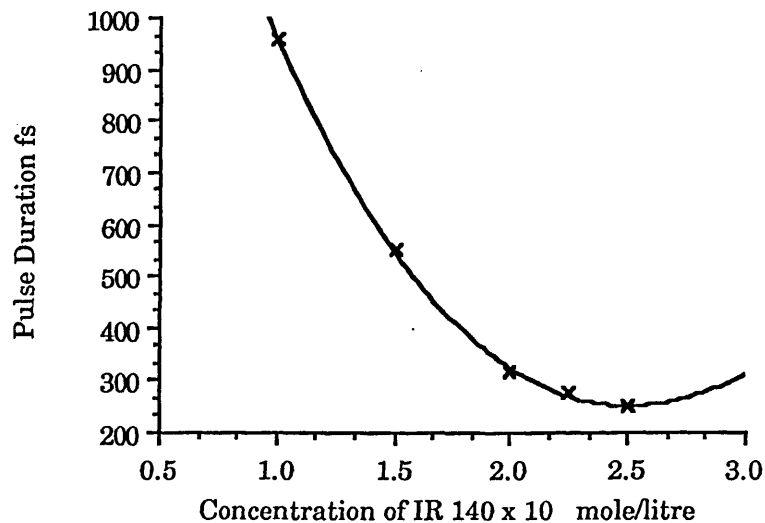
Fig 7.13: The variation of pulse duration as a function of absorber concentration for the 25 ns linear cavity.

it has been shown that the magnitude of the effect is determined by the cavity length of the laser [44]), a simple linear passive cavity was constructed with a round trip time of 25 ns. Wavelength selection was accomplished using a single prism. Mode-locked

operation was observed for pump powers between 200 mW and 400 mW above the laser threshold. The concentration of the passive dye was optimised and fig 7.13 shows the evolution of pulse duration as a function of dye concentration. At a concentration of 2.5×10^{-4} mole/litre with a pump power of 2.8 W, pulses as short as 250 fs were observed with bandwidths of 5.2 nm (see fig 7.14). This gave a time bandwidth product of 0.5 nm. The output power from the laser was approximately 16 mW which corresponds to a peak power of 1.6 kW.
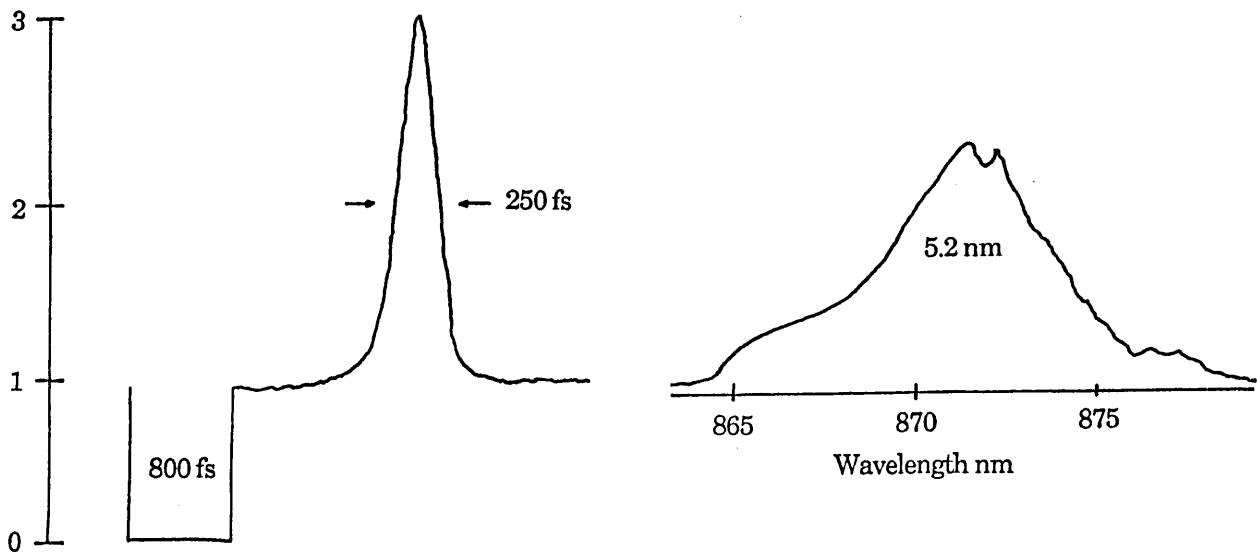
Fig 7.14: (a) The shortest pulses generated from the seven mirror passively mode-locked laser and (b) their associated spectrum.

It should be noted that when the output pulse train was monitored on a photodiode/oscilloscope combination the pulse train was observed to consist of two pulses per cavity period. The temporal separation of the two pulses was found to correspond to the separation between the passive folded section and the output coupler. Increasing the pump power to ~3 W resulted in the observation of another form of pulse splitting and this is illustrated in fig 7.15. Again the recorded autocorrelation signal did not exhibit a three to one contrast ratio. This effect was attributed to the introduction of the seventh mirror into the cavity as similar autocorrelation shapes are predicted by Christodouliodes et al [18]. This mirror was supposed to be a single stack mirror with layer thicknesses of $\frac{\lambda}{4}$ but after discussions with the manufacturers (Tec Optics,

→| |← 150 fs

→ |← 150 fs

7.2 nm

865   870   875

Wavelength nm
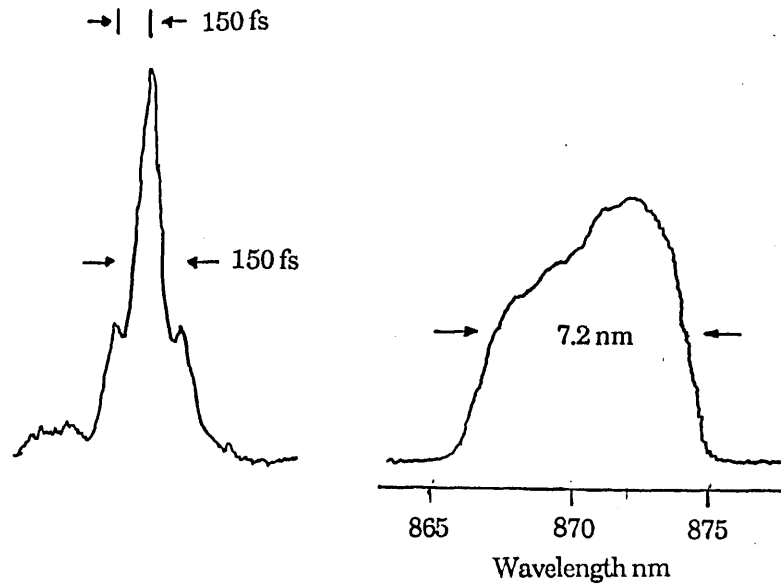
Fig 7.15:   Pulse fragmentation in the seven mirror cavity due to
the presence of a mirror with a geometrical layer
progression.

Onchan, Isle of Man) it was found that the mirror was a single stack mirror with layer

thicknesses varying in a simple geometrical progression. The presence of such a

mirror in the cavity can have dire consequences on the phase of the various spectral

components as was discussed in 7.4. For the broad spectrum associated with the pulse

recorded in fig 7.15 the components in the wings of the spectrum may interact with the

layers forming the mirror in a different manner to the central components. This can

be understood with reference to fig 7.8 which illustrates the variation of phase with

respect to frequency. It can be seen that the mirror phase can take the form of either a

rapidly varying function or a slowly varying function. If the operating wavelength

lies in a region of rapidly varying phase then there is only a small constant phase

region. It is thought that for the 250 fs pulse the spectrum associated with the pulse lies in

such a constant phase zone, however as the pump power is increased and the pulse

shortens, the spectrum broadens and the outer lying spectral components lie upon a

changing phase zone. Thus they are affected by quadratic and cubic phase terms and so

lose their phase relationship with the rest of the pulse spectra. This loss of phase is

further enhanced by the various dispersive elements in the cavity and so results in the

observed autocorrelation traces.
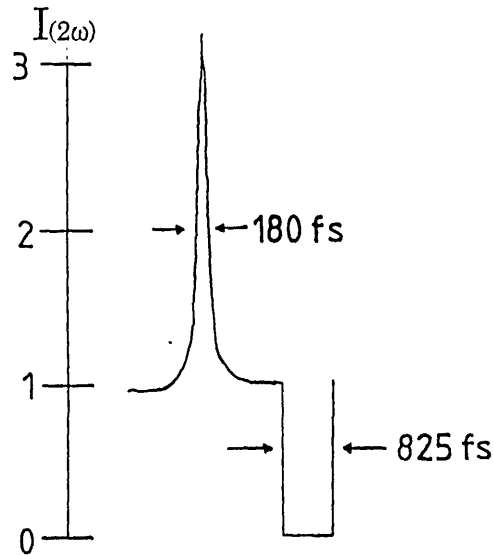
Fig 7.16: The Pulses generated from the linear dispersion compensated cavity.

When the seven mirror, four prism, dispersion-compensated resonator was finally configured it had a cavity round period of 33 ns. With the cavity optimised with respect to the amount of intracavity glass, the position of the passive dye jet and the passive concentration (2×10^{-4} mole/litre), pulses as short as 180 fs (see fig 7.16) were routinely generated with output powers of 15 mW corresponding to peak powers of 2.75 kW. The operating wavelength of the laser was controlled using the dielectric wedge and the wavelength was found to be 870 nm. Altering the magnitude of GVD in the cavity by varying the position of the passive dye jet and the amount of intracavity glass resulted in the generation of pulses as short as 150 fs, however these pulses exhibited the sub-pulses described earlier due to the presence of the seventh mirror. Thus the shortest pulses generated from this laser were ~180 fs.

7.4.6. The Colliding Pulse Mode-Locked Dispersion-Optimised Resonator.

To complete the studies on the dispersion-optimisation of the passively mode-locked $LiF:F_2^+$ colour centre laser a dispersion compensated colliding pulse resonator was constructed as depicted in fig 7.17. The separation of the prisms was 60 cm (this value is less than the 70 cm used in the linear cavity as the pulses circulating in the resonator only pass through each window once), and the cavity period was ~25 ns. The mirrors used to form the optical cavity were different to those used in the linear cavity. Initial

studies on the passive mode-locking of the colour centre were performed with mirrors which only allowed laser operation between 865 nm and 880 nm (see fig 6.5). To overcome this a set of double stack mirrors were fabricated with the bottom stack high reflecting for the pump laser wavelengths and the upper stack totally reflecting over the luminescence band of the colour centre (tunability from the re-designed colour centre laser has now been observed to cover the entire spectral region mentioned in 4.2). Once the travelling-wave resonator was constructed with the four prism sequence inserted, the threshold for laser operation was ~400 mW. Frequency selection was performed
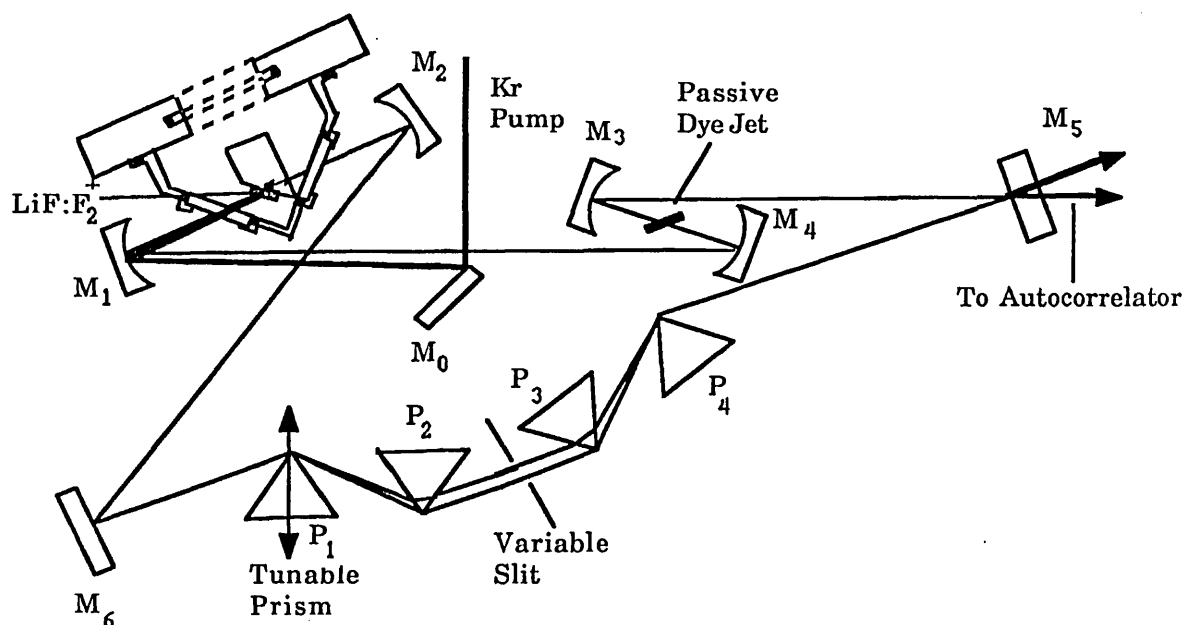
Fig 7.17: The resonator configuration of the dispersion-optimised colliding pulse mode-locked colour centre laser.

using a variable aperture slit [46] which was inserted between P_2 and P_3. This slit was translated across the dispersed beam until the mode-locking was attained. The pulses produced from the laser were monitored as the slit width was increased. The maximum aperture size was determined when mode-locking was lost due to the colour centre lasing at a different wavelength where it experienced lower losses and no attempt was made to investigate the effect of decreasing the aperture size on the pulse duration.

The concentration of the saturable absorber was set at 3×10^{-5} mole/litre and the wavelength was selected to be 850 nm. Operating at this wavelength resulted in a larger

value of the S parameter (see eqn. 3.2) as the emission cross-section of the gain medium is much lower than that at 870 nm. Increasing the absorber concentration tended to cause the colour centre laser to operate at slightly longer wavelengths. At this concentration, once the laser had been fully optimised with respect to prism and passive dye jet position, the duration of the pulses produced from the laser was ~180 fs with bandwiths of 4.2 nm as illustrated in Fig 7.18. This corresponds to a time bandwidth product of 0.317 which should be compared to that for the assumed value for Sech^2 pulses, 0.315. The pump power at which these pulses were generated was ~5 W and at the peak average output power from the colour centre laser was 15 mW per arm which corresponds to a pulse peak power of 2 kW.
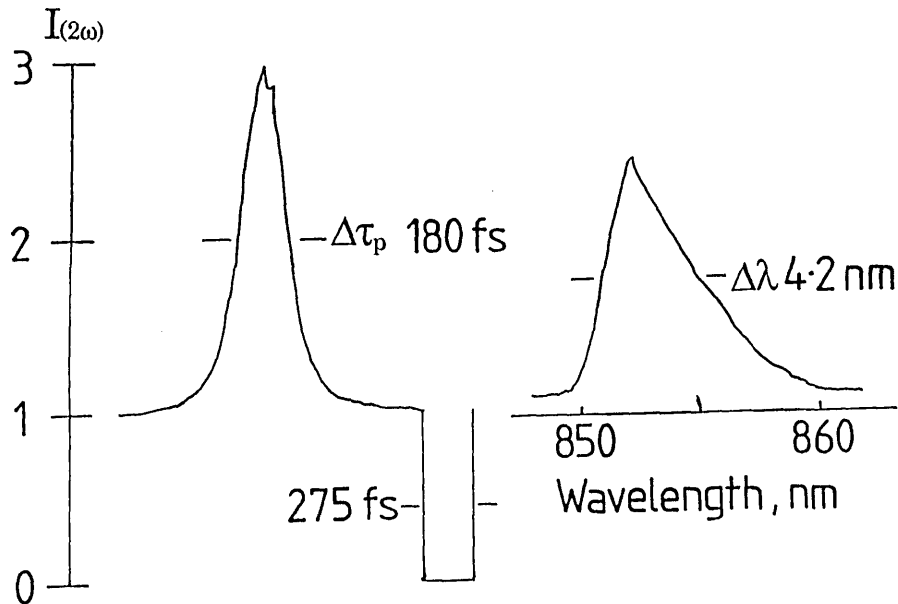
Fig 7.18:   (a) the autocorrelation trace of the dispersion-compensated ring colour centre laser together with (b) its associated spectrum.

It was noticed, however, that after prolonged periods of operation at such high pump powers the laser stability decreased, the pulses broadened and the threshold increased from 400 mW to ~ 1.5 W. The threshold could only be reduced by altering the position of the pump spot and hence the laser active spot in the gain medium. This was attributed to a thermal deionisation of the laser active centres due to the fact that the heat dissipated into the laser active crystal by the pump beam could not be removed rapidly enough

from the laser active spot. This was contrary to the behaviour reported in earlier chapters where no significant deterioration in the performance of the laser was observed, however for the work reported in earlier chapters the maximum power incident was ~3 W. This problem was overcome by reducing the open time of the chopper window from 6 ms to 4 ms, by increasing the speed of the chopper wheel, and thus decreasing the exposure time of the laser active crystal to the pump beam. Although the total heat load introduced to the crystal in one second was the same, the instanteous heating of the crystal was reduced to a level with which the crystal could cope. As the open time of the chopper window was reduced then the autocorrelation window was also reduced which affected the recording of the pulses on the real time autocorrelator as the background level could not be fully displayed. Hence the window time was increased to ~ 5 ms and operating with this open time did not fully irradicate the fading problem. As a result the effects of altering the amount of GVD in the cavity could not be investigated since the performance of the laser deteriorated whilst the autocorrelation traces were being recorded. The digital storage oscilloscope used to record the real time second harmonic autocorrelation trace took ~2 minutes to plot out the trace. The above fading described seemed to take place in about 10 minutes and thus it was difficult to obtain sufficient data points before the laser crystal had to be repositioned and the cavity re-aligned. Also as the crystal faded the pulse duration broadened and it was difficult to determine whether the change in pulse duration was a result of altering the group velocity dispersion in the cavity or a result of the crystal degrading. To overcome these problems a data logger is being designed so that the results can be stored directly on a computer and then plotted out at a later time. This will enable results to be recorded almost instaneously and so reduce the effects of variations, such as pump power drift or crystal fading, on the recorded results.

7.5. Conclusions.

In this chapter the passive mode-locking of a cw chopped $LiF:F_2^+$ colour centre laser is reported for the first time. Using the laser active dye IR140 as the saturable absorber pulses as short as 360 fs were generated, (which were tunable from 865 nm to 880 nm),

from a colliding pulse mode-locked resonator. By replacing the optics which formed the gain folded section and constructing a dispersion-optimised colliding pulse cavity pulses as short as 180 fs were routinely generated which were tunable from 850 nm to 880 nm. However the pump power required to generate these pulses resulted in strong fading of the centres which was partly rectified by reducing the open time of the optical chopper. Thus it has been shown that passive mode-locking of the $LiF:F_2^+$ colour centre laser is a viable technique for the generation of ultrashort pulses in the 850 nm to 880 nm spectral region.

References:

1. M.A. Aegerter and F. Luty; Phys.Sol. Stat. B., 43, 245, 1971.

2. P.M.W. French and J.R. Taylor; Appl. Phys. Lett., 50, 1708, 1987.

3. E.P. Ippen C.V. Shank and A. Diennes; Appl. Phys. Lett., 21, 348,1972.

4. K. Smith, N. Langford, W. Sibbett and J.R. Taylor; Opt. Lett., 10, 559, 1985.

5. J.A. Valdmanis, R.L. Fork and J.P. Gordon; Opt. Lett., 10, 131, 1985.

6. A. Finch private communication.

7. P.W. Smith, Y. Silverberg and D.A.W. Miller; J.O.S.A. B, 2, 1985.

8. G.H.C. New; Opt. Commun., 6, 188, 1972.

9. G.H.C. New; I.E.E.E. J. Quant. Elect ., QE- 10, 115, 1974.

10. L. Bosi, C. Bussolati and G. Spinolo; Phys. Lett., 32A, 159, 1970.

11. J.P. Fouassier, D.J. Lougnot and J. Faure; Opt. Commun., 18, 293, 1978.

12. M.S. Stix and E.P. Ippen; I.E.E.E. J. Quant. Elect ., QE- 19, 520, 1983.

13. R.L. Fork, B.I. Greene and C.V. Shank; Appl. Phys. Lett., 38, 671, 1981.

14. See Sellmeier eqn.n and coeffs in D. Marcuse; Appl. Opts., 19, 1916, 1980.

15. American Institute of Physics Handbook Vol. 3. p6-34

16. S. De Silvestri, P. Laporta and O. Svelto; I.E.E.E. J. Quant. Elect , QE- 20, 533, 1984.

17. W. Dietel, E. Dopel, K. Hehl, W. Rudolph and E. Schimdt; Opt. Commun., 50, 179, 1984.

18. D.N. Christodouliodes, E. Bourkhoff, R. Joseph and T. Simos; I.E.E.E. J. Quant. Elect .., QE- 22, 186, 1986.

19. R.L. Fork, C.V. Shank, R.Yan and C. Hirlimann; I.E.E.E. J. Quant. Elect .., QE- 19, 500, 1983.

20. P.M.W. French; PhD. Thesis University of London 1987.

21. S. De Silvestri, P. Laporta and O. Svelto; Opt. Lett., 9, 335, 1984.

22. A.M. Weiner, J.G. Fujimoto and E.P. Ippen; Opt. Lett., 10, 71, 1985.

23. P. Laporta and V. Magni; Appl. Opts., 24, 2014, 1985.

24. J.C. Diels, W. Dietel, J.J. Fontaine, W. Rudolph and B. Wilhelmi; J.O.S.A. B, 2, 682, 1985.

25. W. Rudolph and B. Wilhelmi; Opt. Commun., 49, 371, 1984.

26. D. Kulhke, W. Rudolph and B. Wilhelmi; I.E.E.E. J. Quant. Elect ., QE- 19, 570, 1983.

27. W.Dietel, J.J. Fontaine, and J-C. Diels; Opt. Lett., 8, 4, 1983.

28. R.A. Fisher, P.L. Kelly and T.K. Gustafuson; Appl. Phys. Lett., 14, 140, 1969.

29. O.E. Martinez, R.L. Fork, and J.P. Gordon; J.O.S.A. B, 2, 753, 1985.

30. R.S. Miranda, G.R. Jacobovitz, C.H. Brito-Cruz and M.A.F. Scarparo; Opt. Lett., 11, 224, 1986.

31. E.B. Treacy; I.E.E.E. J. Quant. Elect ., QE- 5, 454, 1969.

32. J.P. Gordon and R.L. Fork; Opts. Lett., 9, 153, 1984.

33. F. Gires and P. Tournois; C.R. Acad. Sci. Paris., 258, 6112, 1964.

34. J. Heppner and J. Kuhl; I.E.E.E. J. Quant. Elect .., QE- 22, 182, 1986.

35. P.M.W. French, G.F. Chen and W. Sibbett; Opt. Commun., 57, 263, 1986.

36. J. Kuhl, M. Serengi and E.O. Gobel; Opts. Lett., 12, 334, 1987.

37. J. Heppner and J. Kuhl; Appl. Phys. Lett., 47, 453, 1985.

38. D. Grishkowsky and A.C. Balant; Appl. Phys. Lett., 41, 1, 1982.

39. A.S.L. Gomes; PhD. Thesis University of London 1986.

40. F. Salin, P. Grangier, G. Roger and P. Brun; Phys. Rev. Lett., 56, 1132, 1986.

41. P.M.W. French, J. Williams, G.H.C. New, H. Avermeropopulos and J.R. Taylor; Paper 102 QE-8th National Conference on Quantum Electronics, St. Andrews, 1987.

42. D. Von Der Linde; I.E.E.E. J. Quant. Elect .., QE- 8, 292, 1972.

43. J.A. Valdmanis and R.L. Fork; I.E.E.E. J. Quant. Elect ., QE- 22, 112, 1986.

44. P.N. Keen, K. Smith and W. Sibbett; I.E.E. Proceedings, 134, 163, 1987.

45. A.I. Ferguson and M.H. Dunn; Opt. Commun., 20,14, 1977.

46. R.L. Fork; Opt. Lett 11, 189, 1986.

Chapter 8. Electrical Excitation of Intrinsic Defects in Alkali Halide Crystals.

8.1. Introduction.

In the previous chapters the operation of near-infrared colour centre and dye lasers was described. To achieve the power densities necessary to take the gain medium above laser threshold, high average power pump lasers and complicated resonator designs with regions of tight focussing were employed. The pump laser used in this work was a Kr^+ laser, which like most high power ion lasers, was unreliable and very inefficient. This results in the overall efficiency of the laser system being relatively low. (The need for dye jets and associated plumbing for dye lasers, and cryogenic cooling for colour centre lasers also introduces a wide range of operating problems.) At present a variety of different schemes are being tried to increase the input to output power efficiency of lasers and to develop room temperature tunable solid state lasers. A good deal of research has been undertaken into the development of high power III-V semiconductors [1] which can then be used to optically excite a wide variety of solid state materials either in bulk form [2] or in optical fibres [3]. However the shortest wavelength obtained directly from semiconductor diode devices is 650 nm [4]. For some applications solid state blue lasers would be advantageous. There are several possible ways to achieve this goal. The first involves developing II- VImaterials, such as ZnSe which has been shown to electroluminesce in the 500-600 nm spectral region [5]. The second possible avenue to explore is the development of electrically pumped colour centre lasers and a brief report of the electrical pumping of colour centres as a method of obtaining laser action from extremely thin NaCl crystals has been made by Vorob'ev et al [6]. The centre believed to be responsible for the laser action is the self-trapped exciton. The pertinent physics of this centre as a luminescence source have been outlined in section 2.5 and they have been studied by several research workers [7,8,9] and shown to produce electroluminescence in the near-ultraviolet spectral region.

8.2. Electrical Excitation of the Self-Trapped Exciton in Alkali Halide Crystals.

8.2.1. Electrical Contacts.

The mechanism responsible for the electroluminescence observed from alkali halide crystals is thought to be impact ionisation [10,11] . The application of a high potential to the crystal results in the injection of electrons, and the field ionisation of electrons trapped in the crystal. These electrons are accelerated, and scatter off the ions in the lattice during which sufficient energy may be transferred from the electron to the ion and result in the formation of the self-trapped exciton (see chapter 2). Electrical contacts must be applied to the crystal so that the necessary fields can be established across the crystal to allow the injection and field ionisation processes to occur. There are two distinct types of contact: ohmic, which allows the injection of electrons, and blocking, which hinders the injection of electrons. The nature of the contact is determined by the difference between the workfunction of the electrode material and that of the crystal. For an ohmic contact the workfunction of the crystal must be greater than that of the contact, whilst for blocking contacts the reverse applies. The distinction between blocking and ohmic contacts can be understood as follows. For the case of an ohmic contact electrons flow from the metal to the insulator, so that the Fermi levels across the contact can equalise, thus establishing a region of negative space charge in the insulator. This space charge produces a 'built-in' electric field raising the electronic energy levels in the insulator with respect to those in the metal (see fig 8.1).
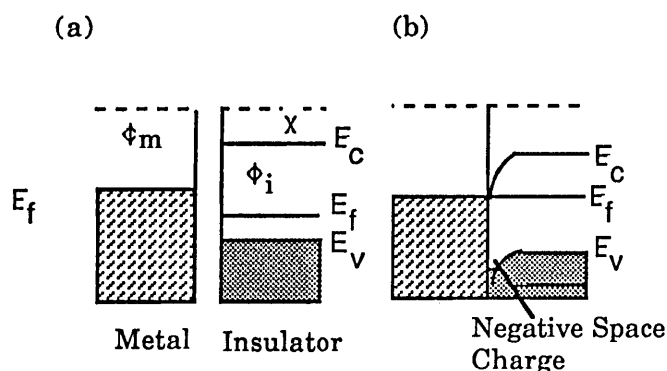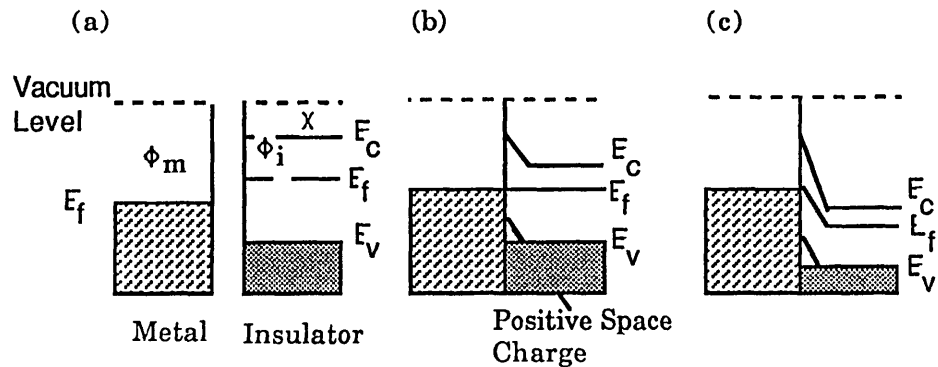

Fig 8.1: (a) A schematic of the energy levels associated with an ohmic contact ($\phi_i > \phi_m$) before a contact between the two is made. (b) The energy levels after a contact has been made.

It also acts as a reservoir of electrons allowing the unrestricted flow of current from the metal to the insulator. In the case of the blocking contact, equalisation of the Fermi levels across the contact requires electrons to flow from the insulator to the metal. This results in the build up of a positive space charge in the insulator, which leads to the formation of a depletion layer. The depletion layer acts as a potential barrier and so inhibits the injection of electrons. When an external potential is applied to the metal-insulator system the potential drops across the depletion region. If the applied potential is high enough then the depletion layer is narrowed significantly and allows the quantum-mechanical tunnelling of electrons through it and into the conduction band of the insulator (see fig 8.2c).

Fig 8.2: (a) A schematic of the energy levels associated with a blocking contact ($\phi_m > \phi_i$) before a contact between the two is made. (b) The energy levels after a contact has been made and (c) the energy levels after an external field, bias for injection has been applied.

The electrons which tunnel through the potential barrier are known as hot electrons as they are injected into electron states well above the edge of the conduction band. These hot electrons have sufficient energy to undergo multiple collisions with the phonon field of the lattice and so enable the formation of the self-trapped exciton. The injected electrons penetrate the crystal and enter regions where the effective field is low. The electrons are then captured in empty trapping states of the crystal. This trapping results in the build-up of an internal space charge field inside the crystal which inhibits the injection of further electrons. This can be interpreted as a broadening of the depletion layer at the contact/insulator interface.

The nature of the electric field distribution is determined by the energy distribution of the trapping centres present in the crystal [12]. If the crystal contains shallow traps the internal field E, is related to the applied potential V by $E \sim V^{\frac{1}{2}}$ [13]. If the traps are distributed uniformly with respect to energy then the internal field is related to the applied potential by $E \sim V$ [14]. Measuring the current flowing through the insulator with respect to the applied voltage enables the determination of the current-voltage characteristics for the insulating crystal. From this relationship the nature of the trapping states may be determined [12].

In chapter 2 the threshold current necessary for laser action to be observed from an alkali halide crystal was evaluated and found to be ~ 20 Amps. Currents of this magnitude have been observed in organic crystals such as anthraceane [15] using ohmic contacts. In order to determine whether it was possible to inject such a current into an alkali halide crystal the current-voltage characteristics of a thin sample of KCl were studied. The experimental configuration employed is illustrated in fig 8.3. The KCl crystal was thinned, in a manner similar to that described in chapter 5, to a thickness of approximately 2 mm and electrodes were attached. On one surface of the crystal a simple evaporated gold electrode was applied whilst on the other surface a sodium/potassium amalgam electrode was attached. This electrode was formed in the following way. A glass tube was glued to the crystal surface and then filled with the amalgam which was formed by melting a small piece of sodium metal on a hot plate and then adding the potassium. The resulting mixture was then drawn into a syringe and injected into the glass tube. A wire was then inserted into the amalgam and the
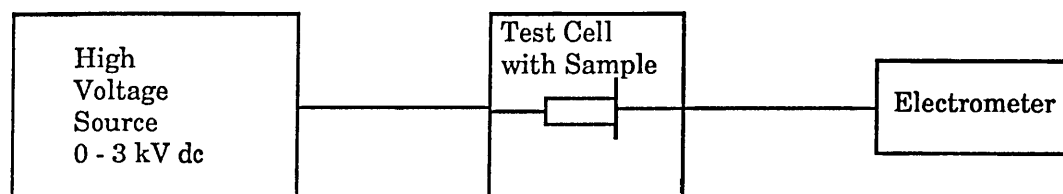
Fig 8.3:   The experimental arrangement used to measure the current-voltage characteristics of a sodium/potassium electrode.
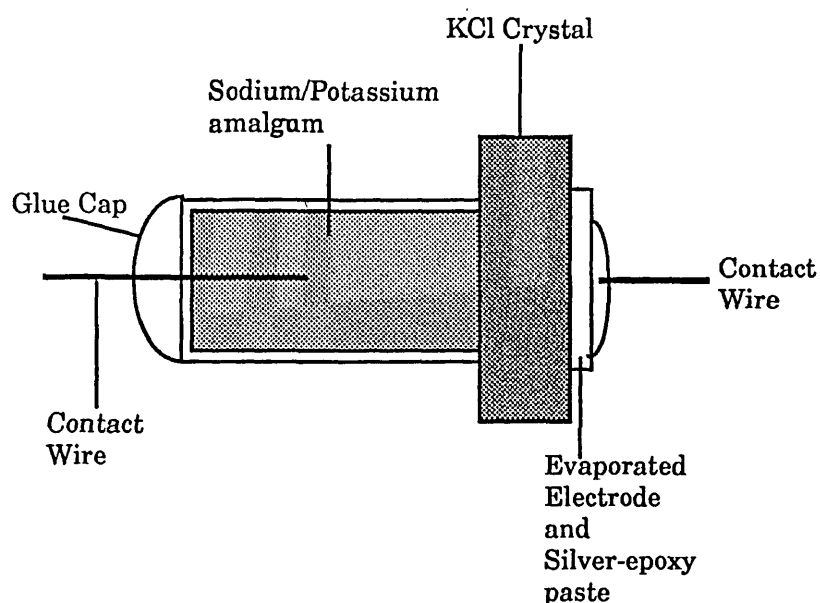
Fig 8.4: A schematic of the sodium/potassium electrode.

glass tube was sealed. The injection process had to be performed rapidly as the amalgam tended to form an oxide layer at the crystal surface which resulted in poor electrical contact being made between the two. To complete the circuit a contact was made between the evaporated electrode and the test cell. This consisted of a piece of wire bonded to the crystal by a silver-epoxy paste. A schematic of the electrode configuration is shown in fig 8.4. The resulting assembly was then placed in a test chamber, which was basically a metal box with two high voltage B.N.C. bulk heads, and a variable DC voltage applied across the crystal. The voltage was biased such that the sodium/potassium electrode should inject electrons into the sample. Care was taken throughout all the experiments to ensure that only the current passing through the sample was measured and not the combined current due to the test cell and the crystal.

As the voltage to the sample was increased a very rapid increase in the current occurred. This was then followed by a decay to a steady-state value. The transient current was typically two or three times greater than the steady state voltage but attempts to measure the exact magnitude of the transient proved fruitless as the electrometer did not have a peak hold system. A chart recorder was inserted into the circuit but the response time of the recorder was not fast enough to record the transient. This behaviour was attributed to the injection of electrons which filled electron traps in the crystal. Thus it was decided to record the data 30 seconds after changing the voltage.

The resulting current was then measured using an electrometer and the results obtained are shown in fig 8.5.
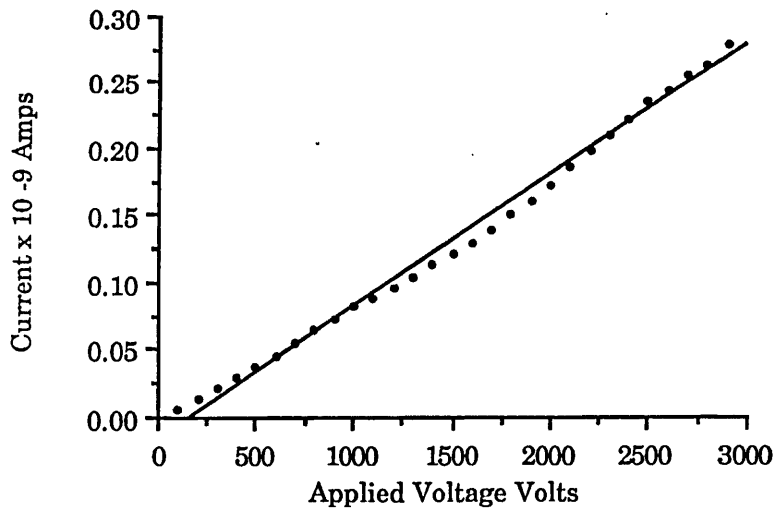
Fig 8.5:   The   current-voltage   relationship   for   the sodium/potassium electrode applied to the KCl crystal. The electrode was biased for injection.

The current-voltage relationship expected for an ohmic contact on an insulating crystal takes the form of

$$I = \frac{\varepsilon A V^2}{\mu d^3}$$ (8.1)

where μ is the mobility of the carriers in the material, ε is the relative permeability of the crystal,A the area of the contact, and d the thickness of the crystal. Thus a quadratic relationship between the current and applied voltage is to be expected. However from the results illustrated in fig 8.5 it can be seen that there is a linear relationship between the current-voltage.

This result was not expected and was attributed to the formation of an oxide layer between the sodium/potassium amalgam and the crystal. Re-making the electrode and monitoring the amalgam/crystal interface as the amalgam was injected indicated that the oxide-layer formed almost as soon as the amalgam was injected into the glass tube. The presence of this oxide-layer acts as a barrier between the crystal and amalgam and so inhibits the injection of electrons. It should be noted however that Boyd et al [16] have observed injected current densities of up to 0.15 A/cm^2 with an ohmic contact applied to

a sample of KI. However this current is still well below the predicted 20 A/cm^2. Boyd et al [16] also reported that they did not observe electroluminescence with ohmic contacts but infact only saw electroluminescence with blocking electrodes. To this extent the current-voltage characteristics of an approximately 500 μm thick piece of KCl with two gold electrodes were studied. The experimental arrangement used was the same as that shown in fig 8.3 and the results obtained are illustrated in fig 8.6. Again the same transient behaviour was observed and so the current was again recorded 30 seconds after the voltage was altered.
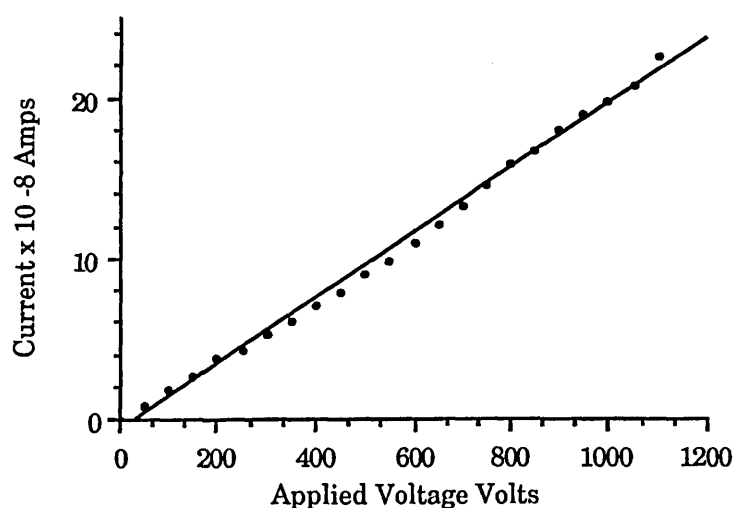
Fig 8.6:   The current-voltage charactersitics for a sample of
           KCl with evaporated blocking electrodes.

The current recorded for this type of blocking electrode was greater than that previously recorded for the ohmic contacts and this may arise from better electrical contact being made to the crystal by the evaporated material than in the case of the amalgam electrode.

8.3. Experimental Observations of Electroluminescence

8.3.1. The Liquid Nitrogen Cryostat.

The studies made on the current-voltage characteristics of the KCl crystal were performed at room temperature with DC applied fields, however the recombination luminescence produced by self-trapped excitons is radiative for temperatures around

77 K and has only been observed with AC applied fields. To attain this temperature, liquid nitrogen can be used as the coolant and to minimise effects associated with water vapour condensation and high liquid nitrogen boil-off rates a cryostat was designed. The cryostat, shown in fig 8.7, can be divided into two distinct portions. The top portion comprised the outer wall of the dewar and the liquid nitrogen can. Attached to the base of the liquid nitrogen can was a copper cold finger. Mounted on the surface of the cold finger was a P.T.F.E. platform which acted as a clamp and guide for the pressure contact. The pressure contact consisted of a copper disc attached to a spring-loaded rod (see fig 8.8). This form of contact was selected to ensure that the crystal sample was kept in good thermal contact with the copper coldfinger. Problems, however, arose from the degree of electrical contact made between the crystal sample and the copper disc, and at present different schemes are being investigated to try and identify the optimum method of electrical and thermal contacting. The temperature of the cold finger and hence that of the crystal sample was measured by inserting a platinum resistance
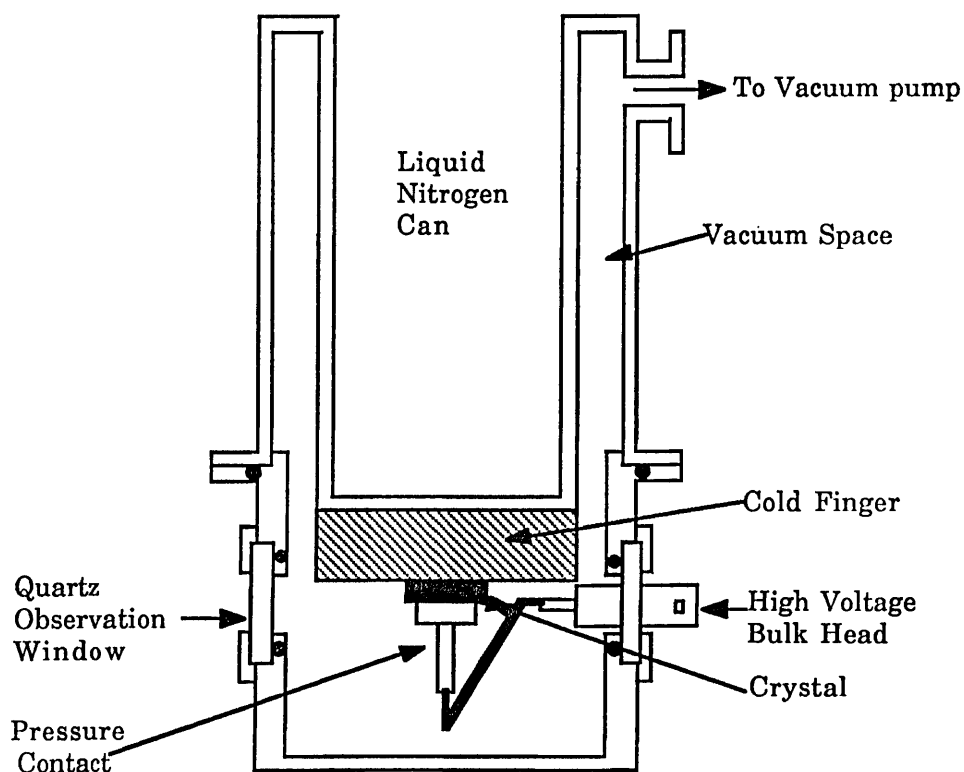
Fig 8.7:   A schematic of the electrical pumping cryostat.
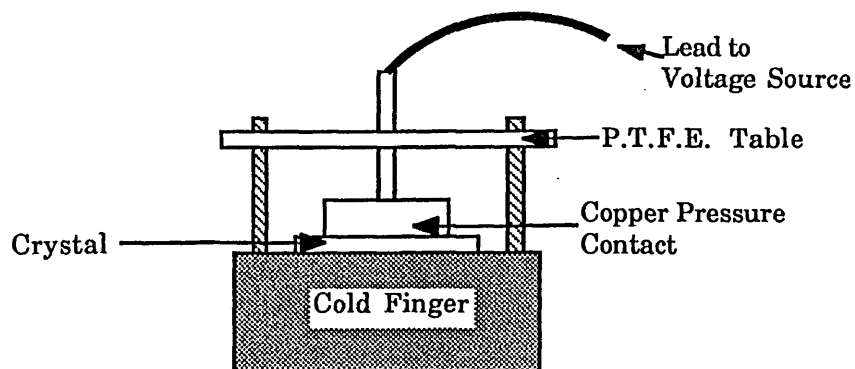
Fig 8.8:   An enlargement of the cold finger of the electrical pumping dewar showing the P.T.F.E. table.

thermometer into the coldfinger.The bottom portion contained the quartz observation windows and the high voltage connectors. Electrical insulation between the crystal and the coldfinger was provided by a thin film of mylar. Initial studies were made with a thin disc of P.T.F.E. as the insulator but this material was found to be a very poor thermal conductor and the crystal sample did not reach the temperature required for the exciton recombination process to be radiative.

8.3.2. Preparation of The Crystal Sample.

Electroluminescence from alkali halide crystals is normally observed when the applied field across the sample is of the order of 10^5 V/cm [8]. Thus for a crystal with a thickness of 1 cm the ^{voltage} applied to the crystal has to be 10^5 V. Voltages of this size are extremely difficult to manipulate. To reduce the applied field the crystal must be thinned down and for the case of the crystals used in the initial studies outlined here, the thinning followed a similar pattern to that described for the production of the LiF crystals used in chapters 5-8. The crystals were polished to typical thicknesses of 150 μm and on one of the surfaces a simple aluminium electrode was evaporated. The majority of the luminescence work presented here was performed using CsI as the sample crystal. The workfunction of aluminium is 4.25 eV [17] whilst for a CsI crystal the workfunction is 1.45 eV [18] and so the contacts were blocking in nature. It should be noted that KCl was tried but no electroluminescence was observed with our set-up. The KCl sample was studied when the P.T.F.E. disc was used to provide the electrical

insulation and so the the sample may not have been at the correct temperature, however, Lebedeva et al have reported luminescence from an ~ 10 μm film of KCl [19]. The production of such thin films by polishing is extremely difficult and at present the thinnest achieved is ~50 μm.

8.3.3. Experimental Observations of Electroluminescence.

An outline of the experimental procedure is now given. A ~150 μm thick sample of CsI was mounted on the copper coldfinger and electrical contact was made between the crystal and the pressure contact. The cryostat was then sealed and evacuated to a typical working pressure of 10^{-5} Torr to avoid Paschen breakdown effects [20], where the applied voltage ionises the gas surrounding the crystal and results in the applied field being dissipated in the gas rather than across the crystal. This effect can also be controlled by limiting the applied voltage to the crystal but this reduces the amount of light emitted from the sample.The pressure was measured at the exit port and so gave a good indication of the actual pressure inside the vacuum space. With the dewar evacuated to the correct working pressure the voltage was then applied to the crystal. The voltage source was a simple step-up transformer which operated at frequencies between 50 Hz and 100 Hz and gave a fixed voltage output of 2.5 kV. This corresponds to fields ~1.5 x 10^6 V/cm being applied to the crystal which should be above the threshold field for electroluminescence. The resulting electroluminescence from the CsI sample was then coupled onto a spectrometer/PMT arrangement so that both the pulse shape of the luminescence signal and its wavelength could be monitored. The signal from the PMT was then fed into a phase-sensitive-detector before being passed to the monitoring device (chart recorder or oscilloscope).

A typical electroluminescence spectrum observed from the CsI sample is shown in fig 8.9. The luminescence extends from 300 nm to 400 nm peaking at 325 nm and is similar to that observed by Parachinni [21]. The temporal features of the observed luminescence signal (shown in the oscillogram of fig 8.9.) were however very different from that reported by Parachinni [21]. This was attributed to the fact that the electroluminescence depends upon the rate of change of voltage with respect to time,
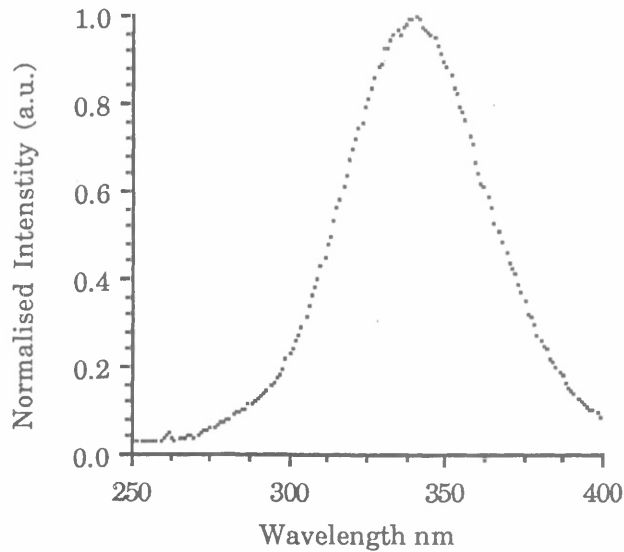
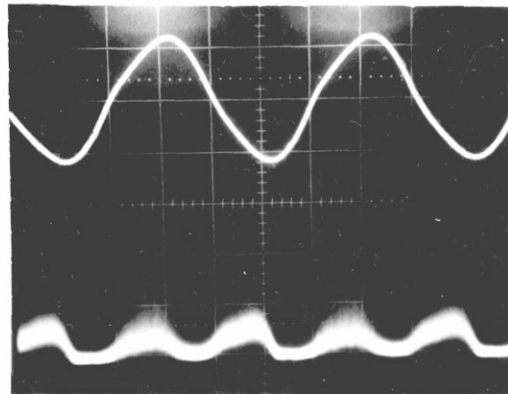Fig 8.9:   The recorded luminescence spectrum from the CsI sample studied.

Fig 8.10: The luminescence signal recorded on the PMT. The upper trace is the voltage signal (1 kV/div). The lower trace is the luminescence signal (1 V/ div). Horizontal scale 0.1 s/div.

$\frac{dV}{dt}$, and at 50 Hz the $\frac{dV}{dt}$ associated with the sine wave excitation signal may not be fast enough to ensure a strong luminescence signal. This can be understood if the following argument which was first proposed by Paracchini [9] is considered. If α is the ionisation rate (that is the number of electron-hole pairs created by a single electron travelling a unit distance in the direction of the applied field) and ϖ is the drift velocity, then the number of photons emitted per unit time, $\frac{dn}{dt}$, is given by

$$\frac{dn}{dt} = \alpha(F)\sigma(F)$$

(8.2)

From this equation it can be seen that both $\alpha(F)$ and $\sigma(F)$ are functions of the internal local field F. The nature of this internal field depends upon the potential difference which appears at the metal insulator contact and this in turn is governed by the energy distribution of the trapping centres (see 8.2.1). Due to the formation of a space charge, the internal field F decreases exponentially in time with respect to the applied potential. (This explains why electroluminescence is not observed for an applied DC voltage.) After a time t' from the beginning of the excitation signal the internal field can be described as

$$F(t') \sim \frac{1}{d} \int_0^{t'} \frac{dV(t)}{dt} \exp{-\frac{(t-t')}{\tau}} dt.$$

(8.3)

where τ is a constant given by the time delay between the applied voltage and the onset of the electroluminescence and d the thickness of the crystal sample. Also any distortion of the applied sinusodial applied voltage may also lead to a decrease in the electroluminescence efficiency. By increasing the drive frequency to 100 Hz, results comparable to those observed by Paracchini were recorded (see fig 8.11).
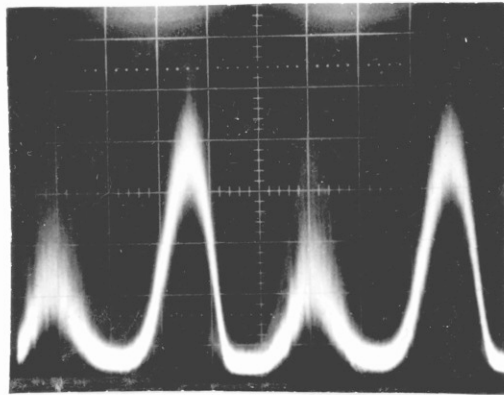
Fig 8.11:   The electroluminescence signal recorded from the CsI
sample with the applied voltage operating at 100 Hz.
Vertical scale 1V/div, horizontal scale .05 s/div.

From this oscillogram it can be seen that there are two distinct components to the recorded signal: one low intensity and the other high intensity . The appearance of the two signals can be attributed to the fact that only one electrode is attached to the crystal and that the excitation signal exhibits both positive and negative $\frac{dV}{dt}$ variations which

means that the crystal is biased for the injection of electrons only on the negative voltage gradient.

With the aluminium electrode on the crystal, and before the voltage signal is applied to the sample, electrons are exchanged between the metal and insulator interface in order to keep the vacuum and Fermi levels constant. This results in a considerable distortion of the insulator conduction band leading to the production of a depletion region inside the crystal as described in section 8.2 and in fact when the driving potential applied to the crystal sample most of it drops across this depletion region. The nature of the potential barrier generated by this depletion region is determined by the distribution of traps in the crystal as mentioned in 8.2.The presence of the negative bias potential results in the injection of hot electrons and also the field-induced ionisation of electrons traps. Both sets of electrons are accelerated up to impact ionisation energies and induce the formation of self-trapped excitons which then recombine to generate the observed luminescence . The electrons penetrate the crystal and enter regions where the space charge field is low. They then are captured in empty traps and form a layer of negative space charge inside the crystal which opposes the further injection of electrons and hence the electroluminescence ceases. When the field is reversed some of these trapped electrons are liberated from the traps and accelerated back towards the contact until they again reach impact ionisation energies. However, the number of electrons which are accelerated during this stage is less than that in the previous portion of the excitation cycle and so the associated secondary electroluminescence signal is reduced.

Although the voltage source was frequency tunable time did not permit an investigation of the effects of frequency variations on the luminescence output. For the sine wave excitation signal used in this work, $\frac{dV}{dt}$ also changed as the frequency changed. By considering eqn. 8.3 it can be seen that the electroluminescence observed from alkali halides is directly dependent upon the rate of change of the external applied potential. Thus for the sine wave excitation signal employed here any changes made in the frequency also affect the rate of change of the applied voltage and so would devalue the results of frequency variations. To investigate these effects and those of

variations in the applied potential a new excitation source should be constructed which will deliver square wave excitation signals.

8.4. Conclusions

In this chapter initial studies into the feasibility of electrically pumping colour centres were made by studying some of the electroluminescence properties of the self-trapped exciton in CsI. This centre was shown to electroluminesce from 300 - 400 nm when an applied field of approximately 1.5×10^6 V/cm was applied to the crystal. At present this work is only in its infancy and in order to attain an electrically pumped colour centre laser studies into the optimum form of electrodes, the shape of these electrodes and the most efficient luminescent host will have to be undertaken. The blocking contacts used in this work are suitable for electroluminescence for they allow the development of a depletion region inside the crystal which then accelerates the injected hot electrons up to energies necessary for field ionisation. However, for laser action to be established it is thought that current densities ~20A/cm^2 must be injected into the insulator (see chapter 2). To achieve cuurent densities of this magnitude ohmic contacts must be used [15] and so the possibility of establishing ohmic contacts onto the alkali halide crystal must be re-addressed.

Nonetheless, it may be concluded at this stage that electrical excitation of alkali halide media does show some promise and the prospects of a blue/ultraviolet laser of this type would be very interesting indeed. Thus the preliminary work described here can be regarded as laying a useful foundation upon which substantial subsequent work could be built.

References:

1. W. Striefer, R.D. Burnham, T.L. Paoli and D.R. Scifres; Laser Focus/Electro-Optics June 1984 page 100.

2. T.Y. Fan and R.L. Byer; Opt. Lett., 12, 809, 1987.

3. I. Alcock, A.I. Ferguson, D.C. Hanna and A.C. Tropper; Opt. Commun., 58, 405, 1986.

4. T. Hayakawa, T. Sutuma, K. Takahashi, M. Kondo, S. Yamamoto and T. Hijikata; Appl. Phys. Letts., 51, 707, 1987.

5. Y.S. Park and B.K. Shin in Electroluminescence. Ed. J.I. Pankove, Springer Verlag Berlin 1977.

6. G.A. Vorob'ev, S.G. Ekhanin, N.I. Lededva, S.N. Morev and N.S. Nesmelov; Sov. J. Phys., 18, 1774, 1976.

7. C. Paracchini and G. Schianchi; Solid State Commun., 8, 1769 1970.

8. S. Unger and K. Teegarden; Phys. Rev. Lett., 19, 1229, 1967.

9. C. Paracchini; Phys. Rev. B., 7, 1603, 1973.

10. W.W. Piper and F.E. Williams; Brit. J. Appl. Phys., 6, 39, 1955.

11. G.F. Alfrey and J.B. Taylor; Proc. Phys. Soc. London., B68, 775, 1955.

12. G.P. Owen and A. Charleby; J. Phys. C., 7, 1400, 1974. and references therein.

13. N.F. Mott and R.W. Gurney; *Electronic Processes in Ionic Crystals*, Oxford University Press, Oxford. 1940.

14. A. Rose; Concepts in Photoconductivity and Allied Problems, Interscience, New York 1963.

15. R.W. Smith; Phys. Rev., 97, 1525, 1955.

16. R.W. Boyd, M.S. Malcuit and K.J. Teegarden; I.E.E.E. J. Quant. Elect ., Q E-18, 1202, 1982.

17. N.W. Ashcroft and N.D. Mermin in *Solid State Physics*, Holt Sanders New York 1976 p. 364.

18. D.W. Lynch; Phys. Rev., 118, 468, 1960.

19. N.I. Lebedeva and N.S. Nesmelov; Sov. Phys-Sol. Stat., 14, 1106, 1972.

20. See for example page 486 of *Conduction of Electricity Through Gases* by J.J. Thompson and G.P. Thompson, Cambridge University Press 1933.

21. C. Paracchini; Phys. Rev. B., 7, 1603, 1973.

Chapter 9: General Conclusions.

The work presented in this thesis has mainly been concerned with the generation and the characterisation of ultrashort pulses in the near-infrared spectral region using both the laser active dye Rhodamine 700 and the F_2^+ colour centre in a LiF host crystal as the gain media. These two gain media were directly excited by a krypton-ion pump laser and tunability was observed from 690 - 810 nm for the dye laser and 815 - 1050 nm for the colour centre laser. The laser active colour centre was operated in two different resonator/cryostat combinations and by the selection of suitable optics tunability was observed over the spectral region just mentioned for both cryostats. Both the gain media were demonstrated as highly efficient sources with slope efficiencies ~40 % and 22 % being observed for the dye and colour centre laser respectively. It should be noted that the colour centre laser output was 'under-coupled' and higher slope efficiencies are to be expected by using an output coupler with the optimum transmissivity (see chapter 5).

To exploit the large tuning range and high output powers offered by these two gain media the possibilities of ultrashort pulse generation were investigated. Both the dye and colour centre lasers were synchronously mode-locked using an acousto-optically mode-locked krypton-ion laser as the pump source. Synchronous mode-locking of the dye laser resulted in the realisation of pulses as short as 1 ps which were tunable over the entire lasing bandwidth of the gain medium (see chapter 4). Attempts to synchronously mode-lock the $LiF:F_2^+$ colour centre using the original resonator/cryostat combination failed, due to inherent design problems, as discussed in chapter 5. Re-design of the resonator/cryostat system (chapter 6), such that only the laser active crystal was maintained in the vacuum space, allowed the generation of pulses as short as a 0.7 ps from a synchronously mode-locked ring colour centre laser. The need for precise matching of the slave laser cavity period to some multiple, or sub-multiple, of the pump laser period is well known [1]. The effects of introducing a timing mis-match between the cavity periods on the pulse shape and duration were studied for both the dye and colour centre laser. The results obtained agree with those reported by other researchers [2,3] in that the shortest pulses were always observed for

positions just beyond (~2 μm) the point of maximum second harmonic.

Although the pulses generated from the synchronously mode-locked colour centre laser are the shortest pulses yet reported further pulse compression can be achieved by the addition of a saturable absorber into the laser cavity allowing the combination of gain and absorber saturation as the pulse shaping mechanisms. Hybrid mode-locking was applied to both the dye and colour centre lasers and using the laser active dye IR 140 as the saturable absorber, pulses as short as 550 fs were generated from the colour centre laser. In the case of the R700 dye laser two different saturable absorbers were employed, DOTCI and HITCI, which led to the generation of 470 fs and 550 fs pulses respectively.

The dependence of the pulse duration on the degree of matching between the pump and slave laser cavity periods is a restrictive constraint on ultrashort pulse generation from both dye and colour centre lasers. This constraint can be alleviated by the use of the technique of passive mode-locking. Until recently this technique had been applied solely to the cw Rhodamine 6G dye laser [4,5] and to quasi-cw flash lamp pumped dye lasers [6]. In this thesis several new active/passive combinations were described. The Rhodamine 700 dye laser was shown to passively mode-lock with DOTCI and HITCI as the saturable absorbers together with a composite saturable absorber of DOTCI/DCI. These led to the generation of pulses of 850 fs (DOTCI),850 fs (HITCI) and 430 fs (DOTCI/DCI) (see chapter 4). Passive mode-locking of the LiF:F_2^+ colour centre laser was demonstrated for the first time and the studies were extended to include both non-dispersion-compensated and dispersion-compensated standing-wave and travelling-wave resonators. The duration of the pulses produced from the dispersion-compensated travelling-wave resonator were ~180 fs in duration with time-bandwidth products implying Sech^2 intensity profiles.

Although ultrashort pulses have been generated from both dye and colour centre lasers little attention has been paid to applications for these pulses. In chapter 4 the characterisation of a weakly multimode optical fibre using the synchronously mode-locked Rhodamine 700 dye laser in conjunction with a synchronously scanning streak camera was described. This allowed the core radius together with the refractive index difference between the core and the cladding to be evaluated. Recent theoretical studies

on the propagation of optical pulses in a single mode optical fibre at wavelengths close to the zero dispersion wavelength indicate that reshaping of either the leading or trailing edge of the pulse should occur [7]. (Since this could have some importance in digital optical communications or data-storage schemes it is worthy of quantitative assessment.) By using a synchronously mode-locked colour centre laser together with recently developed streak cameras containing photocathodes which respond to 1.3 μm light [8] it should be possible to observe directly these pulse reshaping effects. For such a study there are two possible colour centre lasers which could be used as the pulse source. These are the $NaF:(F_2^+)^{**}$[9] and the $KF:F_2^+$ [10] colour centres. The absorption peak of the $NaF:(F_2^+)^{**}$ is centred around 900 nm and can be excited directly by either the $LiF:F_2^+$ colour centre laser described here or by the near-infrared dye laser HITCP [11]. The photochemical and thermal stability, as well as the efficiency of this dye, are poor, however by taking the necessary precautions the photochemical and thermal stablity may be improved. Similarily by adding the laser active dye Rhodamine 700 to the HITCP dye solution an efficient energy transfer laser could be constructed to give output powers comparable to those observed from the $LiF:F_2^+$ colour centre laser [12].By synchronously mode-locking the energy transfer dye laser or the $LiF:F_2^+$ colour centre laser it is believed that pulses of the appropriate picosecond duration should be generated from the $NaF:(F_2^+)^{**}$ laser to observe the pulse propagation effects.

A more direct method to access the relevant wavelength range is to use the F_2^+ centre in KF. This centre is attractive as it can be excited directly by a mode-locked Nd:YAG laser [10]. The technique of pulse compression using an optical fibre and grating pair has been clearly demonstrated for the Nd:YAG laser [13] and by using this technique it should be possible to study the effect of varying the pump pulse duration on the output pulse from the colour centre. However it should be noted that the KF crystal is hygroscopic and any advantages that direct excitation offer may be outweighed by problems encountered in the handling and preparation of the crystal.

The development of the soliton laser [14], whereby the pulses from a synchronously mode-locked KCl:Tl colour centre laser are compressed in an optical fibre and then re-injected back into the cavity of the colour centre laser, has resulted in the generation of

highly stable ultrashort pulses in the 1.55 μm region. This effect can be due to the production of optical solitons arising from a balancing of the negative group velocity dispersion in the optical fibre with the positive dipsersion introduced by the self-phase modulation in the fibre [15]. In addition a recent theoretical treatment has indicated that any external-cavity modulation applied to a laser, be it gain saturation or absorber saturation, should lead to a better phase-locking of the modes in the pulse and hence greater stability [16]. This effect will be investigated for the $LiF:F_2^+$ colour centre laser.

Further studies planned for the $LiF:F_2^+$ colour centre laser involve the use of the resonator/cryostat described in chapter 6 and configuring a unidirectional single frequency travelling-wave resonator. The better frequency definition offered by colour centre lasers over dye lasers [17] should allow for precise studies to be made of narrow band gap semiconductor materials in the 850 nm spectral range. Similar studies can be performed in the 1.3 μm and 1.5 μm regions by simply changing the laser active crystal and pump laser.

Other avenues to explore are the development of new frequency-tunable solid state materials either in bulk form or in optical fibres. Two such materials which have attracted a large amount of interest are alexandrite and Ti:sapphire which have been demonstrated as laser active materials in the 700 - 800 nm [17] and 650 - 1050 nm [17] spectral regions respectively. From these tuning ranges it can be seen that the output wavelengths cover the same spectral regions as the dye and colour centre lasers described in this thesis but they do not require the necessary plumbing and cryogenic cooling. Similarly the development of rare-earth doped materials should provide another possible source for tunable laser action in the visible and near-infrared spectral regions [18]. For work in the 1.5 μm region, the colour centre laser, based on either the KCl:Tl or the $NaCl:O_2^-$ systems, offers the most versatile source of ultrashort pulses at present and the fact that they offer greater ouput powers and tunability when compared to 'new' laser materials and semiconductor diodes lasers operating in the same wavelength region is likely to ensure their continued use for the foreseeable future.

The proposed schemes outlined above all rely on the use of inefficient optical pump sources to provide the necessary excitation. There is a clearly recognised need to develop highly efficient electrically pumped lasers or new materials to serve as laser active media which are tunable in the visible and blue spectral regions. To this end the electroluminescence from the self-trapped exciton in CsI was studied. For ultraviolet/blue laser emission the direct electrical pumping of alkali-halide materials offers exciting new possibilities. The preliminary research relating to CsI which has been discussed here indicates that electroluminescence can be reliably obtained in the 300 - 400 nm spectral region from the self-trapped exciton. It must be recognised that these initial results represent the beginning of the investigations into direct electrical excitation and many extensions in terms of active media and electrical driving schemes can be envisaged. By replacing the CsI crystal with a sample of KBr it may be possible to extend the wavelength range out to 600 nm as this crystal has been demonstrated as a luminescence source over the 400 - 600 nm range by Lebedeva et al [19]. Similarily using NaCl crystals which have been doped with Ag or other heavy elements it should be possible to access the deep ultraviolet around 220 nm. In fact electroluminescence has been demonstrated from NaCl:Ag crystals over the 200 - 500 nm range [20]. At present the excitation scheme used for this work simply consisted of a step-up transformer operating between 50-100 Hz. Although this proved to be a useful system for the direct excitation of the self-trapped exciton a more interesting approach would be to use an Austen switch [21,22] to provide the necessary voltage pulse. Using such a device driven by a mode-locked laser would enable a form of actively mode-locking to be exploited, simply by matching the cavity length to the drive frequency, thus allowing the possibility of ultrashort pulse generation in the ultraviolet/blue spectral region without having to use complicated frequency conversion techniques [23,24]. The luminescence generated by the NaCl:Ag sample has been shown to peak at a wavelength 247 nm [20] and a short pulse laser based on this centre might prove to be an ideal source for seeding a KrF amplication system. As mentioned in chapter 8 investigations are underway to find the best method of applying electrical and thermal contacts to the sample and a new design of dewar is being

developed in which the sample is mounted in a vertical plane. This system will also have an electric heater attached to the cold arm, so that the temperature of the sample can be varied. This should allow the optimum temperature for efficient electroluminescence to be determined [25].

References:

1. N.J. Frigo, T. Daly and H. Mahr; I.E.E.E. J. Quant. Elect. .., QE-13, 101, 1977.

2. C.P. Ausschnitt, R.K. Jain and J.P. Heritage; I.E.E.E. J. Quant. Elect. .., QE-15, 912, 1979.

3. R. Illingworth and I. Ruddock; Opt. Commun., 61, 120, 1987.

4. E.P. Ippen C.V. Shank and A. Diennes; Appl. Phys. Lett., 21, 348, 1972.

5. P.M.W. French and J.R. Taylor; Appl. Phys. Lett., 50, 1708, 1987.

6. W. Sibbett and J.R. Taylor;I.E.E.E. J. Quant. Elect. ., QE-20, 108, 1984.

7. D. Marcuse; Appl. Opts., 19, 1916, 1980.

8. X. Hou, W. Sibbett and B. Weekley; Rev. Sci. Inst., 52, 1487, 1981.

9. L.F. Mollenauer; Opt. Lett., 6,342,1981.

10. L.F. Mollenauer and D.M. Bloom; Opt. Lett., 4, 247, 1979.

11. M.Leduc and C. Weibusch; Opt. Commun., 45,36, 1978.

12. N.Langford, K. Smith and W.Sibbett; Opt. Lett.,12,813, 1987.

13. A.S.L. Gomes; PhD. Thesis University of London 1986.

14. L.F. Mollenauer and R. Stolen; Opt. Lett. 9,13,1984.

15. H.Haus and M. Islam; I.E.E.E. J. Quant. Elect ., QE- 22, 1785, 1986

16. D.Blow and D. Nelson; To be published in J.O.S.A. B, March 1988.

17. L.F. Mollenauer in *Tunable Solid State Lasers* Eds J.C. White and L.F. Mollenauer Springer Verlag, Berlin 1986 Chp 6.

18. J.C. Walling in *Tunable Solid State Lasers* Eds J.C. White and L.F. Mollenauer Springer Verlag, Berlin 1986 Chp 9.

19. N.I. Lebedeva and N.S. Nesmelov; Sov. Phys-Sol. Stat., 14, 1106, 1972.

20. N.I. Lebedeva, N.S. Nesmelov and A.V. Vladimirov; Sov. Phys-Sol. Stat., 19, 372, 1977.

21. D.H. Austen; Appl. Phys. Lett., 26, 101, 1975.

22. W. Margulis, W. Sibbett, and J.R. Taylor; Opt. Commun.; 35, 153, 1980.

23. P.G. May; PhD. Thesis University of London 1983.

24. S.J. Bastow and M.H. Dunn; Opt. Commun.; 35, 259, 1980.

25. Initial investigations performed on a sample of CsI:Na indicate that as the temperature of the crystal is raised from 77 K to ~ 150 K the intensity of the luminescence signal recorded is observed to increase by a factor of three.

175

Acknowledgements

I wish to thank Professor Wilson Sibbett , my supervisor, Dr. Gari Owen, my C.A.S.E. supervisor, and Dr. Kevin Smith for their encouragement and guidance during this work. I would also like to thank those in the Optics Group of Imperial College for assistance before my move to St. Andrews, most notably Dr. Roy Taylor. Special thanks are also extended to Mr. Bob Mitchell and to Mr. Derek Bayne, of the University of St. Andrews, for their specialist help in vacuum testing the various cryostats. Also Dr. Bill Sleat, Colin Johnston and Robert Grant plus the rest of the laser group at St. Andrews deserve to be acknowledged.

The technical staff of the Optics Group of Imperial College, Mr. R. Morrison and Mr. R. Wilkins, the Physics Department of the University of St. Andrews, Mr. G. Radley and Mr. J. Lindsey, and the Royal Armaments Research and Development Establishment (R.A.R.D.E.) are thanked for the speed and efficiency with which various cryostats, optical mounts and components were produced.

Financial support from the Science and Engineering Research Council and R.A.R.D.E. is gratefully acknowledged.

Finally I would like to thank my wife Alison for the many hours spent reading and correcting the initial drafts of this thesis and 2 year old Alexander for scribbling on them.

Publications

STREAK CAMERA STUDY OF ULTRASHORT PULSE PROPAGATION IN A WEAKLY MULTIMODE OPTICAL FIBRE

Indexing term: Optical fibres

A mode-locked dye laser in conjunction with a synchronously operating streak camera has been used to study ultrashort light pulse propagation in a weakly multimode optical fibre. Measurements of the intermodal temporal dispersion allowed the effective core radius a, the refractive index difference Δ and the cutoff wavelengths of the LP_{21} and LP_{11} mode groups to be determined. The LP_{21} cutoff wavelength was experimentally verified and the temporal dispersion of the LP_{01} and LP_{11} mode groups investigated as a function of the fibre length.

The 'Synchroscan' streak camera[1] has proved to be an extremely useful tool in the study of light events in the picosecond time domain,[1] including the propagation of ultrashort light pulses in optical fibres.[2] In this letter we employ such a system in conjunction with a highly tunable synchronously mode-locked CW Rhodamine 700 dye laser to provide a real-time display of the intermodal temporal dispersion in a weakly multimode optical fibre.
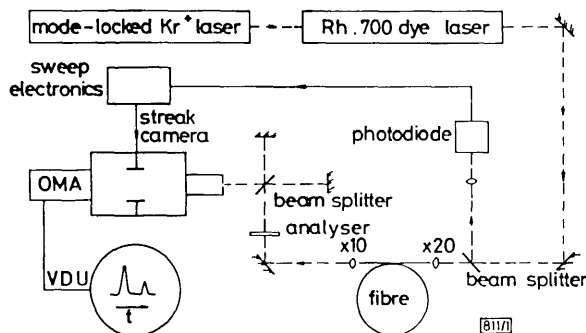
Fig. 1 *Experimental arrangement*

The 51·5 m-long sample of optical fibre investigated in this experiment was manufactured commercially and was nominally single-mode at 1·3 μm. However, for the operational wavelength range of the synchronously mode-locked Rhodamine 700 dye laser (subpicosecond pulses were generated over the 700–800 nm spectral range with average output powers ~100 mW), the optical fibre was expected to be weakly multimode. Fig. 1 shows the experimental arrangement used in this letter. A fraction of the laser output (~10 mW average power) was coupled into the optical fibre using a ×20 microscope objective. Output coupling was achieved with a ×10 microscope objective which allowed the propagating mode groups to be directed into an optical delay line (for calibration purposes) and then on to the input slit of the streak camera. The output from the fibre was also studied with an analyser (to determine the mode polarisation state) and a screen (to observe the transverse mode structure). The rest of the dye laser output was used to trigger the RF sweep electronics for the synchronously operating Photochron II[3] streak camera. The streak images were then coupled to the optical multichannel analyser (OMA), which provided a real-time display of the fibre output pulses. A temporal resolution (measured before the fibre) of 15 ps was quite sufficient for this study of modal dispersion. (However, it is worth noting that a temporal resolution of close to 1 ps has been demonstrated for a Photochron II streak camera used in conjunction with a passively mode-locked CW ring dye laser.)[4]

With the dye laser operating at a wavelength of 705 nm, three mode groups were observed and identified: the LP_{01}, LP_{11} and LP_{21} mode groups. Fig. 2 shows the temporal displacement of these modes after propagating through the 51·5 m-long fibre. Simultaneous observations of the transverse mode structure of the fibre output and the real-time Synchroscan display allowed the propagation order to be easily ascertained. (The relative amplitudes of the mode groups were found to be highly sensitive on both the launching conditions and the alignment of the analyser.) According to the theory,
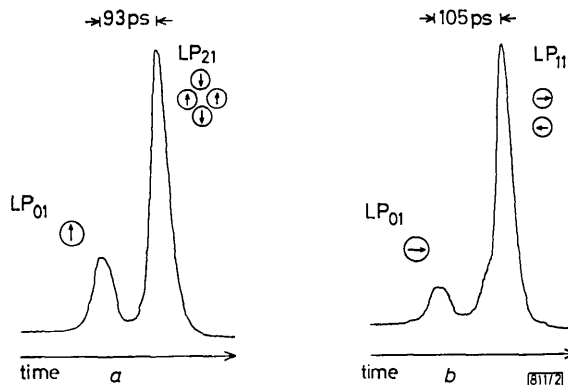

Fig. 2 *Temporal displacement of (a) LP_{01} and LP_{21} mode groups (vertically polarised) and (b) LP_{01} and LP_{11} mode groups (horizontally polarised) for $\lambda = 705$ nm*

for a weakly guiding step-index fibre,[5] the group delay T_{gr} of a particular mode group is dependent on both material dispersion (which is the same for all mode groups) and the waveguide dispersion, which is dependent on the derivative $d(vb)/dv$, the normalised group delay. From Reference 5 we have the following expression for this group delay:

$$T_{gr} = (L/c)[(d(nk)/dk) + n\Delta(d(vb)/dv)] \qquad (1)$$

where L is the fibre length, n is the core refractive index ($= 1·45$), Δ is the core/cladding refractive index difference, c is the velocity of light and k ($= 2\pi/\lambda$) is the wavenumber in free space. The relative group delays of the LP_{21} and LP_{11} mode groups with respect to the fundamental Gaussian, LP_{01} mode group (ΔT_{21} and ΔT_{11}, respectively) shown in Fig. 2 arise from the modal variation of $d(vb)/dv$ (see Fig. 4 of Reference 5), and are given by

$$\Delta T_{21} = (Ln\Delta/c)[(d(vb)/dv)_{21} - (d(vb)/dv)_{01}] \qquad (2)$$

$$\Delta T_{11} = (Ln\Delta/c)[(d(vb)/dv)_{11} - (d(vb)/dv)_{01}] \qquad (3)$$

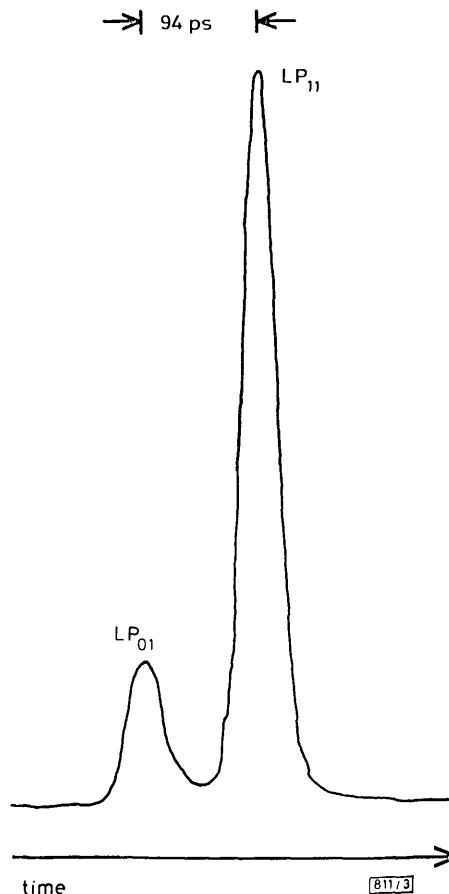A knowledge of these relative group delays ($\Delta T_{21} = 93$ ps and

Fig. 3 *Temporal displacement of LP_{01} and LP_{11} mode groups for $\lambda = 745$ nm*

$\Delta T_{11} = 105$ ps) allowed an effective normalised frequency parameter V $(= 2\sqrt{(2)}\pi a(n\Delta)^{1/2}/\lambda)$ to be deduced,[2,5] and from our data a value of $V = 4\cdot11 \pm 0\cdot01$ was obtained. Using this value and the associated values of $d(vb)/dv$ for the three mode groups, the effective refractive index difference Δ was determined to be $(3\cdot4 \pm 0\cdot2) \times 10^{-3}$ from either of eqns. 2 or 3. The effective core radius a was then calculated from Δ via the expression for V, and found to be $4\cdot64 \pm 0\cdot1$ μm. These values are in very good agreement with those supplied by the optical fibre manufacturer, whose quoted step-index values for a and Δ are $4\cdot66$ μm and $3\cdot4 \times 10^{-3}$, respectively, for this fibre sample.* From the above values of a and Δ, the cutoff wavelengths for the LP_{21} and LP_{11} mode groups were calculated to be $0\cdot755 \pm 0\cdot040$ μm and $1\cdot203 \pm 0\cdot060$ μm, respectively. As the former cutoff wavelength lay well within the tuning range of the synchronously pumped Rhodamine 700 dye laser, the laser output was tuned to longer wavelengths, and at $\lambda = 745$ nm the LP_{21} mode group was no longer observed to propagate. In Fig. 3 the temporal displacement is indicated for the two remaining mode groups $(LP_{11}$ and $LP_{01})$ at the new value of the normalised frequency parameter corresponding to $\lambda = 745$ nm. The measured relative group delay of 94 ps is in excellent agreement with the value of 96 ps calculated from eqn. 3 for the new V number and associated dispersion data. Fig. 4 shows the temporal displacement of the

LP_{11} and LP_{01} mode groups as a function of the optical fibre length. A linear relationship, as expected from eqn. 3, was obtained with a gradient of $1\cdot84$ ps/m.

In conclusion, a synchronously operating streak camera in conjunction with a mode-locked dye laser has been employed in the determination of important optical fibre parameters and cutoff wavelengths for the LP_{21} and LP_{11} mode groups. By utilising the high tunability of the synchronously pumped dye laser, it was possible to investigate the region of cutoff for the LP_{21} mode group. Current work relates to ultrashort pulse propagation studies in the $1\cdot0-1\cdot4$ μm spectral range in respect of mode cutoff wavelengths and temporal profile characterisation.

K. SMITH
W. SIBBETT*
N. LANGFORD

4th September 1985

Photonics Group
Blackett Laboratory
Imperial College
Exhibition Road, London SW7 2BZ, United Kingdom

* Present address: Department of Physics, University of St. Andrews, North Haugh, St. Andrews, Fife KY16 9AJ, United Kingdom

Fig. 4 *Plot of relative group delay of* LP_{01} *and* LP_{11} *mode groups* (ΔT_{11}) *as a function of fibre length* $(\lambda = 745$ nm$)$

* HAUGE, S.: 'Optical fibres', Deeside, Clwyd, Wales (private communication)

References

1 SIBBETT, W.: 'Synchroscan streak camera systems'. Proceedings of 15th international congress on high-speed photography and photonics, San Diego, 1982, *SPIE*, 348, pp. 15–26
2 WILLSON, J. P., SIBBETT, W., and MAY, P. G.: 'Synchroscan streak camera measurements of mode propagation in optical fibres'. Proceedings of 3rd international conference on picosecond phenomena, Garmisch-Partenkirchen, 1982, pp. 149–152
3 BRADLEY, D. J., and SIBBETT, W.: 'Subpicosecond chronoscopy', *Appl. Phys. Lett.*, 1975, 27, pp. 382–384
4 WILLSON, J. P., SIBBETT, W., and SLEAT, W. E.: 'Pulsewidth and interpulse jitter measurements of a passively mode-locked ring CW dye laser', *Opt. Commun.*, 1982, 42, pp. 208–210
5 GLOGE, D.: 'Weakly guiding fibres', *Appl. Opt.*, 1971, 10, pp. 2252–2258

Subpicosecond-pulse generation in a synchronously mode-locked ring color-center laser

N. Langford, K. Smith, and W. Sibbett

Department of Physics, University of St. Andrews, St. Andrews, Fife KY16 9SS, Scotland, UK

Data are presented for the operation of a versatile color-center laser that permitted the generation of stable trains of subpicosecond pulses in a synchronously pumped ring configuration. With LiF:F_2^+ as the gain medium, pulses having durations of 0.7 psec (Gaussian pulse shape assumed) were reliably obtained with average powers of 15–20 mW available in each of the two output beams. These pulse widths are more than a factor of 2 shorter than those obtained when this laser was configured with a standing-wave resonator.

Within the last decade, frequency-tunable lasers employing color-center media have gained increasing importance in scientific research. In particular, the generation of picosecond-pulse trains from such lasers by the technique of synchronous pumping was investigated by several authors.[1–6] Early experiments on synchronous mode locking were performed on F_2^+ color-center lasers and revealed optical pulses of several picoseconds in duration for both LiF and KF systems.[1,7] In view of the large homogeneous luminescence bandwidth, the ultimate limit on pulse duration was speculated to be subpicosecond. To date, this femtosecond potential of the color-center laser has been realized only in the case of the soliton laser.[8] In this Letter, we present preliminary data that indicate that stable trains of subpicosecond pulses can be produced directly by a mode-locked LiF:F_2^+ color-center laser.

Laser operation took place at cryogenic temperatures, so the LiF:F_2^+ color-center crystal was mounted on a copper cold finger (maintained at ~77 K) and located in an evacuated enclosure. All the reflecting cavity optics were external to the dedicated crystal enclosure so that our design afforded maximum choice of cavity arrangement. It was therefore straightforward to configure and evaluate both standing-wave and traveling-wave cavities. The basic configuration of the bidirectional ring resonator is shown in Fig. 1. The two thin (~2-mm) Brewster-angled windows (W_1, W_2) that provided optical access to the Brewster-angled LiF crystal also ensured that the necessary vacuum fidelity could be maintained. Mode-locked operation of the Kr-ion pump laser (at 647 nm) provided about 1-W time-averaged power of 90-psec duration pulses at a repetition frequency of 82 MHz. The horizontally polarized pump light was coupled into the active medium through mirror M_0 and one of the folded mirrors (M_1 and M_2 have radii of curvature of 10 cm). The optical resonator for the color-center laser was completed by the two plane mirrors M_3 and M_4, one of which (M_4) served as an output coupler, and frequency tuning was effected by an intracavity dielectric wedge. In part of the work described in this Letter a simple linear-cavity configuration was employed. This was achieved by substituting mirror M_2 for a 5-cm radius-of-curvature mirror and ensuring alignment of the M_1, M_2, and M_4 mirror assembly. It is worth noting that both linear and ring cavities facilitate efficient color-center laser operation with noncollinear pump- and infrared-beam alignments. This feature eliminates the effect of optical feedback and subsequent mode-locking degradation of the pump laser.

The F_2^+ color centers were created in polished 10 mm × 10 mm × 2 mm LiF crystals by the established technique[1] of electron bombardment at low temperatures (~77 K in our case). This process created high densities of F centers and anion vacancies. Subsequent annealing of the crystals at room temperature, at which the anion vacancies became mobile, allowed the aggregation of these centers to form high densities of the required F_2^+ centers. (This latter process took place during the time required to load and cool the crystal in the vacuum enclosure—approximately 10 min.) The absorption band associated with the created F_2^+ centers is strongly peaked in the 650-nm spectral region, which is well suited to the 647- and 676-nm output of a Kr-ion pump laser. Once it was loaded, the crystal could easily be translated (along the x, y, and z axes) in order to position it inside the cavity and obtain optimum laser performance. To minimize thermal degradation of the active F_2^+ centers, we used a chopped pump beam with a duty factor of 8×. The nature and time scale of the observed degradation in efficiency of the LiF:F_2^+ gain medium depended on
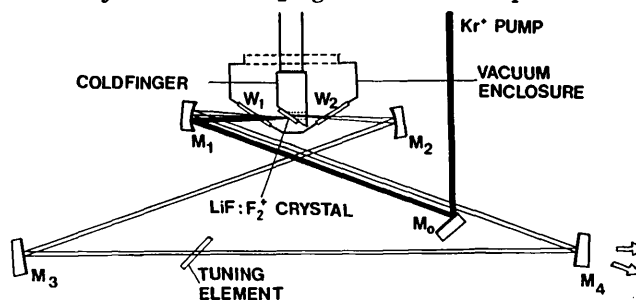

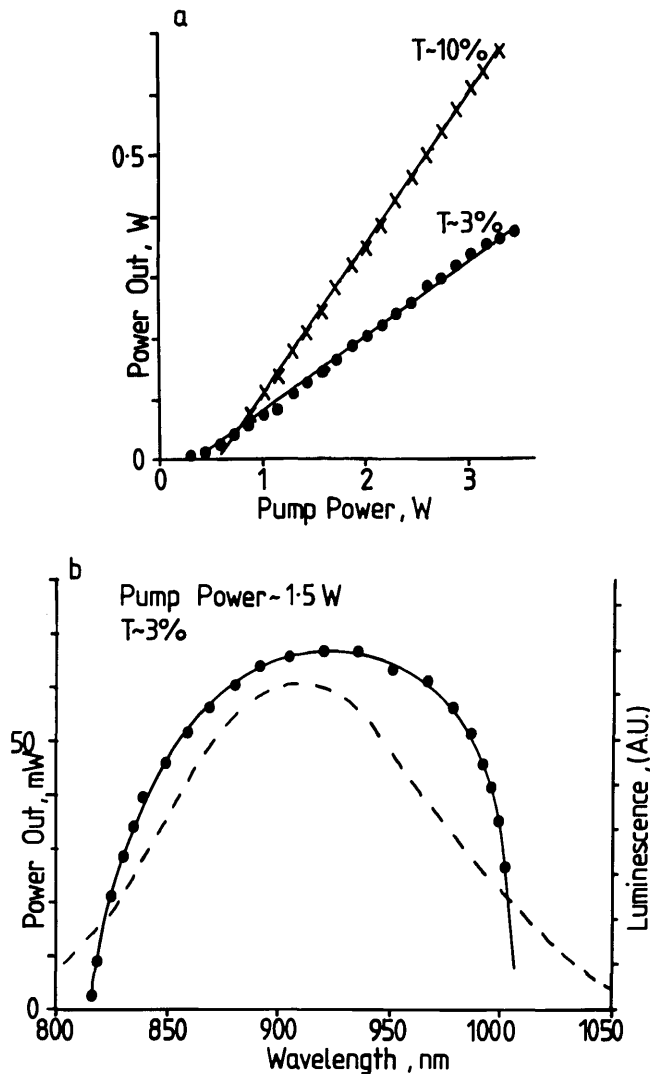Fig. 1. Color-center laser with traveling-wave cavity configuration.

Fig. 2. Peak chopped output power versus a, pump power for $T \sim 3\%$ ($\lambda = 875$ nm) and $T \sim 10\%$ ($\lambda = 922$ nm) output couplers and b, wavelength for a pump power ~ 1.5 W and $T \sim 3\%$ output mirror. The dashed line included in b corresponds to the luminescence band of F_2^+ color centers in LiF.

the peak power of the pump-laser beam. Under the conditions of excitation, using a non-mode-locked cw laser, (4-W) stable laser operation was obtained for more than 200 h from the same active focal volume of the crystal. (This period is defined as the time during which the threshold pump-power level doubles—typically from 300 to 600 mW for the arrangement illustrated in Fig. 1.) When the crystal was moved, a comparable laser performance could be obtained for a further 20 h of operation. The degradation was attributed to the deionization of the F_2^+ color centers.[1] When the laser was synchronously pumped by a mode-locked Kr-ion laser, the period of stable operation was somewhat reduced. In this case, 100 h of operating time could be obtained for the same spot on the crystal. By adjusting the crystal location, the laser could be used for a further 20 h, but the stability period progressively decreased for each spot. This effect was believed to result from orientational bleaching of the F_2^+ centers when these were subjected to the relatively high peak power (~ 100 W) of the pump pulses.[1]

The performance of the $LiF:F_2^+$ laser in a linear configuration is illustrated in Fig. 2 in terms of efficiency and tunability. Figure 2a shows the peak (chopped) output power of the color-center laser as a function of the pump power for 3 and 10% transmission output couplers. Broad-wavelength tunability is demonstrated in Fig. 2b for the 3% output coupler and a somewhat poorer crystal than the one employed in Fig. 2a. The longer-wavelength side of the tuning curve is limited not by the luminescence properties of the active center[9] (illustrated as the *dashed line* in Fig. 2b) but by the cavity optics employed (100% reflectivity; 800–1000 nm). Mode locking of this standing-wave color-center laser was achieved by the technique of synchronous pumping, and, to facilitate cavity-length adjustments of the color-center resonator, mirror M_4 was mounted on a precision translation stage. Pulse durations were monitored by using the standard collinear second–harmonic generation autocorrelation technique, and the durations were calculated from the full width at half-maximum, assuming a Gaussian pulse shape. In the linear-cavity configuration pulse durations of 2–3 psec were typical, with pulses as short as 1.5 psec being measured. Figure 3 shows an autocorrelation trace of the shortest pulses with a corresponding spectrum. A time–bandwidth product of 0.48 is inferred, which is close to the value of 0.44 for a bandwidth-limited Gaussian pulse shape. Considerably shorter pulses were obtained from the mode-locked bidirectional ring-cavity configuration. Figure 4 shows a typical autocorrelation trace for 0.7-psec duration pulses for the laser operating at 880 nm with a pump power of 600 mW. At this wavelength, the peak (chopped) output power in each of the output beams was in the range of 15–20 mW. Simultaneous measurement of the spectral width gave a value of 1.8 nm, implying a time–bandwidth product of 0.49. Mode-locked operation was obtained essentially over the whole wavelength range depicted in Fig. 2b, with appreciably shorter pulses and greater stability than that observed for the conventional linear-cavity configuration. This was attributed to the coherent interaction process in the gain medium for the ring resonator that gives rise to enhanced gain depletion and to cross coupling between the counterpropagating pulses.[10-12]

Preliminary studies of the mode-locked behavior of the linear and ring $LiF:F_2^+$-center color-center configurations reveal a close similarity to the corresponding
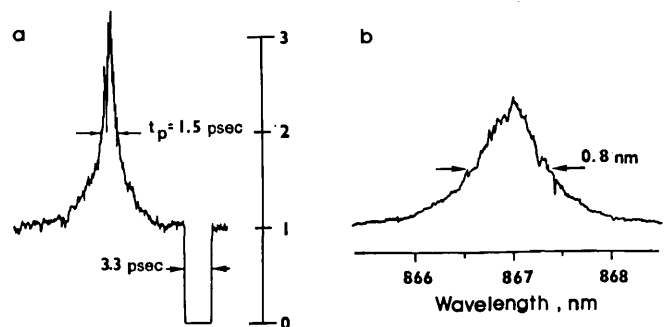

Fig. 3. Autocorrelation trace of the shortest pulses obtained from a, the synchronously pumped standing-wave laser and b, the corresponding laser bandwidth ($T \sim 3\%$).

PERFORMANCE CHARACTERISTICS OF A SYNCHRONOUSLY PUMPED LiF:F$_2^+$ COLOUR CENTRE LASER

N. LANGFORD, K. SMITH [1] and W. SIBBETT

Department of Physics, University of St. Andrews, St. Andrews, Fife KY16 9SS, Scotland, UK

We present data from a versatile colour centre laser design which has permitted the characterisation of the synchronously mode-locked behaviour of linear and ring cavity configurations for the F$_2^+$ centre in LiF. In a linear cavity, we have generated pulses with typical durations in the 2–3 ps range (assuming a gaussian pulse-shape) and observed performance characteristics similar to those of synchronously pumped dye laser systems with regard to cavity length detuning and pump power dependences. Considerably shorter pulse durations (~0.7 ps) were obtained from the mode-locked laser when configured in a bi-directional ring resonator.

1. Introduction

At present, many time-domain spectroscopic studies are undertaken using frequency-tunable, synchronously mode-locked lasers as the primary source of excitation. The most common of these are the argon/krypton ion- or Nd:YAG-pumped dye lasers which have been studied extensively both experimentally and theoretically [1–9]. In recent years, however, the generation of picosecond pulses by synchronously pumped colour centre lasers has received much attention due to their convenient operation in the near infrared spectral region [10–15]. Early experiments on synchronous mode-locking of colour centre systems were performed on F$_2^+$ centre gain media and revealed optical pulses of several picoseconds in duration for both LiF and KF hosts [10,16]. The mode-locked behaviour of these lasers was reported [16] to be remarkably similar to that of their synchronously pumped dye counterparts. However, subsequent work relating to other colour centre media where important parameters such as the radiative decay time and gain cross-section of the centre were very different to those of dyes, has revealed the expected deviation from dye laser-like

mode-locked behaviour [12–15]. In this paper, we present a detailed study of the performance of a synchronously mode-locked LiF:F$_2^+$ standing-wave colour centre laser and the generation of stable trains of subpicosecond pulses in a bidirectional ring configuration is also described.

2. Experimental

Stable long term laser operation of the LiF:F$_2^+$ centre took place at cryogenic temperatures. For the laser employed in this work, all the reflecting cavity optics were external to the dedicated crystal vacuum enclosure so that the design afforded maximum choice of cavity arrangement. It was therefore straightforward to configure and evaluate both standing-wave and travelling-wave resonator geometries. The basic linear cavity configuration is illustrated in fig. 1. The LiF cyrstal was mounted at Brewster's angle (with respect to the resonator axis) on a horizontal copper coldfinger maintained at 77 K and located in the evacuated enclosure. The two thin Brewster-angled windows (W$_1$, W$_2$) which provided optical access to the LiF crystal also ensured that the necessary vacuum fidelity could be maintained. A krypton ion laser generated approximately 4 W pump power when operated simultaneously on
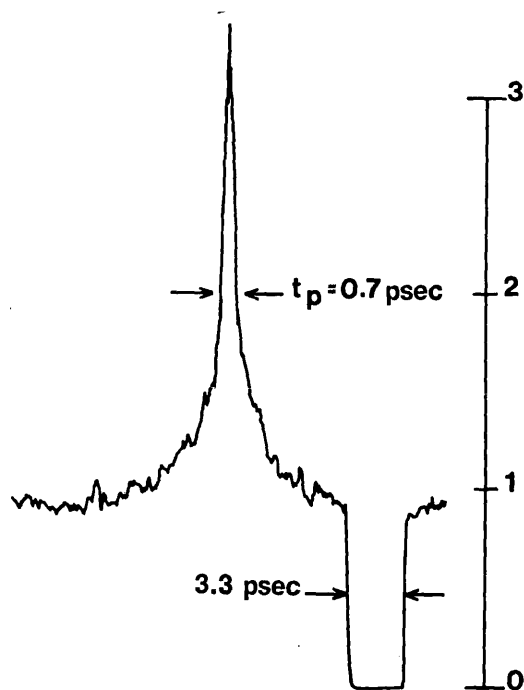
Fig. 4. Autocorrelation trace of shortest pulse obtained from ring laser for a pump power of 600 mW ($T \sim 3\%$).
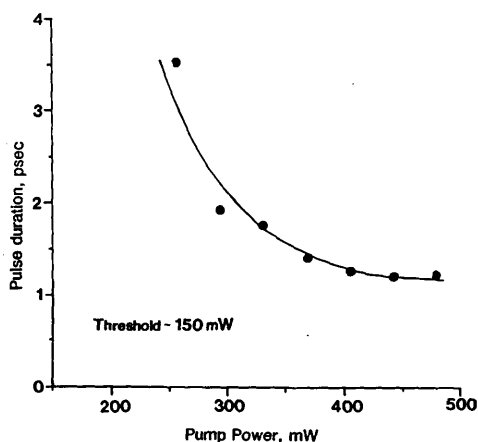

Fig. 5. Plot of pulse duration versus pump power for the ring laser.

performance[11,13] of synchronously pumped dye-laser systems. For instance, the effects of cavity-length detuning were studied, and it was found that satellite pulses were generated at negative mismatches, whereas broader pulses having a distinct dominant coherence spike were observed under conditions of positive mismatch.[14] This dyelike nature is to be expected since, for the LiF:F_2^+ center, the radiative decay time [reported to be 29 nsec at 77 K (Ref. 15)] and the gain cross section [$\sim10^{-16}$ cm^2 (Refs. 1 and 9)] are similar to those of commonly used dyes. Other synchronously pumped color-center systems (with typically much longer radiative decay times than the cavity round-trip time) showed significant deviation from the dyelike behavior.[3-6] In particular, the formation of

pulses in the picosecond domain (~10 psec) was observed only at high pump powers.[3,6] In both cavity configurations, our color-center laser produced good-quality picosecond mode-locked pulses at pump powers of less than twice threshold (Fig. 5).

In conclusion, we have described a versatile color-center laser design that permits the evaluation of both standing-wave and traveling-wave resonators. By exploiting the mechanism of coherent interaction of counterpropagating pulses in the gain medium, we generated stable trains of subpicosecond pulses over the wavelength range 800–1000 nm and, to the authors' knowledge, obtained the shortest pulses (~0.7 psec) yet reported for a purely synchronously pumped color-center laser. The passive mode locking of this LiF:F_2^+ laser by using the polymethine cyanine dye IR140 as a saturable-absorber medium[16] is currently being investigated, and its performance characteristics will be reported in the near future.

References

1. L. F. Mollenaur, in *Handbook of Lasers*, M. L. Stitch and M. Bass, eds. (North-Holland, Amsterdam, 1985), Vol. 4, Chap. 2.
2. T. T. Basiev, N. S. Vorobiev, S. N. Mirov, V. V. Osiko, P. P. Pashinin, V. Postolov, and A. M. Prokhorov, JETP Lett. **31**, 291 (1980).
3. L. F. Mollenaur, N. D. Vieira, and L. Szeto, Opt. Lett. **7**, 414 (1982).
4. L. Isganitis, M. G. Sceats, and K. R. German, Opt. Lett. **5**, 7 (1980).
5. R. Illingworth and I. S. Ruddock, Opt. Commun. **61**, 120 (1987).
6. M. N. Islam, L. F. Mollenauer, and K. R. German, in *Digest of Conference on Lasers and Electro-Optics* (Optical Society of America, Washington, D.C., 1987), paper TUHH1.
7. L. F. Mollenauer and D. M. Bloom, Opt. Lett. **4**, 247 (1979).
8. L. F. Mollenauer and R. H. Stolen, Opt. Lett. **9**, 13 (1984).
9. J. Nahum, Phys. Rev. **158**, 814 (1967).
10. J. P. Heritage and E. D. Isaacs, in *Digest of Conference on Lasers and Electro-Optics* (Optical Society of America, Washington, D.C., 1981), paper WL3.
11. C. P. Ausschnitt, R. K. Jain, and J. P. Heritage, IEEE J. Quantum Electron. **QE-15**, 912 (1979).
12. P. G. May, W. Sibbett, and J. R. Taylor, Appl. Phys. B **26**, 179 (1981).
13. R. L. Fork, B. I. Greene, and C. V. Shank, Appl. Phys. Lett. **38**, 671 (1981).
14. N. Langford, K. Smith, and W. Sibbett, submitted to Opt. Commun.
15. L. Bosi, C. Bussolati, and G. Spinolo, Phys. Lett. **32A**, 159 (1970).
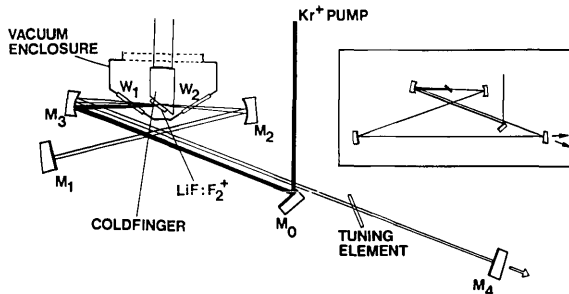16. K. Smith, W. Sibbett, and J. R. Taylor, Opt. Commun. **49**, 359 (1984).

Fig. 1. Colour centre laser with standing-wave resonator configuration. (Inset: ring resonator).
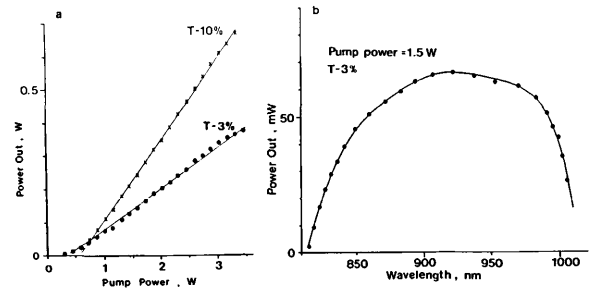

Fig. 2. Peak chopped output power versus (a) pump power for $T \approx 3\%$ ($\lambda = 875$ nm) and $T \approx 10\%$ ($\lambda = 922$ nm) output couplers, and (b) wavelength for a pump power ~ 1.5 W and $T \approx 3\%$ output coupler.

the 647 nm and 676 nm lines. Mode-locked operation of the laser (at 647 nm) provided about 1 W time-averaged power of 90 ps duration pulses at a repetition frequency of 82 MHz (length of cavity ~ 1.8 m). The horizontally polarised pump light was coupled into the active medium via mirror M_0 and one of the mirrors M_2, M_3 (both with radii of curvature of 10 cm). The optical resonator was completed with the plane mirrors M_1 and M_4 and frequency tuning was affected by an intracavity dielectric wedge. Mirror M_4 also served as an output coupler for the resonator. Mode-locking of this standing-wave colour centre laser was achieved by the technique of synchronous pumping whereby the round-trip cavity period of the resonator was precisely matched to that (or one half) of the pump laser. In order to facilitate cavity length adjustments, mirror M_1 was mounted on a precision translation stage. Stable uni-directional mode-locked operation was ensured by asymmetry in the mirror locations (i.e. length $M_1M_2 \ll$ length M_3M_4 (~ 1.4 m)). In part of the work described in this paper a bi-directional ring configuration was employed. This was achieved as illustrated in the inset diagram in fig. 1. Pulse durations were monitored using the standard collinear second harmonic generation autocorrelation technique and the durations calculated from the full-width-at-half-maximum (fwhm) assuming a gaussian pulseshape. It is worth noting that both linear and ring cavities facilitate efficient colour centre laser operation with non-collinear pump and infrared beam alignments. This feature eliminates the effect of optical feedback and subsequent mode-locking degradation of the pump laser.

The F_2^+ colour centres were created in the pol-

ished $10 \times 10 \times 2$ mm LiF crystals by the established technique [10] of the electron bombardment at low temperatures (~ 77 K in our case). This process created a high density of both F-centres and anion vacancies. Subsequent annealing of the crystals at room temperature where the anion vacancies became mobile allowed the aggregation of these centres to form high densities of the required F_2^+ centres (absorption peak ~ 650 nm [17]). This latter process took place during the time required for both loading and cooling of the crystal in the vacuum enclosure which was approximately 10 minutes for our system. Once loaded the crystal position could be finely adjusted to optimise laser performance. To minimise thermal degradation of the active F_2^+ centres the pump laser beam was chopped with a duty reduction factor of $\times 8$. Under these conditions we have generally obtained in excess of 200 hours of stable and efficient laser operation from a single crystal.

2. Results and discussion

The performance of the LiF:F_2^+ laser in a linear configuration is illustrated in fig. 2 in relation to efficiency and tunability. Fig. 2(a) shows the peak (chopped) output power of the colour centre laser as a function of the pump power for the 3% and 10% transmission output couplers. Although broad wavelength tunability is demonstrated in fig. 2(b) (for a somewhat poorer crystal than in fig. 2(a)) the longer wavelength side of the tuning curve is not limited by the luminescence properties of the active centre [17]
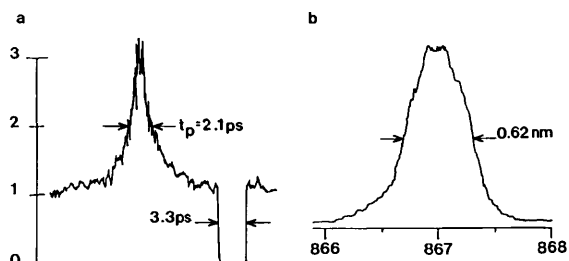
Fig. 3. Autocorrelation trace of typical pulses obtained from the synchronously pumped standing-wave colour centre laser (a) and the corresponding laser spectrum (b). $T \simeq 3\%$.

but by the cavity optics employed (BBHR 800–1000 nm).

When synchronously mode-locked in this linear cavity configuration pulse durations of 2–3 ps were typical (see fig. 3) with a peak (chopped) output power of approximately 30 mW at a pump power of 600 mW. Pulse durations as short as 1.5 ps have been obtained from the linear configuration (matched to one half the pump period) with an associated spectral width of 0.8 nm [18]. The typical time–bandwidth products of approximately 0.5 inferred for these pulses are close to the value of 0.44 which corresponds to a bandwidth-limited gaussian pulseshape.

Fig. 4(a) illustrates the typical behaviour of both the time-averaged fundamental and second harmonic powers as a function of round-trip cavity length detuning for the colour centre laser where its round-trip period is matched to that of the pump. Zero cavity detuning corresponds to the cavity length at which maximum second harmonic occurred. It can be seen that despite an essentially constant fundamental output power over the 80 μm round-trip cavity detuning range depicted in fig. 4(a), the second harmonic signal clearly shows an asymmetric peak with a fwhm ~ 15 μm. This enhancement in second harmonic signal is indicative of significant pulse shortening which takes place when the cavity lengths are closely matched. Once the maximum second harmonic power has been obtained, the shortest pulses were then achieved with a cavity length shortened by a few micrometers beyond the zero detuned position. This behaviour is in good agreement with previous observations on mode-locked F_2^+ colour centre lasers [10,16] and is remarkably similar to the
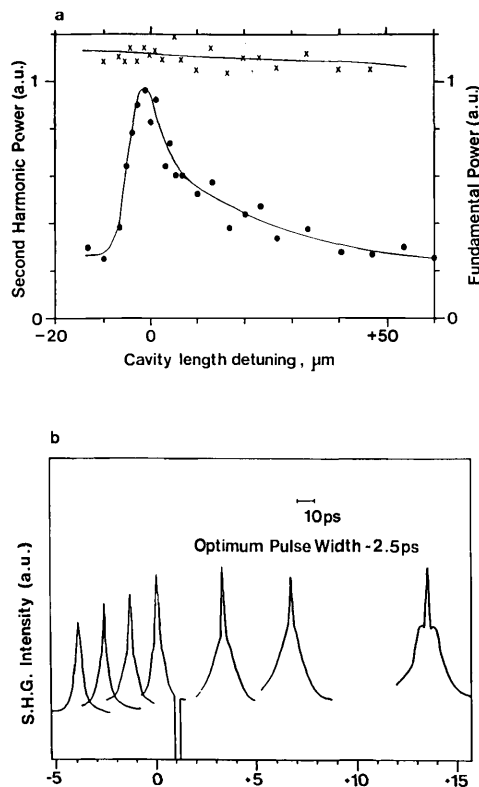
Fig. 4. (a) Plot of time-averaged fundamental (crosses) and second harmonic (dots) powers as a function of the round-trip cavity detuning length). (b) SHG autocorrelation traces of pulses obtained at various cavity detunings.

extensively reported characteristics of synchronously mode-locked dye lasers (see, for example, ref. [5]). Fig. 4(b) illustrates this behaviour by reproducing autocorrelation traces of pulses for various detunings of the colour centre cavity length. For longer cavities (~ 10–15 μm positive detuning) the pulses are clearly broader and the autocorrelation traces are "shouldered". As the cavity is shortened, the pulses narrow and the shoulders become less pronounced. Eventually, at a slightly negative detuning in the cavity length (−2.7 μm in this case) the optimum, (~2.5 ps duration) pulse profiles with contrast ratios of 3:1 are obtained. Further shortening led to pulse broadening and to a rapid decline in contrast ratio. For cavity detunings beyond −5 μm, autocorrelation traces were not obtained with any degree of reliability. The behaviour illustrated in fig. 4 is typical for our laser system but it is expected that
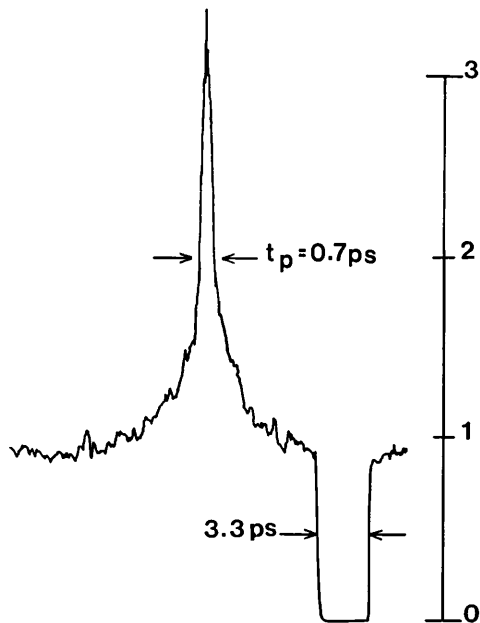
Fig. 5. Autocorrelation trace of short pulses obtained from travelling-wave resonator for a pump power of 600 mW ($T \approx 3\%$).

Fig. 6. Plot of pulse duration versus pump power for (a) linear and (b) ring cavity configurations.

the specific cavity length detuning sensitivity will generally depend upon parameters such as pump power, output coupling and intracavity bandwidth [5].

Considerably shorter pulse durations were obtained from the mode-locked laser when configured in a bi-directional ring resonator (see inset in fig. 1). Fig. 5 shows a typical autocorrelation trace for 0.7 ps duration pulses obtained at a wavelength of 880 nm and a pump power of 600 mW. Simultaneous measurement of the spectral width gave a value of 1.8 nm which implies a time–bandwidth product of 0.49. Under these conditions the peak (chopped) output power in each of the output beams was in the range of 15–20 mW. Mode-locked operation was obtained essentially over the whole wavelength range depicted in fig. 2(b) within which shorter pulses were produced with greater stability than for the conventional linear cavity configuration discussed above. This has been attributed to the coherent interaction process in the gain medium for the ring resonator which gives rise to enhanced gain depletion and to cross-coupling between counter-propagating pulses [19,20]. For both the ring and linear cavity config-

urations it was possible to generate good quality picosecond pulses at pump powers of less than twice the threshold power. This is illustrated in fig. 6 where the optimum pulse duration is shown as a function of the pump power for the linear and ring cavities. (The pump power to the laser was adjusted using an optical attenuator in the Kr^+ laser beam.) The onset of mode-locking at modest pump power levels is another dye-like feature of this synchronously pumped F_2^+ laser.

3. Conclusions

We have described a versatile colour centre laser design which has permitted its performance evaluation with both standing-wave and travelling-wave resonators. In a linear cavity configuration we have generated nearly bandwidth-limited pulses of 1.5 ps duration. Optimum pulses were obtained at a cavity length slightly shorter (~ 2–3 μm) then that at which the maximum second harmonic signal occurred, and in addition, we observed that mode-locking was established at modest pump power levels. These dye-like features are consistent with the radiative decay-times and gain cross-sections which are similar for dyes and the F_2^+ centre in LiF. (The LiF:F_2^+ centre has a radiative decay-time of 29 ns at 77 K [21] and a calculated gain cross-section $\sim 10^{-16}$ cm^2 [10,21]).

We have also exploited the mechanism of coherent interaction of counter-propagating pulses in the gain medium in a bi-directional ring resonator and generated stable trains of subpicosecond pulses over the wavelength range 800–1000 nm. To the authors' knowledge we have obtained the shortest pulses (∼0.7 ps) yet reported for a purely synchronously pumped colour centre laser.

References

[1] A. Scavennec, Optics Comm. 17 (1976) 14.
[2] N.J. Frigo, R. Daly and H. Mahr, IEEE J. Quant. Electron. QE-13 (1977) 101.
[3] D.M. Kim, J. Kuhl, R. Lambrich and D. von der Linde, Optics Comm. 27 (1978) 123.
[4] J.P. Ryan, L.S. Goldberg and D.J. Bradley, Optics Comm. 27 (1978) 127.
[5] C.P. Ausschnitt, R.K. Jain and J.P. Heritage, IEEE J. Quant. Electron. QE-15 (1979) 912.
[6] S.L. Shapiro, R.R. Cavanagh and J.C. Stephenson, Optics Lett. 6 (1981) 470.
[7] P.G. May, W. Sibbett, K. Smith, J.R. Taylor and J.P. Willson, Optics Comm. 42 (1982) 285.
[8] G.H.C. New, Rep. Prog. Phys. 46 (1983) 877.
[9] K. Smith, J.M. Catherall and G.H.C. New, Optics Comm. 58 (1986) 118.
[10] L.F. Mollenauer, Handbook of Lasers, Vol. 4, eds. M.L. Stitch and M. Bass, (North-Holland, Amsterdam, Oxford, New York, Tokyo, 1985) Chapter 2.
[11] T.T. Basiev, N.S. Vorobiev, S.N. Mirov, V.V. Osiko, P.P. Pachinin, V. Postovalov and A.M. Prokhorov, JETP Lett. 31 (1980) 291.
[12] L.F. Mollenauer, N.D. Vieira and L. Szeto, Optics Lett. 7 (1982) 414.
[13] L. Isganitis, M.G. Sceats and K.R. German, Optics Lett. 5 (1980) 7.
[14] R. Illingworth and I.S. Ruddock, Optics Comm. 61 (1987) 120.
[15] M.N. Islam, L.F. Mollenauer and K.R. German, Conf. on Lasers and electro-optics, Baltimore (1987).
[16] L.F. Mollenauer and D.M. Bloom, Optics Lett. 4 (1979) 247.
[18] N. Langford, K. Smith and W. Sibbett, submitted to Optics Lett.
[17] J. Nahum, Phys. Rev. 158 (1967) 814.
[19] J.P. Heritage and E.D. Isaacs, Conf. on Lasers and electro-optics, Washington D.C. (1981).
[20] P.G. May, W. Sibbett and J.R. Taylor, Appl. Phys. B 26 (1981) 179.
[21] L. Bosi, C. Bussolati and G. Spinolo, Phys. Lett. 32A (1970) 159.

Passively mode-locked color-center laser

N. Langford, K. Smith,* and W. Sibbett

Department of Physics, University of St. Andrews, St. Andrews, Fife KY16 9SS, Scotland, UK

Passive mode locking of a cw (chopped) color-center laser using a saturable-absorber polymethine cyanine dye is reported for the first time to our knowledge. By employing the dye IR 140 for passive mode locking, we have obtained stable-output trains of pulses from a LiF:F_2^+ laser at wavelengths around 870 nm. When the technique of colliding-pulse mode locking was implemented in a ring-cavity configuration, pulses having durations as short as 390 fsec were generated.

The passively mode-locked cw dye laser[1] has proved to be a reliable source of ultrashort optical pulses, with the direct generation of pulses as short as 27 fsec reported for an optimized colliding-pulse ring laser.[2] Recent investigations of various active–passive dye combinations have extended the technique to cover a substantial part of the visible and near-infrared spectral regions.[3–6] By employing dispersion-compensated cavity configurations, pulse durations of <100 fsec have been generated for alternative active–passive dye combinations.[7] In this Letter we report on a further extension of this technique by the passive mode locking of a near-infrared color-center laser using a polymethine cyanine saturable absorber.

The color-center laser, which has an active medium of F_2^+ centers in LiF, has been shown to be a highly efficient laser source in the 800–1050-nm wavelength range when pumped by the red output of a krypton-ion laser.[8] The F_2^+ color centers were created in polished 10 mm × 10 mm × 2 mm LiF-crystal samples by the established technique[8] of electron bombardment at low temperatures (77 K in our case) and subsequent annealing of the crystals at room temperature. Since laser operation took place at cryogenic temperatures, the LiF:F_2^+ color-center crystal was mounted on a copper cold finger (maintained at 77 K) and located in an evacuated enclosure. The room-temperature loading of the laser-active crystal into the vacuum enclosure, which takes approximately 10 min, and the subsequent recooling of the crystal to 77 K provided the necessary annealing time for the formation of the F_2^+ centers. Electrical neutrality of the crystal is maintained by the creation of an appropriate density of electron traps. When the crystal is heated by the pump beam these electron traps can be ionized, thus liberating electrons that can subsequently be trapped by the F_2^+ centers to form F_2 centers.[9] This reduces the available F_2^+ concentration and hence the overall gain. To minimize the effects of this thermal degradation, the krypton-ion pump beam was chopped. The duty cycle of the chopper was initially selected to be the 8× (chopping frequency 28 Hz) used for the synchronously mode-locked system,[10] but a factor of 4× (chopping frequency 14 Hz) was later found to be perfectly satisfactory for the continuous-pumping

conditions associated with passive mode locking. Under both chopping conditions we have typically obtained more than 200 h of stable efficient laser operation from a single crystal.

The saturable absorber used for passive mode locking was the dye 5,5'-dichloro-11-diphenylamino-3,3'-diethyl-10,12-ethylenethiatricarbocyanine perchlorate (IR 140, Eastman Kodak). This dye was first employed for subpicosecond pulse generation in the hybrid mode locking of the active dye Styryl-9,[11] and this combination has since led to the generation of femtosecond-duration pulses in dispersion-controlled cavities[12,13] operating around 850 nm. The measured peak-absorption cross section of the IR 140 dye was 6 × 10^{-16} cm^2 at 810 nm for a propylene carbonate solution. The radiative decay lifetime of the dye is believed to be approximately 1 nsec, which is comparable with that of other polymethine cyanine dyes operating in the same spectral region.[14] Photoisomerization of this dye is also a well-known phenomenon,[15] with an equally high peak-absorption cross section occurring at a slightly longer wavelength.

For preliminary mode-locking experiments the cavity depicted in Fig. 1 was employed. A krypton-ion laser generated approximately 3 W of pump power when operated simultaneously on the 647- and 676-nm lines. The horizontally polarized pump light was then coupled into the active crystal through mirror M_0 and one of the folded mirrors (both M_2 and M_3 have radii of curvature of 10 cm). Two thin (~2-mm) Brewster-angled windows (W_1 and W_2) provided optical access to the Brewster-angled LiF crystal and also ensured the necessary vacuum fidelity. The remainder of the optical resonator comprised the totally reflecting plane mirror (M_1), a plane output coupler (M_6, with T ~ 3%), and folded section mirrors M_4 and M_5, both with 5-cm radii of curvature. A free-flowing ~200-μm-thick ethylene glycol jet (in which the propylene carbonate solution of IR 140 was dissolved) was placed at the beam waist between M_4 and M_5. Frequency tuning was effected by an intracavity dielectric wedge. The overall resonator length was close to 2 m, giving a cavity round-trip time of ~13 nsec.

Figure 2a shows the cw (chopped) output train of pulses from the passively mode-locked color-center
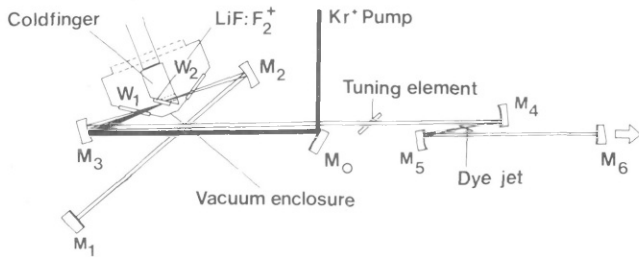
© 1987, Optical Society of America

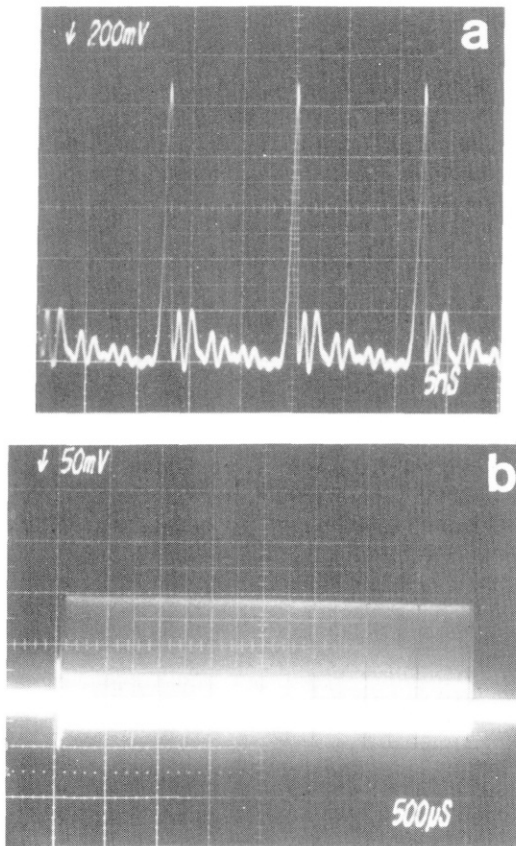Fig. 1.   The experimental passively mode-locked color-center laser.

Fig. 2.   The passively mode-locked cw (chopped) output-pulse train. Time scales: a, 5 nsec/major division; b, 500 sec/major division. (Chopping factor 8×.)

laser, while Fig. 2b shows the highly stable nature of the output-pulse train. Both were recorded using a Telefunken BPW 28 photodiode and Tektronix 7834 oscilloscope arrangement. The laser-pulse durations were determined by employing the standard technique of second-harmonic-generation autocorrelation. With an IR 140 dye concentration of 9×10^{-5} mol/ liter, the laser operated with excellent stability, and pulses having durations of ~1 psec were generated for pump powers 200–400 mW above the threshold power level of approximately 2 W. A typical autocorrelation trace of 1.3-psec-duration pulses (assuming a sech^2 pulse shape) is presented in Fig. 3a for the linear cavity configuration. Simultaneous measurement of the spectral width (Fig. 3b) gave a value of 1.75 nm, imply-

ing a time–bandwidth product of 0.90. The average power associated with these pulses was ~10 mW (evaluated by measuring the chopped output power and multiplying it by the chopping factor).

It is of interest to consider the extensive theoretical literature that has been developed for the slow saturable-absorber mode locking of quasi-continuous dye lasers.[16-19] For the evolution of a stable ultrashort pulse it has been reported that certain system constraints should be satisfied.[16,19] These are the following: (1) the relaxation time of the amplifying medium must be of the order of the cavity round-trip time, (2) the absorber's relaxation time must be less than that of the amplifier, and (3) the so-called s parameter[17] must be large (>2). With regard to the first requirement, practical systems[1-7] operate with a cavity round-trip time longer than the amplifier medium's relaxation time. In the case of our color-center laser the relaxation time of the amplifier medium [reported to be ~29 nsec at 77 K (Ref. 20)] exceeds the round-trip time by a factor of 2. The second constraint, however, is easily fulfilled by our active–passive combination, and the third condition, relating to the s parameter, is aided by the tight focusing afforded by the concave mirrors M_4 and M_5. A calculation of the gain cross section for the F_2^+ center in LiF gives a value of ~10^{-16} cm^2.[8,20]

The most recent advances in the technique of passive mode locking have exploited the coherent interaction processes inherent in colliding-pulse systems, whereby counterpropagating pulses collide in the saturable-absorber dye jet. When applied to cw ring dye lasers this technique has been shown both experimentally and theoretically to give rise to shorter pulses with enhanced stability.[21,22] In our colliding-pulse, passively mode-locked ring color-center laser, the basic cavity configuration was similar to that already described but with mirrors M_1 and M_6 suitably repositioned for the resonator arrangement comprising the six mirrors as illustrated in Fig. 1. The round-trip time was ~15 nsec, and, as for conventional colliding-pulse ring systems, the separation of the gain medium and the saturable absorber was approximately one
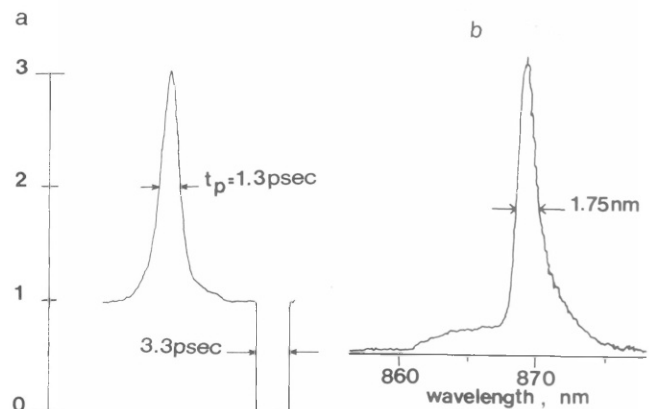

Fig. 3.   a, Typical autocorrelation trace of the passively mode-locked linear color-center laser output; b, corresponding spectrum. (Chopping factor 4×.)
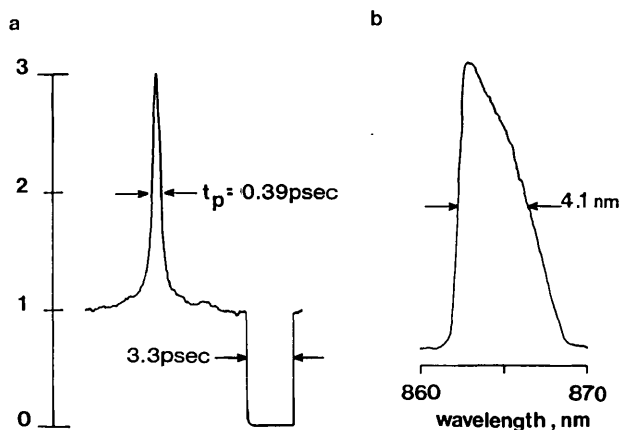
a   b

Fig. 4. a, Typical autocorrelation trace of the output of the colliding-pulse passively mode-locked color-center laser; b, the corresponding spectrum. (Chopping factor 4×.)

quarter of the round-trip cavity length. By employing this experimental setup with a dye concentration of 2 × 10^{-14} mol/liter, we have obtained highly stable output trains of mode-locked subpicosecond-duration pulses. When the typical autocorrelation trace shown in Fig. 4a, which corresponds to 390-fsec-duration pulses, is taken with the associated spectrum (Fig. 4b), the implied time–bandwidth product is 0.65. This somewhat exceeds the product for bandwidth-limited durations for the assumed $sech^2$ pulse shapes, but the laser operation is not yet fully optimized. Under these conditions a (chopped) average power of 6 mW was available in each output beam.

In conclusion, we have demonstrated for the first reported time the passive mode locking of a color-center laser using a saturable-absorber dye. Using an IR 140 dye solution as the saturable-absorber medium, we have generated stable-output trains of picosecond pulses in a standing-wave cavity, and, by exploiting colliding-pulse mode locking, we have obtained subpicosecond-pulse durations (390 fsec). We would expect further improvements when the group-velocity dispersion in the laser has been appropriately controlled.[23] In this work we have not only extended the technique of saturable-absorber passive mode locking to a new laser type but have also demonstrated successful mode locking in a novel system parameter regime. For future work, we have identified other saturable absorbers that should permit the passive mode locking of this color-center system to be evaluated at wavelengths around 1 μm. Furthermore, by changing the active medium to the NaF- and NaCl-based F_2^+-type color-center crystals, it should be possible to adapt the passive mode-locking technique to the 1.0–1.7-μm spectral regions.

References

1. E. P. Ippen, C. V. Shank, and A. Dienes, Appl. Phys. Lett. **21**, 348 (1972).
2. J. A. Valdmanis, R. L. Fork, and J. P. Gordon, Opt. Lett. **10**, 131 (1985).
3. K. Smith, N. Langford, W. Sibbett, and J. R. Taylor, Opt. Lett. **10**, 559 (1985).
4. P. M. W. French and J. R. Taylor, Opt. Lett. **11**, 297 (1986).
5. P. M. W. French and J. R. Taylor, Opt. Commun. **58**, 53 (1986).
6. P. M. W. French and J. R. Taylor, IEEE J. Quantum Electron. **QE-22**, 1162 (1986).
7. P. M. W. French and J. R. Taylor, Opt. Commun. **61**, 224 (1987).
8. L. F. Mollenauer, Methods of Experimental Physics (Academic, New York, 1979), Vol. 15, Part B, Chap. 6.
9. W. Gellermann, A. Muller, D. Wandt, S. Wilk, and F. Luty, J. Appl. Phys. **61**, 1297 (1987).
10. N. Langford, K. Smith, and W. Sibbett, Opt. Lett. **4**, 817 (1987).
11. K. Smith, W. Sibbett, and J. R. Taylor, Opt. Commun. **49**, 359 (1984).
12. J. Dobler, H. H. Schulz, and W. Zinth, Opt. Commun. **57**, 407 (1986).
13. M. D. Dawson, T. F. Boggess, and A. L. Smirl, Opt. Lett. **12**, 254 (1987).
14. J. P. Fouassier, D. J. Lougnot, and J. Faure, Opt. Commun. **18**, 263 (1976).
15. J. P. Fouassier, D. J. Lougnot, and J. Faure, Opt. Commun. **23**, 393 (1977).
16. G. H. C. New, Opt. Commun. **6**, 188 (1972).
17. G. H. C. New, IEEE J. Quantum Electron. **QE-10**, 115 (1974).
18. H. A. Haus, IEEE J. Quantum Electron. **QE-11**, 736 (1975).
19. G. H. C. New, K. E. Orkney, and M. J. W. Nock, Opt. Quantum Electron. **8**, 425 (1976).
20. L. Bosi, C. Bussolati, and G. Spinolo, Phys. Lett. **32A**, 159 (1970).
21. R. L. Fork, B. I. Greene, and C. V. Shank, Appl. Phys. Lett. **38**, 671 (1981).
22. M. S. Stix and E. P. Ippen, IEEE J. Quantum Electron. **QE-19**, 520 (1983).
23. J. A. Valdmanis and R. L. Fork, IEEE J. Quantum Electron. **QE-22**, 112 (1986).

Passive mode locking of a continuous-wave dye laser in the red–near-infrared spectral region

K. Smith, N. Langford, W. Sibbett, and J. R. Taylor

Photonics Group, Optics Section, Blackett Laboratory, Imperial College, London SW7 2BZ, England

Passive mode locking of a cw Rhodamine 700 dye laser is reported for the first time to our knowledge. By using two saturable absorber dyes, DOTCI and HITCI, continuous-output trains of subpicosecond pulses have been obtained in the 727–740- and 762–778-nm spectral regions, respectively. By the addition of a fast-recovery-time dye (DCI) to the DOTCI saturable absorber, pulses as short as 350 fsec at 740 nm have been generated.

The passively mode-locked cw dye laser[1] has proved to be a reliable source of ultrashort optical pulses. Recent advances have exploited the technique of colliding-pulse mode locking, either in a ring cavity[2] or in a linear cavity terminated by an antiresonant ring,[3] and the direct generation of pulses as short as 27 fsec has been reported for an optimized ring-cavity configuration.[4] The main restriction on use of this technique has been the lack of suitable active–passive dye combinations, and, as yet, only one combination, that of Rhodamine 6G/DODCI,[1] is commonly used. In recent years, however, several studies of potential saturable absorbers for new spectral regions have been undertaken using simple flash-lamp-pumped dye-laser systems.[5,6] In this Letter, we report on the passive mode locking of the highly efficient dye Rhodamine 700 with the reliable production of a continuous output of subpicosecond pulses.

Literature on the theory of slow saturable-absorber mode locking for a quasi-continuous dye laser is extensive.[7–10] It is well known that for stable ultrashort pulse evolution it is necessary that there be a net round-trip loss on both the leading and the trailing pulse edges and a net round-trip gain at the pulse peak. In principle these conditions can be easily satisfied, provided that certain system constraints are fulfilled.[7,10] First, the relaxation time of the amplifying medium must be of the order of the cavity round-trip time; second, the absorber relaxation time must be less than the relaxation time of the amplifier; and third, the so-called s parameter [as defined by New in Eq. (4) of Ref. 8] must be large ($\gtrsim 2$). (In the case of the cavity configuration used in this work, this third condition relating to the s parameter reduces essentially to ensuring an appropriate ratio of the absorption cross section to the amplification cross section.) When these requirements are all satisfied, then the laser operates within a region of compression and the intracavity energy can be confined to a circulating stable ultrashort light pulse.

The active dye used in this work was Rhodamine 700 [fluorescence lifetime in ethanol $\sim$ 2.8 nsec (Ref. 11)], which, when pumped with all red lines (647 and 676 nm) from a krypton-ion laser, had a power perfor-

mance similar to that of Rhodamine 6G pumped by an argon-ion laser. The wavelength tuning range, however, extended over the 700–800-nm region. (An alternative method of exciting Rhodamine 700 is to use an energy-transfer dye mixture[12] and an argon-ion pump source.) Two saturable-absorber polymethine cyanine dyes have been used for the passive mode locking described here. These dyes were 3,3′-diethyloxatricarbocyanine iodide (DOTCI) and 1,1′,3,3,3′,3′-hexamethylindocarbocyanine iodide (HITCI) with absorption cross sections measured to be 9.8×10^{-16} at 680 nm and 9.1×10^{-16} cm^2 at 740 nm for ethanolic solutions of DOTCI and HITCI, respectively (Fig. 1). In addition, both dyes exhibit photoisomer formation with equally high absorption cross sections peaking at slightly longer wavelengths.[13] The radiative lifetimes of these dyes have been reported to be 2.3 nsec for DOTCI in ethylene glycol[1] and 1.2 nsec for HITCI in dimethyl sulfoxide.[13] *HITCI has been used as a saturable absorber in the hybrid mode locking of an Oxazine 750 dye laser in a similar spectral region to that reported here.*[15]

A linear cavity configuration, similar to that described in earlier work,[16] was employed. The pump beam was coupled into the four-mirror laser cavity through a telescope arrangement (comprising two biconvex lenses of 6-cm focal length) and an extra independent *5-cm radius-of-curvature* mirror, which focused the pump beam into the $\sim$200-μm Brewster-angled Rhodamine 700 dye jet (concentration 1.6 $\times$ 10^{-3} mol/L in ethylene glycol) *placed at the common focus of the 5-cm radius-of-curvature cavity mirrors.* The telescope, although possessing unity magnification, permitted fine adjustment of both the position and the size of the pump spot in the active medium and therefore permitted the laser performance to be optimized easily. The resonator was completed with a second folded section, which comprised two 5-cm radius-of-curvature mirrors with a $\sim$200-μm-thick Brewster-angled absorber dye jet at their common focus. The respective concentrations of DOTCI and HITCI solutions were 3 $\times$ 10^{-5} and 1 $\times$ 10^{-5} mol/L in ethylene glycol with 5% ethanol to predissolve. An output from the cavity was obtained as a reflection from the intra-

© 1985, Optical Society of America

cavity dielectric tuning wedge, which provided wavelength selection over the mode-locking region. The cavity length of 90 cm gave a round-trip time of 6 nsec.

For the DOTCI dye solution, pulses of ~1-psec duration were maintained over the 727–740-nm region with average output powers as high as 20 mW. In the
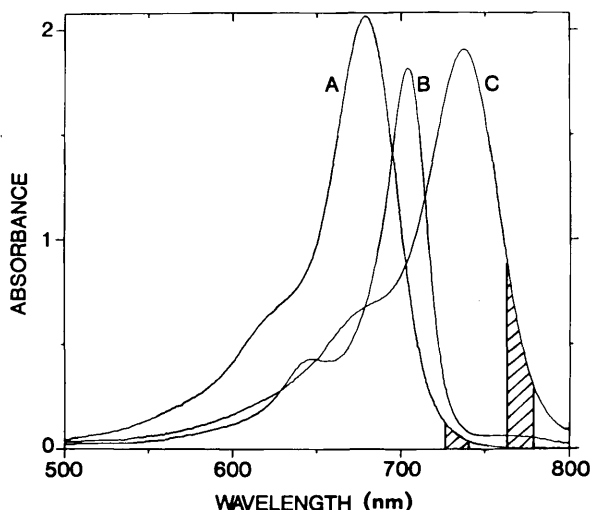

Fig. 1. Absorption traces of 4×10^{-5} mol/L ethanolic solutions of (a) DOTCI, (b) DCI, and (c) HITCI (2-mm sample thickness). *The spectral range (see text) where passive mode locking was obtained is shown by the shaded regions.*
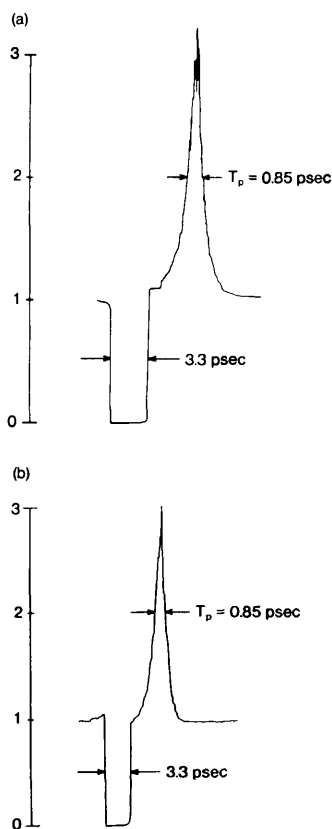
Fig. 2. Autocorrelation traces of the shortest pulses obtained from passively mode-locked cw Rhodamine 700 with (a) DOTCI ($\lambda = 730$ nm) and (b) HITCI ($\lambda = 770$ nm).
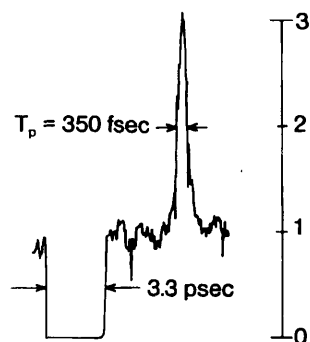
Fig. 3. Autocorrelation trace of the shortest pulses obtained from the passively mode-locked Rhodamine 700–DOTCI–DCI dye-laser system ($\lambda = 740$ nm). (DCI concentration, 3×10^{-5} mol/L.)

case of the HITCI dye solution, the mode-locking range was at the slightly longer wavelengths 762–778 nm, and output powers ~10 mW were more typical. For both saturable absorbers pulses as short as 0.85 psec (Fig. 2) were generated (assuming $sech^2$, a pulse shape that is common for lasers of this type). Also, in both cases the laser was found to operate most successfully between 200 and 400 mW above the threshold power level (~2 W). The maximum available power from the krypton-ion pump laser was 2.5 W, and therefore no attempt fully to optimize the saturable-absorber dye concentration was possible. It has been shown that the addition of a fast-recovery saturable absorber to the slow-recovery system leads to further pulse shortening,[17] and so the fast-recovery-time dye, 1,1'-diethyl-4,4'-carbocyanine iodide (DCI) was added to the DOTCI saturable-absorber solution. The lifetime of this dye is reported to be 48 psec (Ref. 18) in ethanolic solution, and its measured peak absorption cross section at 705 nm (Fig. 1) is 8.7×10^{-16} cm^2. With this saturable-absorber mixture stable pulses of 500-fsec duration were typically generated, although pulses as short as 350 fsec were recorded (Fig. 3). However, for these shortest pulses stability was poor since the addition of the DCI dye forced the optimum lasing wavelength toward the long-wavelength limit of the mode-locking region.

In conclusion, the passive mode locking of a cw Rhodamine 700 dye laser and the production of stable, subpicosecond pulses has been demonstrated. Other suitable active–passive dye combinations have been identified, and we are currently investigating the extension of the operating range of passively mode-locked cw dye lasers over the visible and near-infrared spectral regions.

References

1. E. P. Ippen, C. V. Shank, and A. Dienes, Appl. Phys. Lett. **21**, 348 (1972).
2. R. L. Fork, B. I. Greene, and C. V. Shank, Appl. Phys. Lett. **38**, 671 (1981).
3. H. Vanherzeele, J. C. Diels, and R. Torti, Opt. Lett. **9**, 549 (1984).
4. J. A. Valdmanis, R. L. Fork, and J. P. Gordon, Opt. Lett. **10**, 131 (1985).
5. W. Sibbett and J. R. Taylor, IEEE J. Quantum Electron. **QE 19**, 558 (1983).
6. W. Sibbett and J. R. Taylor, IEEE J. Quantum Electron. **QE-20**, 108 (1984).
7. G. H. C. New, Opt. Commun. **6**, 188 (1972).
8. G. H. C. New, IEEE J. Quantum Electron. **QE-10**, 115 (1974).
9. H. A. Haus, IEEE J. Quantum Electron. **QE-11**, 736 (1975).
10. G. H. C. New, K. E. Orkney, and M. J. W. Nock, Opt. Quantum Electron. **8**, 425 (1976).
11. T. Doust, Royal Institution, London (personal communication).
12. E. G. Marason, Opt. Commun. **40**, 212 (1982).
13. J. P. Fouassier, D. J. Lougnot, and J. Faure, Opt. Commun. **18**, 263 (1976).
14. L. D. Derkacheva, V. A. Petukhov, and E. G. Treneva, Opt. Spectrosc. (USSR) **41**, 574 (1976).
15. G. W. Fehrenbach, K. J. Gruntz, and R. G. Ulbrich, Appl. Phys. Lett. **33**, 159 (1978).
16. K. Smith, W. Sibbett, and J. R. Taylor, Opt. Commun. **49**, 359 (1984).
17. E. P. Ippen and C. V. Shank, Appl. Phys. Lett. **27**, 488 (1975).
18. V. Sundstrom and T. Gillbro, Chem. Phys. **61**, 257 (1981).

THE HYBRID MODE-LOCKING OF A CW RHODAMINE 700 DYE LASER

N. LANGFORD [1], K. SMITH [1], W. SIBBETT [1] and J.R. TAYLOR

Photonics Group, The Blackett Laboratory, Imperial College, London SW7 2BZ, UK

Two saturable absorber dye solutions, HITCI and DOTCI, have been employed to provide hybrid mode-locking of a cw dye laser operating over the 770–781 nm and 710–718 nm spectral ranges respectively. Pulses as short as 0.55 ps and 0.47 ps were obtained in these respective regions.

1. Introduction

Continuous wave (CW) mode-locked dye lasers are a very convenient source of tunable ultrashort light pulses which find many experimental applications [1]. The two mode-locking methods most commonly employed are those of synchronous mode-locking, where the cavity length of the dye laser is matched to that of the actively mode-locked pump laser [2], and passive mode-locking, using a saturable absorber dye solution [3]. Synchronous mode-locking gives rise to highly tunable, energetic pulses, whereas the highest stability and shortest pulse durations are achieved with passive mode-locking. The technique of hybrid mode-locking, where a saturable absorber is incorporated within a synchronously pumped laser configuration, appears to offer a compromise, in which highly stable, ultrashort pulses are available with some degree of tunability. The main restriction to this technique, however, is the lack of suitable saturable absorbers for the wide range of active dyes now available in the visible and near infra-red regions, and only a limited number of hybrid systems have been reported [4–8]. In this paper, we report on the generation of frequency-tunable subpicosecond pulses from a CW rhodamine 700 dye laser by hybrid mode-locking.

[1] Present address: Photonics Group, Department of Physics, University of St Andrews, North Haugh, St Andrews KY16 9SS, Scotland.

2. Experimental and results

Fig. 1 shows the experimental configuration used in the preliminary stages of this work. The mode-locked CW dye laser was synchronously pumped with the 80 ps pulses (measured using a synchronously operating Photochron II streak camera [9]) at $\sim$82 MHz from an acousto-optically mode-locked krypton ion laser operating on the 647 nm line. Average pump powers of $\sim$1 W were typically obtained. The synchronously pumped rhodamine 700 laser comprised a standard linear, four mirror (M_1-M_4) dye laser cavity configuration in which the 200 μm thick Brewster-angled dye jet was situated at the common focus of the two 10 cm radius of curvature mirrors M_2 and M_3. These mirrors were nominally 100% reflecting in the 640–860 nm range. The plane mirror, M_1, had identical reflectivity characteristics to those of mirrors M_2 and M_3, and had a hole in the centre to allow the krypton ion pump beam to be coupled directly into the dye jet by mirror M_2. Two extracavity krypton ion beam steering mirrors facilitated the fine
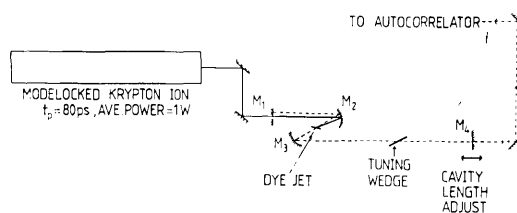

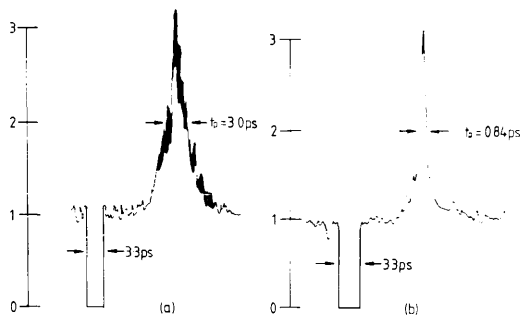Fig. 1. The experimental arrangement.

Fig. 2. The duration of the dye laser pulses at 771 nm with (a) no saturable absorber and (b) an absorber concentration of 3.4 × 10⁻⁵ mol/ℓ.
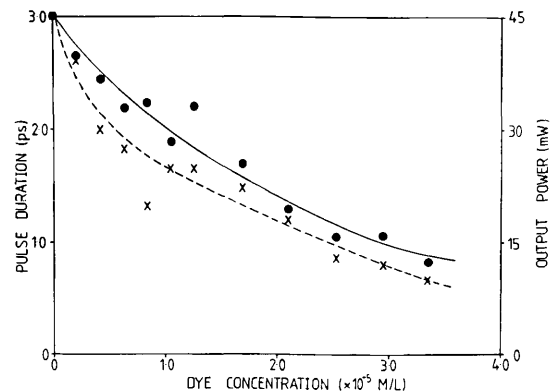

Fig. 3. The dependence of the pulse duration (dots) and average output power (crosses) on the absorber dye concentration for hybrid mode-locked operation at 771 nm.

adjustment of the pump spot position in the dye jet. Output coupling was achieved via mirror M_4 which had a reflectivity of approximately 95% over the 700–800 nm spectral region. Wavelength selectivity was accomplished with an intracavity dielectric tuning wedge. Since the processes for ultrashort pulse formation by the techniques of synchronous and hybrid mode-locking require the pump and slave laser cavity lengths to be appropriately matched, the output coupler was mounted on a differential micrometer controlled translation stage. The overall length of the dye laser cavity was ~1.8 m giving a round-trip time of ~12.4 ns, and the mode-locked pulse train was monitored using a real-time autocorrelator with a resolution of better than 0.1 ps.

The optimum concentration of the active dye rhodamine 700 (in ethylene glycol) was 1.6×10^{-3} mol/ℓ and pulse durations ~3 ps (assuming a gaussian pulse profile) were recorded essentially over the entire tuning range (690–790 nm) of the laser dye (see fig. 2(a)). Average output powers ~50 mW were typically observed at the peak of the tuning curve. Hybrid mode-locking was obtained by introducing the saturable absorber into the rhodamine 700 dye circulation system so that the gain and absorber dyes formed a composite medium. For this work, the saturable absorber dye was 1,1′,3,3,3′,3′-hexamethylindotricarbocyanide iodide (HITCI) which displays an absoption band peaking around 740 nm in ethanolic solution ($\sigma_{max} = 9.1 \times 10^{-16}$ cm²). With the laser operating at a wavelength of 771 nm simultaneous autocorrelations of the output pulse width were taken as the concentration of the HITCI absorber dye

was increased. These results are illustrated in fig. 3. Although low concentrations of saturable absorber (~25 × 10⁻⁵ mol/ℓ) did lead to some small degree of pulse shortening, the major action of this low dye concentration was to increase the pulse stability with no significant reduction in the average output power. Further additions of the HITCI dye caused continued pulse shortening, eventually giving rise to the 0.84 ps duration pulses (gaussian pulse profile assumed) shown in fig. 2(b) where the dye concentration was 3.4×10^{-5} mol/ℓ and an average output power of 10 mW was recorded. At this absorber concentration significant pulse shortening was observed in the 770–781 nm wavelength range. The shortest pulses, obtained at a wavelength of 776 nm, had durations of 0.55 ps with an average output power of 15 mW (shown in fig. 4).

During the later stages of this work a different cavity configuration (similar to that described in ref. [8]) was employed. This 1.8 m long cavity comprised an independent passive dye folded section with two 10 cm radius of curvature mirrors and a 200 μm thick Brewster-angled ethylene glycol jet at their common focus. An output coupler with a 90% reflecting coating over the 700–750 nm region was used. Hybrid mode-locking in this configuration using the dye HITCI gave similar results to those already reported. A further experiment was performed using the saturable absorber dye 3,3′-diethyloxatricarbocyanine iodide (DOTCI) which has an absorption band peaking around 680 nm in ethanolic solution ($\sigma_{max} = 9.1$
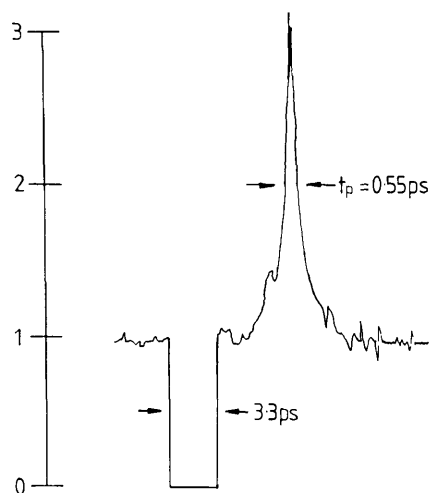
Fig. 4. The shortest pulses obtained from the rhodamine 700/ HITCI hybrid dye laser (HITCI concentration = 3.4×10^{-5} mol/ℓ, λ = 776 nm).
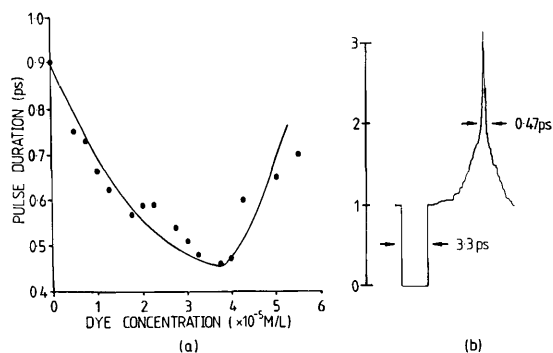
Fig. 5. (a) The dependence of the pulse duration on the DOTCI absorber concentration for hybrid mode-locked operation (λ = 713 nm) and (b) a typical autocorrelation trace taken with an absorber concentration of 4×10^{-5} mol/ℓ (λ = 713 nm).

$\times 10^{-5}$ cm^2). Pulse duration variations as a function of DOTCI dye concentration are illustrated in fig. 5(a) and a typical autocorrelation trace of 0.47 ps duration pulses (taken at a dye concentration of 4×10^{-5} mol/ℓ) with an average output power of 12 mW is reproduced in fig. 5(b). At this absorber concentration, hybrid operation was observed for wavelengths between 710 and 718 nm.

3. Conclusion

We have demonstrated that the laser dyes HITCI and DOTCI can be employed as saturable absorbers in the hybrid mode-locking of a synchronously pumped CW rhodamine 700 dye laser system. By further optimisations of the dye concentrations it should be possible to generate stable, subpicosecond pulses over most of the 685–820 nm wavelength range with the two saturable absorber dyes employed here.

Acknowledgement

References

[1] Ultrafast Phenomena, IV; Proc. Fourth Intern. Conf., eds. D.H. Auston and K.B. Eisenthal (Springer-Verlag, 1984).

[2] C.K. Chan and S.O. Sari, Appl. Phys. Lett. 25 (1974) 403.

[3] E.P. Ippen, C.V. Shank and A. Dienes, Appl. Phys. Lett. 21 (1972) 348.

[4] G.W. Fehrenbach, K.J. Gruntz and R.G. Ulbrich, Appl. Phys. Lett. 33 (1978) 159.

[5] J.P. Ryan, L.S. Goldberg and D.J. Bradley, Optics 27 (1978) 127.

[6] Y. Aoyagi, Y. Segawa and S. Namba, Japan J. Appl. Phys. 20 (1981) L1595.

[7] Y. Ishida, K. Naganuma and T. Yajima, Japan J. Appl. Phys. 21 (1982) L312.

[8] K. Smith, W. Sibbett and J.R. Taylor, Optics Comm. 49 (1984) 359.

[9] M.C. Adams, W. Sibbett and D.J. Bradley, Advances in Electronics and Electron Physics 52 (1979) 265.

A passively mode-locked c.w. rhodamine 700 dye laser

K. SMITH, N. LANGFORD, W. SIBBETT and J. R. TAYLOR†

Department of Physics, University of St Andrews,
North Haugh, St Andrews, Fife KY16 9SS, Scotland

Abstract. Passive mode-locking of a c.w. rhodamine 700 dye laser is reported for the first time. Continuous output trains of subpicosecond pulses have been obtained with two saturable absorber dyes, DOTCI and HITCI, in the 727–740 nm and 762–778 nm spectral regions respectively. By the addition of a fast recovery time dye (DCI) to the DOTCI saturable absorber solution, pulses as short as 350 fs at 740 nm have been generated in a linear cavity configuration.

1. Introduction

The passively mode-locked c.w. dye laser [1], first demonstrated in 1972 as a successful development of the flashlamp pumped system [2], has proved to be a reliable source of ultrashort optical pulses. The most recent advances have employed the technique of colliding pulse mode-locking and have led to the direct generation of pulses as short as 27 fs in an optimized cavity configuration [3]. An unfortunate restriction of passive mode-locking has been in the lack of suitable active/passive dye combinations and, as yet, only the combination of rhodamine 6G/DODCI [1], finds common usage. We now report on the successful c.w. passive mode-locking of a new system generating tunable picosecond pulses in the near infrared spectral region. The use of streak cameras to record the decay characteristics of many saturable absorber species [4] has, in recent years, led to the successful passive mode-locking of flashlamp-pumped dye laser systems over the complete visible and near infrared regions [5, 6]. The c.w. system we report on here used the highly efficient active dye rhodamine 700.

2. Theoretical considerations

Literature on the theory of slow saturable absorber mode-locking for a quasi-continuous dye laser is extensive [7–10]. It is well known that for stable ultrashort pulse evolution it is necessary that there be a net round-trip loss on both the leading and trailing pulse edges and a net round-trip gain at the pulse peak. In principle these conditions can be easily satisfied provided that certain system constraints are fulfilled [7, 10]. Firstly, the relaxation time of the amplifying medium must be of the order of the cavity round-trip time, secondly, the absorber relaxation time must be less than the relaxation time of the amplifier, and thirdly, the so called 's' parameter (as defined by New in equation (4) of [8]) must be large (> 2). For the configuration used in this work, the third condition relating to the s parameter reduces to ensuring an

† Photonics Group, Optics Section, Blackett Laboratory, Imperial College, London SW7 2BZ, England.

appropriate ratio of the absorption cross-section to the amplification cross-section. When these requirements are all satisfied, then the laser operates within a region of compression and the intracavity energy can be confined to a stable ultrashort light pulse.

The active dye used. in this work was rhodamine 700 with a measured fluorescence lifetime of 2·8 ns in ethanol [11]. When pumped with all red lines (647, 676 nm) from a krypton ion laser, rhodamine 700 had a power performance very similar to that of rhodamine 6G pumped by an argon ion laser but with a 700–800 nm tuning range. Two saturable absorber polymethine cyanine dyes were used for the passive mode-locking described here. These dyes were DOTCI (3,3′-diethyloxa-tricarbocyanine iodide) and HITCI (1,1′,3,3,3′,3′-hexamethylindotricarbocyanine iodide) with absorption cross-section measured to be $9·8 \times 10^{-16}$ cm^2 at 680 nm and $9·1 \times 10^{-16}$ cm^2 at 740 nm for ethanolic solutions of DOTCI and HITCI respectively (figure 1). In addition, both dyes exhibit photoisomer formation with equally high absorption cross-sections peaking at slightly longer wavelengths [12]. The radiative lifetimes of these dyes have been reported to be 2·3 ns for DOTCI in ethylene glycol [13] and 1·2 ns for HITCI in DMSO [12].
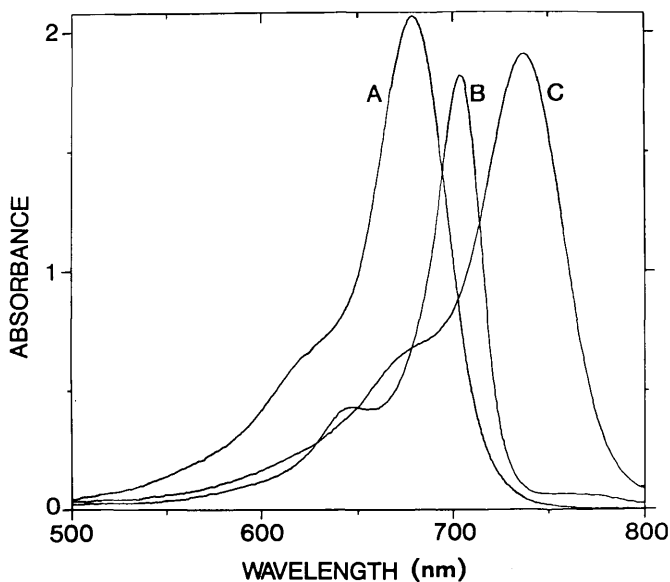

Figure 1.   Absorption traces of 4×10^{-5} mol l^{-1} ethanolic solutions of A, DOTCI; B, DCI and C, HITCI (2 mm sample cell thickness).

3. Experimental procedure

A ~ 90 cm long linear cavity configuration (shown in figure 2) was employed giving a round-trip time of ~ 6 ns. The pump beam was coupled into the four-mirror laser cavity via a telescope arrangement (comprising two biconvex lenses of 6 cm focal length) and an extra independent mirror (5 cm radius of curvature) which focused the pump beam into the $\sim 200\,\mu$m Brewster-angled rhodamine 700 dye jet (concentration $1·6 \times 10^{-3}$ mol l^{-1} in ethylene glycol). The active folded section
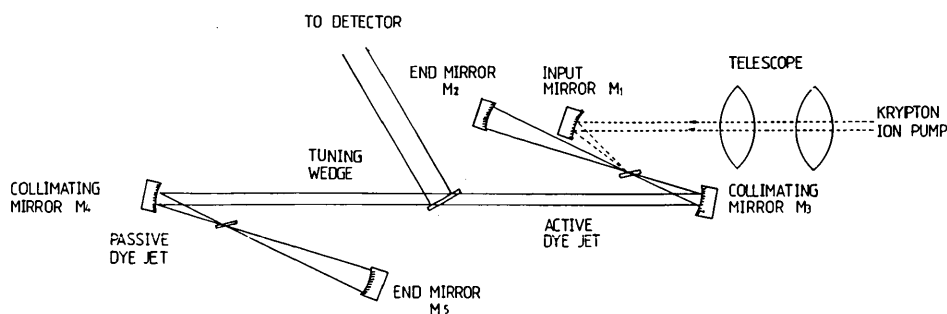
Figure 2.　The experimental cavity configuration.

comprised two 5 cm radius of curvature mirrors highly reflecting in the 700–800 nm spectral region. The telescope, although possessing unity magnification, allowed fine adjustment of both the position and size in the active medium. The resonator was completed with a second folded section which comprised two 5 cm radius of curvature mirrors with a ~200 μm thick Brewster-angled absorber dye jet at their common focus. The respective concentrations of DOTCI and HITCI solutions were 3×10^{-5} mol l^{-1} and 1×10^{-5} mol l^{-1} in ethylene glycol with 5% ethanol to predissolve. An output from the cavity was obtained as a reflection from the intracavity dielectric tuning wedge which provided wavelength selection over the mode-locking region.

4.　Results

For the DOTCI absorber dye solution, pulses of approximately 1 ps duration were maintained over the 727–740 nm wavelength region with average output powers as high as 20 mW. In the case of the HITCI absorber dye solution, the mode-locking range was at the slightly longer wavelengths 762–778 nm and output powers of 10 mW were more typical. Figure 3 shows the c.w. output train of pulses for the case of the mode-locked rhodamine 700/DOTCI dye laser system as recorded by a photodiode/sampling oscilloscope combination. Using the technique of SHG autocorrelation the laser pulse durations were determined. For both saturable absorbers pulses as short as 0·85 ps (figure 4) were generated (a $sech^2$ pulse profile is assumed). Also, in both cases the laser was found to operate most successfully between 200 and 400 mW above the threshold power level of 2 W. Since the maximum available pump power from the krypton ion laser was ~2·5 W no attempt to fully optimize the saturable absorber dye solution concentration was possible.

The addition of a fast recovery time dye to the slow recovery system has been shown to lead to further pulse shortening [14]. Consequently, the fast recovery time dye DCI (1,1'-diethyl-4,4'-carbocyanine iodide) was added to the DOTCI saturable dye solution. The lifetime of this dye is reported to be 48 ps [15] in ethanolic solution and its measured peak absorption cross-section at 705 nm (figure 1) is $8·7 \times 10^{-16}$ cm^2. With this saturable absorber dye mixture stable pulses of 500 fs duration were typically generated, although pulses as short as 350 fs were recorded (figure 5). However, for the shortest pulses stability was noted to be poor since the addition of the DCI dye forced the optimum lasing wavelength towards the long wavelength limit of the mode-locking region.
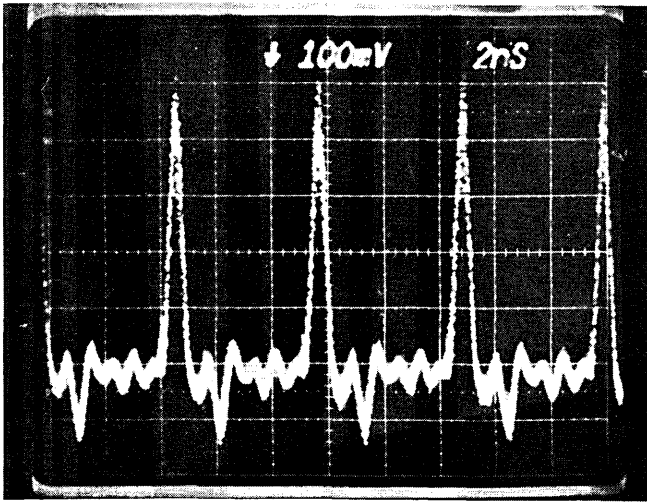
K. *Smith* et al.

Figure 3. The mode-locked c.w. rhodamine 700/DOTCI dye laser output recorded using a photodiode/sampling oscilloscope combination.

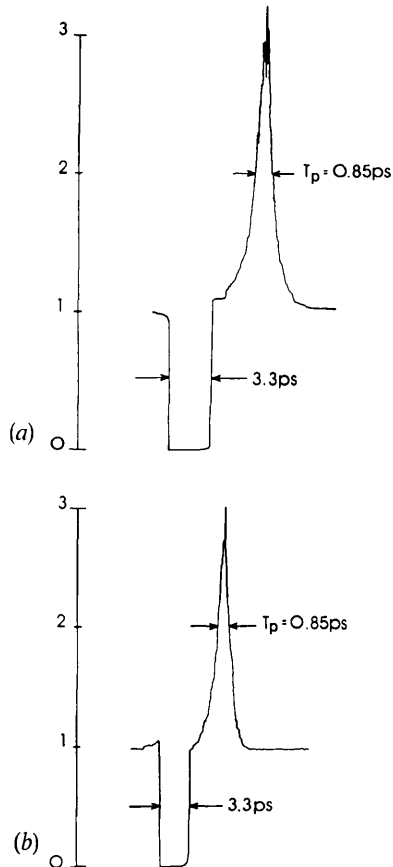

Figure 4. Autocorrelation traces of the shortest pulses obtained from the passively mode-locked c.w. rhodamine 700 dye laser with (a) DOTCI ($\lambda = 730$ nm) and (b) HITCI ($\lambda = 770$ nm).
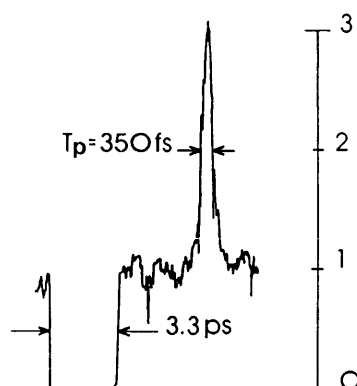
Figure 5.   Autocorrelation trace of the shortest pulses obtained from the passively mode-locked rhodamine 700/DOTCI/DCI dye laser system ($\lambda = 740$ nm) (DCI dye concentration $= 3 \times 10^{-5}$ mol l^{-1}).

5. Conclusions

The passive mode-locking of a c.w. rhodamine 700 dye laser and the production of stable, subpicosecond pulse trains in the red/near infrared spectral region has been demonstrated. Such a system could easily be extended to a useful femtosecond laser pulse source by exploiting the technique of colliding pulse mode-locking in optimized cavity configurations [3]. Other suitable active/passive dye combinations have been identified and we are currently investigating the extension of the operating range of passively mode-locked c.w. dye lasers over the visible and near infra-red spectral regions.

Acknowledgments

References

[1] Ippen, E. P., Shank, C. V., and Dienes, A., 1972, *Appl. Phys. Lett.*, **21**, 348.
[2] Schmidt, W., and Schäfer, F. P., 1968, *Physics Lett.* A, **26**, 558.
[3] Valdmanis, J. A., Fork, R. L., and Gordon, J. P., 1985, *Optics Lett.*, **10**, 131.
[4] Sibbett, W., Taylor, J. R., and Welford, D., 1981, *IEEE Jl quant. Electron.*, **17**, 500.
[5] Sibbett, W., and Taylor, J. R., 1983, *Optics Commun.*, **46**, 32.
[6] Sibbett, W., and Taylor, J. R., 1984, *IEEE Jl quant. Electron.*, **20**, 108.
[7] New, G. H. C., 1972, *Optics Commun.*, **6**, 188.
[8] New, G. H. C., 1974, *IEEE Jl quant. Electron.*, **10**, 115.
[9] Haus, H. A., 1975, *IEEE Jl quant. Electron.*, **11**, 736.
[10] New, G. H. C., Orkney, K. E., and Nock, M. J. W., 1976, *Opt. quant. Electron.*, **8**, 425.
[11] Doust, T., 1985, private communication.
[12] Fouassier, J. P., Lougnot, D. J., and Faure, J., 1976, *Optics Commun.*, **18**, 263.
[13] Derkacheva, L. D., Petukhov, V. A., and Treneva, E. G., 1972, *Optika Spectrosk.*, **41**, 574.
[14] Ippen, E. P., and Shank, C. V., 1975, *Appl. Phys. Lett.*, **27**, 488.
[15] Sundstrom, V., and Gillbro, T., 1981, *Chem. Phys.*, **61**, 257.